## ENHANCEMENT IN RESISTIVITY RESOLUTION BASED ON DATA AMALGAMATION TECHNIQUE

 $\mathbf{B}\mathbf{y}$ 

## ANDY ANDERSON ANAK BERY

Thesis submitted in fulfilment of the requirements for the degree of Doctor of Philosophy

**DECEMBER 2015** 

#### **ACKNOWLEDGMENTS**

First and foremost, praises and thanks to the Almighty God for showers of blessing throughout my PhD study to complete the research successfully.

I would like to express my deep sincere thanks and gratitude to my main supervisor, Associate Professor Dr. Rosli Saad, for his motivations, advices, and immense knowledge. His guidance and kindly supervision helped me in completing my PhD study. I also would like to express my sincere gratitude to my co-supervisor Dr. Nordiana Mohd Muztaza for her helps and suggestions. Special thanks to Professor Dato' Dr. Mohd Mokhtar Saidin, Director of Centre for Global Archaeological Research (CGAR) for permission conducting research allowing the use of data and borehole records.

Secondly, I would like to give my appreciation to all the laboratory assistants, Mr. Yaakub Othman, Mr. Shahil Ahmad Khosaini and Mr. Azmi Abdullah that helps and guided me throughout period of my PhD study.

I would like to thank and give my appreciation to colleagues Dr. Nur Azwin Ismail and Dr. Noer El Hidayah Ismail. Thanks also to postgraduates, Mr. Yakubu Mingyi Samuel, Mr. Kiu Yap Chong, Mr. Mark Jinmin, Mr. Ragu Ragava Rao Satinaranan and lastly Madam. Nur Aminuda Kamaruddin. I would like to send my deep sincere thanks to them all for helps and supports.

I also would like to thanks Kementerian Pelajaran Malaysia and Universiti Sains Malaysia for the Skim Latihan Akademik Bumiputera (SLAB) scholarship and financial support throughout period of my PhD study.

Last but not least, my sincere thanks and profound appreciation to my beloved parents Mr. Bery Sidos and Mdm. Pauline Pungga, my sister Eva Diana Bery, my brother Jeff Steven Bery and my special one Cassandra Warnes Tueng who have provided me with their prayers, encouragements and supports throughout my PhD study.

## TABLE OF CONTENTS

		Page
Ackı	nowledgments	ii
Tabl	e of Contents	iii
List	of Tables	vi
List	of Figures	vii
List	of Symbols	xi
List	of Abbreviations	xii
Abst	trak	xiii
Abst	tract	xv
CHA	APTER 1: INTRODUCTION	1
1.0	Background	1
1.1	Problem statements	3
1.2	Research objectives	4
1.3	Motivation and research novelty	5
1.4	Layout of thesis	6
СНА	APTER 2: LITERATURE REVIEW	8
2.0	Introduction	8
2.1	Electrical resistivity theory	9
2.2	Basic concept of 2-D resistivity imaging	11
2.3	The general four-electrode method	13
2.4	Selecting electrode array for 2-D resistivity survey	15
	2.4.1 D-D array	16
	2.4.2 P-D array	17
	2.4.3 W array	18

	2.4.4	W-S array		19
2.5	Electr	ode arrays		20
2.6	Invers	sion of resisti	vity data	21
2.7	Previo	ous studies		23
	2.7.1	Critical con	nments on resistivity data processing technique	27
2.8	Chapt	er summary		32
	D.T.D. 4			22
СНА	PTER	3: RESEARC	CH METHODOLOGY	33
3.0	Introd	uction		33
3.1	Resea	rch methodol	ogy flowcharts	34
3.2	Phase	1: 2-D comp	uterized models and field model	37
	3.2.1	Forward mo	odelling	37
	3.2.2	Geological	models test	38
		3.2.2.1	A block model	38
		3.2.2.2	Two blocks model	39
		3.2.2.3	Contact zone model	40
		3.2.2.4	Vertical dyke model	40
		3.2.2.5	Fault model	41
	3.2.3	The DLA to	echnique for two different arrays	42
	3.2.4	Field mode	1	42
	3.2.5	The DLA to	echnique for field model data	43
	3.2.6	Inversion m	nodelling	43
3.3	Phase	2: The nume	erical comparative assessment	44
3.4	Phase 3: Validation of the DLA technique		46	
	3.4.1	Minden, US	SM, Penang	47
	3.4.2	Bukit Bunu	ih, Perak	48
3.5	Chapt	er summarv		50

CHA	PTER 4	4: RESULTS AND DISCUSSIONS	51
4.0	Introd	luction	51
4.1	Resul	ts of 2-D computerized models	51
	4.1.1	A block model	51
	4.1.2	Two blocks model	61
	4.1.3	Contact zone model	71
	4.1.4	Vertical dyke model	81
	4.1.5	Fault model	91
	4.1.6	The numerical comparative assessment	101
	4.1.7	Conclusion of 2-D computerized models	103
4.2	Field	model study	109
	4.2.1	The buried bunker, USM, Penang	109
	4.2.2	The numerical comparative assessment	119
	4.2.3	Conclusion of field model	121
4.3	Field	studies	123
	4.3.1	Minden, USM, Penang	123
	4.3.2	Bukit Bunuh, Perak	124
4.4	Chapt	er summary	126
СНА	PTER 5	5: CONCLUSION AND RECOMMENDATIONS	127
5.0	Concl	usion	127
5.1	Recor	nmendations for future research	129
REFERENCES			130

## LIST OF TABLES

		Page
Table 3.1	Parameters of forward modelling for four different arrays used.	38
Table 4.1	The numerical comparative assessment for a block model.	104
Table 4.2	The numerical comparative assessment for two blocks model.	105
Table 4.3	The numerical comparative assessment for contact zone model.	106
Table 4.4	The numerical comparative assessment for vertical dyke model	107
Table 4.5	The numerical comparative assessment for fault model.	108
Table 4.6	The numerical comparative assessment for the buried bunker.	122

## LIST OF FIGURES

		Page
Figure 2.1	Common electrodes array for resistivity measurement.	12
Figure 2.2	Arrangement of four-electrode in electrical resistivity method.	13
Figure 2.3	Electrode's arrangement for D-D array.	16
Figure 2.4	Electrode's arrangement for P-D array.	17
Figure 2.5	Electrode's arrangement for W array.	18
Figure 2.6	Electrode's arrangement for W-S array	19
Figure 2.7	Common arrays used in resistivity and their geometric factors.	21
Figure 3.1	Research methodology flowchart for the Phase 1.	35
Figure 3.2	Research methodology flowchart for the Phase 2.	36
Figure 3.3	The synthetic model showing a block embedded in homogenous medium.	39
Figure 3.4	The synthetic model showing two blocks embedded in homogenous medium.	39
Figure 3.5	The synthetic model showing contact zone attached with homogenous medium.	40
Figure 3.6	The synthetic model showing vertical dyke crossed with homogenous medium.	41
Figure 3.7	The synthetic model showing fault attached with homogenous medium.	41
Figure 3.8	Penang Island geological map.	48
Figure 3.9	Geological map of Bukit Bunuh study area with blue triangle.	49
Figure 4.1	The block model results given by D-D array.	52
Figure 4.2	The block model results given by P-D array.	53
Figure 4.3	The block model results given by W array.	54
Figure 4.4	The block model results given by W-S array.	55
Figure 4.5	The block model results given by the DLA technique of (D-D+P-D) arrays.	56
Figure 4.6	The block model results given by the DLA technique of (D-D+W) arrays.	57

Figure 4.7	(D-D+W-S) arrays.	58
Figure 4.8	The block model results given by the DLA technique of (P-D+W) arrays.	59
Figure 4.9	The block model results given by the DLA technique of (P-D+W-S) arrays.	60
Figure 4.10	The block model results given by the DLA technique of (W+W-S) arrays.	61
Figure 4.11	The two blocks model results given by D-D array.	62
Figure 4.12	The two blocks model results given by P-D array.	63
Figure 4.13	The two blocks model results given by W array.	64
Figure 4.14	The two blocks model results given by W-S array.	65
Figure 4.15	The two blocks model results given by the DLA technique of (D-D+P-D) arrays.	66
Figure 4.16	The two blocks model results given by the DLA technique of (D-D+W) arrays.	67
Figure 4.17	The two blocks model results given by the DLA technique of (D-D+W-S) arrays.	68
Figure 4.18	The two blocks model results given by the DLA technique of (P-D+W) arrays.	69
Figure 4.19	The two blocks model results given by the DLA technique of (P-D+W-S) arrays.	70
Figure 4.20	The two blocks model results given by the DLA technique of (W+W-S) arrays.	71
Figure 4.21	The contact zone model results given by D-D array.	72
Figure 4.22	The contact zone model results given by P-D array.	73
Figure 4.23	The contact zone model results given by W array.	74
Figure 4.24	The contact zone model results given by W-S array.	75
Figure 4.25	The contact zone model results given by the DLA technique of (D-D+P-D) arrays.	76
Figure 4.26	The contact zone model results given by the DLA technique of (D-D+W) arrays.	77
Figure 4.27	The contact zone model results given by the DLA technique of (D-D+W-S) arrays.	78
Figure 4.28	The contact zone model results given by the DLA technique of (P-D+W) arrays.	79

Figure 4.29	The contact zone model results given by the DLA technique of (P-D+W-S) arrays.	80
Figure 4.30	The contact zone model results given by the joint-inversion of (W+W-S) arrays.	81
Figure 4.31	The vertical dyke model results given by D-D array.	82
Figure 4.32	The vertical dyke model results given by P-D array.	83
Figure 4.33	The vertical dyke model results given by W array.	84
Figure 4.34	The vertical dyke model results given by W-S array.	85
Figure 4.35	The vertical dyke model results given by the DLA technique of (D-D+P-D) arrays.	86
Figure 4.36	The vertical dyke model results given by the DLA technique of (D-D+W) arrays.	87
Figure 4.37	The vertical dyke model results given by the DLA technique of (D-D+W-S) arrays.	88
Figure 4.38	The vertical dyke model results given by the DLA technique of (P-D+W) arrays.	89
Figure 4.39	The vertical dyke model results given by the DLA technique of (P-D+W-S) arrays.	90
Figure 4.40	The vertical dyke model results given by the DLA technique of (W+W-S) arrays.	91
Figure 4.41	The fault model results given by D-D array.	92
Figure 4.42	The fault model results given by P-D array.	93
Figure 4.43	The fault model results given by W array.	94
Figure 4.44	The fault model results given by W-S array.	95
Figure 4.45	The fault model results given by the DLA technique of (D-D+P-D) arrays.	96
Figure 4.46	The fault model results given by the DLA technique of (D-D+W) arrays.	97
Figure 4.47	The fault model results given by the DLA technique of (D-D+W-S) arrays.	98
Figure 4.48	The fault model results given by the DLA technique of (P-D+W) arrays.	99
Figure 4.49	The fault model results given by the DLA technique of (P-D+W-S) arrays.	100
Figure 4.50	The fault model results given by the DLA technique of (W+W-S) arrays.	101
Figure 4.51	The buried bunker model results given by D-D array.	110
Figure 4.52	The buried bunker model results given by P-D array.	111

Figure 4.53	The buried bunker model results given by W array.	112
Figure 4.54	The buried bunker model results given by W-S array.	113
Figure 4.55	The buried bunker model results given by the DLA technique of (D-D+P-D) arrays.	114
Figure 4.56	The buried bunker model results given by the DLA technique of (D-D+W) arrays.	115
Figure 4.57	The buried bunker model results given by the DLA technique of (D-D+W-S) arrays.	116
Figure 4.58	The buried bunker model results given by the DLA technique of (P-D+W) arrays.	117
Figure 4.59	The buried bunker model results given by the DLA technique of (P-D+W-S) arrays.	118
Figure 4.60	The buried bunker model results given by the DLA technique of (W+W-S) arrays.	119
Figure 4.61	Inversion of model resistivity results at Minden, USM, Penang.	124
Figure 4.62	Inversion of model resistivity results at Bukit Bunuh, Perak.	125

#### LIST OF SYMBOLS

A Cross-sectional area
C Current electrode

Electric field intensity

E East

F Forward operator

J Current density

J Number of integer

I Current

k Geometric factor

km Kilometre

L Length of conductor

m metre N North

P Potential electrode

r Radius

R Resistance

V Potential difference

 $\sigma$  Conductivity

 $\pi$  pi (3.14159)

 $\Omega$  Ohm

 $\Omega$ .m Ohm.meter

 $\rho$  Resistivity

 $\rho_a$  Apparent resistivity

γ Gamma

% Percentage

 $\Delta$  Changes

#### LIST OF ABBREVIATIONS

2-D Two-dimensional

3-D Three-dimensional

a Distance between two electrodes

BGS British Geological Survey

CGAR Centre for Global Archaeological Research

CR Compare-R

D Depth of investigation

DC Direct current
D-D Dipole-Dipole

DP Number of data points

DLA Data Levels Amalgamation

EHR Enhancing Horizontal Resolution et al. et alia which means "and others"

GPR Ground Penetrating Radar
i.e. id est which means "that is"

IM Inversion model resistivity data point

max Maximum

n Ratio n(a) over a

No. Number

OD Number of overlapping inversion of

model resistivity data

P-D Pole-Dipole

PO Percentage of overlapping data point

RES2DINV Resistivity two-dimensional inversion

RES2DMOD Resistivity two-dimensional modelling

SAS Statistical Averaging System

TEM Transient electromagnetic
USM Universiti Sains Malaysia

W Wenner

W-S Wenner-Schlumberger

## PENINGKATAN DALAM RESOLUSI KERINTANGAN BERDASARKAN TEKNIK PENGGABUNGAN DATA

#### **ABSTRAK**

Kaedah pengimejan kerintangan 2-D menentukan taburan kerintangan pada bawah permukaan Bumi. Peningkatan dalam kualiti data kerintagan 2-D dilakukan menggunakan kaedah penggabungan tahap data (DLA) berdasarkan pertindihan tahap data dengan kombinasi dua susunatur berlainan. Ojektif pertama kajia ini adalah membangunkan penilaian perbandingan berangka bagi susunatur individu dan kaedah DLA. Tujuan kedua adalah meningkatkan resolusi dengan kaedah DLA bagi dua susunatur berlainan. Tujuan terakhir adalah mengesahsahihkan kaedah DLA bagi dua susunatur berlainan. Dalam usaha untuk mencapai ketiga-tiga objektif, kajian dijalankan dalam tiga fasa yang berlainan. Fasa pertama melibatkan model-model berkomputer 2-D atau dikenali sebagai model-model sintetik dan model lapangan ditunjukkan. Lima model berkomputer berlainan dicipta dan digunakan bagi menyiasat keupayaan pengimejan menggunakan empat susunatur. Dalam fasa kedua, penilaian perbandingan berangka telah diperkenalkan bagi susunatur tunggal dan kaedah DLA. Dua susunatur terbaik dan sesuai ditentukan berdasarkan keputusan penilaian perbandingan berangka. Dalam fasa ketiga, pengesahsahihan bagi kaedah DLA menggunakan dua susunatur yang terbaik dan sesuai diaplikasikan pada tinjauan lapangan yang sebenar. Bedasarkan kepada penilaian perbandingan berangka, bagi model-model berkomputer 2-D dan model lapangan, ia menunjukkan bahawa kaedah DLA bagi dua susunatur Pole-Dipole (P-D) dan Wenner-Schlumberger (W-S) dapat memberikan kualiti data yang baik. Ini disumbangkan oleh jumlah bilangan data kerintagan ketara berbanding kombinasi yang lain. Pertimbangan kedua adalah peratusan pertindihan data songsangan bagi kaedah DLA adalah baik dengan nilai 79 % keatas. Pertimbangan terakhir adalah kaedah DLA bagi dua susunatur berlainan dapat memberi gambaran sasaran yang baik dalam kedua-dua model kajian. Oleh itu, dua susunatur ini dipilih bagi kajian lapangan di dua tempat berbeza. Keputusan-keputusan pengimejan kerintangan 2-D daripada dua kajian lapangan ditentusahkan dengan data-data lubang bor. Keputusan-keputusan kajian lapangan menunjukkan bahawa kaedah DLA ini adalah berupaya dalam menghasilkan dan meningkatkan resolutsi songsangan bagi kaedah pengimejan kerintangan 2-D. Bagaimanapun, keadaan ini hanya dapat dicapai jika pemilihan susunatur-susunatur yang baik dilakukan. Kesimpulan, kesemua ketiga-tiga objektif kajian telah berjaya dicapai.

# ENHANCEMENT IN RESISTIVITY RESOLUTION BASED ON DATA AMALGAMATION TECHNIQUE

#### **ABSTRACT**

The 2-D electrical resistivity imaging measured resistivity distribution at the subsurface. Improvement in 2-D resistivity data quality was carried out by the data levels amalgamation (DLA) technique which is based on overlapping data levels with two different arrays combination. The first study objective is to develop the numerical comparative assessment for individual array and the DLA technique of two different arrays. The second objective is to improve resolution using the DLA technique on two different arrays. The final objective is to validate the DLA technique of two different arrays. In order to achieve all three objectives, the study was carried out in three different phases. The first phase involved 2-D computerized models or namely synthetic models and a field model are presented. Five different synthetic models are created and used to investigate the imaging capabilities using four different arrays. In second phase, the numerical comparative assessment is introduced for the individual array and the DLA technique. The two best and suitable arrays were determined based on the numerical comparative analysis results. In phase three, validation of the DLA technique using two best and suitable arrays are applied to the actual field surveys. Based on the numerical comparative assessment for both 2-D computerized models and a field model, it shows that the DLA technique of Pole-Dipole (P-D) and Wenner-Schlumberger (W-S) arrays are able to provide good data quality of image. This is given by a greater total number of apparent resistivity data compared to any other combinations. The second consideration is the percentage of overlapping in inversion data for the two models using the DLA technique which is also good with a value of greater than 79 %. The last consideration is ability of the DLA technique using two different arrays to resolve image of the known target in both study models. Therefore, these two arrays are chosen for the real field studies in two different areas. The 2-D resistivity imaging results from these two field studies are validated by borehole data. The field study results show that the DLA technique is very capable of producing and enhancing the resolution of inversion of the 2-D resistivity imaging method. However, this condition can only be achieved if proper selection of arrays is made. In conclusion, all of three research objectives were successfully achieved.

#### CHAPTER 1

#### **INTRODUCTION**

#### 1.0 Background

Geophysics is one of the branches of applied earth science which uses principles of physics to study the subsurface. Geophysics has been developing rapidly through the years and has become the main technology in various studies and investigations on the subsurface. Nowadays, it has also helped geoscientists to understand the Earth's phenomena. By measuring different physical parameters and nature of materials in and/or on the Earth, geophysicists are able to study and explore various ground resources such as groundwater, minerals and hydrocarbon. The exploitation of these resources helps many countries generate income including developing countries such as Malaysia.

The 2-D resistivity imaging method is one of the most popular geophysical methods used for the subsurface imaging in environmental and engineering studies. It is chosen for this study due to its ability to provide information of the subsurface structure, water content, depth to bedrock and overburden thickness (Loke 2004; 2014; Reynolds, 1997). In addition, this geophysical method has also been successfully used in complex and noisy geological areas where other geophysical techniques such as seismic refraction/reflection, transient electromagnetic (TEM) and ground penetrating radar (GPR) methods cannot be used for the Earth's subsurface imaging works (Reynolds, 1997).

The purpose of 2-D resistivity imaging is to determine the distribution of subsurface resistivity. 2-D resistivity imaging measurements are taken on the ground surface. From these measurements, estimation of the subsurface true resistivity values can be done by inversion RES2DINV software (Loke, 2001) and MATLAB software (Candansayar, 2008). The subsurface true resistivity values are narrated to many geological parameters: soil mineral, fluid content and water saturation degree in soils/rocks. 2-D resistivity imaging has been used for many years in hydrogeological, mineral exploration and subsurface engineering investigations (Loke, 2004; 2014). More recently, 2-D resistivity imaging method has been used in archaeology, geological structure and groundwater surveys (Martorana et al. 2009; Berge and Drahor, 2009; Muztaza, 2013; Ishola et al. 2014; Ishola, 2015).

With the suitable or right array, the 2-D resistivity imaging method is one of the most suitable geophysical method in engineering and environmental field studies (Dahlin and Zhou, 2004; Loke, 2004; 2014; Neyamadpour et al. 2010a, 2010b, Muztaza, 2013). However, depth and size of the target is very critical in the resistivity study. Resolution is decreased when current travels away from electrodes at the surface (Loke, 199a; Loke, 2014). In addition, poor scalability of electrode spacing, wrong array selection and poor ground contact lead to bad interpretation and improper use of the 2-D resistivity imaging method.

In electrical resistivity surveys, high resolution, reliable and good imaging depends on the choice of electrode configuration or namely array. The electrode configuration used should provide adequate information about the Earth's model (Dahlin and Zhou, 2004). The selection of the most appropriate array has continued to be a topic of discussion among researchers in view of their merits and limitations (Olayinka and Yaramanci, 1999). The debate about how to select the most

appropriate electrode array has been a long and continuing history in electrical resistivity survey (Candansayar, 2008).

Several studies have been carried out regarding the performance of various arrays. There are many types of arrays to be used for data acquisition in field survey. Some of the common arrays are Dipole-Dipole (D-D), Pole-Dipole (P-D), Wenner (W) and Wenner-Schlumberger (W-S) (Candansayar, 2008; Reynolds, 1997; Chambers et al., 1999; Storz et al., 2000). It is generally recognized that W and W-S arrays are less sensitive to noise and high vertical resolution (Dahlin and Zhou, 2004). Roy and Apparao (1971) and Barker (1979) studied the depth of investigation of different array types. The resolution and accuracy of inverted data sets have been investigated by various researchers (Sasaki, 1992; Dahlin and Zhou, 2004).

#### 1.1 Problem statements

At present, data processing techniques using only one type of resistivity array have a few disadvantages such as low horizontal coverage, low vertical coverage, low resolution, low signal strength, high noise level, and shallow penetration depth (Loke, 2004; 2014). D-D, P-D and W-S arrays are easily contaminated by noise compared to W arrays (Dahlin and Zhou, 2004). This is due to a good signal strength by W array compared to other arrays. D-D array has low vertical resolution compared to P-D, W and W-S (Barker, 1979).

D-D array is very sensitive to resistivity horizontal changes. However, this array is insensitive to resistivity vertical changes (Loke, 2004; 2014). P-D array has good horizontal coverage in 2-D resistivity imaging (Loke, 2004; 2014). This array

also has good depth of investigation compared to other arrays (Muztaza, 2013). W array is sensitive to resistivity vertical changes. However, this array is less sensitive to resistivity horizontal changes in subsurface. W-S array is moderately sensitive both vertical and horizontal changes in resistivity (Loke, 2004; 2014). The horizontal data coverage of W-S array is wider than W array (Loke, 2004; 2004).

To overcome these problems, the numerical comparative assessment is carried out for individual array and the DLA technique for two different arrays. The DLA technique used in this study is lightly similar to the joint-inversion technique. The numerical comparative assessment is carried out for three main parameters. These parameters are also vital in producing high resolution in the 2-D resistivity imaging method. Based on the numerical comparative assessment and the DLA technique, selection of the two best and suitable arrays can be made for the real field studies to get the 2-D resistivity imaging results. Borehole records were used as geological references in interpretation work.

#### 1.2 Research objectives

The objectives in this research are:

- i. To compare the numerical comparative assessment for individual array and the DLA technique of two different arrays.
- ii. To improve resolution in data processing using the DLA technique on two different arrays.
- iii. To validate the DLA technique of two different arrays to provide significant improvement in 2-D resistivity imaging data quality.

#### 1.3 Motivation and research novelty

A previous study by as de la Vega et al. (2003) concluded that the joint-inversion technique of W and D-D arrays can improves the depth of investigation. Neyamadpour et al. (2010a) claimed that the joint-inversion technique of W and D-D arrays can be highly useful for cavity detection. However, Berge and Drahor (2003) claimed that the combination or joint-inversion technique of different arrays would not be useful in every situation. Athanasiou et al. (2007) indicated that algorithm used in combined weighted inversion does not necessarily gives optimum results. It shows that, there are many debates in the joint-inversion technique of the 2-D resistivity imaging. Critical comments on previous studies on the joint-inversion technique in the 2-D resistivity imaging method are carried out in Chapter 2.

This research aims to modify the conventional resistivity data processing technique. The originality of this research lies in the numerical comparative assessment between the results obtained using individual array and the DLA technique for the two best and suitable different arrays. The numerical comparative assessment was developed and carried out with respect to (i) number of apparent resistivity data, (ii) percentage of overlapping inversion model data and lastly (iii) ability to resolve the known target. This novel approach allows the 2-D resistivity imaging method to be carried out on the two best and suitable arrays rather than using three or four arrays. In addition, this approach only focused on the use of geophysical inversion software rather than using non-geophysical software. The DLA technique for these two suitable arrays is a useful approach in data processing strategy to enhance resolution of the 2-D resistivity imaging method.

#### 1.4 Layout of thesis

In general, the thesis content is systematized as follows.

In Chapter 1, the background of this research is introduced. Problem statements and objectives to be achieved in this research are highlighted. Furthermore, motivation and research novelty as well as the layout of thesis are presented in this chapter.

In Chapter 2, the general method and principle of electrical resistivity method used are discussed. Several previous studies done by other researchers using geophysical methods applied in environmental and engineering problems are also discussed. In addition, recent development of resistivity method and critical comments on the joint-inversion technique are also discussed to give an overview as a stepping stone for this research.

In Chapter 3, research methodology is discussed on the development of the DLA technique. This chapter continues to discuss five different 2-D computerized models and a field model. The development of the numerical comparative assessment is presented for the selection of the two best and suitable arrays for the actual field studies. In addition, geological setting and survey geometry for two field study areas are discussed.

Chapter 4 discusses the study results according to the flow of research; the 2-D computerized models, a field model and the numerical comparative assessment. Based on the conclusion of these two model tests and the numerical comparative assessment, two best and suitable arrays are chosen to be used for the real field

studies in two different areas. The discussion is followed by the results from these field studies.

Lastly, Chapter 5 discusses the conclusion of the 2-D resistivity imaging method using the DLA technique in data processing. The summary of the whole research together with the advantages of the DLA technique are also discussed. Finally, some recommendations for the future research are proposed.

#### **CHAPTER 2**

#### LITERATURE REVIEWS

#### 2.0 Introduction

Geotechnical studies are normally related to soils or rocks properties, manmade structures, foundations and environmental works. Geophysical studies are capable of providing supporting relevant imaging (data) in order to reduce operation cost and time effective. Using drilling borehole only provides information in discrete locations and incurs high cost to study the subsurface characterizations. Geophysical methods such as the 2-D resistivity imaging method can be used to identify the bedrock depth and overburden (soils) materials (Samsudin et al. 1998). In addition, this geophysical method is capable of detecting or imaging some near-surface structures such as sinkholes, faults and boulders. Selection of suitable and appropriate geophysical method is closely related to the objective of a study or project and the site's conditions (Reynolds, 1997). Geophysical methods allow the ground subsurface conditions to be examined indirectly, quickly, reliably and cost effectively with sufficient results. These geophysical methods utilize different physical properties of the ground's material to study the subsurface structures as described by Samsudin et al. (1998). Geophysical methods are routine procedures to delineate geological structures and other subsurface phenomena (Dahlin, 1996). Proper usage of these geophysical methods could leads to an increase in resolution of the ground subsurface model or pseudosection.

The 2-D resistivity imaging method is used to detect groundwater and subsurface characterizations (Araffa et al. 2015). IP method is normally used in waste landfills mapping while self-potential method is normally used in seepage tracks mapping (Loke, 2004). The electrical method's applications in environmental and engineering studies are widely used for many aspects such as slope monitoring, soil characterizations as well as mineral and groundwater explorations (Samsudin et al. 1998; Samsudin et al. 2008; Nordiana et al. 2012; Seaton and Burby, 2000).

#### 2.1 Electrical resistivity theory

The general partial differential equation governing electrical resistivity method can be derived from basic electrical principle. The fundamental physical law used in electrical resistivity method is Ohm's Law that governs the flow of current in the ground. Equation 2.1 shows Ohm's Law in vector form for current flow in a continuous medium:

$$\overrightarrow{J} = \overrightarrow{\sigma} \overrightarrow{E} \tag{2.1}$$

where  $\vec{\sigma}$  is conductivity of the medium,  $\vec{J}$  is current density and  $\vec{E}$  is electric field intensity. In practice, what is measured is an electric field potential. Note that for electrical resistivity method, medium resistivity,  $\vec{\rho}$  is equal to a reciprocal of the conductivity, and  $\vec{\rho} = 1/\vec{\sigma}$ , is more commonly used. In 1827, a German scientist, Georg Simon Ohm found that an electrical current, (I) in a conducting wire is proportional to potential difference, (V) across it (Equation 2.2).

$$V \alpha I$$
 (2.2)

To grasp the theory of resistivity, potential difference, (V) and current, (I) that flows through the circuit are measured. Thus, an increase in resistance, (R) value across the circuit will result in the dropping of current, (I) (Equation 2.3). It shows that current is inversely proportional to resistance.

$$I = \frac{V}{R} \tag{2.3}$$

The potential difference is measured experimentally using a voltmeter while the current is measured using an ammeter. The SI unit for resistance is volts per ampere or Ohm,  $(\Omega)$ . The resistivity can be calculated using Equation 2.4.

$$\rho = R \frac{A}{L} \tag{2.4}$$

where:

 $\rho$  = Resistivity of the conductor material ( $\Omega$ .m)

R = Resistance

A = Cross-sectional area (m<sup>2</sup>)

L = Length of the conductor (m)

For a homogeneous media with one electrode, the potential will separate radially outwards from the current source where area, (A) will be a half sphere,  $(2\pi r^2)$  with radius, (r). Equation 2.4 is rewritten as Equation 2.5.

$$\rho = k R \tag{2.5}$$

where,  $k = 2\pi r$  for the half sphere. Equation 2.5 consists of two parts. The first part is resistance, (R) and the second part is geometric factor, (k) which describes the geometry of electrode configuration.

#### 2.2 Basic concept of 2-D resistivity imaging

A fundamental property of any volume of material is its resistance measured in the unit of Ohm. The resistance is defined as the material's opposition to the flow of electrical current (Reynold, 1997). Resistivity (in unit of  $\Omega$ .m) is related to this property and is expressed as resistance through a distance, which makes it independent of material geometry (Reynold, 1997).

Resistivity is considered as functions of rock porosity, volumetric fraction of saturated pores and resistivity of pore water (Archie, 1942). In many cases, it is the pore fluid of rock that accounts for the overall resistivity signature rather than the host rock (Lowrie, 1997). In 2-D resistivity imaging measurement, the basic procedure is to establish a subsurface distribution of resistivity by injecting current into the underground between two current electrodes planted on ground surface. The resulting potential difference are measured between two potential electrodes in a line or grid (Ramirez et al., 1993). The ground (Earth) can be considered as one component of an electrical circuit known as the resistor. An interpretation of the measured parameters yield information about the electrical conductivity beneath, the ground's surface.

The 2-D resistivity imaging measurements for a homogeneous medium are normally made by injecting current into the ground through two current electrodes (C1 and C2) and measuring the resulting voltage difference between two potential electrodes (P1 and P2) (Figure 2.1). From the current, (I) and voltage, (V), an apparent resistivity, ( $\rho_a$ ) value is calculated (Equation 2.6).

$$\rho_{\rm a} = \frac{\rm kV}{\rm I} \tag{2.6}$$

where, k is the geometric factor which depends on the arrangement of the four electrodes. Figure 2.1 shows common electrodes array for resistivity measurement.

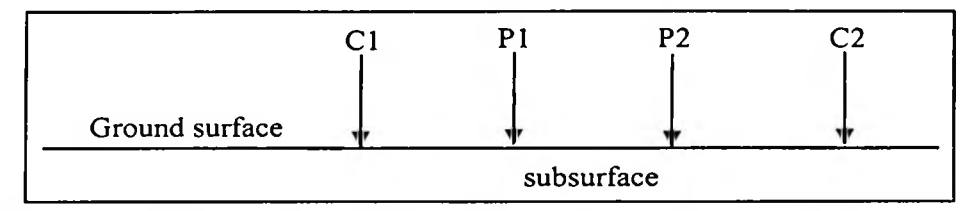


Figure 2.1: Common electrodes array for resistivity measurement.

Therefore, for an inhomogeneous case, the resistivity meter normally measures resistance value, (R) as given by Equation 2.3. In practice, the apparent resistivity value is calculated by Equation 2.7.

$$\rho_{a} = k R \tag{2.7}$$

The geological structures of the Earth's subsurface are inhomogeneous and the resistivity, that is collected, does not represent the true resistivity, but it represents an apparent resistivity (Paul, 2007). The relationship between the "apparent" and "true" resistivity values is a multiplex connection. In order to determine true subsurface resistivity values from its apparent values, an inversion using a computer program is needed for measured apparent resistivity data (Loke, 1999a; Loke, 2014).

#### 2.3 The general four-electrode method

Consider an arrangement which consists of a pair of current electrodes and a pair of potential electrodes. Figure 2.2 shows a diagram of the four-electrode method. This arrangement will be used to illustrate the current flow into the ground.

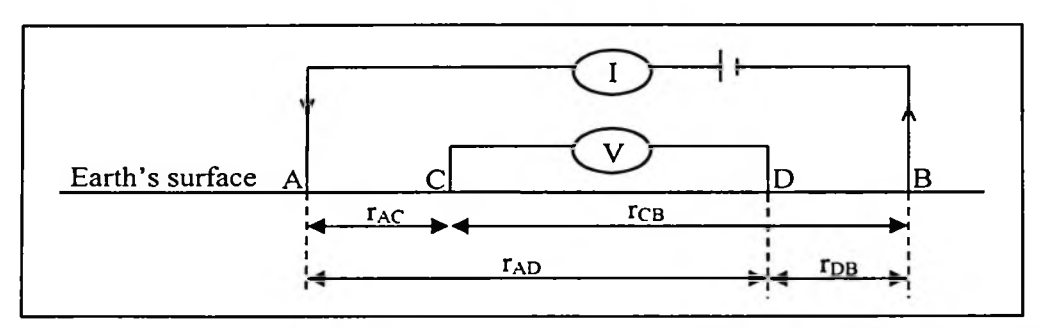


Figure 2.2: Arrangement of four-electrode in electrical resistivity method.

The current electrodes A and B act as the source and sink. At the detection electrode C, potential due to the source A is  $+\rho I/(2\pi r_{AC})$ , while potential due to the sink B is  $-\rho I/(2\pi r_{AC})$ . The combined potential at C is given by Equations 2.8–2.10.

$$V_C = \frac{\rho I}{2\pi r_{AC}} + \left(-\frac{\rho I}{2\pi r_{CB}}\right) \tag{2.8}$$

$$V_C = \frac{\rho I}{2\pi r_{AC}} - \frac{\rho I}{2\pi r_{CR}}$$
 (2.9)

$$V_C = \frac{\rho I}{2\pi} \left( \frac{1}{r_{AC}} - \frac{1}{r_{CB}} \right)$$
 (2.10)

This is similar to the resultant potential at D. This is given by Equation 2.11.

$$V_{D} = \frac{\rho I}{2\pi} \left( \frac{1}{r_{AD}} - \frac{1}{r_{DB}} \right)$$
 (2.11)

The potential difference measured by a voltmeter connected between C and D is given by Equation 2.12–2.14.

$$V = V_C - V_D \tag{2.12}$$

$$V = \frac{\rho I}{2\pi} \left( \frac{1}{r_{AC}} - \frac{1}{r_{CB}} \right) - \frac{\rho I}{2\pi} \left( \frac{1}{r_{AD}} - \frac{1}{r_{DB}} \right)$$
(2.13)

$$V = \frac{\rho I}{2\pi} \left[ \left( \frac{1}{r_{AC}} - \frac{1}{r_{CB}} \right) - \left( \frac{1}{r_{AD}} - \frac{1}{r_{DB}} \right) \right]$$
 (2.14)

All quantities in this Equation (2.14) can be measured at the ground surface except the resistivity value, which is given by Equation 2.15.

$$\rho = 2\pi \frac{V}{I} \left[ \frac{1}{\left( \frac{1}{r_{AC}} - \frac{1}{r_{CB}} \right) - \left( \frac{1}{r_{AD}} - \frac{1}{r_{DB}} \right)} \right]$$
(2.15)

This  $\rho$  is called apparent resistivity. Therefore, Equation 2.15 can be rewritten as Equation 2.16.

$$\rho_{a} = 2\pi \frac{V}{I} \left[ \frac{1}{\left( \frac{1}{r_{AC}} - \frac{1}{r_{CB}} \right) - \left( \frac{1}{r_{AD}} - \frac{1}{r_{DB}} \right)} \right]$$
(2.16)

Then, Equation 2.16 can be rearranged as Equation 2.17 to get the final equation as Equation 2.18. Therefore, Equation 2.18 is equal to Equation 2.6 and Equation 2.19 is equal to Equation 2.7.

$$\rho_{a} = 2\pi \left[ \frac{1}{\left(\frac{1}{r_{AC}} - \frac{1}{r_{CB}}\right) - \left(\frac{1}{r_{AD}} - \frac{1}{r_{DB}}\right)} \right] \frac{V}{I}$$
 (2.17)

$$\rho_{\rm a} = k \frac{\rm V}{\rm I} \tag{2.18}$$

$$\rho_{\rm a} = k R \tag{2.19}$$

#### 2.4 Selecting electrode array for 2-D resistivity survey

The 2-D resistivity survey has remained an essential tool for over two decades (Dahlin, 1996; Seaton and Burby, 2000; Loke, 2014) as geophysical investigations are used for hydrogeology, subsurface exploration, mining, geotechnical engineering and archaeological prospecting. The success of the 2-D resistivity imaging method in mapping Earth's subsurface structures depends on other factors in the choice of suitable electrode array.

Among the several electrode arrays that are commonly used in 2-D resistivity imaging are standard arrays; Dipole-Dipole (D-D), Pole-Dipole (P-D), Wenner (W) and lastly Wenner-Schlumberger (W-S) (Chambers et al., 1999; Storz et al., 2000). The difference between these array types lies in separation between the electrodes pairs that provide variation or differences in the geometric factor for each electrode

array (Loke, 2004; Loke et al., 2010). In view of advantages and limitations of one electrode array over another, several researchers have investigated electrical resistivity survey capabilities of different electrode arrays by comparison (Dahlin and Zhou, 2004; Perren, 2005, Putiska et al., 2012; Alwan, 2013).

#### 2.4.1 **D-D** array

In D-D array (Figure 2.3), a pair of potential electrode are on the outside of a pair of current electrode. Each pair of electrode has a constant electrode separation (a) and the distance between two innermost electrodes is (na). The measured apparent resistivity,  $\rho_a$  is given by Equation 2.20.

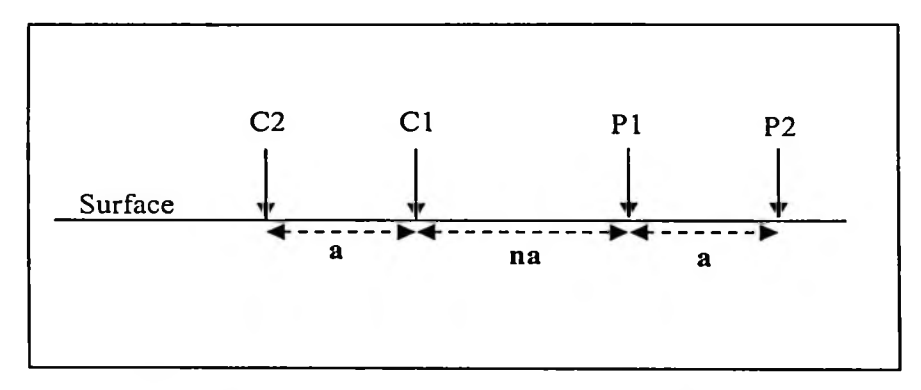


Figure 2.3: Electrode's arrangement for D-D array.

$$\rho_{\rm a} = \pi n a (n+1)(n+2) R \tag{2.20}$$

where;

n = Ratio of n(a) over a

a = Distance between two electrodes

#### 2.4.2 P-D array

P-D array (Figure 2.4) is an electrical array for 2-D resistivity imaging that contains four co-linear electrodes with one of the current electrodes (which acts as the source) positioned at an infinity distance. Usually, it is positioned at approximately five to ten survey depth (Loke, 2001). The other current electrode is placed in vicinity of a pair of potential (receiver) electrode. This geometry is used because it reduces the distortion of equipotential surfaces (Smith, 1986). The measured apparent resistivity,  $\rho_a$  is given by Equation 2.21.

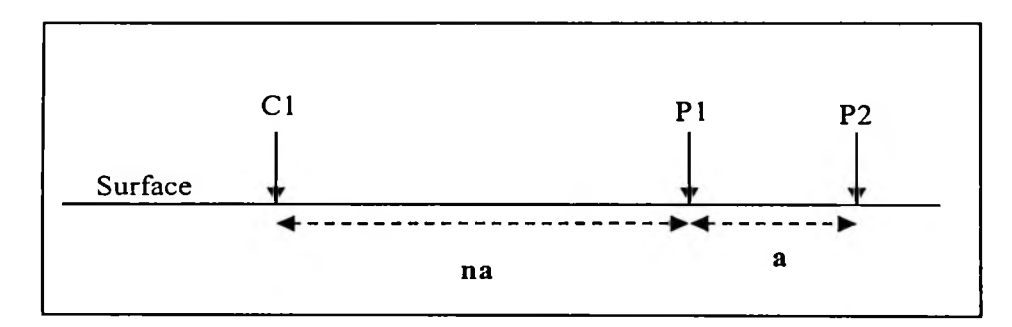


Figure 2.4: Electrode's arrangement for P-D array.

$$\rho_{\mathbf{a}} = 2\pi \mathbf{n} \mathbf{a} (\mathbf{n} + 1) \mathbf{R} \tag{2.21}$$

where;

n = Ratio of n(a) over a

**a** = Distance between two electrodes

#### 2.4.3 W array

In W array (Figure 2.5), a pair of current electrodes and a pair of potential electrodes are arranged collinearly and separation between adjacent four electrodes are equal. This separation is denoted by (a). Due to simplicity in its geometry, this array is often used in electrical resistivity survey. In normal electrical resistivity sounding measurement using W array, distance (a) is increased step by step, while keeping middle-point of electrodes fixed. The measured apparent resistivity,  $\rho_a$  is given by Equation 2.22.

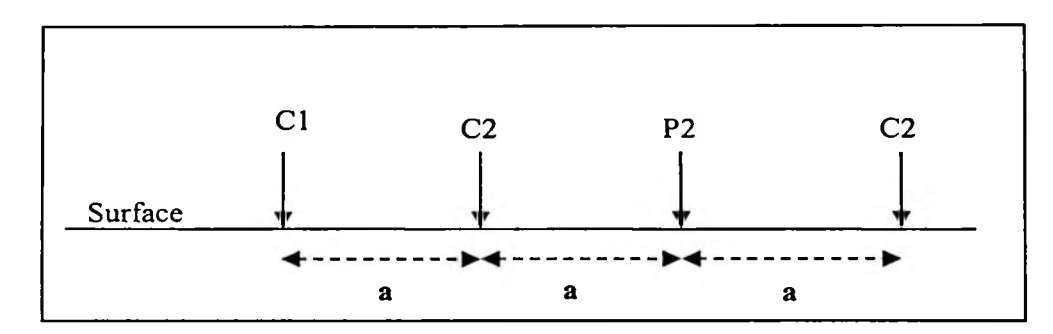


Figure 2.5: Electrode's arrangement for W array.

$$\rho_{\rm a} = 2\pi a R \tag{2.22}$$

where;

**a** = Distance between two electrodes

#### 2.4.4 W-S array

W-S (Figure 2.6) array is also one of the most commonly used array for the ground subsurface investigation. This array has a pair of current electrodes and a pair of potential electrodes are arranged collinearly. In this array, separation between the pair of current electrodes is much larger than separation between the pair of potential electrodes. In this array, the electrode layout for the first data level (n=1) is same as W array. The measured apparent resistivity,  $\rho_a$  is given by Equation 2.23.

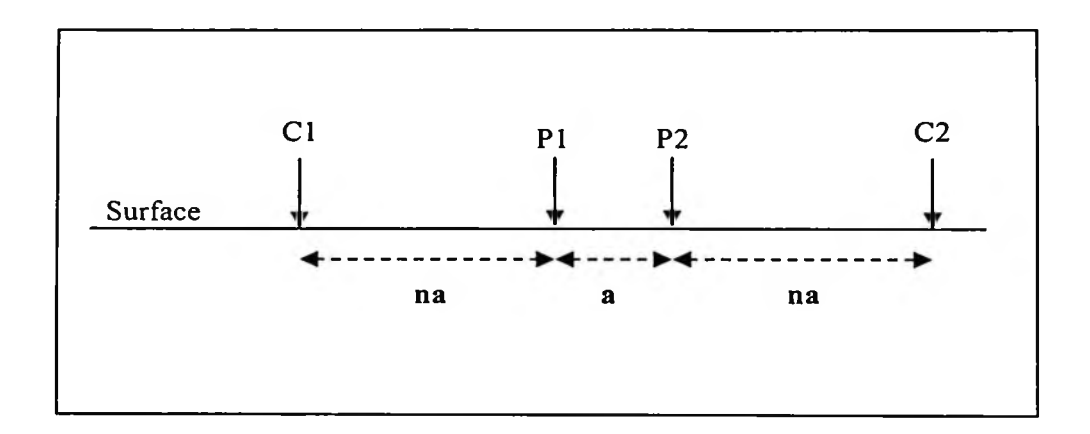


Figure 2.6: Electrode's arrangement for W-S array.

$$\rho_{\rm a} = \pi \rm na(n+1)R \tag{2.23}$$

where;

n = Ratio of n(a) over a

**a** = Distance between two electrodes

#### 2.5 Electrode arrays

An arrangement of the electrodes is called an electrode array. The apparent resistivity value depends on the geometry of the electrodes (geometric factor, k) (Reynolds, 1997). The geometric factor depends on the position of electrodes in the array. Resistivity imaging employs different types of electrode arrays.

According to Norman and Fujita (1997), the most common arrays used in resistivity imaging survey are W, D-D and W-S. Choosing the right array for a resistivity survey is important for two reasons. The first one is that for each array, there are varying degrees of advantages and disadvantages when compared with other arrays. The second reason is that the resistivity image of the same structure is different when produced by a different array.

Choosing the appropriate array depends on the survey's objective. Moreover, choosing the appropriate array requires some considerations such as depth of the object, vertical and horizontal changes of the subsurface and signal strength (Loke, 2001; Dahlin and Zhou, 2004). Figure 2.7 shows some common arrays used in resistivity surveys together with their geometric factors.

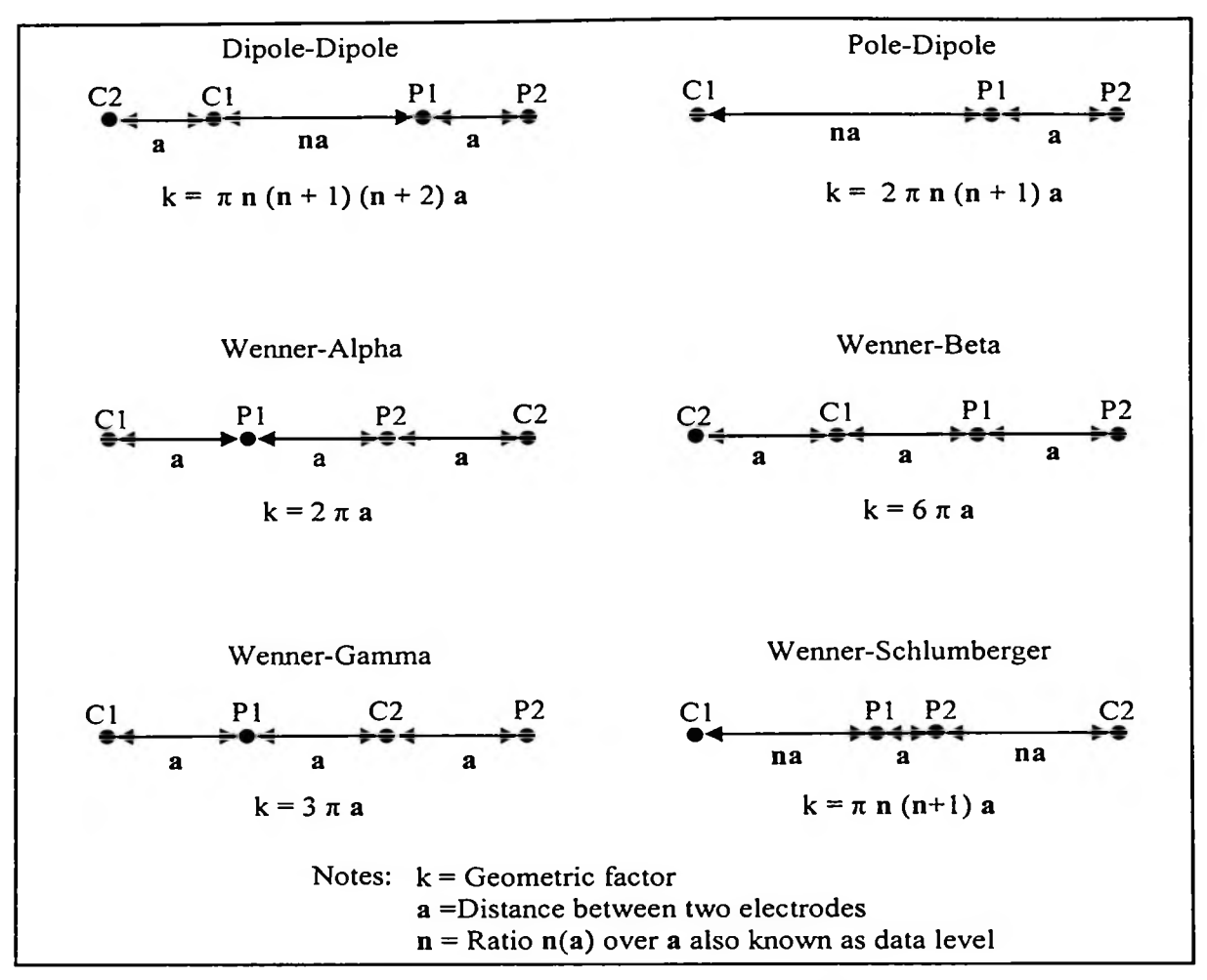


Figure 2.7: Common arrays used in resistivity and their geometric factors (ABEM, 2006).

## 2.6 Inversion of resistivity data

The objective of electrical resistivity inversion is to find a model which adequately reproduces the observed data (Oldenburg, 1978). In recent years, several methods have been developed for the direct interpretation of the 2-D electrical resistivity data. Since most of the direct current electrical resistivity problems are non-unique, iterative methods are commonly used for practical inversion of the data (Jupp and Vozoff, 1975). The iterative method successively improves the model parameters by reducing the error between the model response and observed data.

The ridge regression method (Imam, 1975) has been used by other researchers (Rijo et al., 1977; Petrick, et al., 1977) in inversion of one-dimensional electrical resistivity sounding data. This method was extended by Pelton et al. (1978) to invert electrical resistivity and induced polarization data over two-dimensional structure. This method requires many forward modelling evaluations for each ridge regression inversion as well as large memory space. Furthermore, this method gives an erratic electrical resistivity distribution when many model layers are used in the inversion (Constable et al., 1987).

Tripp et al. (1984) used the transmission surface analogy to generate the initial model of D-D electrical resistivity data. For noisy data, the resulting model after inversion is diverged from the real model. Shima (1990, 1992) used the alpha centre method for the 2-D inversion of surface and cross-hole electrical resistivity data. The main disadvantage of the alpha centre method is that it is not suitable for complex structures with high contrast and sharp boundary.

The effect of topography plays a significant role in the inversion scheme (Fox et al., 1980; Spiegel et al., 1980). Tong and Yang (1990) proposed a finite element forward modelling scheme that takes into account topographic feature in the inversion of electrical resistivity data. The Zohdy-Barker method (Barker, 1992) uses a modification of Zohdy's optimization technique (Zohdy, 1989) to convert the 2-D data pseudosection. Although improvements were made by Loke and Barker (1995a) to overcome problems of the relatively slow convergence and instability, this method does not converge to the real model for complex geological structures.

It is obvious from the literature that most of these algorithms are implemented on mini or mainframe or workstation computers. Many electrical

resistivity surveys are carried out by small companies for mineral, hydrogeological and engineering purposes. The computing resources needed may not be available, and it would not be practical to carry out the inversion during the field survey or data acquisition.

The recent improvements to data acquisition equipment for electrical resistivity surveys require a similar development of more sophisticated inversion algorithms to fully utilize electrical resistivity data (Griffiths and Turnbull, 1985; Griffiths et al., 1990). Loke and Barker (1995b, 1996) have developed a fast inversion algorithm whereby a 2-D structure can be modelled on a computer during field survey or data acquisition of electrical resistivity.

### 2.7 Previous studies

Several case studies are discussed in this chapter, which involve the application of electrical resistivity with other geophysical methods and electrical resistivity with some geotechnical engineering methods. These previous geophysical studies are related to engineering and environmental perspectives. Furthermore, the discussion includes recent developments of 2-D resistivity imaging method by various researchers.

Samsudin et al. (2008) combined 2-D resistivity imaging and seismic reflection survey with hydro-chemical methods. The study was carried out to map saline water intrusion into coastal groundwater aquifers in Kelantan, Malaysia. Integration of all results apart from delineating the subsurface geologic units also indicated the extent of presence of total dissolved solids among other components in the water.

Saad et al. (2011) presented integrations between 2-D electrical resistivity and seismic refraction methods to study shallow subsurface. The study was carried out in Selangor, Malaysia.

Giang et al. (2013) presented results of geophysical methods such as vertical electrical sounding, very low frequency, seismic refraction and electrical resistivity imaging. The work's purpose was to locate the aquifers and to assess the hydrogeological conditions for groundwater potential. The research location is in the industrial zones of North Hanoi, Vietnam.

Geophysical methods-seismic refraction, electrical resistivity tomography and microgravity were applied to Dead Sea sinkhole problem in the Ein Gedi area at an earlier stage of the sinkhole development. The methods allowed the determination of the sinkhole formation mechanism and localization of the hazardous sinkhole zones. This study was conducted by Ezersky et al. (2013). The suitability of the combined microgravity and resistivity tomography to detect and characterize caves deeply buried in limestone is proposed by Martinez-Moreno et al. (2013). At the investigation site, microgravity, electrical resistivity and IP data was collected along four profiles.

Hamdan and Vafidis (2013) presented the development of joint-inversion strategies. The research was conducted to improve on electrical resistivity and seismic velocity models for delineating saline water zones in karst geological formations. The 2-D resistivity imaging method was carried out to provide a better means of bridging information. This electrical resistivity method is used to map geotechnical properties of the subsurface. The study was presented by Rucker and Noonan (2013) at Panama Canal. Dahlin et al. (2013) proposed calibration of

electrical resistivity method and cone penetration tests with resistivity measurement (CPTU-R). These methods were successful to map the quick clay site which is located at Frastad, Sweden.

Dahlin et al. (2014) presented the application of electrical resistivity monitoring in soils to trace the water transport during an irrigation study. Chambers et al. (2014) proposed electrical resistivity tomography monitoring research to be used in observing and characterizing the ground embankments. Meanwhile, Cho et al. (2014) studied the effects of the 2-D electrical resistivity monitoring created on the Earth-filled dams. Heenan et al. (2015) presented an attempt to monitor natural degradation processes in hydrocarbon impacted beach sediments. In this study, an autonomous electrical resistivity monitoring system was deployed on Grand Terre, Louisiana.

Robinson et al. (2015) performed a 3-D cross-borehole electrical resistivity method on a limestone quarry in which transport and flow are controlled by a bedding plane feature. Static and time-lapse of electrical resistivity data sets were used to perform the 3-D model's evaluation.

An electrical resistivity method was performed by Oladunjoye and Jekayinfa (2015). The study compared vertical electrical sounding data using conventional Schlumberger array and modified Schlumberger array to assess the effectiveness of modified Schlumberger array for groundwater exploration. The study found that the modified Schlumberger array is a good alternative compared to the conventional Schlumberger array.

Juhojuntti and Kamm (2015) developed a method for joint inversion of seismic refraction and electrical resistivity data. A method is developed using sharp

boundary models with few layers. The study demonstrated the usefulness of the approach using some examples from case studies related to the shallow groundwater exploration and geotechnical investigations.

Recent developments of electrical resistivity method are discussed where these research are the continuation of all these research works proposed by geophysicists throughout the recent years.

Recently, various studies have described the use of electrical resistivity method for environmental and engineering studies. Ward (1990) has studied the combination of aluminium and soaked soil with salt water used as a current electrode in an investigation area where it is difficult to plant electrodes into ground surface. The combination of horizontal long electrodes with vertical long electrodes, i.e., pipes was proposed by Ramirez et al. (2003). Meanwhile, inclined wells were proposed by Hatanaka et al. (2005). Stainless steel electrodes are widely used in the 2-D resistivity imaging methods. LaBrecque and Daily (2008) have investigated different metals and graphite (carbon) types as electrodes. Tsokas et al. (2008) successfully used a flat base or plate as a new alternative for electrodes. Zhu and Feng (2011) proposed that the combination of long electrodes with a large number of short electrodes planted on the ground surface would enhance the vertical resolution.

Several different approaches have been suggested which led to novel survey design in the 2-D resistivity imaging method. An independent configuration on multielectrode array is proposed by Lehmann (1995). The multiscale survey technique was proposed by Abdul Nassir (1997). Moller et al. (2001) proposed a rapid data inversion by multichannel deconvolution. Mitigation measures were also proposed by many researchers; roll-along (or multiple line) data acquisition (Dahlin

et al., 2002), survey line in orthogonal directions (Chambers et al., 2002) and no more than two-electrode distance used as line separations (Gharibi and Bentley, 2005). Muztaza (2013) developed a new technique called Enhancing Horizontal Resolution (EHR) for 2-D resistivity survey in various environmental perspectives.

# 2.7.1 Critical comments on resistivity data processing technique

In recent years, there has been a significant development in the algorithms to automatically determine non-conventional arrays such as D-D and P-D that would be able to produce a better image resolution. This approach is conducted by using the same number of datum points as the selected array (Stummer et al., 2004; Wilkinson et al., 2006b). Minimization of data error and model parameters errors is significantly a good inversion method especially in resistivity data processing (Narayan et al. 1994).

A large amount of time series monitoring data set which leads to the time-lapse development was proposed by Loke (1999b). Some other different approaches have also been proposed in order to design arrays that maximize the image resolution, including optimized or modified arrays development (White et al., 2001; Wilkinson et al., 2006a; Nyquist et al., 2007; Saad, 2009), maximizing Jacobian sensitivity matrix elements summation (Furman et al., 2007), maximizing the sensitivity of cumulative while minimizing the distribution of mutual current (Nenna et al., 2011), maximizing the normal matrix determinant (Coles and Morgan, 2009) and maximizing the model resolution matrix elements summation (al Hagrey, 2012).

Loke and Dahlin (2010) proposed horizontal diagonal roughness filters used in inversion setting and Blome et al. (2011) proposed the concept of experimental

design which is based on complete data sets in linear independence term. Donohue et al. (2012) proposed overlapping sections to be used for very long 2-D survey lines. A new array type, the γ1 ln arrays is introduced by Szalai et al. (2015). The sequence of current and potential electrodes for this new array is CPCP. These arrays are called quasinull arrays which can be useful as they complement the traditional arrays.

Reliability assessment of 2-D inversion in apparent resistivity data was proposed by Olayinka and Yaramanci (2000). An important development is resistivity data processing made by Stummer et al. (2004) who successfully proposed an accurate and fast method in selecting arrays that could maximize the model resolution. In the study, an experimental design procedure is developed to identify electrode configurations to provide information of subsurface which is based on predefined optimization criteria. The study suggested that the best images are determined from comprehensive data sets of much larger data points. Then, it was further improved by Wilkinson et al. (2006a) who proposed novel methods to enhance quality of optimized arrays.

Szalai and Szarka (2008) proposed surface geoelectric arrays classification. Loke et al. (2010) proposed four different methods to automatically in choose an optimal array. This approach was carried out to give maximum information on subsurface with limited number of measurements. Four methods used in this study are the Compared-R (CR), Original GF (ETH), Modified GF (BGS) and Combined Modified GF and Compare-R (BGS-CR) methods.

Comparison study between smooth and blocky inversion in 2-D resistivity data processing is carried out by Loke et al. (2003). The results are tested for both several synthetic and field surveys with smooth and blocky inversion method. The study

concluded that blocky inversion is suitable where there are sharp boundaries. Meanwhile, the smooth inversion method is suitable for areas where the subsurface resistivity changes in a gradual manner. However, Adiat et al. (2013) proposed an appropriate inversion algorithm and suitable electrode spacing effect on the efficacy in the 2-D resistivity imaging. In the study, poor selection of electrode spacing will gives unsuccessful result, even though both standard constraint and robust constraint inversions were used.

Loke et al. (2013) presented a review of the electrical resistivity method which includes recent development over the past few decades. Fraquharson and Oldenburg (2004) studied two automatic ways namely the generalized cross-validation and L-curve criteria. Both criteria provide means of estimating regularized parameters when only size of uncertainties are known. The linearized least-squares optimization method was proposed by (deGroot-Hedlin and Constable, 1990; Ellis and Oldenburg, 1994). This approach studied the relationship between the measured data and model parameters.

Zhou and Greenhalgh (2000) studied the relative advantages and effectiveness of cross-hole resistivity imaging using four arrays. They are Pole-Pole, Pole-Dipole, bipole-pole and bipole-bipole on synthetic models. The results show that images yielded by these arrays are very competitive. The best images are given by Pole-Pole array because it contains maximum information on electric properties around boreholes. Schwarzbach et al. (2005) introduced the concept of multi-objective optimization. This approach is to cast regularized inverse resistivity problem into the general formulation.

Ishola et al. (2014a) and Ishola (2015) combined the results from three arrays using image processing technique after the 2-D resistivity data inversion took place. After inversion, data sets were merged using basic statistical parameters such as minimum, maximum, median and average. This approach was carried out using the PCI Geomatica Software which is commonly used in remote sensing. Ishola et al. (2014b) proposed multiple electrode combination for 2-D resistivity imaging. This approach was carried out using unsupervised classification technique for post-inversion of resistivity data.

In data processing, the joint-inversion in the 2-D resistivity imaging method has been used by various researchers. The joint-inversion in the 2-D resistivity imaging method was used only for two or three different arrays without specific consideration on other arrays (de la Vega et al. 2003; Neyamadpour et al. 2010a; 2010b).

Candansayar (2008) suggested the application of three and four electrode array data for combined inversion. There are four different arrays used in the study, which are W, W-S, D-D and P-D. Comparison study was carried out for a single array combined inversion of any two arrays. Comparison study showed that the combined inversion of two different sets of arrays is able to provide better resolution than an individual array. However, inversion of the P-D and D-D data set arrays jointly gave a better result than the single use of array. This approach was carried out by developing a new inversion algorithm using MATLAB software.

The 3-D resistivity imaging survey was carried out along seven parallel lines using D-D and W arrays (Neyamadpour et al. 2010a). In the study, only two different arrays were used for synthetic model analysis and field study. Based on the study, they

proposed that the joint-inversion for both arrays is suitable and useful for engineering and environmental applications especially cavity detection. Neyamadpour et al. (2010b) investigated applicability of three different arrays in 3-D resistivity imaging. Based on the study, the joint-inversion of W-S with D-D or W with D-D in combination with an appropriate 3-D inversion method is capable of being highly useful when then site condition is not suitable for P-D and P-D arrays.

Comparative test on different arrays such as W, D-D and W-S was proposed by Martorana et al. (2009). In the 2-D simulation model, different levels of Gaussian noise was added. Comparison study was carried out between interpretive models and the initial models to estimate the quality of the match.

The 2-D resistivity imaging survey was conducted to study a gasoline-contaminated soil by de la Vega et al. (2003). In order to improve the inversion of resistivity model, the joint-inversion of W and D-D data sets was carried out. From the analysis of the inversion resistivity model, it shows that depth of investigation is improved to 25 m compared to the results from each array separately. The study concluded that the joint-inversion improves the depth of investigation while maintaining shallow lateral resolution.

Athanasiou et al (2007) examined combined weighted inversion in electrical resistivity data using different arrays. An algorithm for the 2-D combined inversion was examined too. The study introduced weighting factor from Jacobian matrices for each array data set. The results indicate that algorithm provides 2-D resistivity model of all data sets which is not necessarily optimal. In conclusion, the combined weighted inversion would probably give low quality of the 2-D resistivity results which is caused by low quality of individual inversion data sets.

More than two different arrays used in the joint-inversion of 2-D resistivity data was carried out by Berge and Drahor (2009). The study demonstrated that conductive structure and resistive increase or decrease is based on type of array and number of array used in combined different array. In the study, the optimum electrical resistivity tomography revealed was given by the usage of combined different array. The conclusion of the study was that the combined or the joint-inversion of different arrays would not be useful in very situation.

# 2.8 Chapter summary

This chapter was to review the foundation of the 2-D resistivity imaging method in geophysics. Furthermore, previous studies by many researchers in application of 2-D resistivity imaging, recent development in electrical resistivity method and the joint-inversion technique were reviewed. This approach is carried out to identify any gap or space left by the previous studies. Resolution enhancement in 2-D resistivity imaging method is a focussed matter in this research. An overview from various data processing and the joint-inversion techniques by different researchers showed that different parameters and a few arrays was used. An overview of the DLA technique in the 2-D resistivity imaging method, provides a platform for this research to take place. Therefore, in the next chapter the research methodology to comprehensively improve understanding about the near surface condition are described.

#### CHAPTER 3

### RESEARCH METHODOLOGY

### 3.0 Introduction

This chapter discusses the methodology and technique used in this study. Methodological framework overview that is used in data acquisition and data analysis is presented. The DLA technique used in this study is based on the overlapping data levels in apparent resistivity data set. In this study, an improvement in data quality for the 2-D resistivity results was carried out using the DLA technique which consisted of different combinations of number of electrode spacing (a) and number of data levels (n) values. The results in 2-D resistivity model were presented with the overlapping number of data levels for two different arrays.

In order to achieve all the objectives, the study methodologies were carried out in three different phases. The first phase involved 2-D computerized models or namely synthetic models and a field model is presented. Five different synthetic models were created and used to investigate the imaging capabilities using four different arrays. In the second phase, the numerical comparative assessment was introduced for individual array and the DLA technique. The two best and suitable arrays was determined which is based on this numerical comparative assessment results. In the phase three, validation of the DLA technique using two best and suitable arrays were applied to the actual field surveys.

# 3.1 Research methodology flowcharts

The summary of both Phase 1 and Phase 2 as parts of the research methodology are shown in Figure 3.1 and Figure 3.2. These flowcharts summarise all the steps including preparation of the data sets for the DLA technique and the numerical comparative assessment used in this study. In addition, these flowcharts can be used as a guide for other researchers to use the DLA technique in the 2-D resistivity data processing. For the filtering section, the resistivity data set can be viewed from the RMS error statistics section in RES2DINV program. After carrying out inversion, switch to the 'Display' window in RES2DINV program. Then the INV file consisting the inversion results is read. The 'RMS error statistics' option is selected that will display the percentage of difference in distribution between the measured and calculated apparent resistivity data (Appendix A).

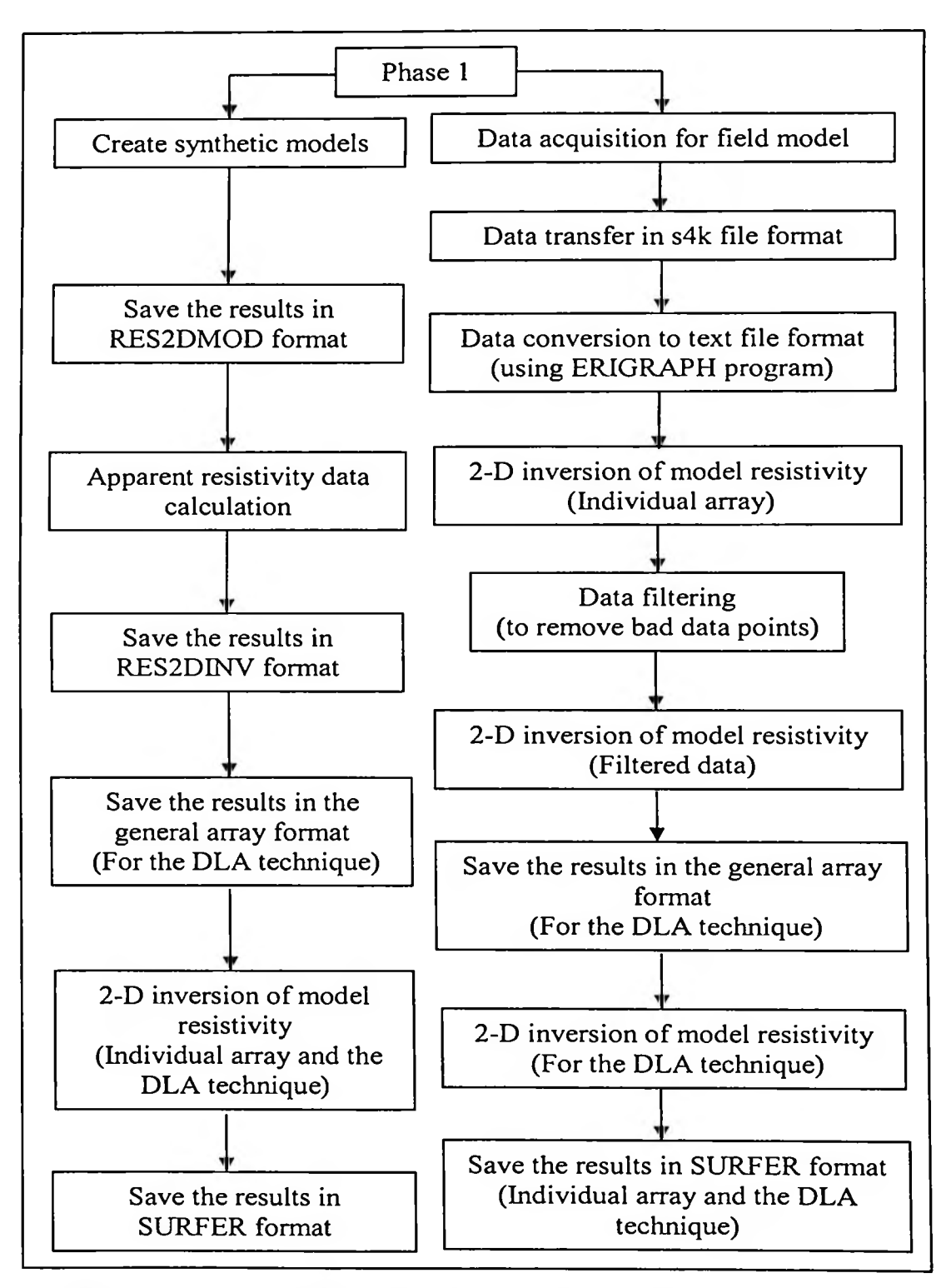


Figure 3.1: Research methodology flowchart for the Phase 1.

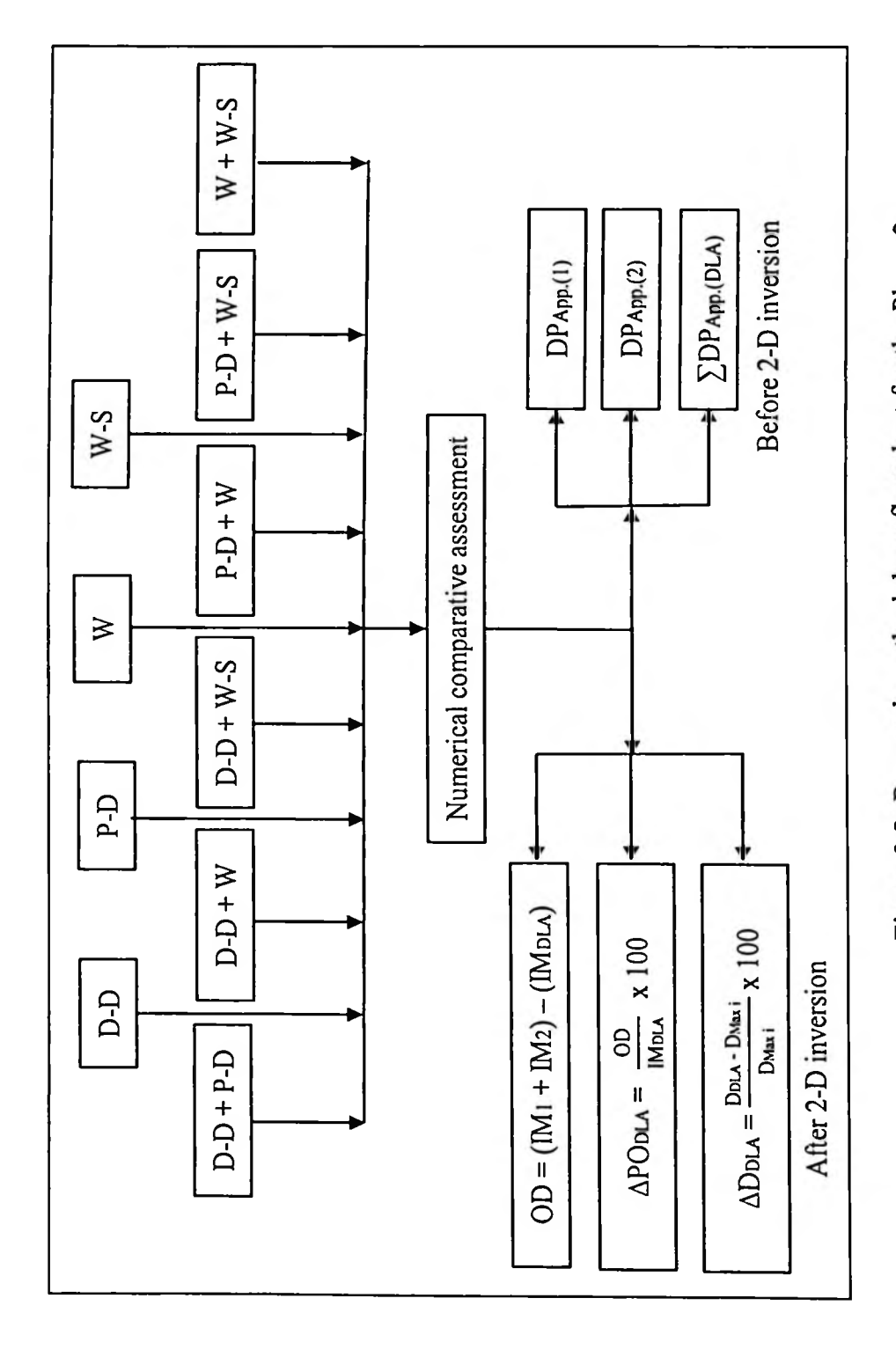


Figure 3.2: Research methodology flowchart for the Phase 2.

# 3.2 Phase 1: 2-D computerized models and field model

Four different computerized (synthetic) models were used for the simulation purpose. Each of the created models were transformed into sets of physical property by assigning true resistivity values to each cell unit. Once the physical property models were created, then the forward modelling was performed to establish the synthetic apparent resistivity data.

# 3.2.1 Forward modelling

The main objective of this approach is to numerically study the capabilities of four different arrays used on near surface imaging targets on the synthetic resistivity data. Dipole-Dipole (D-D), Pole-Dipole (P-D), Wenner (W) and Wenner-Schlumberger (W-S) arrays were used to implement these simulations. The 2-D computerized models were constructed using 41 number of electrodes and minimum electrode spacing of 1 m. The forward modelling responses were calculated using RES2DMOD program (Loke and Barker, 1996). It is a 2-D forward modelling program that calculates apparent resistivity values for 2-D subsurface model. This forward modelling program uses finite-difference scheme which was based on a method described by Dey and Morrison (1979a). However, modification was made by Loke (1994) to correct for minor inconsistency in discrimination of Dey and Morrison by area method.

# 3.2.2 Geological models test

In this stage, the geometry and dimensions of the targets were specified. These included the size, value and number of block for the model and lastly its resistivity value. A summary of the model parameters used in all synthetic models for four different arrays was presented in Table 3.1.

Table 3.1: Parameters of forward modelling for four different arrays used.

Parameters	D-D	P-D	W	W-S
Number of electrode	41	41	41	41
Number of a spacing (m)	1	1	1	1
Number of data points	741	780	245	380

### 3.2.2.1 A block model

The model consists of a rectangular block as the target with resistivity value of 100  $\Omega$ .m (blue) embedded in a high resistive homogenous medium of 417  $\Omega$ .m (light green) as background as shown in Figure 3.3. A block is positioned between distance of 18 m and 24 m. The dimension of a block is 8 m in length and 3.25 m in height.

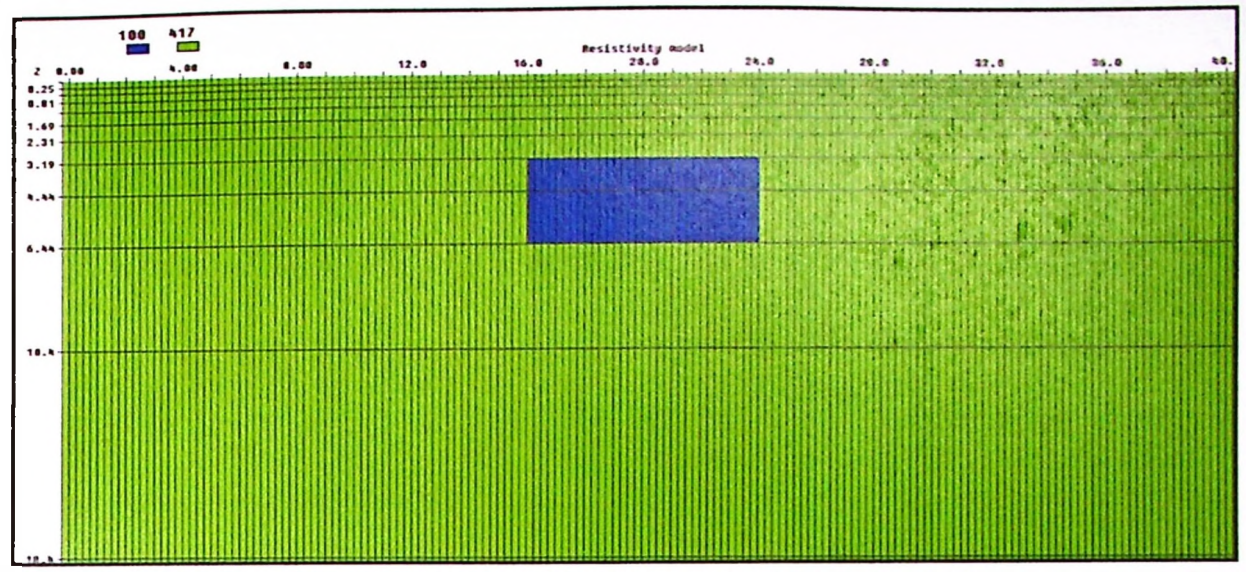


Figure 3.3: The synthetic model showing a block embedded in homogenous medium.

#### 3.2.2.2 Two blocks model

The model consists of two rectangular block as targets with resistivity values of 50  $\Omega$ .m (blue) and 100  $\Omega$ .m (light blue) embedded in high resistive homogenous medium of 700  $\Omega$ .m (green) as background as shown in Figure 3.4. The first block of 50  $\Omega$ .m is positioned between the distance of 13 m and 16 m. The second block of 100  $\Omega$ .m is position between 24 m and 27 m. The dimension of a block is 3 m in length and 2.13 m in height.

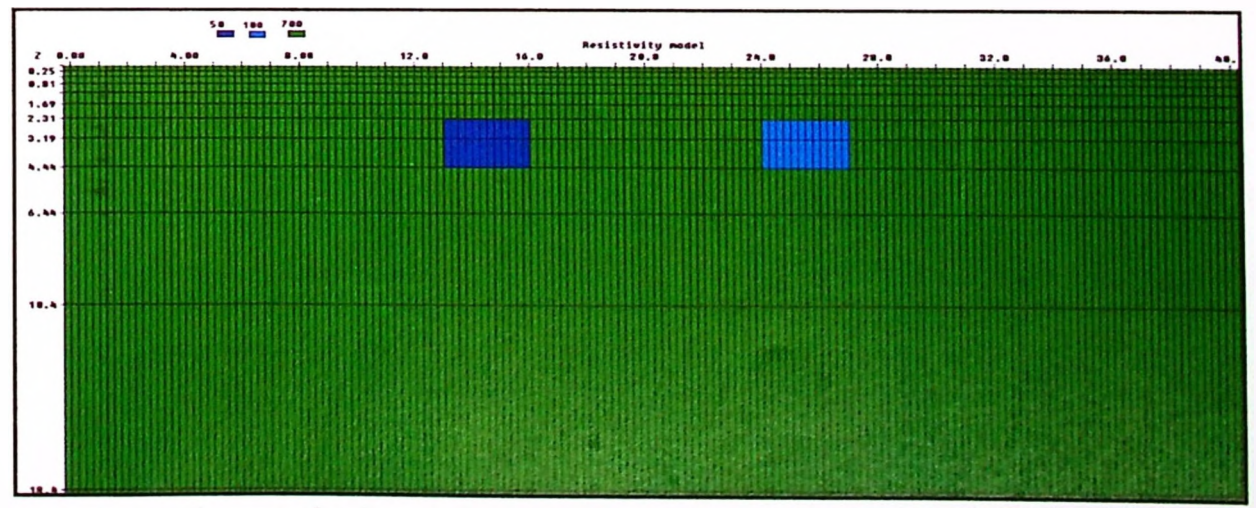


Figure 3.4: The synthetic model showing two blocks embedded in homogenous medium.

### 3.2.2.3 Contact zone model

The model consists of two different layers as targets with contact zone of resistivity value of 100  $\Omega$ .m (light blue) attached with a high resistive homogenous medium of 700  $\Omega$ .m (green) as shown in Figure 3.5. The contact zone is positioned between distance of 20 m and 40 m. The dimension of the contact zone is 20 m in length and 4.44 m thick from the surface.

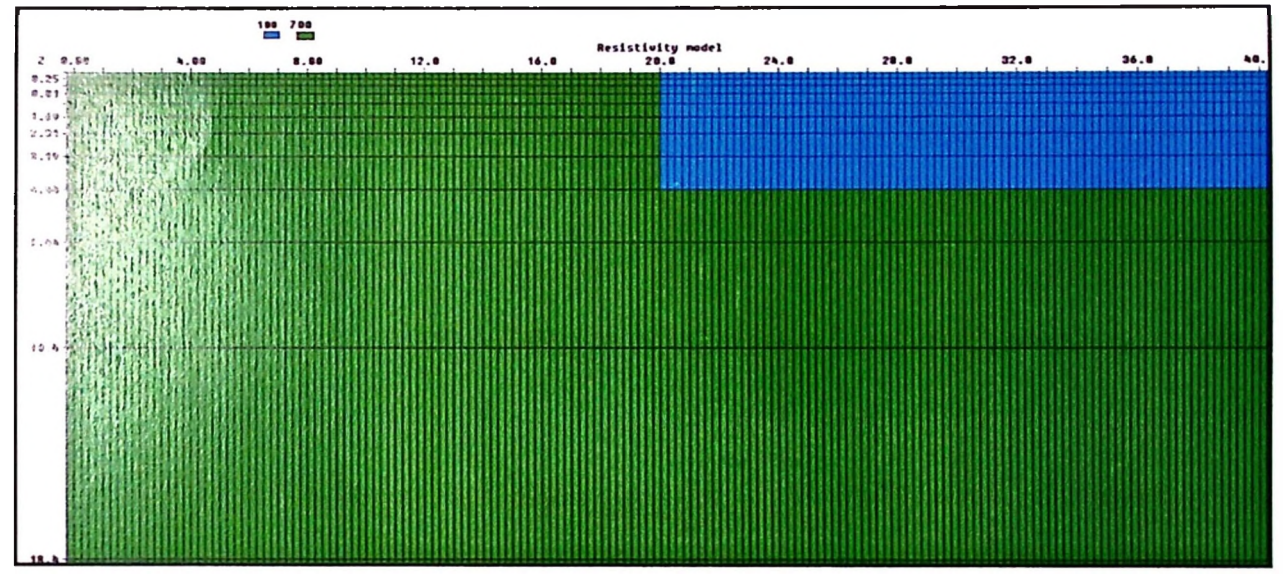


Figure 3.5: The synthetic model showing contact zone attached with homogenous medium.

## 3.2.2.4 Vertical dyke model

The model consists of an intrusive vertical dyke of infinite extent as the target with resistivity value of 70  $\Omega$ .m (blue) crossed high resistive homogenous medium of 700  $\Omega$ .m (green) as shown in Figure 3.6. The vertical dyke is positioned between the 18 and 22 electrodes. The dimension of a block is 4 m in width.

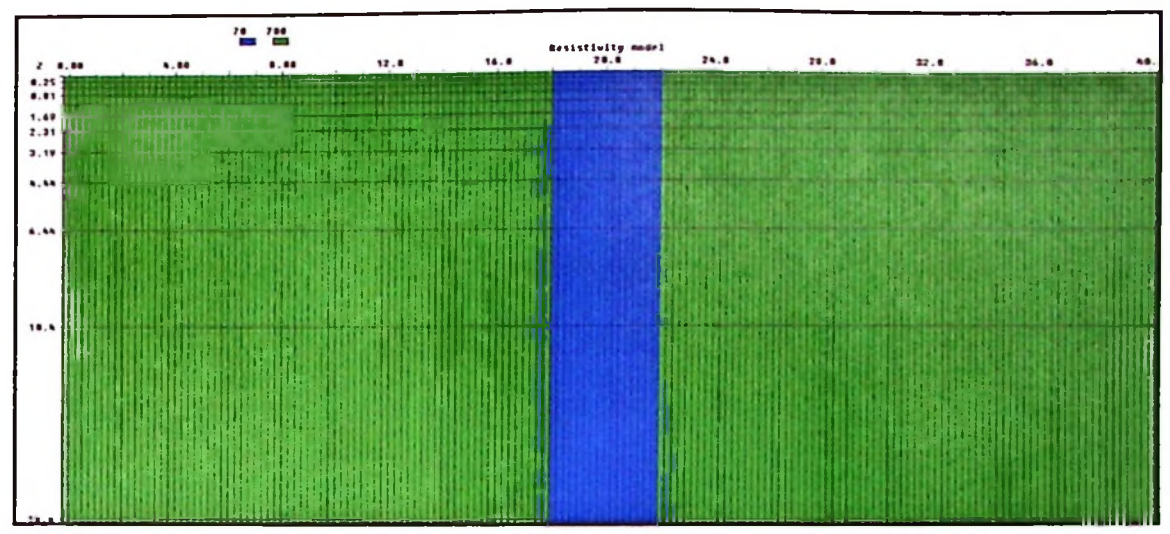


Figure 3.6: The synthetic model showing vertical dyke crossed with homogenous medium.

### 3.2.2.5 Fault model

The model consists of two different layers as targets with fault of resistivity value of 70  $\Omega$ .m (blue) attached with a high resistive homogenous medium of 700  $\Omega$ .m (green) as shown in Figure 3.7. The fault is positioned between distance of 20 m and 40 m. The dimension of the fault is 20 m in length and 3.19 m thick from the surface.

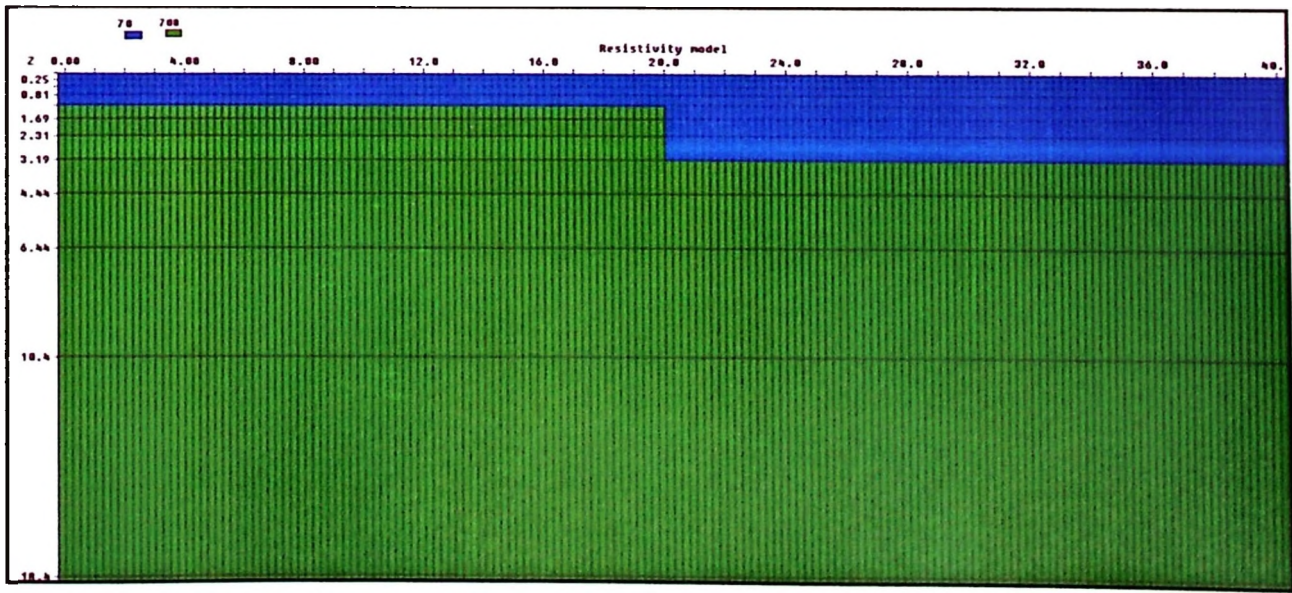


Figure 3.7: The synthetic model showing fault attached with homogenous medium.

# 3.2.3 The DLA technique for two different arrays

For each synthetic model data sets reproduced using RES2DMOD program (copyright by M.H. Loke), the reconstructed new data set is needed for two different arrays. This approach was carried out using the general array format (\*.dat) for the DLA technique in inverse modelling RES2DINV program (copyright by M.H. Loke). The general array format is used to cater for arrangement of electrode that do not fall under the conventional array types. This approach gives the user greater latitude in the arrangement of electrode. The general array format used in this study is shown in Appendix B. Two separate data sets from each individual arrays were combined together using the general array format. A new data set was obtained and the number of apparent resistivity data is the summation of these two data sets. Therefore, the DLA technique used in this study is capable of providing a dense data set from two different arrays.

#### 3.2.4 Field model

A bunker in Universiti Sains Malaysia (USM) main campus was selected for field model study using the 2-D resistivity imaging method. The spread length of study line is 60 m with minimum electrode spacing of 1.5 m and crossing the buried bunker. The dimension of this target is known.

# 3.2.5 The DLA technique for field model data

For each data conversion in SAS4000 utilities program (copyright by ABEM Instrument AB), the user will get raw data set for individual array in the s4k file format (\*.s4k). ERIGRAPH program (copyright by Torleif Dahlin) was used for conversion from the s4k file format (\*.s4k) to the text file format (\*.dat). The general array format which was used in this study is shown in Appendix B. Two separate data sets from each individual arrays were combined together using the general array format. A new data set was obtained and the number of apparent resistivity data is the summation of these two data sets. Therefore, the DLA technique used in this study is capable of providing a dense data set from two different arrays.

# 3.2.6 Inversion modelling

Prior to inversions of apparent resistivity values for all synthetic models, 1 % random noise level is added to each inversion model to reflect field condition (Olayinka and Yaramanci, 2000). The type of noise added in was apparent resistivity. The 2-D inversion modelling was carried out using RES2DINV, a commercially available inversion program (Loke and Barker, 1996). This inversion software uses smooth-constrained inversion routine (deGroot-Hedlin and Constable, 1990; Ellis and Oldenburg, 1994).

For all the synthetic models, the inversion routine took between 5 to 7 number of iterations depending on models and array types used to converge to misfit data to less than 10 %. This inverse modelling calculates resistivity distribution that is consistent with true values of models. Once, the resistivity data inversion has been

carried out, the 2-D inverse resistivity models for all four different arrays were saved in the SURFER format or the text file format (\*.dat). SURFER software (copyright by Golden Software, LLC) is a contouring and surface modelling package for visualization purposes.

# 3.3 Phase 2: The numerical comparative assessment

After obtaining the inversion of model resistivity for all selected arrays, the numerical comparative assessment of individual model resistivity and the DLA model resistivity for two different arrays were carried out. The numerical comparative assessment is used for quality assessment. There are three different parameters were used in this quality assessment. They are (i) total number of data points (apparent resistivity) ( $\sum DP_{App,(DLA)}$ ), (ii) percentage of overlapping inversion of model resistivity data ( $\Delta PO_{DLA}$ ) and (iii) the ability to resolve the known target. Total number of data point (apparent resistivity) used in the inversion modelling is given by Equation 3.1.

$$\Sigma DP_{App,(DLA)} = DP_{App,(1)} + DP_{App,(2)}$$
 (3.1)

where; DP<sub>App.(1)</sub> is number of apparent resistivity data for array 1.

DP<sub>App.(2)</sub> is number of apparent resistivity data for array 2.

In addition, two new formulations were developed to determine the percentage of overlapping inversion of model resistivity data. Two formulations were developed in this study for numerical comparative assessment. They are the number of overlapping inversion of model resistivity data (OD) and the percentage of overlapping in the DLA technique ( $\Delta PO_{DLA}$ ) which are given by Equation (3.2) and Equation (3.3) as below.

$$OD = (IM_1 + IM_2) - (IM_{DLA})$$
 (3.2)

where; IM<sub>1</sub> is inversion of model resistivity data array 1.

IM<sub>2</sub> is inversion of model resistivity data array 2.

IM<sub>DLA</sub> is the DLA of model resistivity data for both arrays.

$$\Delta PO_{DLA} = \frac{OD}{IM_{DLA}} \times 100$$
 (3.3)

where; OD is the number of overlapping inversion of model resistivity data.

IM<sub>DLA</sub> is the DLA of model resistivity data for both arrays.

For overview of the characteristics of the DLA technique for two different arrays, the percentage change in inversion depth of investigation ( $\Delta D_{DLA}$ ) was developed which is given by Equation (3.4). This approach is not the main parameter to be used in the selection of the best two arrays, but it is more on general knowledge about the DLA technique in the 2-D resistivity imaging method.

$$\Delta D_{DLA} = \frac{(D_{DLA} - D_{Maxi})}{D_{Maxi}} \times 100$$
 (3.4)

where; D<sub>DLA</sub> is depth of investigation of the DLA model resistivity.

D<sub>Max i</sub> is the maximum depth of investigation of model resistivity of any individual array used for the DLA technique.

The numerical comparative assessment was used for the quality assessment to select the two best and suitable arrays for the DLA technique. Decision and consideration will be based on the three main parameters as stated previously. The decision to select only the two best and suitable arrays for the DLA technique is due to cost constraints and also limitation of work force. In addition, the approach in this research can be a guideline for other researchers to use the DLA technique in the 2-D resistivity imaging method especially for those with non-geophysics background.

# 3.4 Phase 3: Validation of the DLA technique

Based on the final decision of the numerical comparative assessment in the Phase 2, validation of the DLA technique using the two best and suitable arrays was applied to actual field surveys. The subsurface investigation for site characterization using the joint-inversion technique have been receiving growing attention (de la Vega et al. 2003; Athanasiou et al. 2007; Candansayar, 2008; Berge and Drahor, 2009; Neyamadpour et al. 2010a, 2010b). The reduction in processing time and data acquisition has made this approach economically viable to acquire complementary of the 2-D resistivity imaging method. Therefore, the DLA technique used in this study

for the best and suitable arrays was carried at two different sites for validation purposes. The first field study was located at Minden, USM, Penang and the second field study was located at Bukit Bunuh, Lenggong, Perak.

## 3.4.1 Minden, USM, Penang

Penang is the second smallest of the 11 states of Peninsular Malaysia. It is situated in the northern region. The island and mainland are linked by regular ferry service, a 13.5 km long Penang First Bridge and a 24 km long Penang Second Bridge. Penang Island is located between latitudes of 5° 8' North and 5° 35' North and longitudes of 100° 8' East and 100° 32' East. The climate is tropical with an average mean daily temperature of approximately 27 °C and mean daily maximum and minimum temperatures between 31.4 °C and 23.5 °C respectively (Fauziah et al., 2006). Penang Island consists of coastal plains, hills and mountains with three main geological formations of igneous rock (Figure 3.8). All igneous rocks are granites in terms of Streckeisen classification (Ong, 1993). The granite is classified based on the basis of the proportions of alkali feldspar to total feldspars which is divided into two main groups. The first one is North Penang Pluton and second one is South Penang Pluton (Ong, 1993; Pradhan et al., 2012). Minden, USM area is classified as medium to coarse grained biotite granite. The orientation of the Minden valley is along the North-South direction. The valley marks the position of Central Penang Fault Zone (Streckeisen, 1967; Ong, 1993; Fauziah et al., 2006).

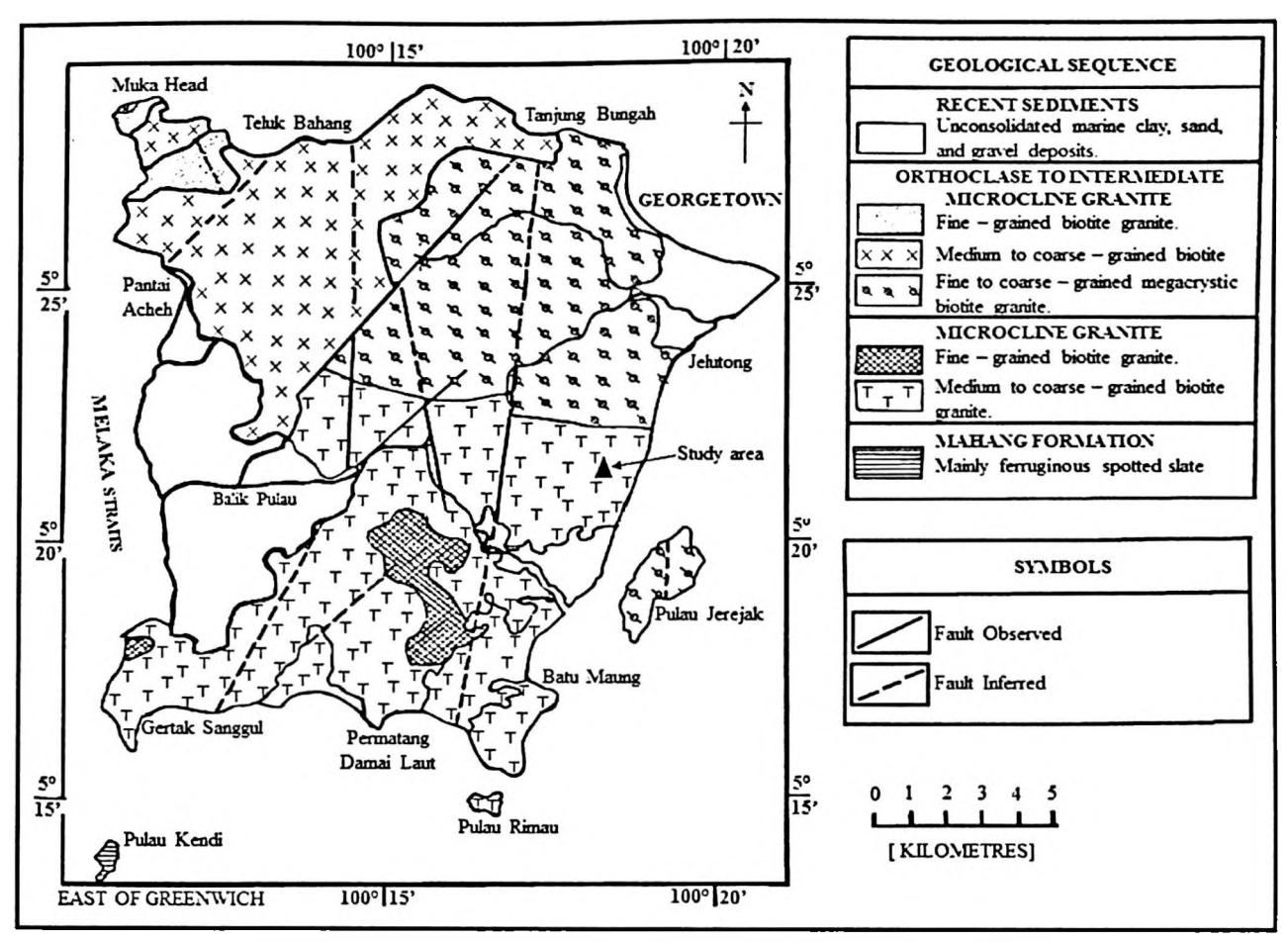


Figure 3.8: Penang Island geological map (Ong, 1993).

The spread length of the 2-D resistivity survey is 200 m with minimum electrode spacing of 5 m. The borehole location was located at 90 m and 120 m in the 2-D resistivity survey line.

# 3.4.2 Bukit Bunuh, Lenggong, Perak

Bukit Bunuh, Lenggong, Perak is the second field study located at latitude of 5° 3' North and longitude of 100° 59' East (Figure 3.9). This area is surrounded by mountainous terrain underlain by granitic rock which is from Jurassic end-Carbonaceous low era. This area originates from Bintang Range in the west of Lenggong town (Saidin, 1997; Azwin et al., 2015). Bukit Bunuh is about 10

Tampan which was discovered by Mokhtar Saidin (Talib et al., 2009). The first excavation revealed on site a stone tool-making workshop dating 40,000 years ago and suevite boulders area which is dated 1.83 million years ago.

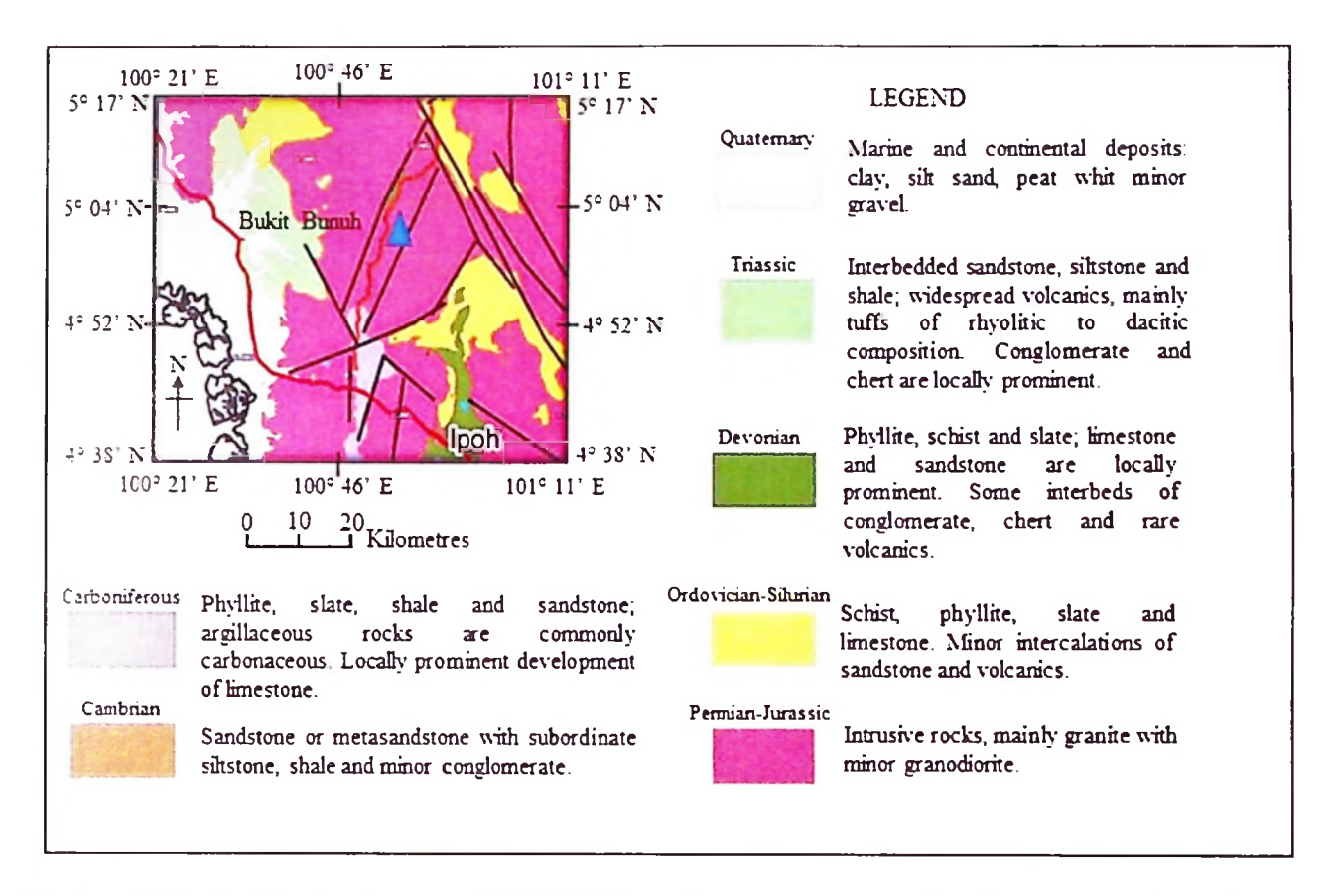


Figure 3.9: Geological map of Bukit Bunuh study area with blue triangle (Jabatan Mineral dan Geosains Malaysia, 1985).

The spread length of the 2-D resistivity survey is 200 m with minimum electrode spacing of 5 m. The borehole location was located at 90 m and 120 m in the 2-D resistivity survey line.

## 3.5 Chapter summary

This chapter discusses the research methodology and technique used in this research. Methodological framework overview that was used in data acquisition and data analysis is presented. In order to achieve all the objectives, the methodologies employed were carried out in three different phases. The decision for these two arrays was made after full consideration of all investigated parameters. There are two field study areas in this research, which are Minden, USM, Penang and Bukit Bunuh, Lenggong, Perak respectively. In short, these two different areas were selected for the validation of the DLA technique using a combination of two different arrays data sets. This approach is carried to answer the third objective in this study.

### **CHAPTER 4**

### RESULTS AND DISCUSSIONS

### 4.0 Introduction

The results of this research will be presented and discussed in the ways the research methodology were carried out. The following discussions are summaries of the obtained results which are followed by the figures and tables to give more insight into the results' explanation.

## 4.1 Results of 2-D computerized models

The results of reconstructed 2-D resistivity imaging for the synthetics models using individual inversion and the DLA technique are presented in this section as shown by the figures and tables. In addition, the results of the reconstructed numerical comparative analysis approach which was explained in Chapter 3 are presented too.

### 4.1.1 A block model

Some 2-D resistivity imaging results for individual array data sets recover image of a block as shown in Figures 4.1 until 4.4. From the results, it shows that image of a block is well resolved only by D-D array. This array is able to image a

block with the right location and the same resistivity value. P-D and W-S arrays are able to resolve the image of a block moderately, which means they give the right location, but with high resistivity value. However, W array cannot resolve image of a block with good results. W array gives wrong location of a block and higher resistivity than the true resistivity value. The reason is because this array is less sensitive to resistivity horizontal changes (Loke, 2004; 2014).

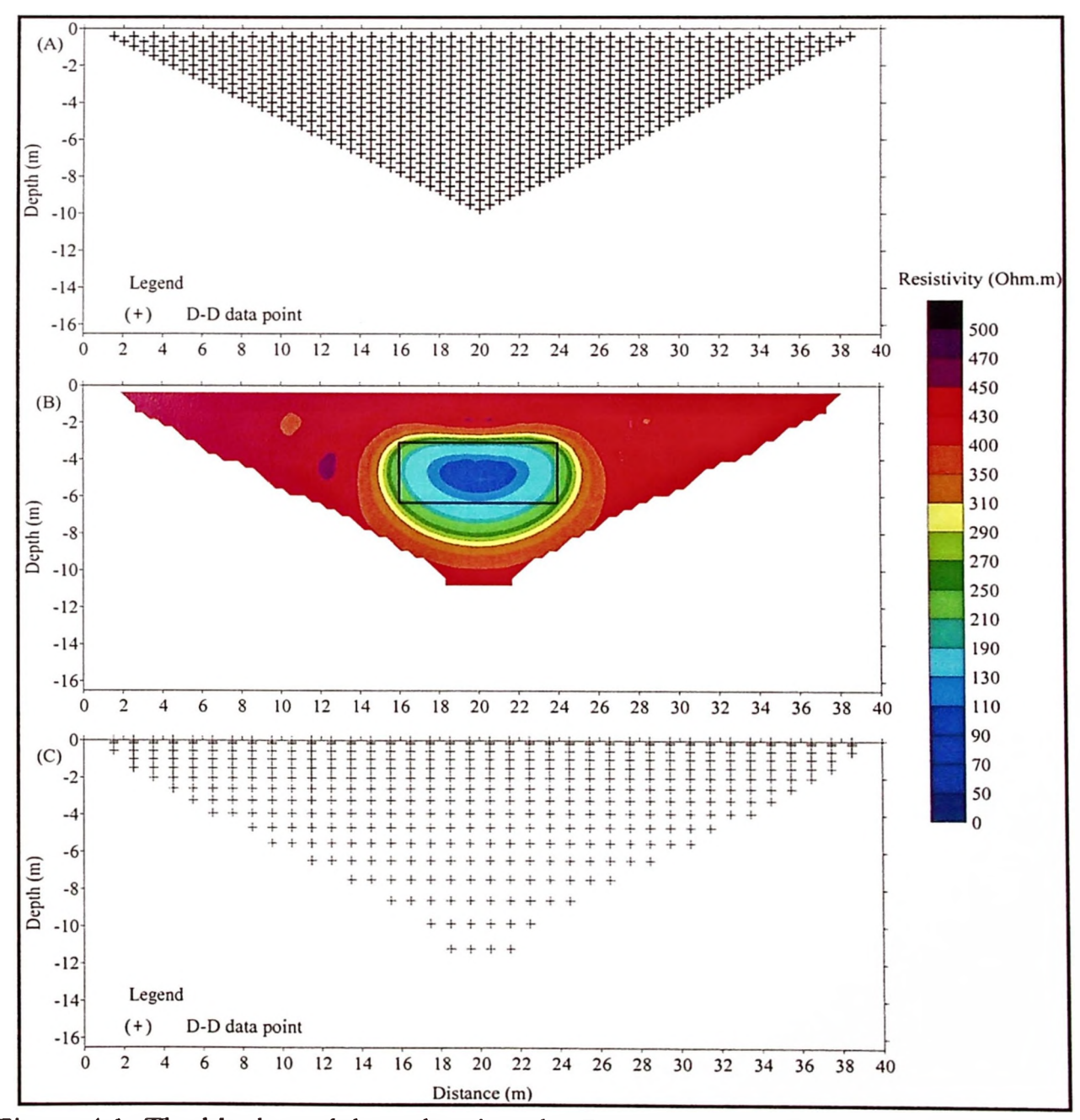


Figure 4.1: The block model results given by D-D array. A) Apparent resistivity data points arrangement. B) 2-D resistivity model result and C) Model resistivity data points.

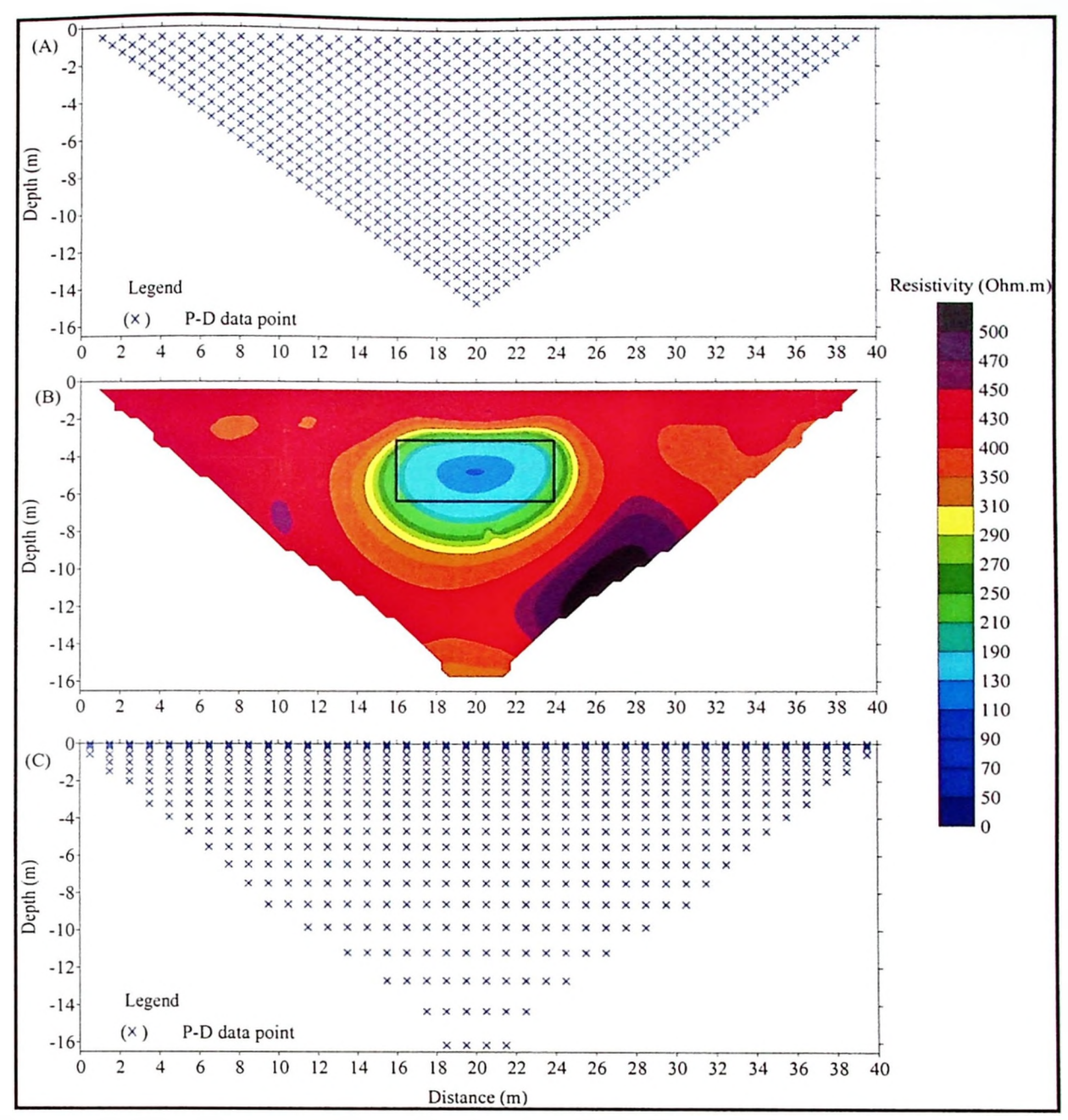


Figure 4.2: The block model results given by P-D array. A) Apparent resistivity data points arrangement. B) 2-D resistivity model result and C) Model resistivity data points.

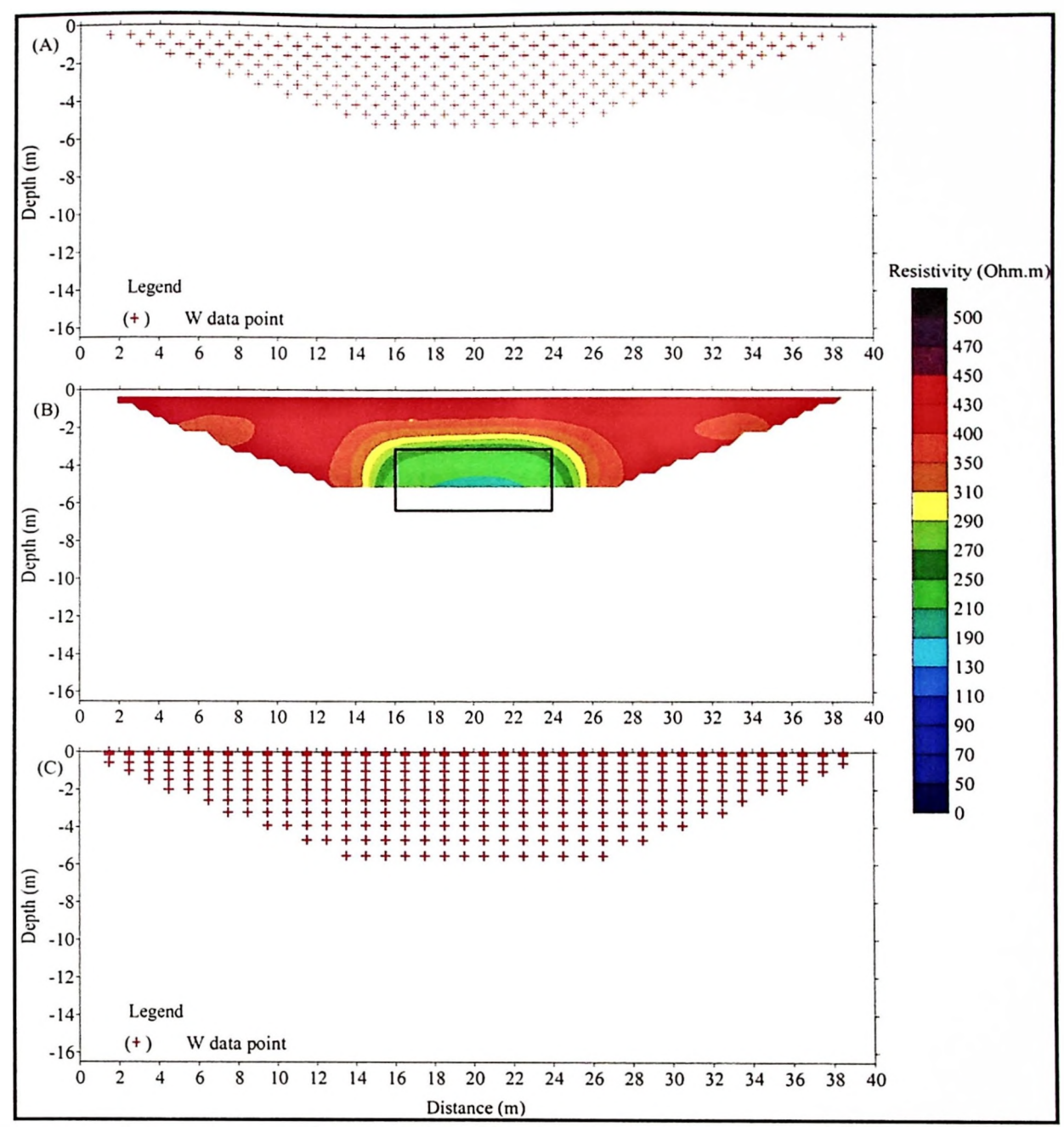


Figure 4.3: The block model results given by W array. A) Apparent resistivity data points arrangement. B) 2-D resistivity model result and C) Model resistivity data points.

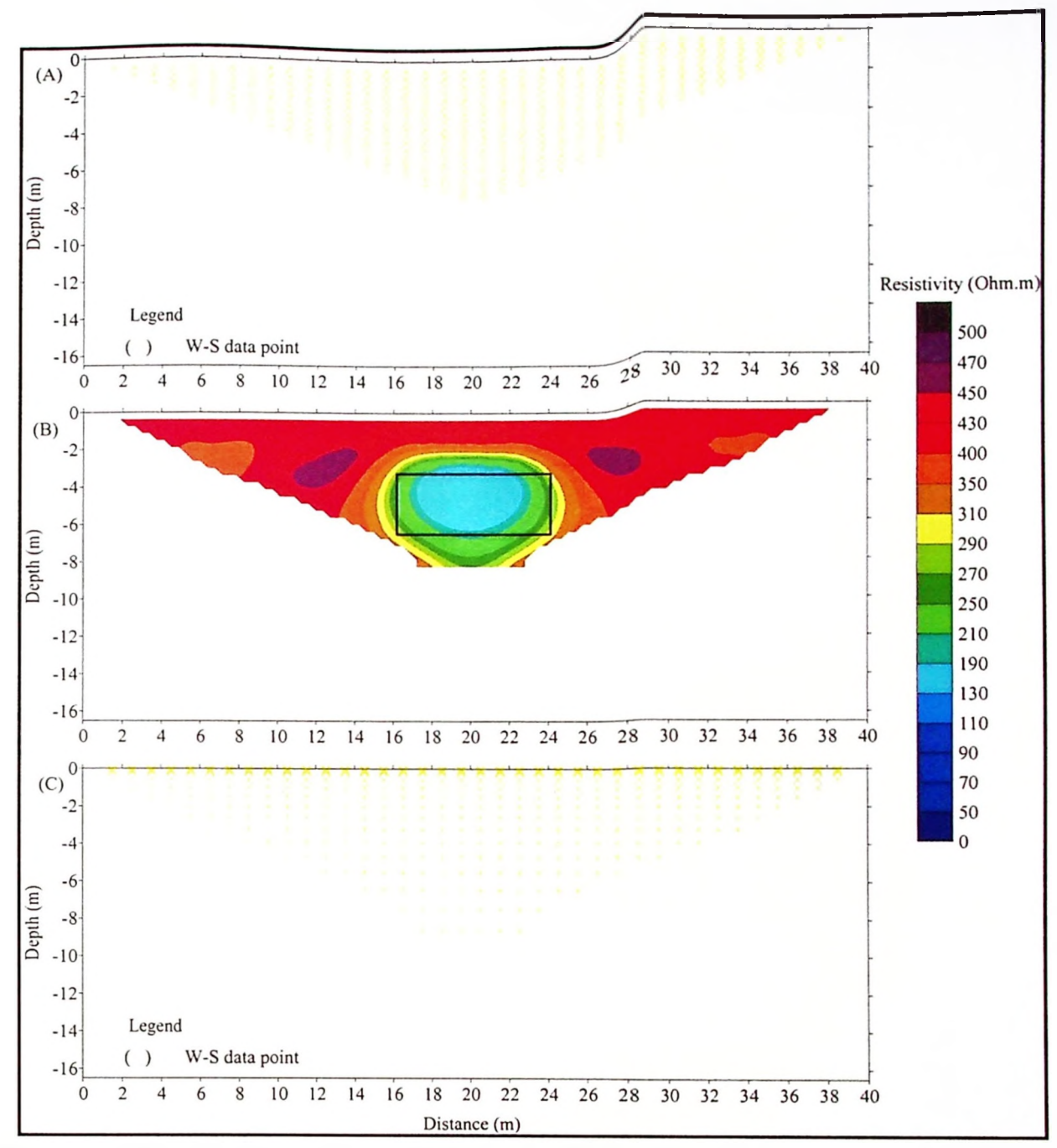


Figure 4.4: The block model results given by W-S array. A) Apparent resistivity data points arrangement. B) 2-D resistivity model result and C) Model resistivity data points.

Some of the 2-D resistivity imaging results for the DLA technique data sets recover the target of a block image as shown in Figures 4.5 until 4.10. From the results, it shows that a block image is resolved well by (D-D+P-D, D-D+W, D-D+W-S, P-D+W and P-D+W-S) arrays. All of them are able to image the right location and the same resistivity value of a block. However, only the DLA technique of (W+W-S) is able to resolve a block image with moderate results, which gives the right location

but with high resistivity value. This may be due to domination of W array in the DLA technique. W array is less sensitive to resistivity horizontal changes (Loke, 2004; 2014).

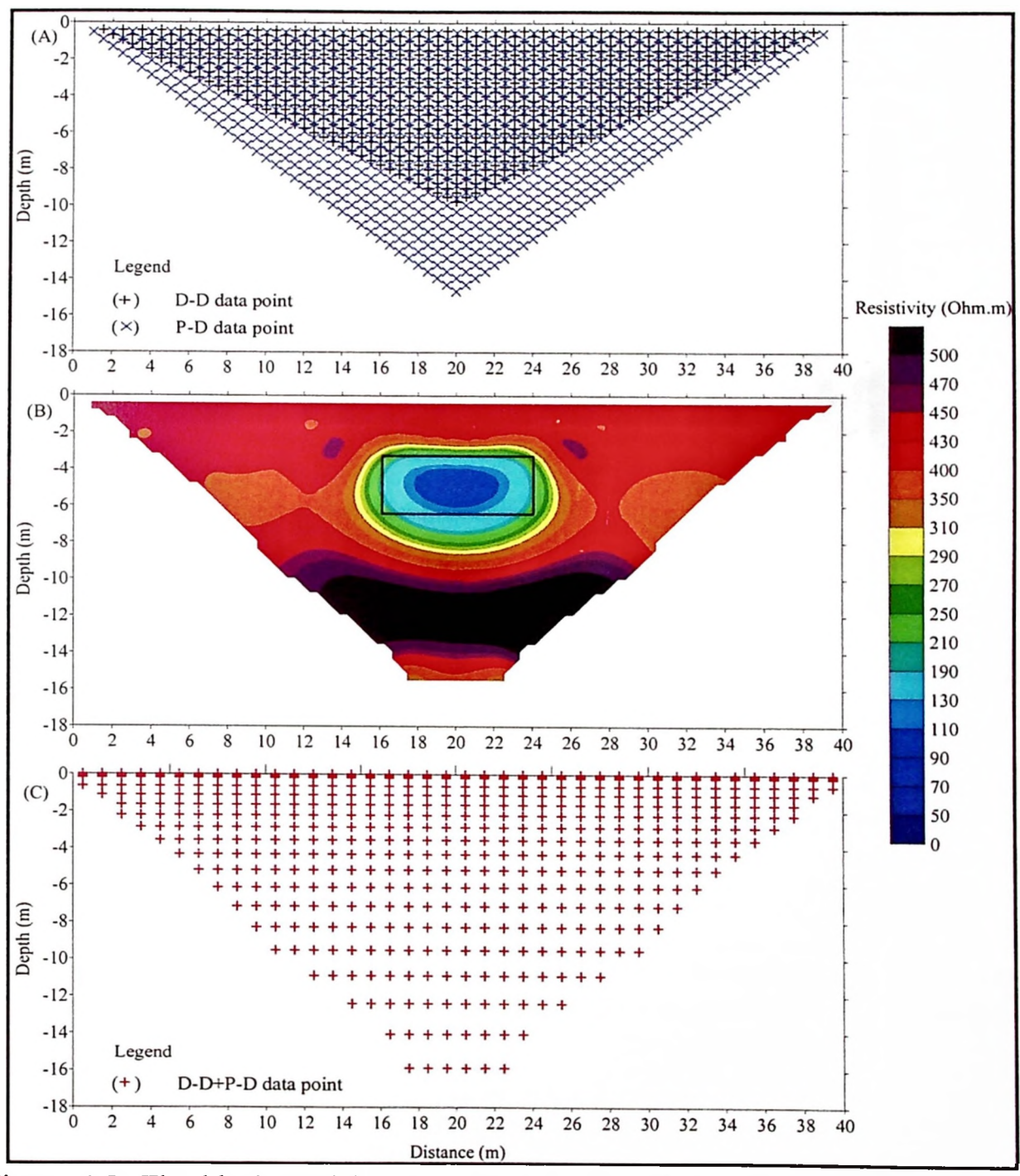


Figure 4.5: The block model results given by the DLA technique of (D-D+P-D) arrays. A) Apparent resistivity data points arrangement. B) 2-D resistivity model result and C) Model resistivity data points.

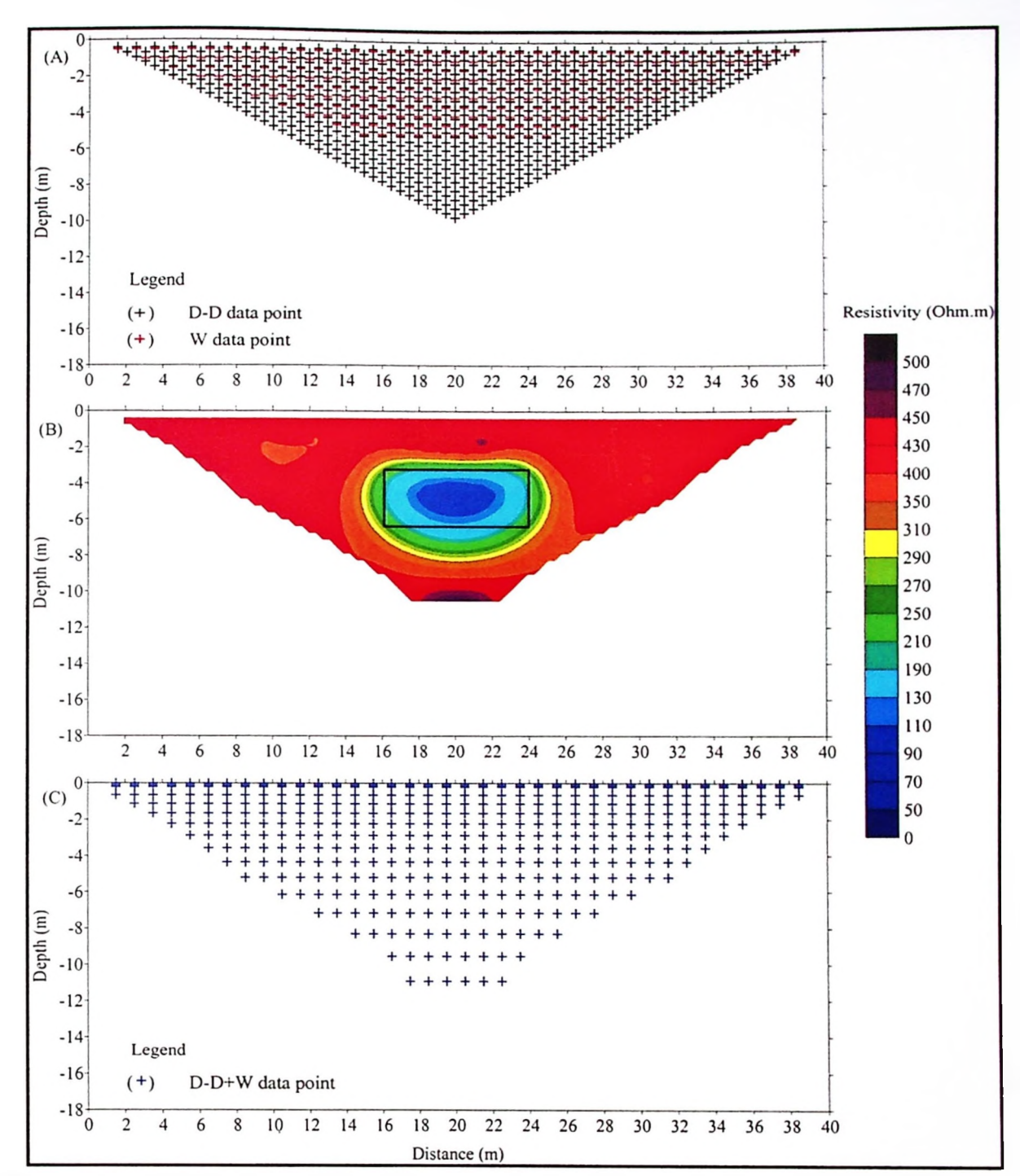


Figure 4.6: The block model results given by the DLA technique of (D-D+W) arrays. A) Apparent resistivity data points arrangement. B) 2-D resistivity model result and C) Model resistivity data points.

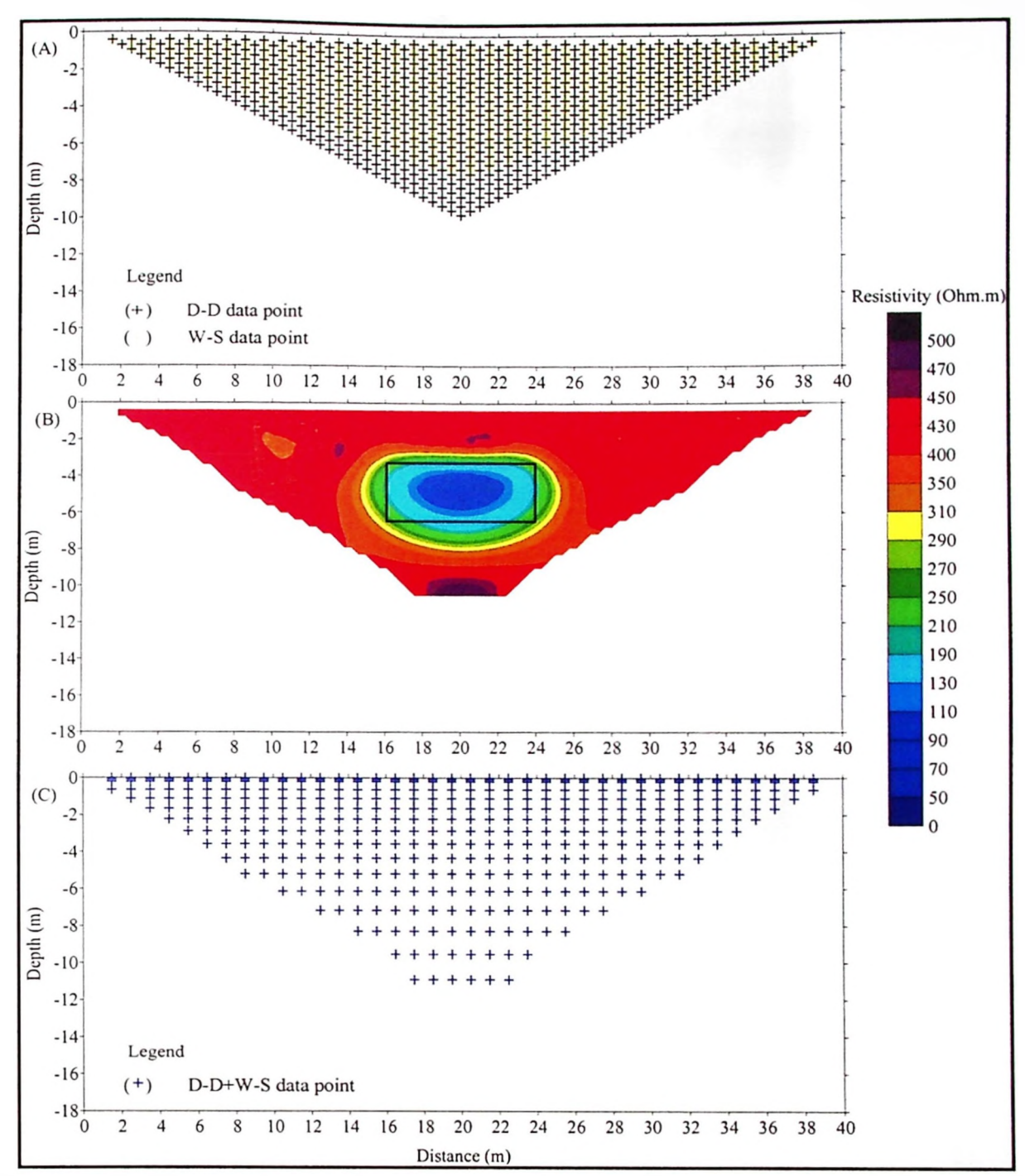


Figure 4.7: The block model results given by the DLA technique of (D-D+W-S) arrays. A) Apparent resistivity data points arrangement. B) 2-D resistivity model result and C) Model resistivity data points.

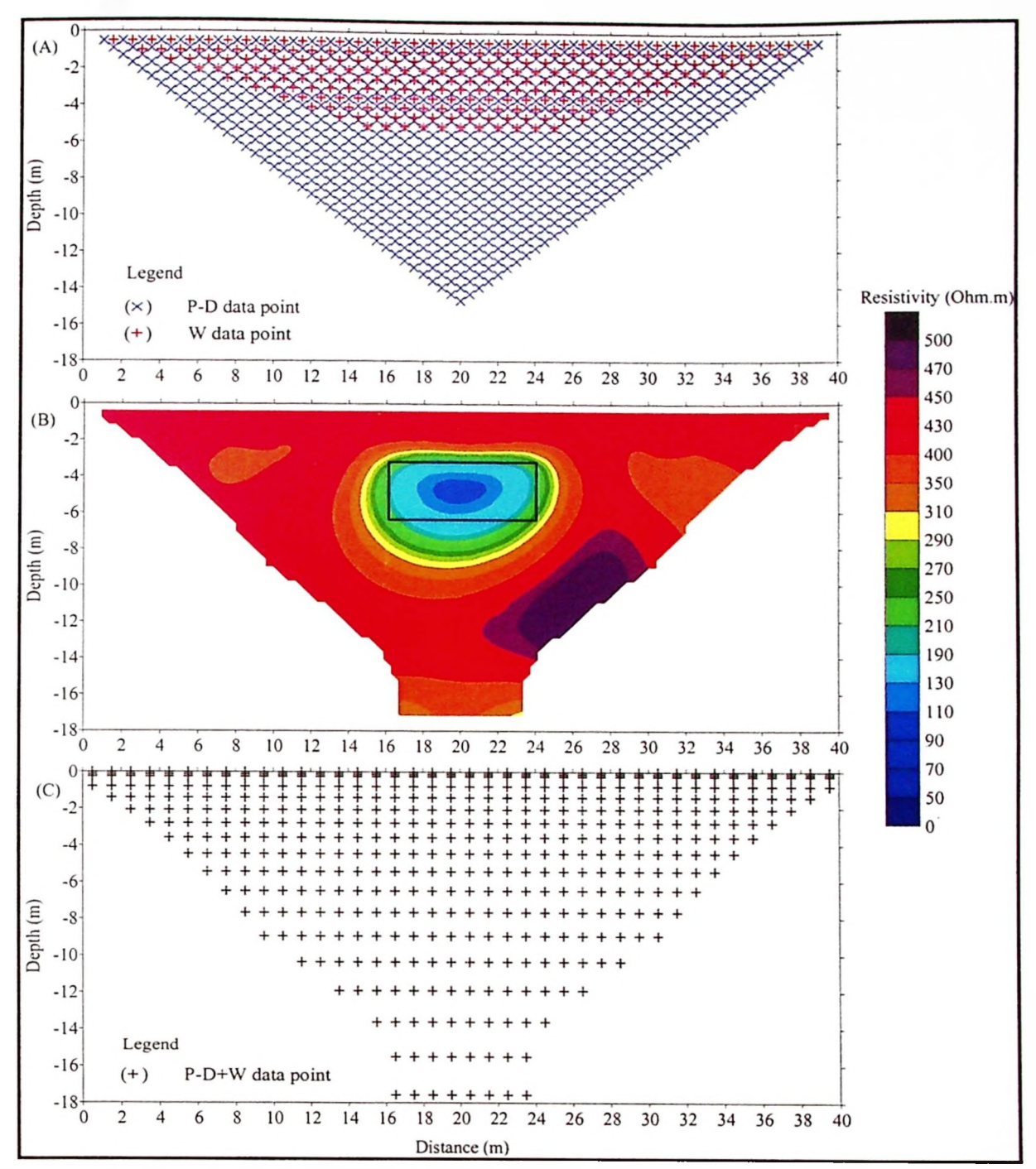


Figure 4.8: The block model results given by the DLA technique of (P-D+W) arrays. A) Apparent resistivity data points arrangement. B) 2-D resistivity model result and C) Model resistivity data points.

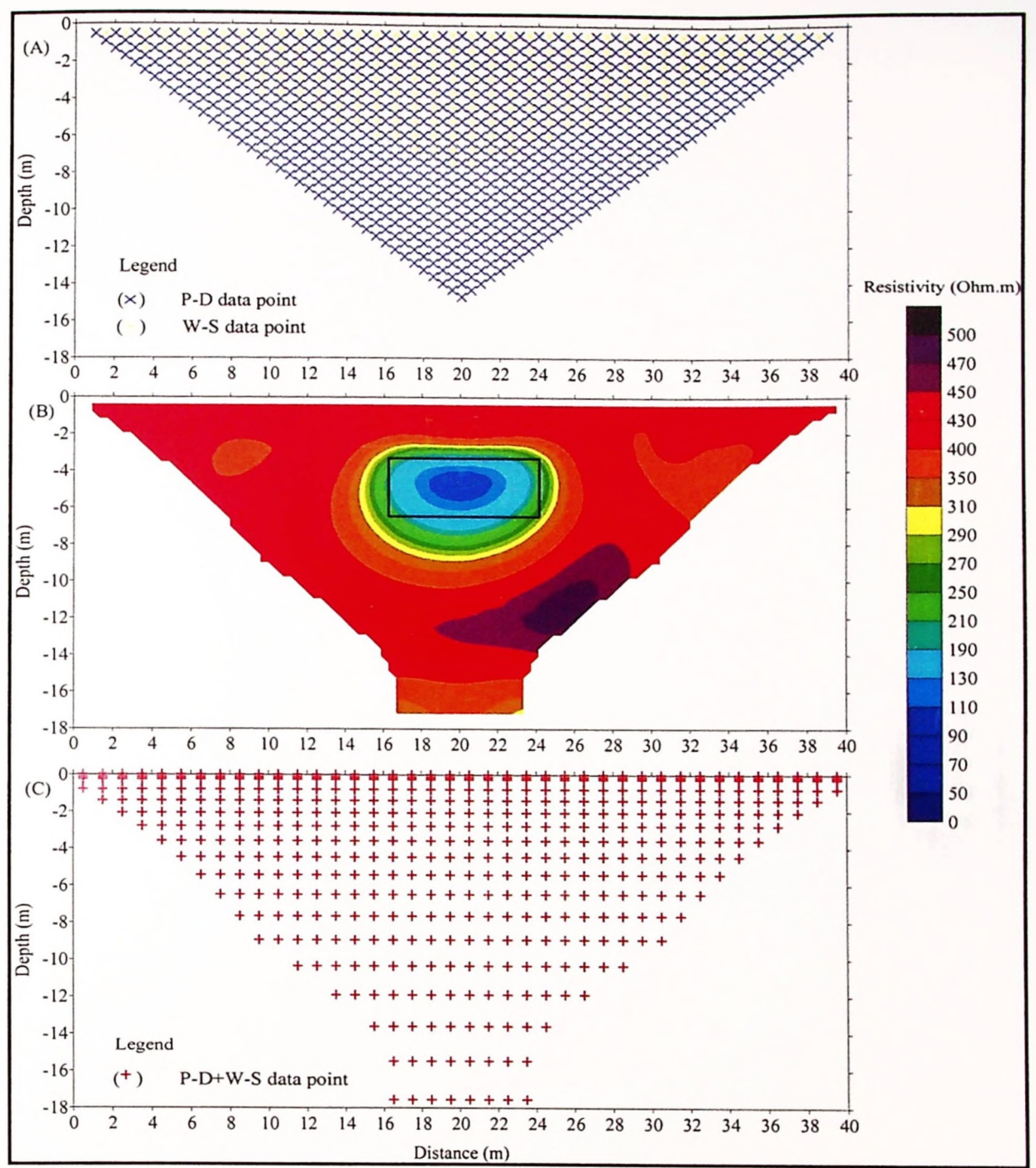


Figure 4.9: The block model results given by the DLA technique of (P-D+W-S) arrays. A) Apparent resistivity data points arrangement. B) 2-D resistivity model result and C) Model resistivity data points.

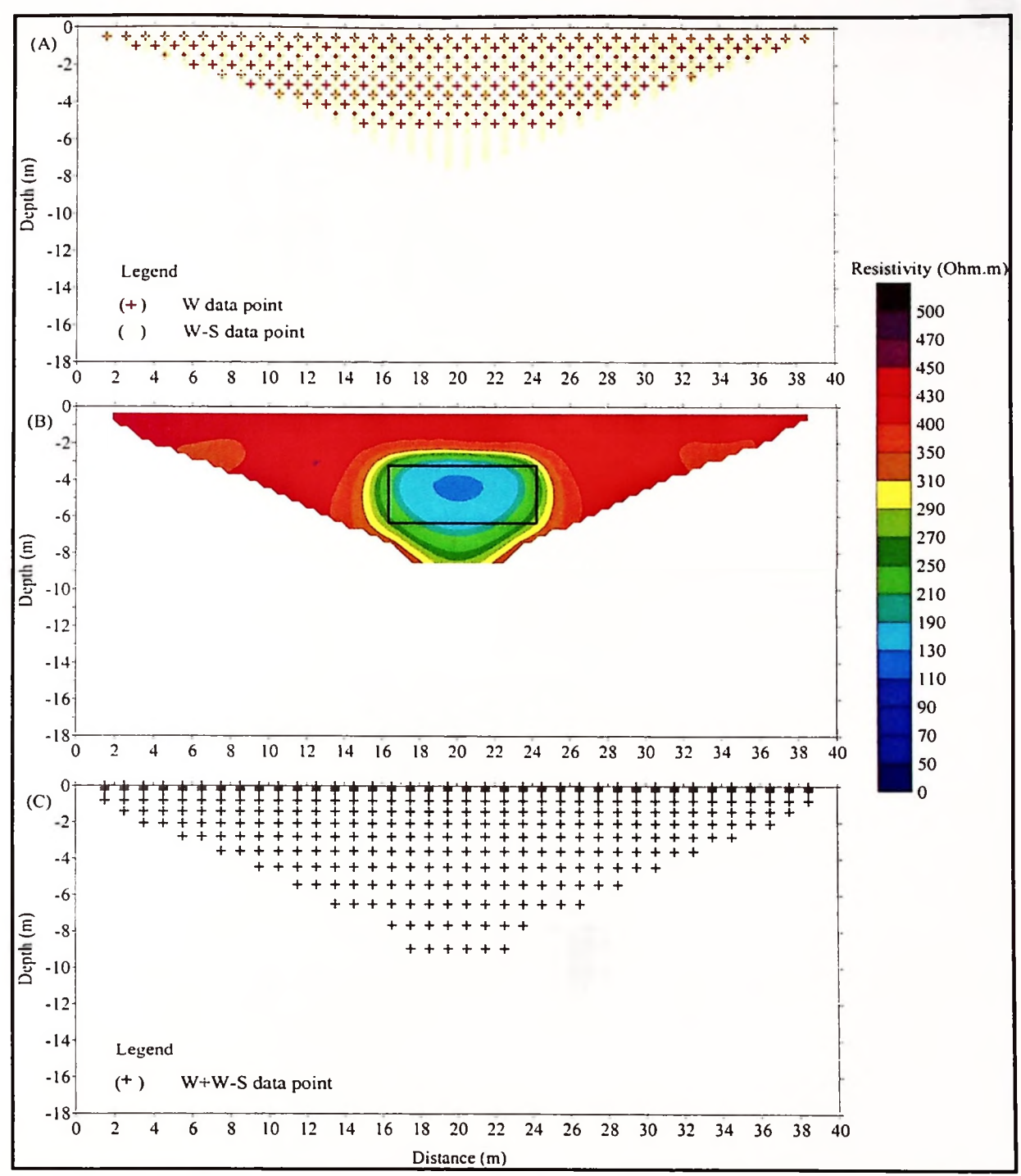


Figure 4.10: The block model results given by the DLA technique of (W+W-S) arrays. A) Apparent resistivity data points arrangement. B) 2-D resistivity model result and C) Model resistivity data points.

## 4.1.2 Two blocks model

Some 2-D resistivity imaging results for individual array data sets recover the targets of two blocks images as shown in Figures 4.11 until 4.14. From the results, it

shows that two block (50  $\Omega$ .m and 100  $\Omega$ .m) images are fairly well resolved by D-D and P-D arrays with the right location and acceptable resistivity values. However, W array cannot resolve image with well. W array gives the wrong location of a block and higher resistivity value than the true resistivity value. W array gives unclear image about the location of the two blocks and it gives higher resistivity value than the true one. This is due to poor ability to resolve vertical structure (Loke, 1999a; 2014). W-S array is able to resolve image of two blocks with moderate results. W-S arrays is able to image these two blocks with the right location, but it gives higher resistivity than true resistivity value. It shows that W-S array is moderately sensitive to both vertical and horizontal changes in resistivity (Loke, 2014).

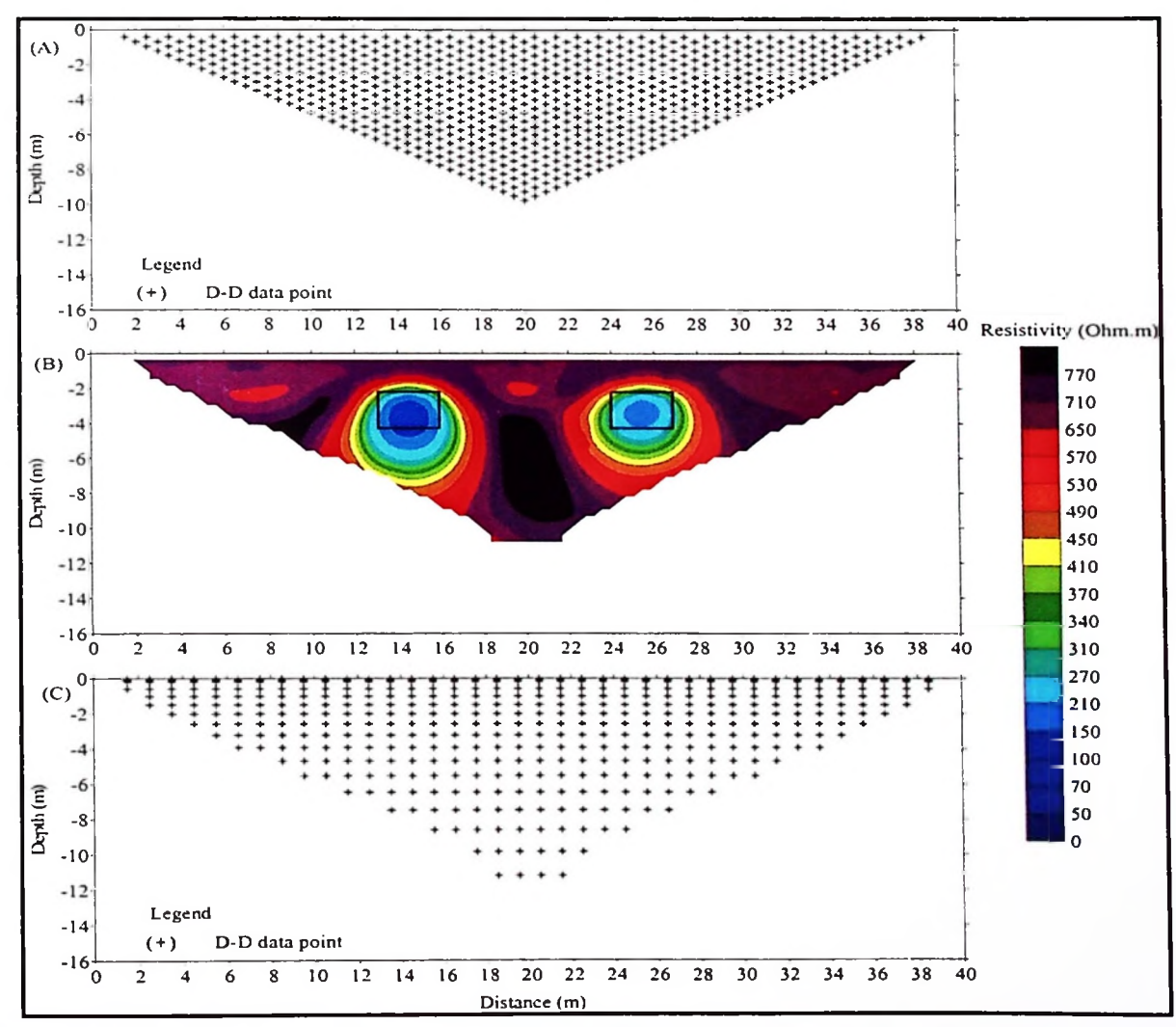


Figure 4.11: The two blocks model results given by D-D array. A) Apparent resistivity data points arrangement. B) 2-D resistivity model result and C) Model resistivity data points.

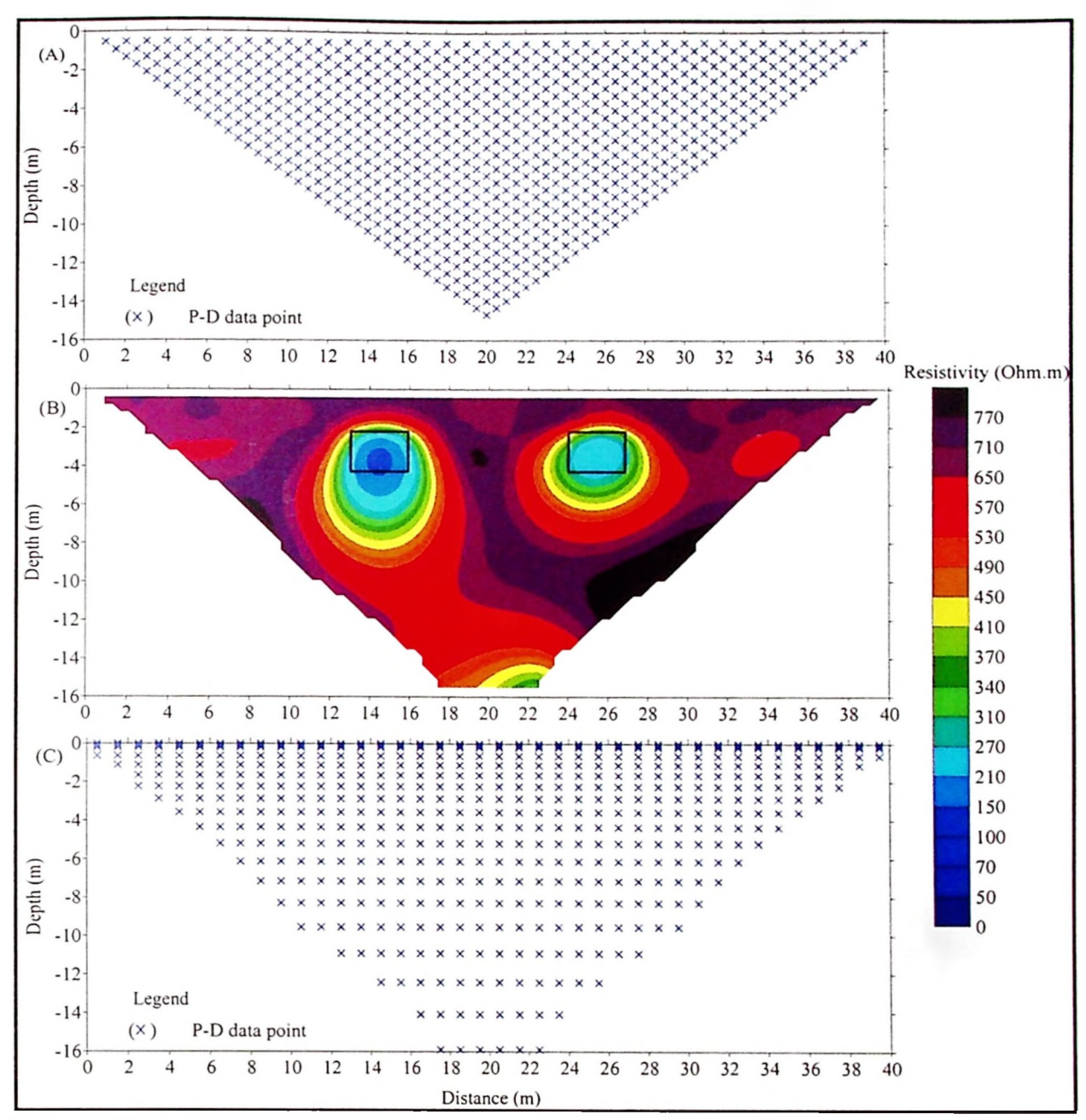


Figure 4.12: The two blocks model results given by P-D array. A) Apparent resistivity data points arrangement. B) 2-D resistivity model result and C) Model resistivity data points.

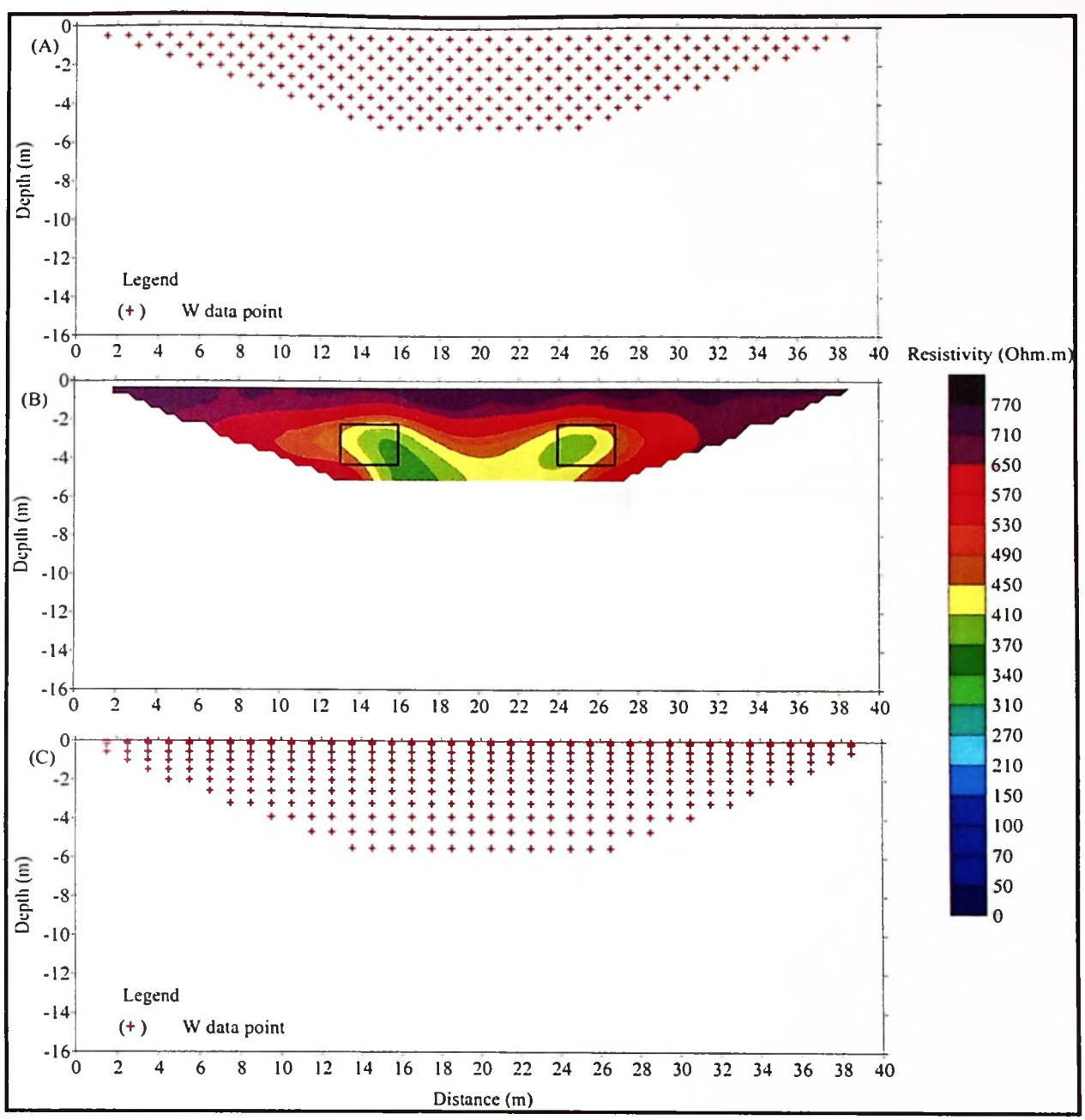


Figure 4.13: The two blocks model results given by W array. A) Apparent resistivity data points arrangement. B) 2-D resistivity model result and C) Model resistivity data points.

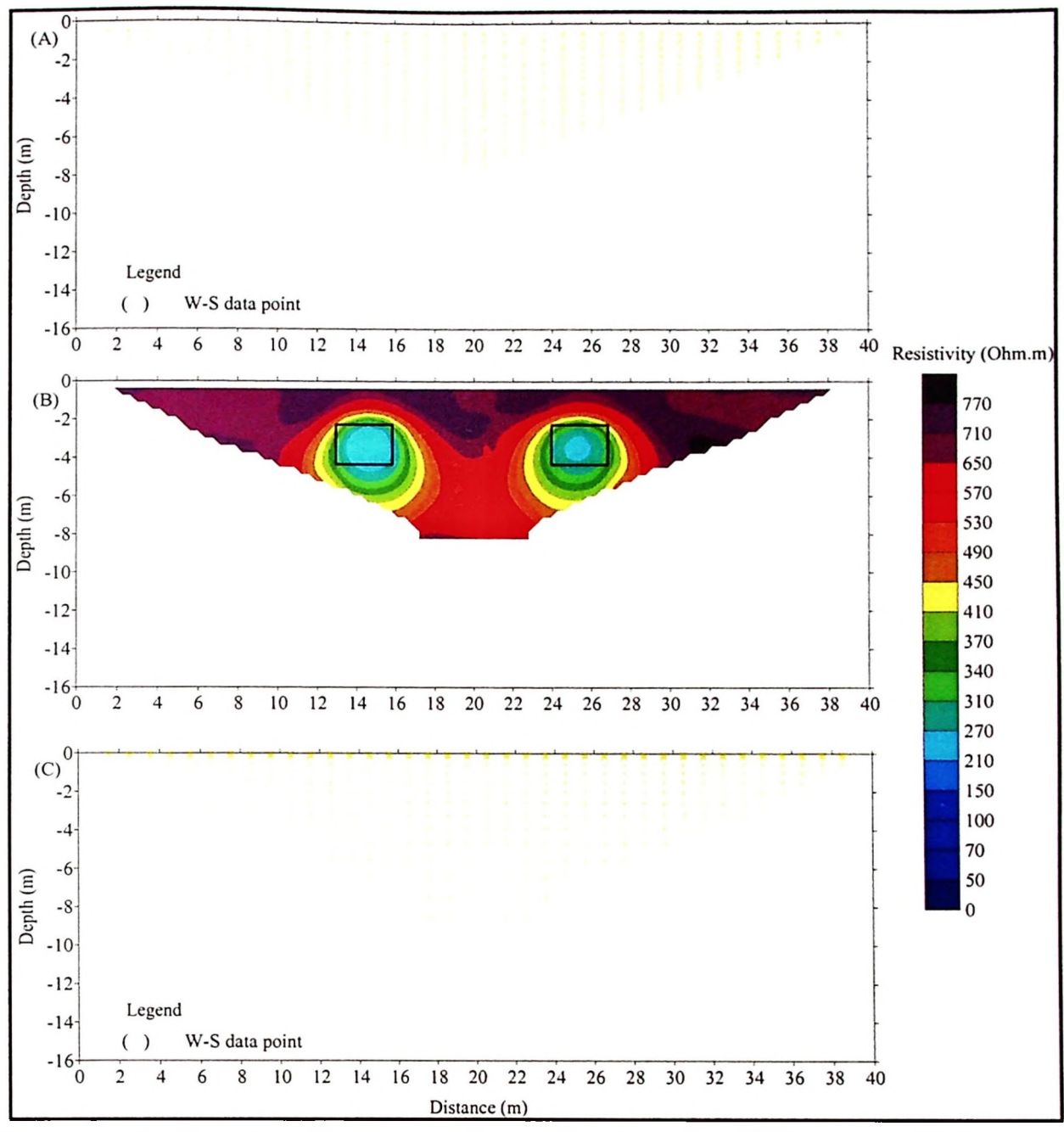


Figure 4.14: The two blocks model results given by W-S array. A) Apparent resistivity data points arrangement. B) 2-D resistivity model result and C) Model resistivity data points.

Some of the 2-D resistivity imaging results for the DLA technique data sets recover the targets of two blocks (50  $\Omega$ .m and 100  $\Omega$ .m) as shown in Figures 4.15 until 4.20. From the results, it shows that the two block images are resolved with good results by (D-D+P-D, D-D+W, D-D+W-S, P-D+W and P-D+W-S) arrays. All of them are able to image these two blocks with the right location and acceptable resistivity values. Only the DLA of (W+W-S) is able to resolve the two block images

with moderate results, which gives the right location but high resistivity values. This is may be due to domination of W array in the DLA technique. W array is less sensitive to resistivity horizontal changes (Loke, 20014).

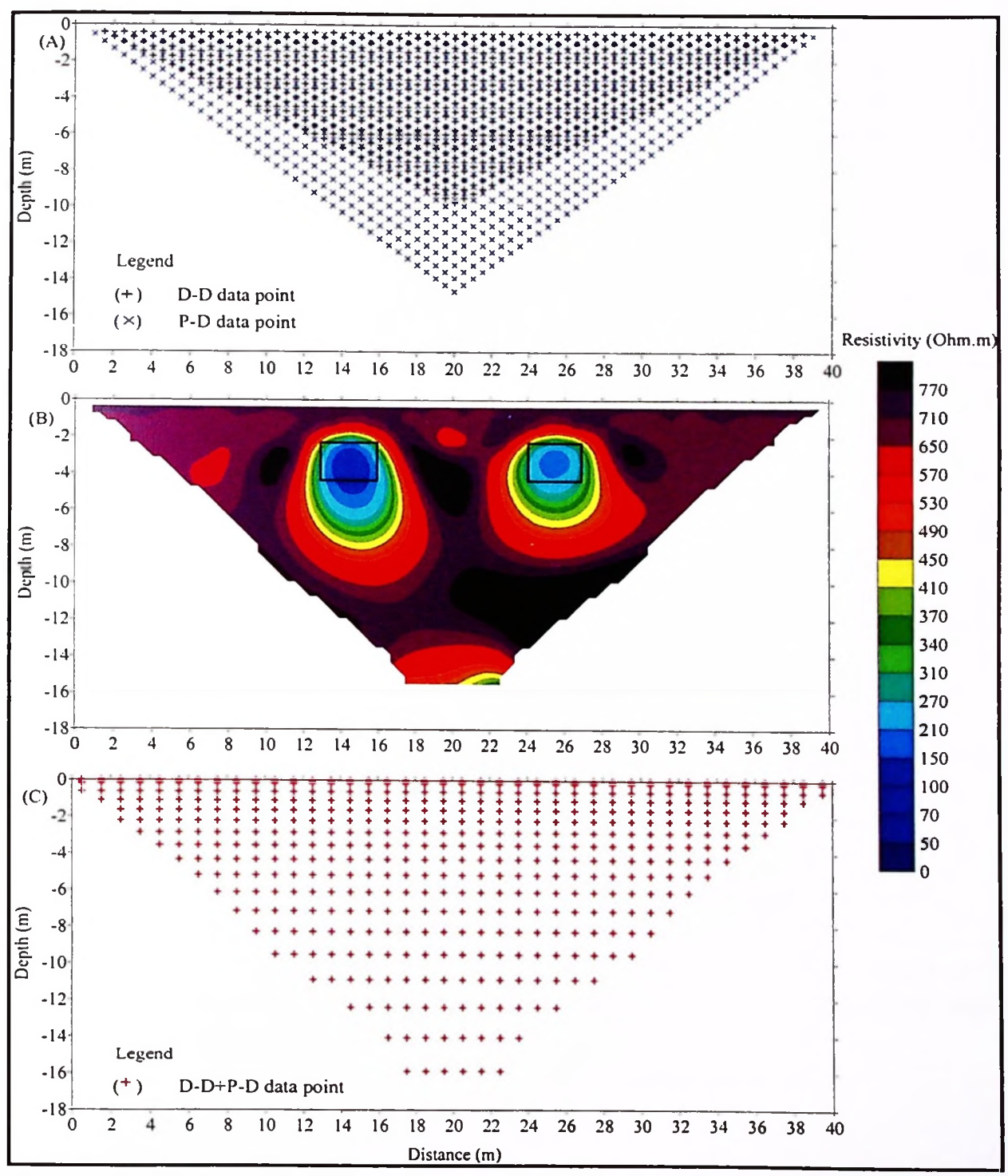


Figure 4.15: The two blocks model results given by the DLA technique of (D-D+P-D) arrays. A) Apparent resistivity data points arrangement. B) 2-D resistivity model result and C) Model resistivity data points.

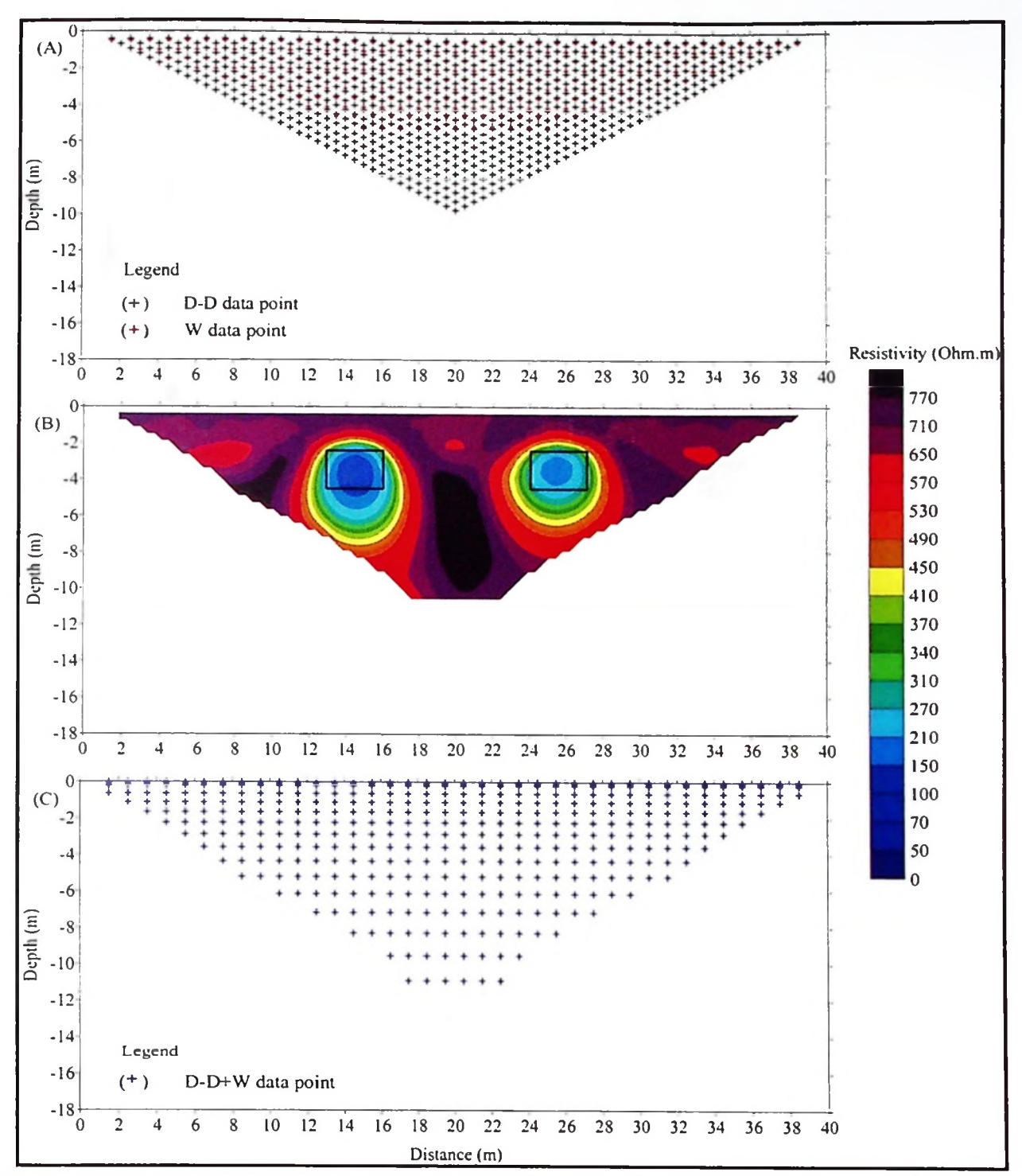


Figure 4.16: The two blocks model results given by the DLA technique of (D-D+W) arrays. A) Apparent resistivity data points arrangement. B) 2-D resistivity model result and C) Model resistivity data points.

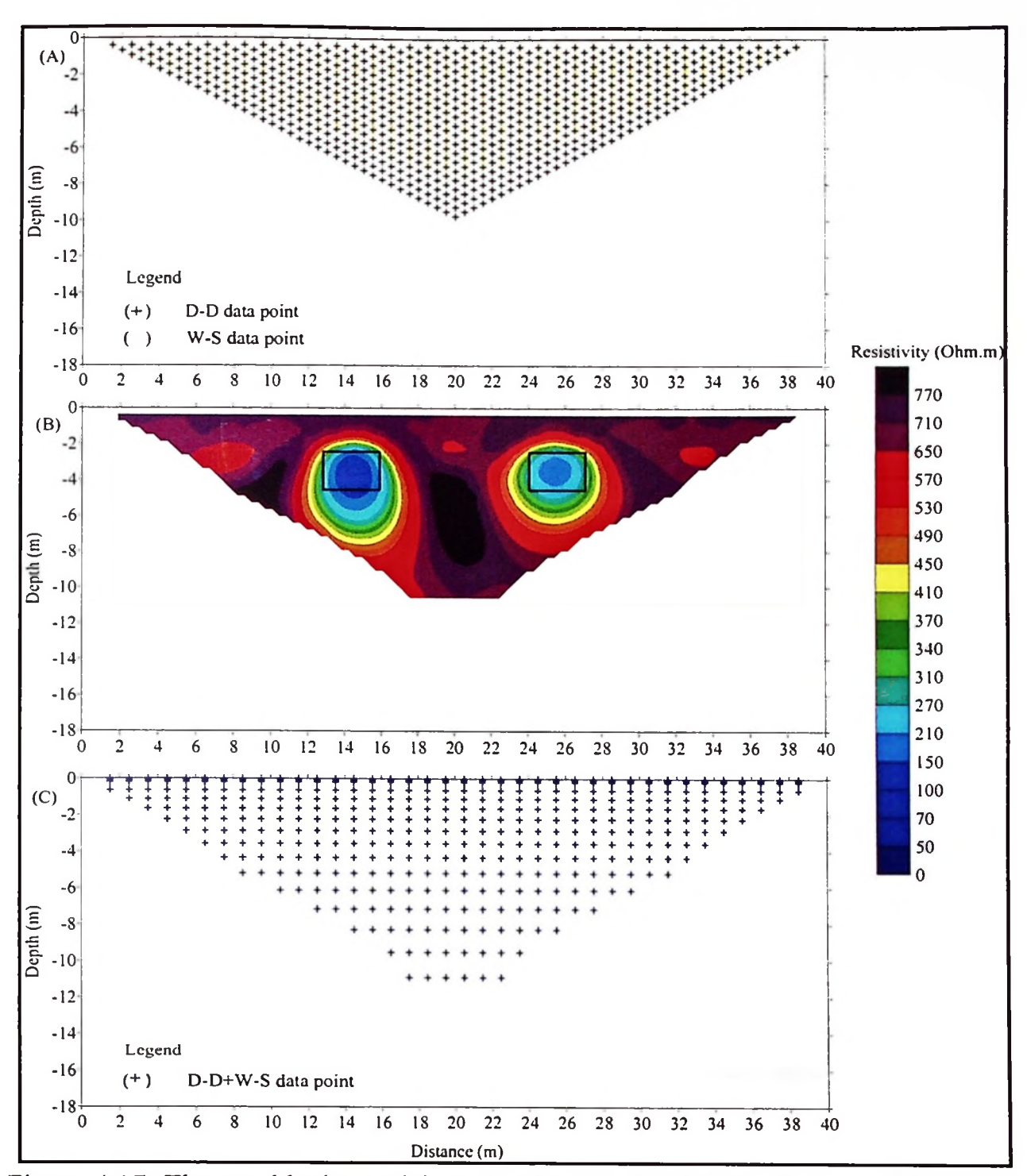


Figure 4.17: The two blocks model results given by the DLA technique of (D-D+W-S) arrays. A) Apparent resistivity data points arrangement. B) 2-D resistivity model result and C) Model resistivity data points.

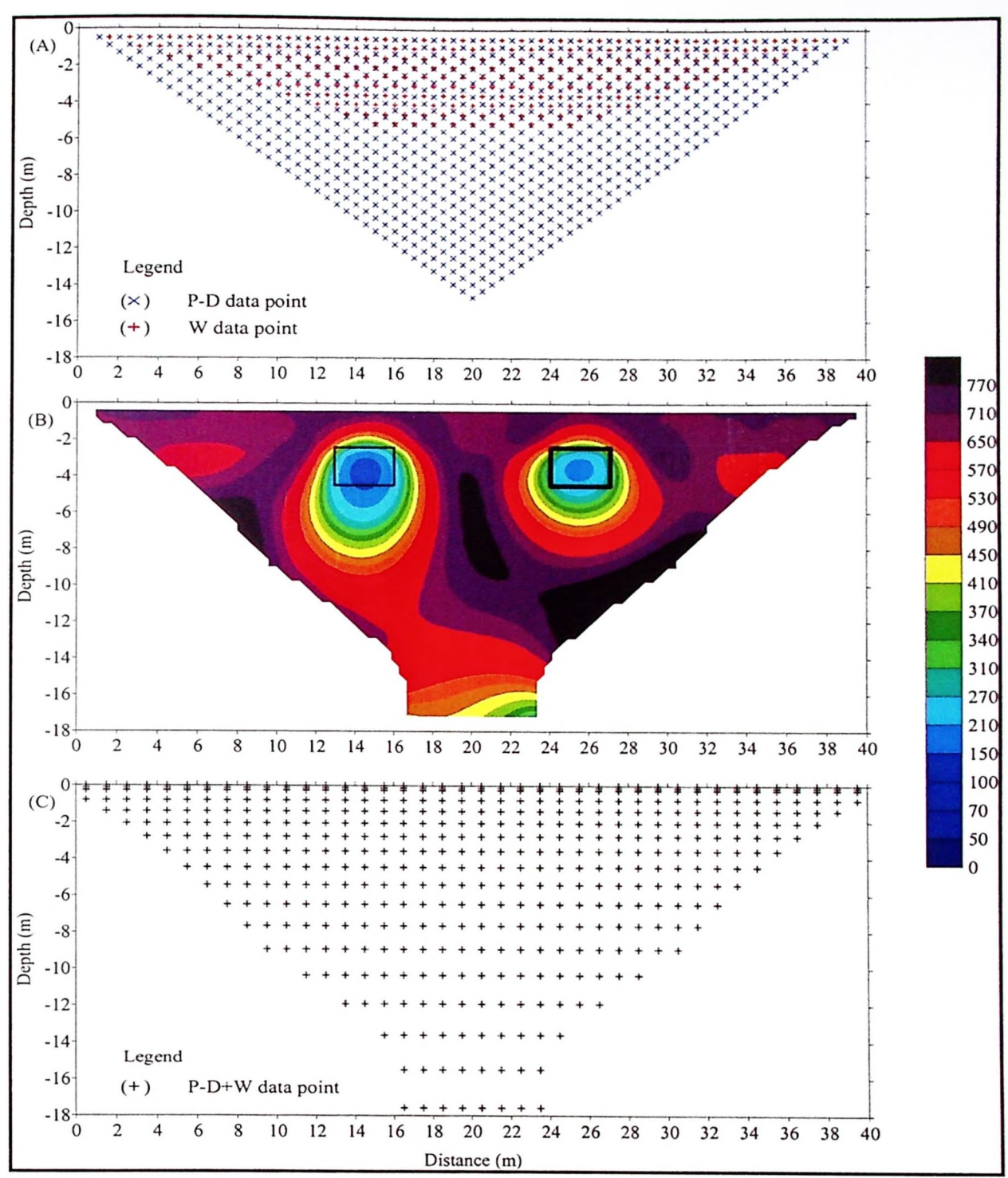


Figure 4.18: The two blocks model results given by the DLA technique of (P-D+W) arrays. A) Apparent resistivity data points arrangement. B) 2-D resistivity model result and C) Model resistivity data points.

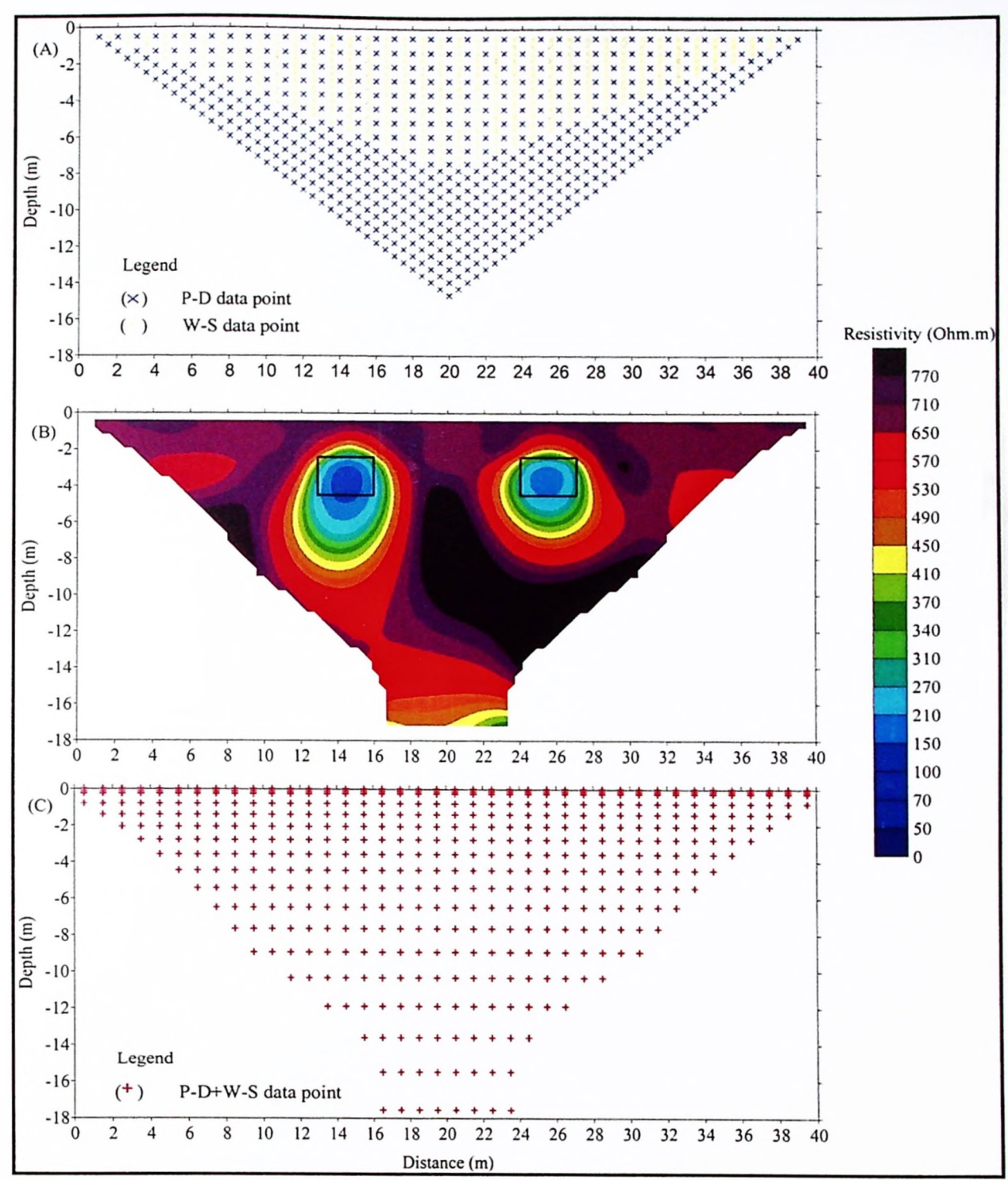


Figure 4.19: The two blocks model results given by the DLA technique of (P-D+W-S) arrays. A) Apparent resistivity data points arrangement. B) 2-D resistivity model result and C) Model resistivity data points.

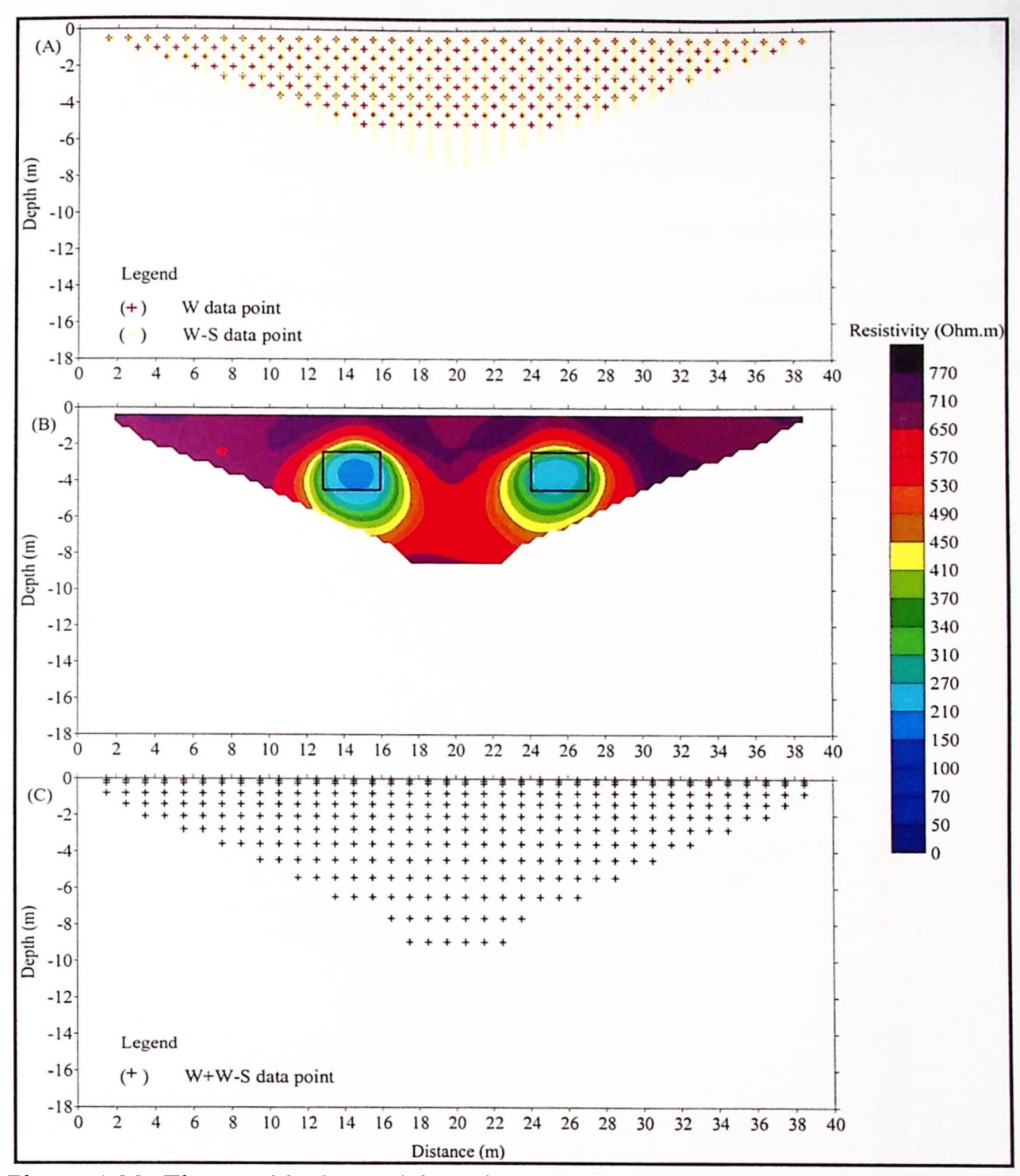


Figure 4.20: The two blocks model results given by the DLA technique of (W+W-S) arrays. A) Apparent resistivity data points arrangement. B) 2-D resistivity model result and C) Model resistivity data points.

## 4.1.3 Contact zone model

Some 2-D resistivity imaging results for the individual array data sets recover the targets of the contact zone images as shown in Figures 4.21 until 4.24. From the

results, it shows that the contact zone (100  $\Omega$ .m) images are fairly well resolved by D-D array with acceptable shape and right resistivity value. However, P-D, W, and W-S arrays are only able to resolve image of the contact zone with moderate results. The results show that these three arrays able to give right resistivity of the contact zone. However the bottom part of the contact zone is not imaged well enough. The reason is because these three arrays is less sensitive to resistivity changes (Loke, 2004; 2014).

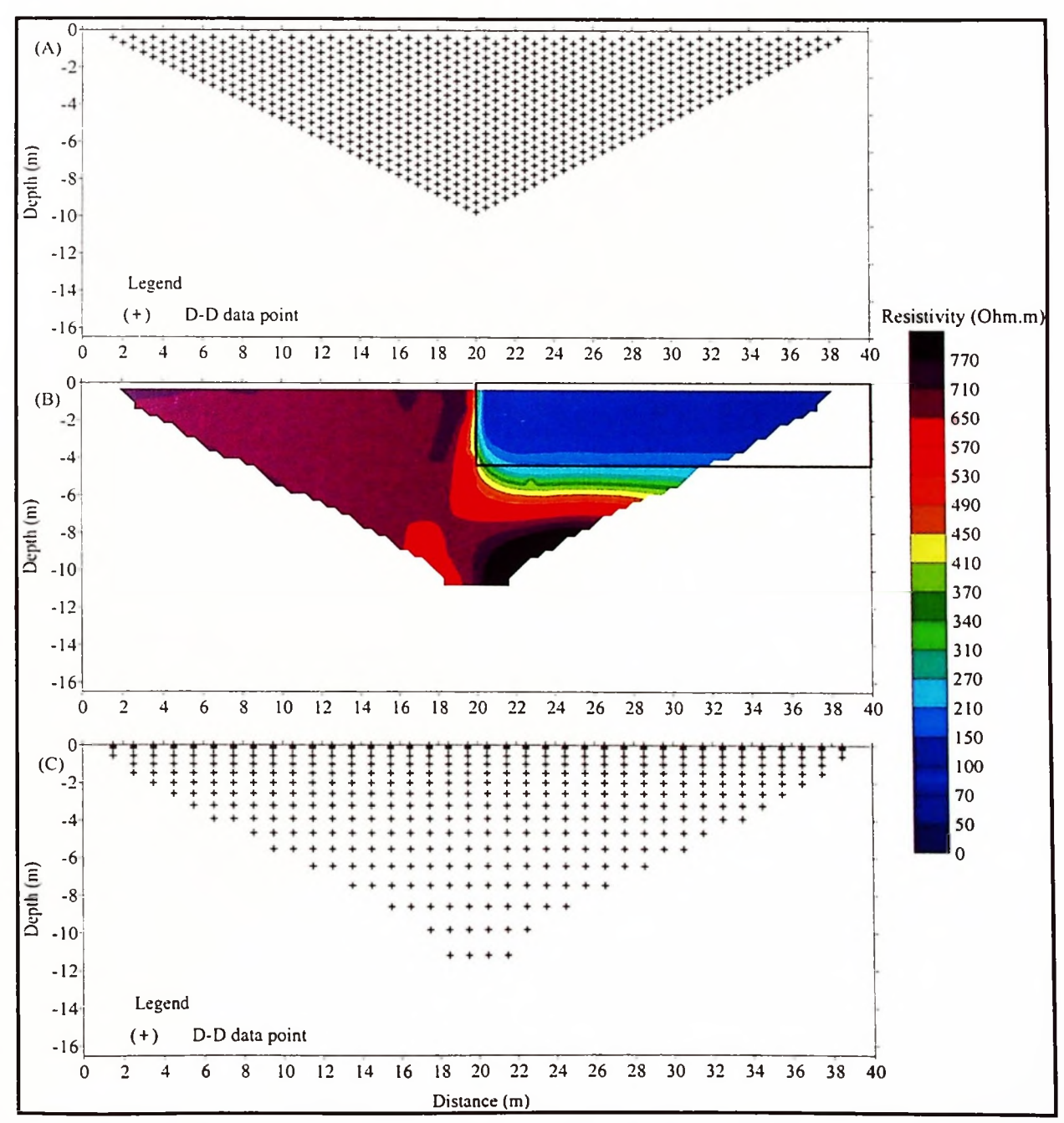


Figure 4.21: The contact zone model results given by D-D array. A) Apparent resistivity data points arrangement. B) 2-D resistivity model result and C) Model resistivity data points.

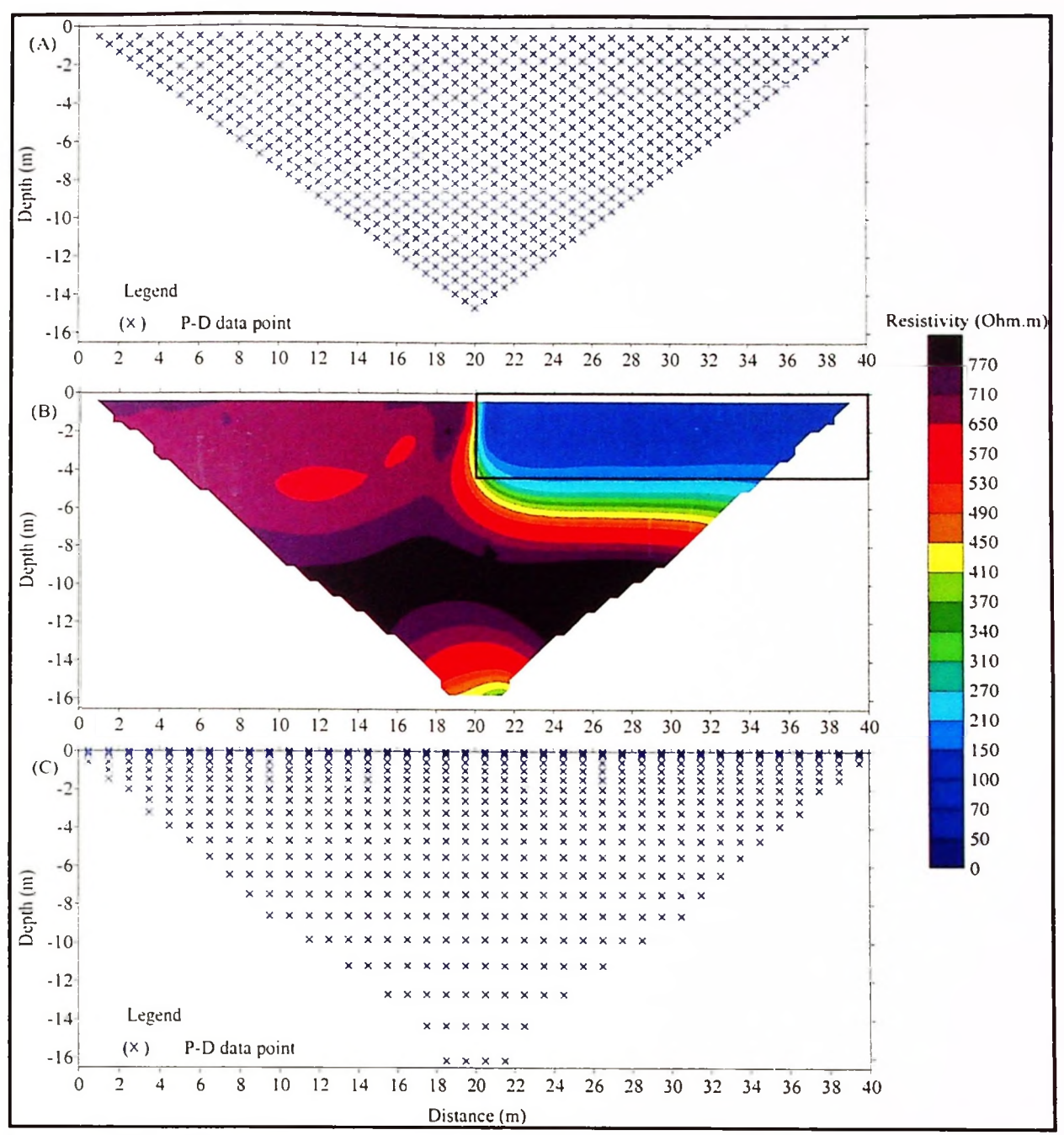


Figure 4.22: The contact zone model results given by P-D array. A) Apparent resistivity data points arrangement. B) 2-D resistivity model result and C) Model resistivity data points.

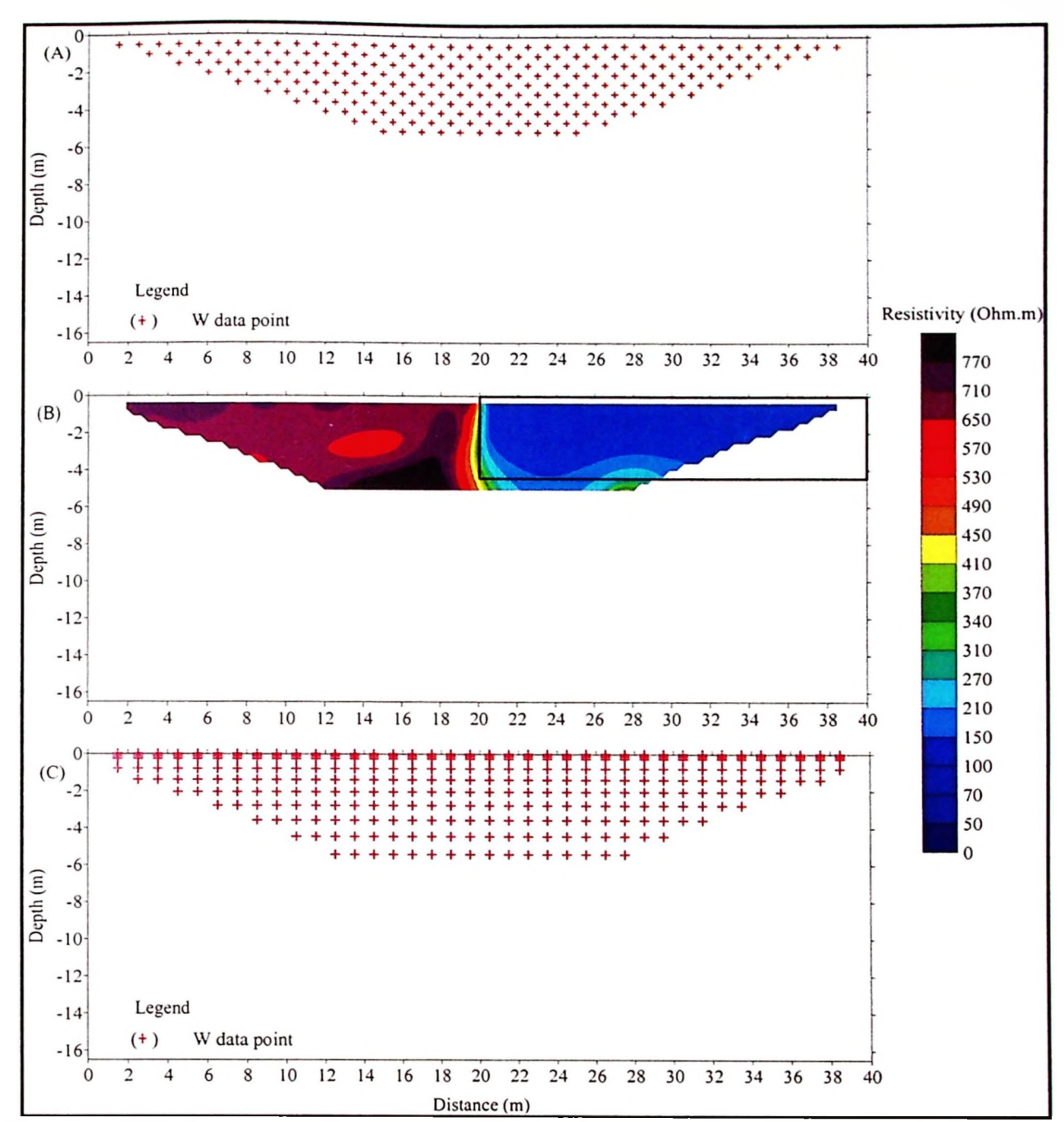


Figure 4.23: The contact zone model results given by W array. A) Apparent resistivity data points arrangement. B) 2-D resistivity model result and C) Model resistivity data points.

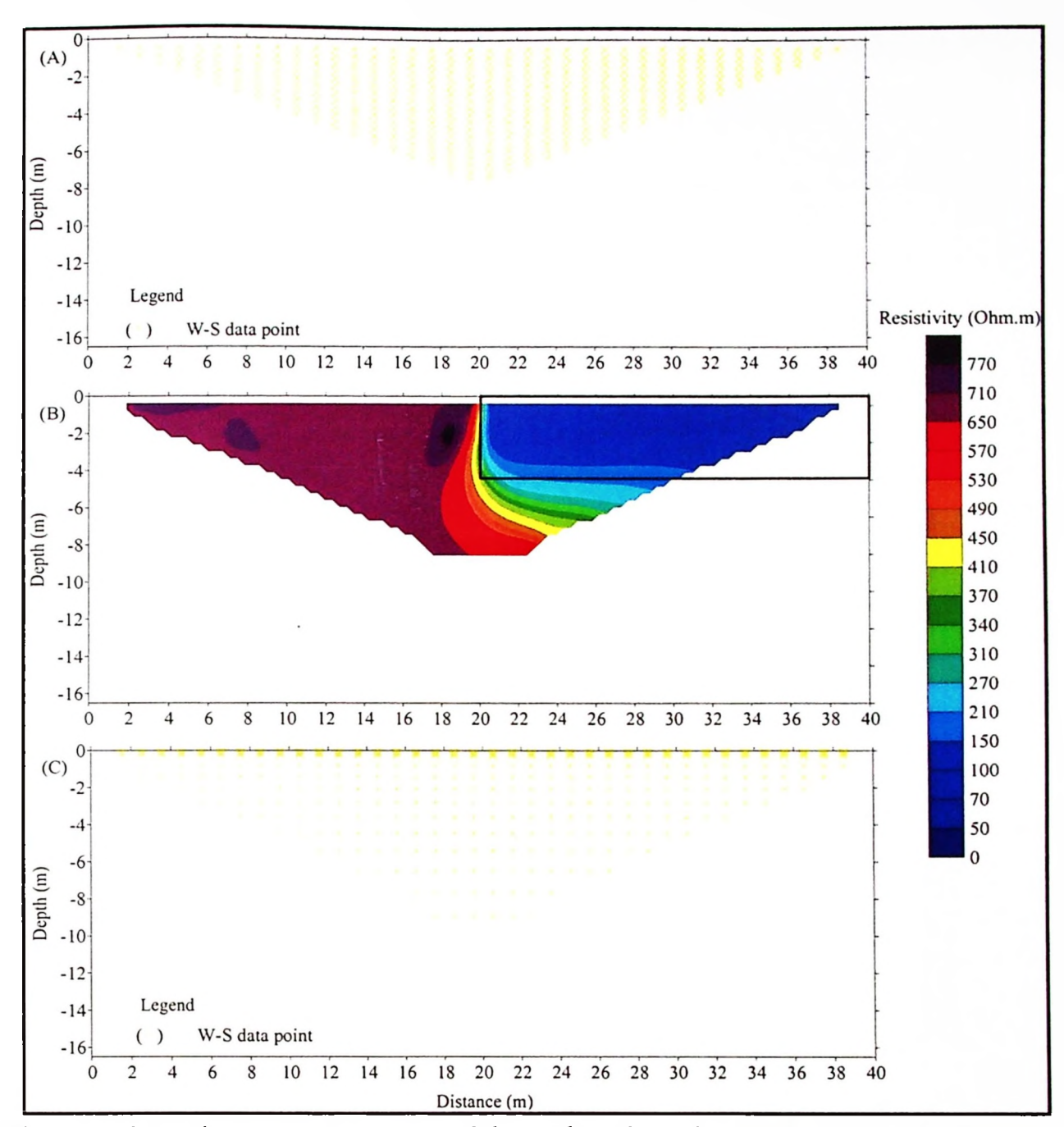


Figure 4.24: The contact zone model results given by W-S array. A) Apparent resistivity data points arrangement. B) 2-D resistivity model result and C) Model resistivity data points.

All of the 2-D resistivity imaging results for the DLA technique data sets recover the target of contact zone (100  $\Omega$ .m) as shown in Figures 4.25 until 4.30. From the results, it shows that the contact zone is resolved with good results by all models using the DLA technique (D-D+P-D, D-D+W, D-D+W-S, P-D+W, P-D+W-

S and W+W-S). All of the DLA models are able to image the contact zone with the acceptable shape and the right resistivity value.

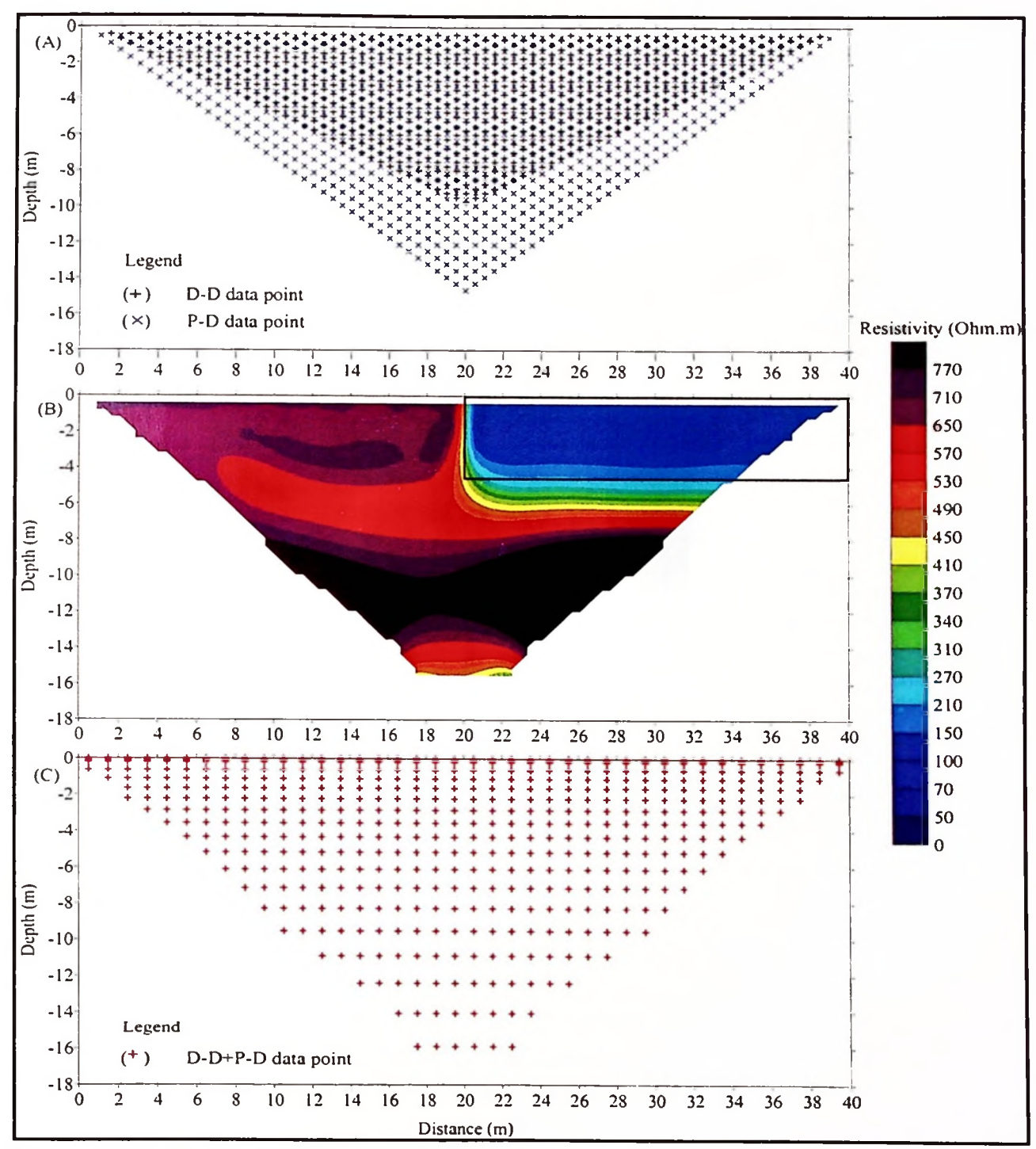


Figure 4.25: The contact zone model results given by the DLA technique of (D-D+P-D) arrays. A) Apparent resistivity data points arrangement. B) 2-D resistivity model result and C) Model resistivity data points.

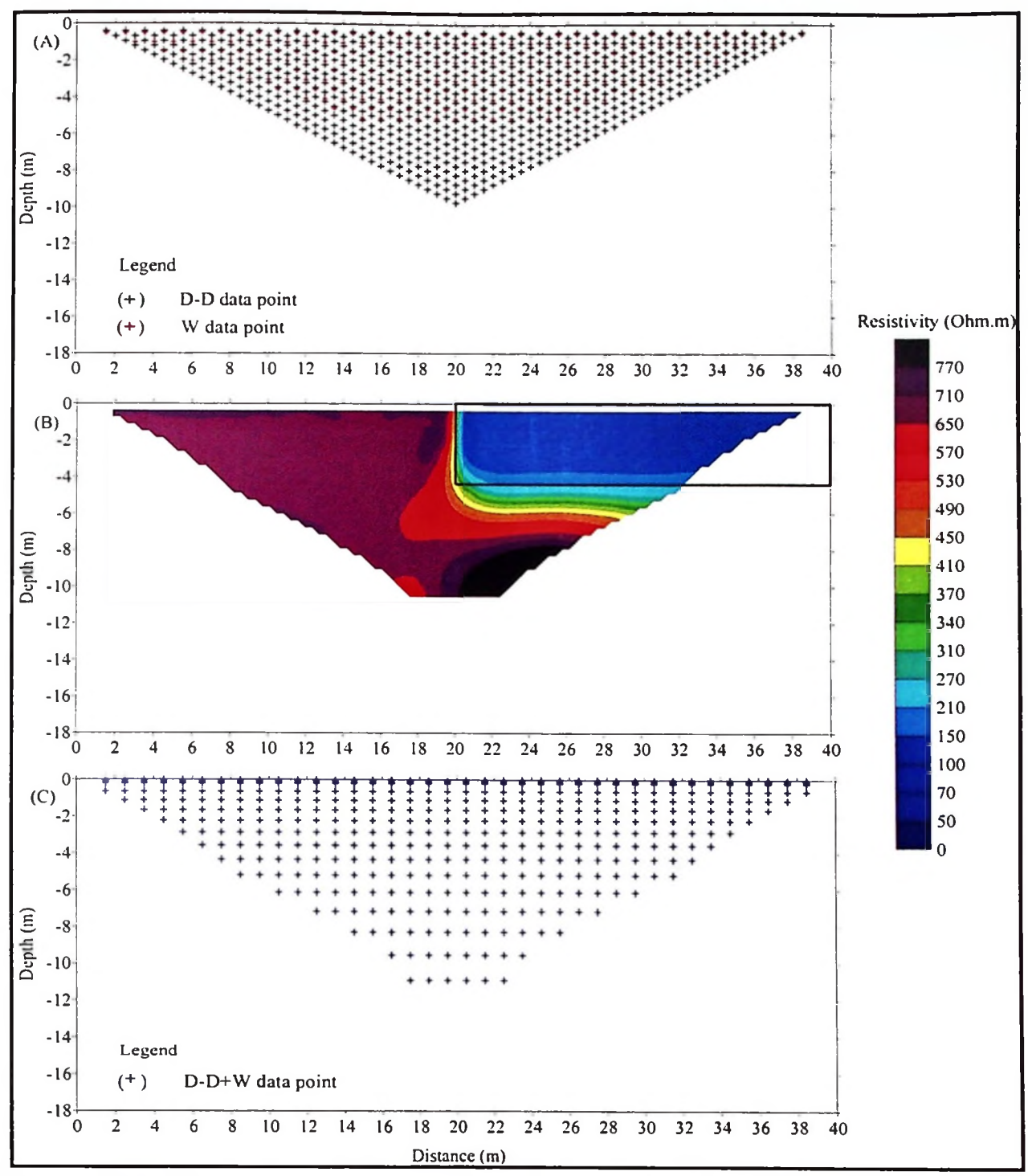


Figure 4.26: The contact zone model results given by the DLA technique of (D-D+W) arrays. A) Apparent resistivity data points arrangement. B) 2-D resistivity model result and C) Model resistivity data points.

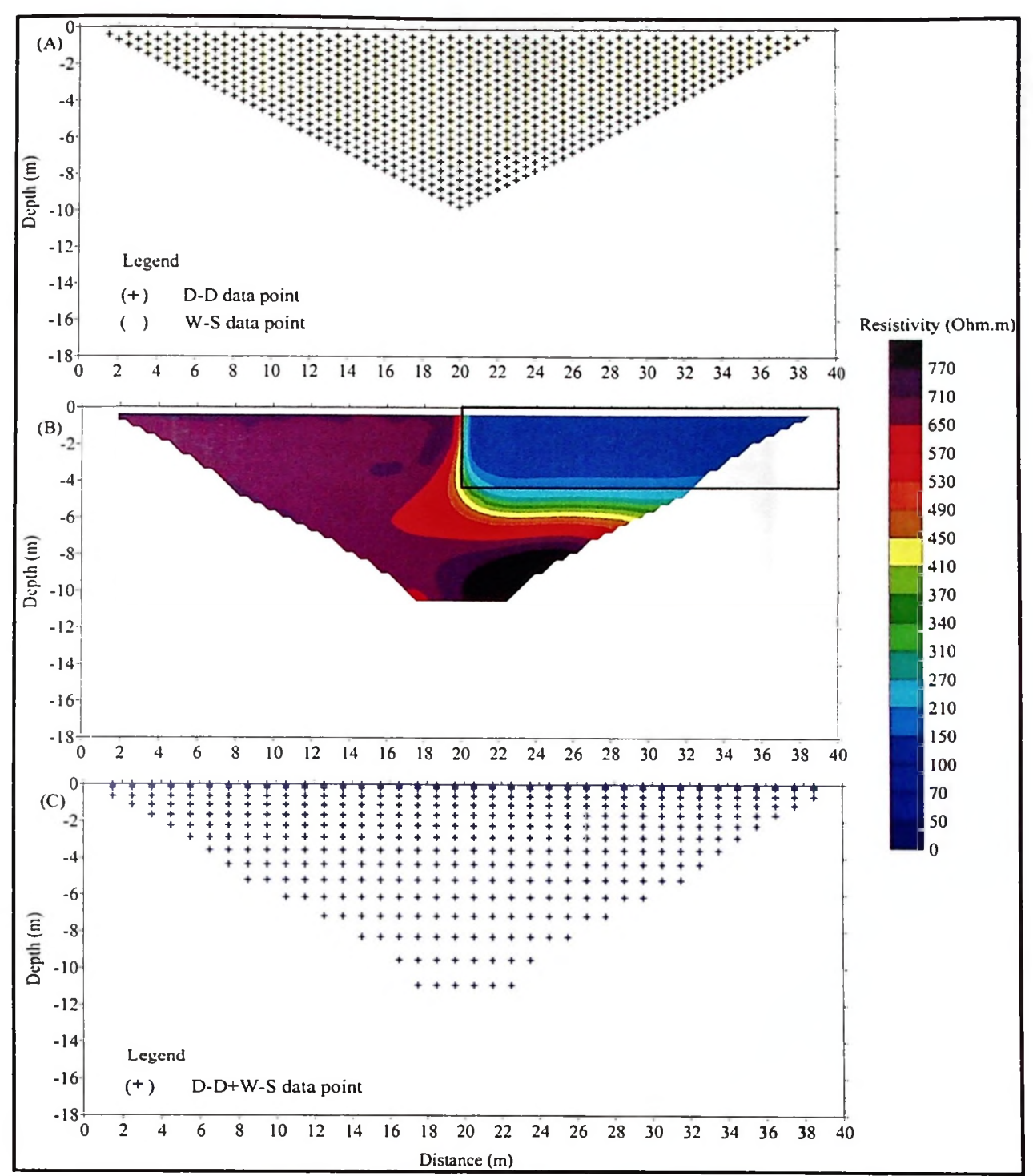


Figure 4.27: The contact zone model results given by the DLA technique of (D-D+W-S) arrays. A) Apparent resistivity data points arrangement. B) 2-D resistivity model result and C) Model resistivity data points.

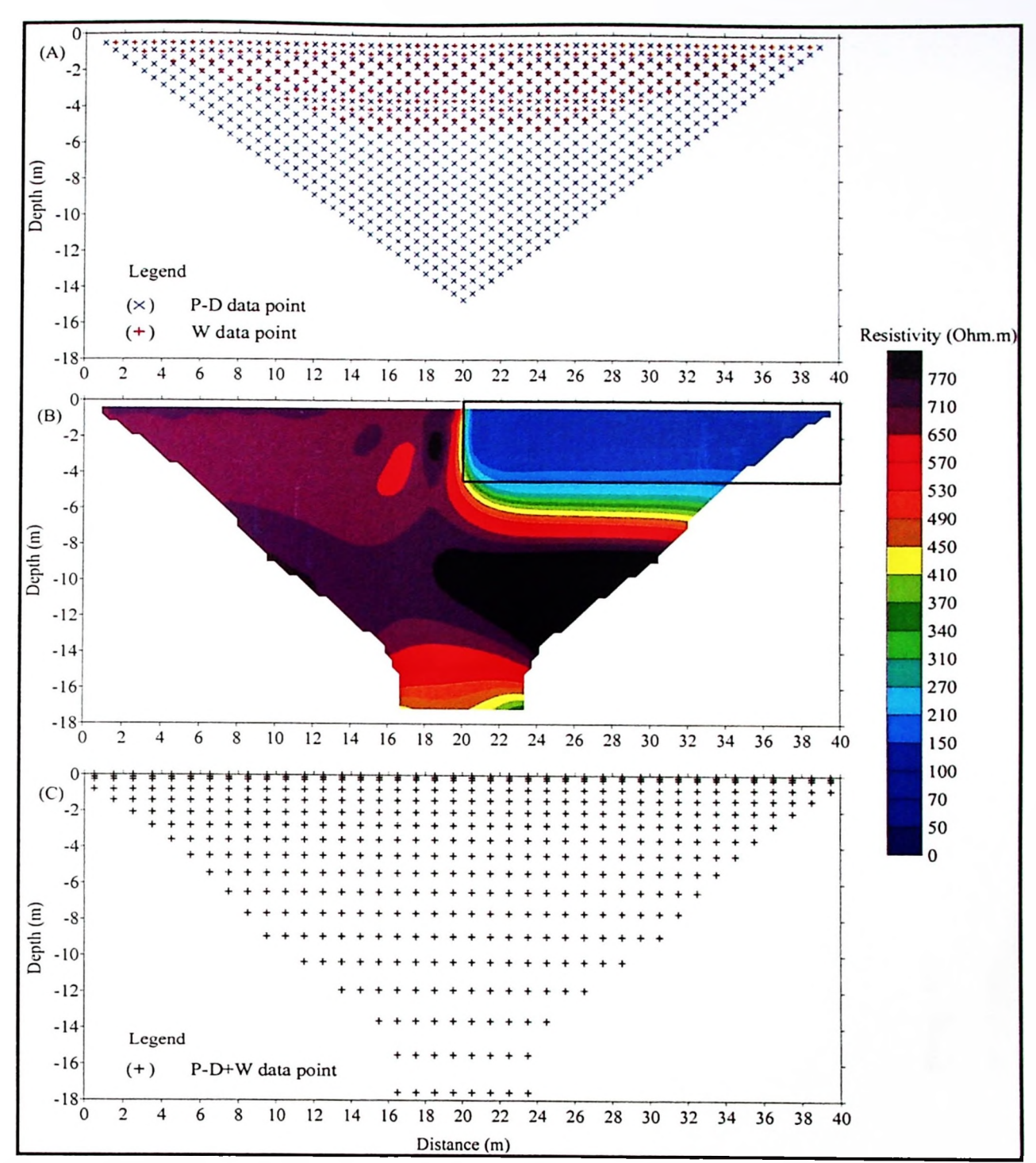


Figure 4.28: The contact zone model results given by the DLA technique of (P-D+W) arrays. A) Apparent resistivity data points arrangement. B) 2-D resistivity model result and C) Model resistivity data points.

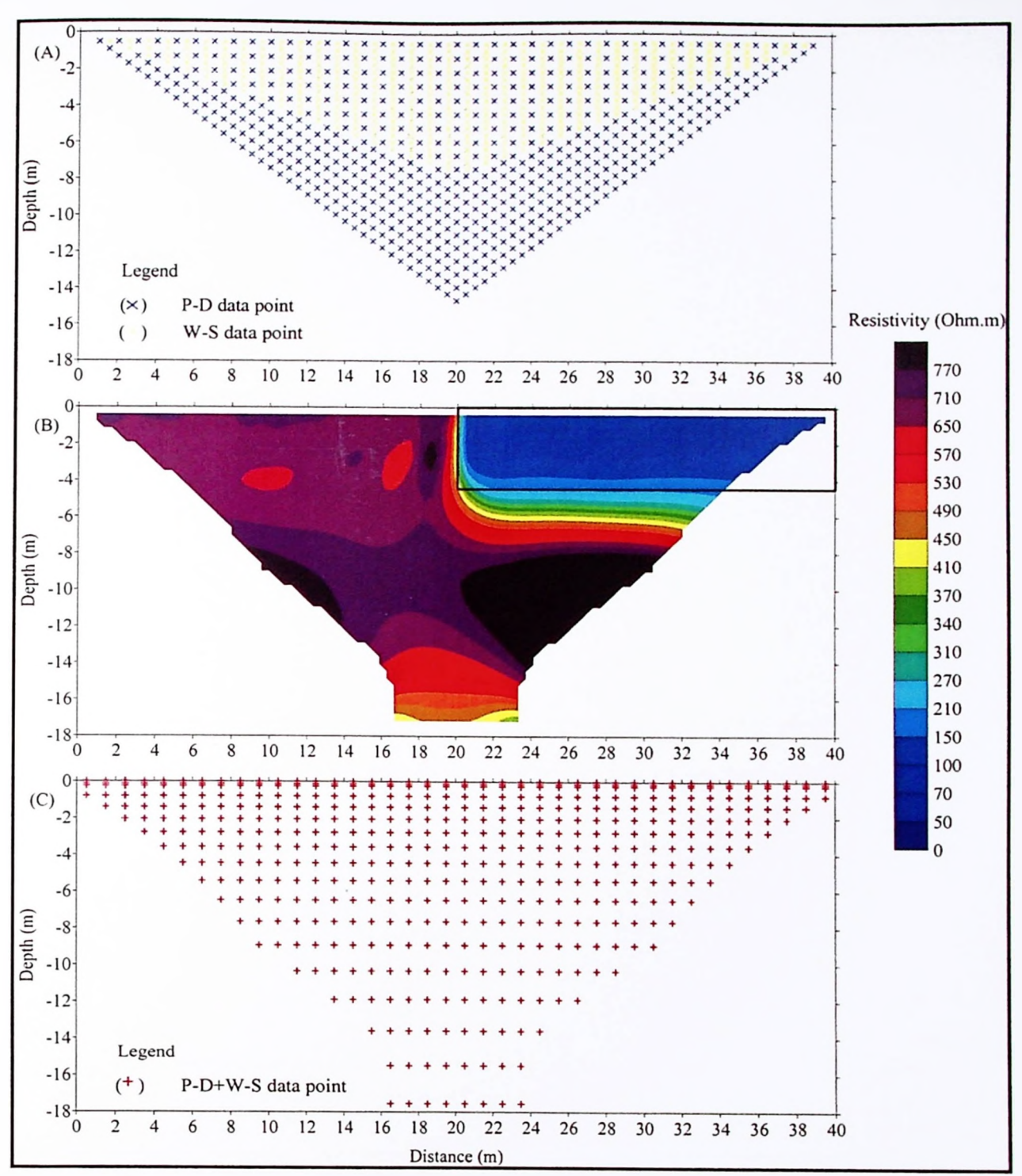


Figure 4.29: The contact zone model results given by the DLA technique of (P-D+W-S) arrays. A) Apparent resistivity data points arrangement. B) 2-D resistivity model result and C) Model resistivity data points.

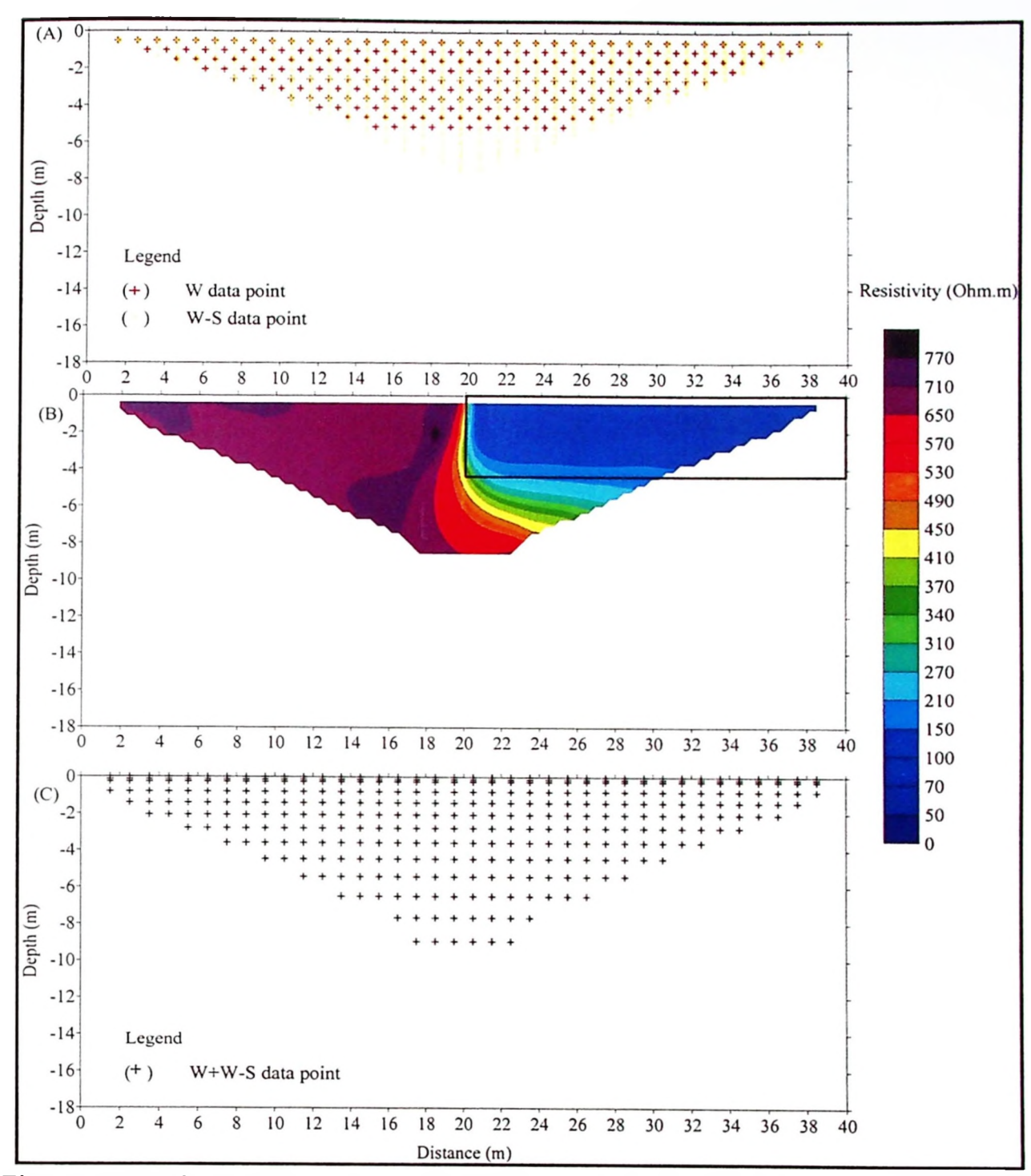


Figure 4.30: The contact zone model results given by the DLA technique of (W+W-S) arrays. A) Apparent resistivity data points arrangement. B) 2-D resistivity model result and C) Model resistivity data points.

## 4.1.4 Vertical dyke model

Some 2-D resistivity imaging results for individual array data sets recover the targets of the vertical dyke images as shown in Figures 4.31 until 4.34. From the

results, it shows that the vertical dyke (70  $\Omega$ .m) images are fairly well resolved by these three arrays only (D-D, P-D and W) with right shape and right resistivity value. However, W-S array is able to resolve image of the fault with moderate results. W-S array is able to image the vertical dyke with right resistivity value. However, the vertical extension of the fault is not imaged with well enough. The reason is because W-S array has moderate sensitivity to resistivity horizontal changes (structure of the vertical dyke) (Loke, 2004; 2014).

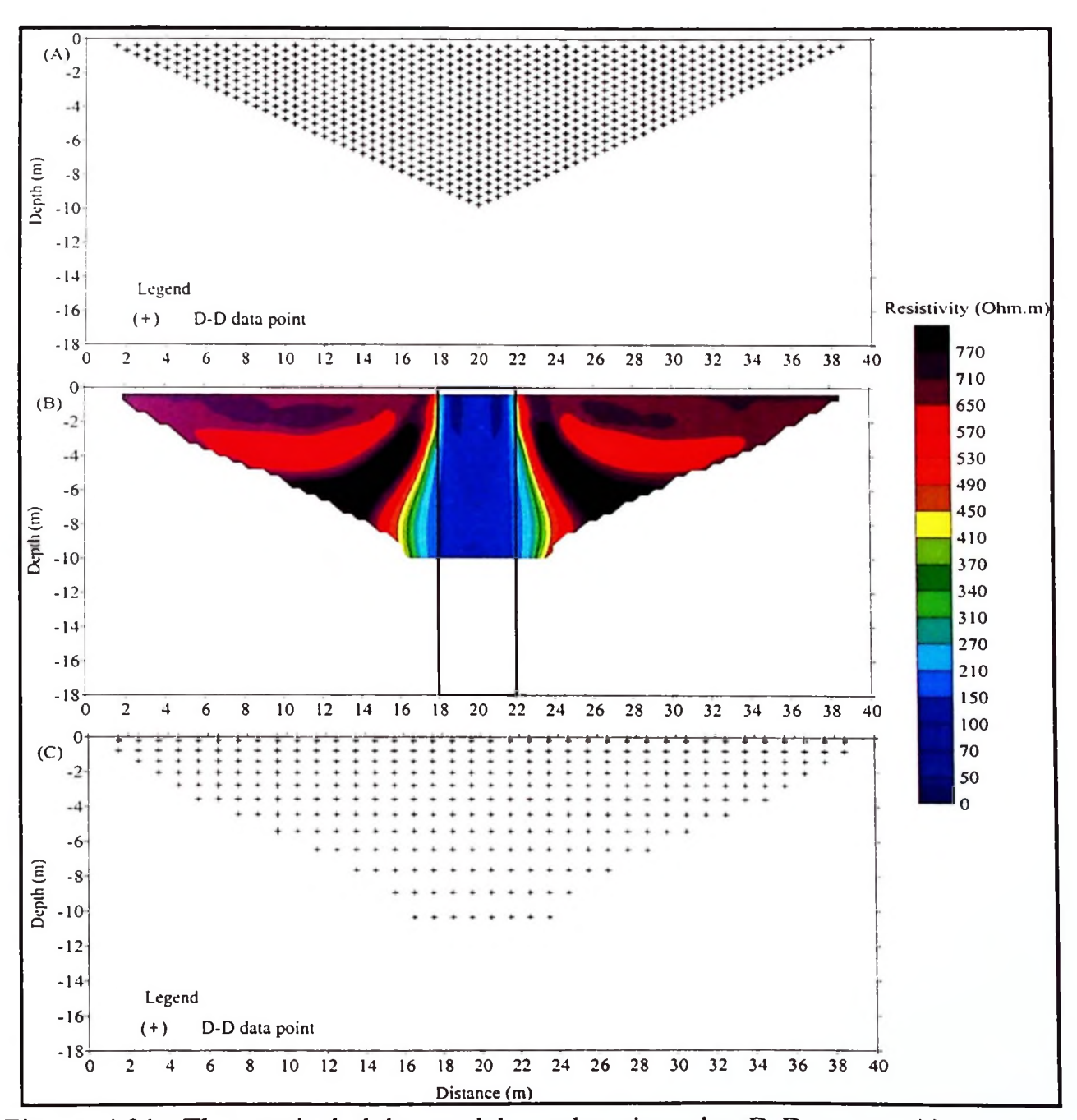


Figure 4.31: The vertical dyke model results given by D-D array. A) Apparent resistivity data points arrangement. B) 2-D resistivity model result and C) Model resistivity data points.

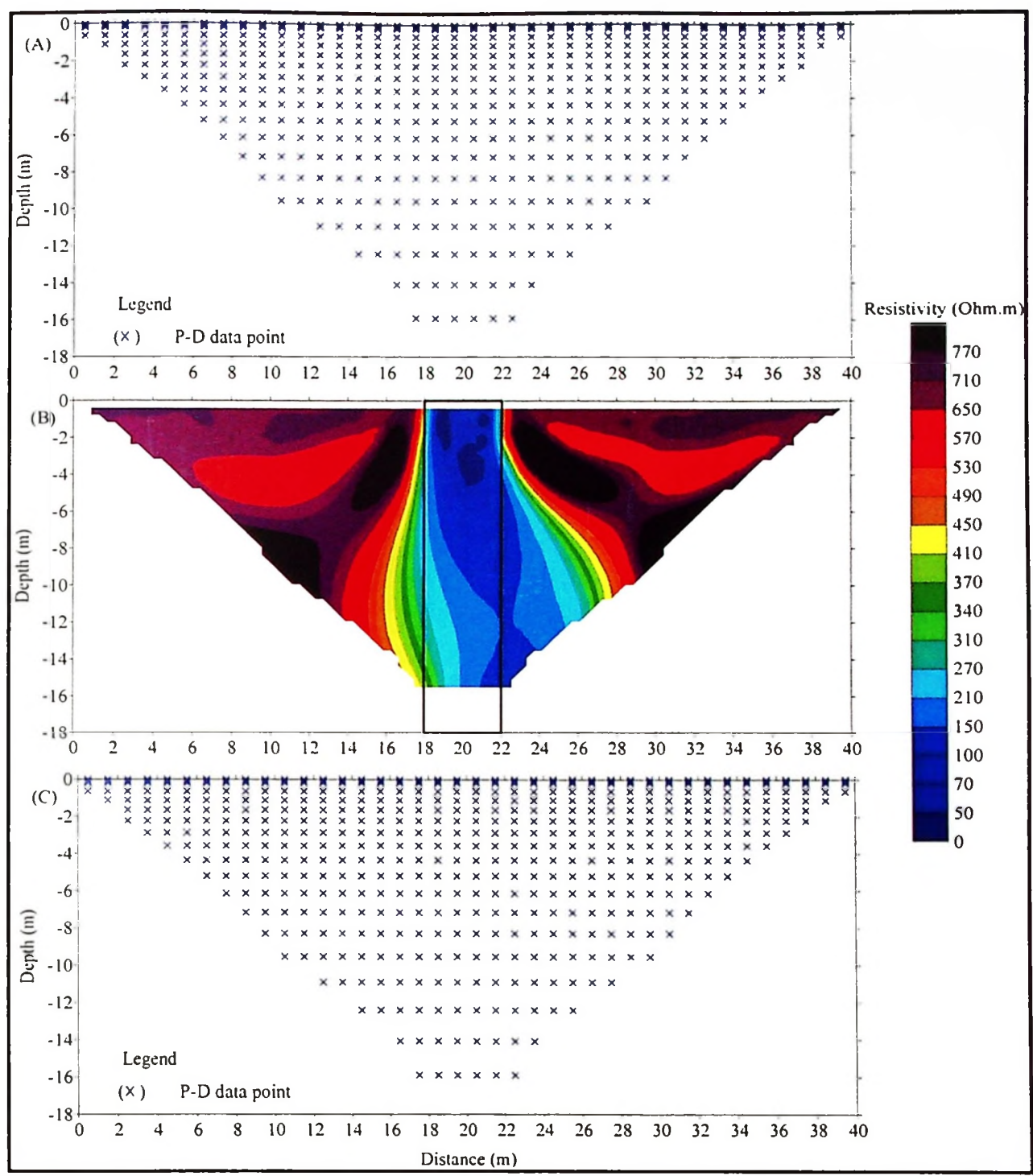


Figure 4.32: The vertical dyke model results given by P-D array. A) Apparent resistivity data points arrangement. B) 2-D resistivity model result and C) Model resistivity data points.

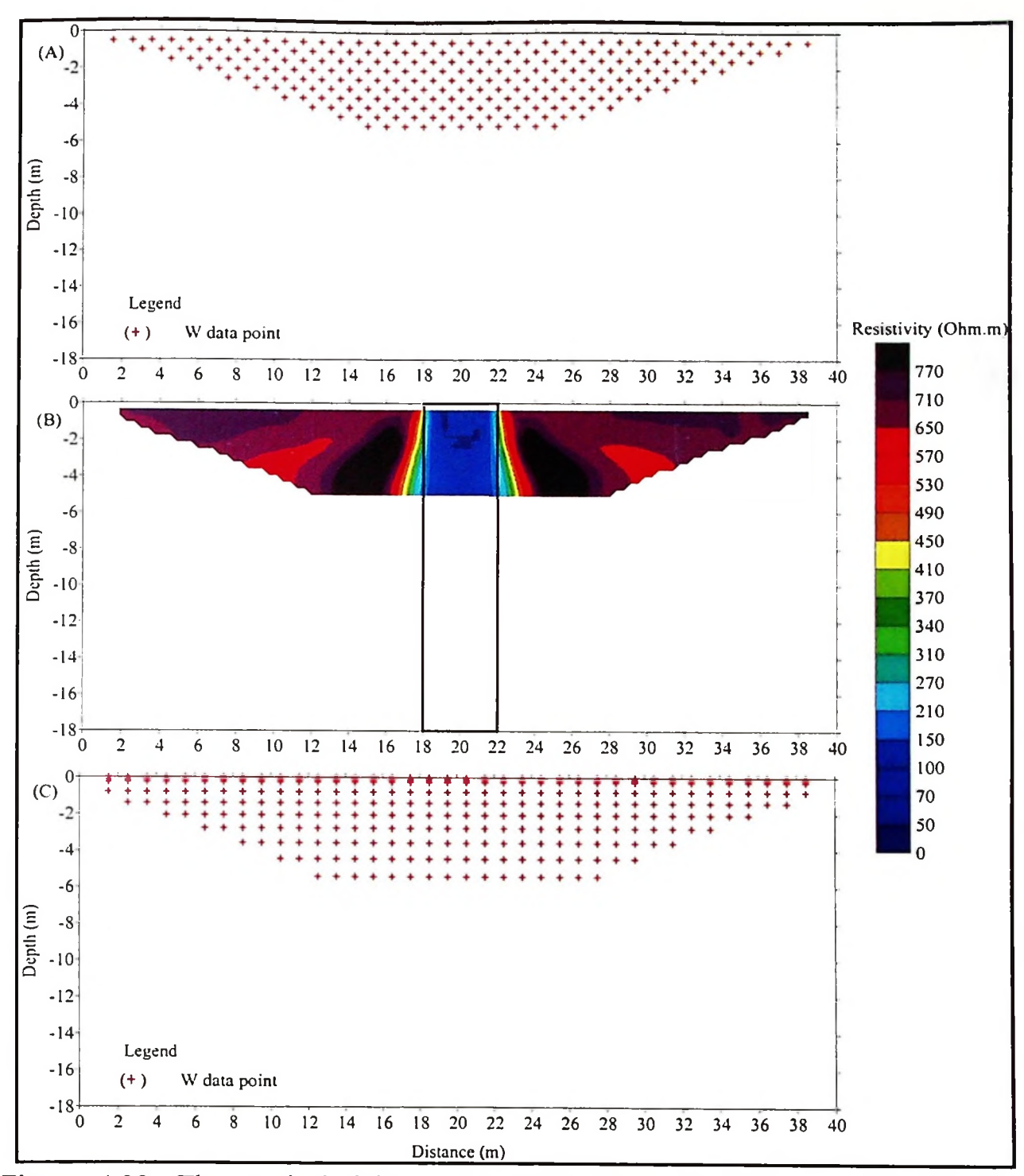


Figure 4.33: The vertical dyke model results given by W array. A) Apparent resistivity data points arrangement. B) 2-D resistivity model result and C) Model resistivity data points.

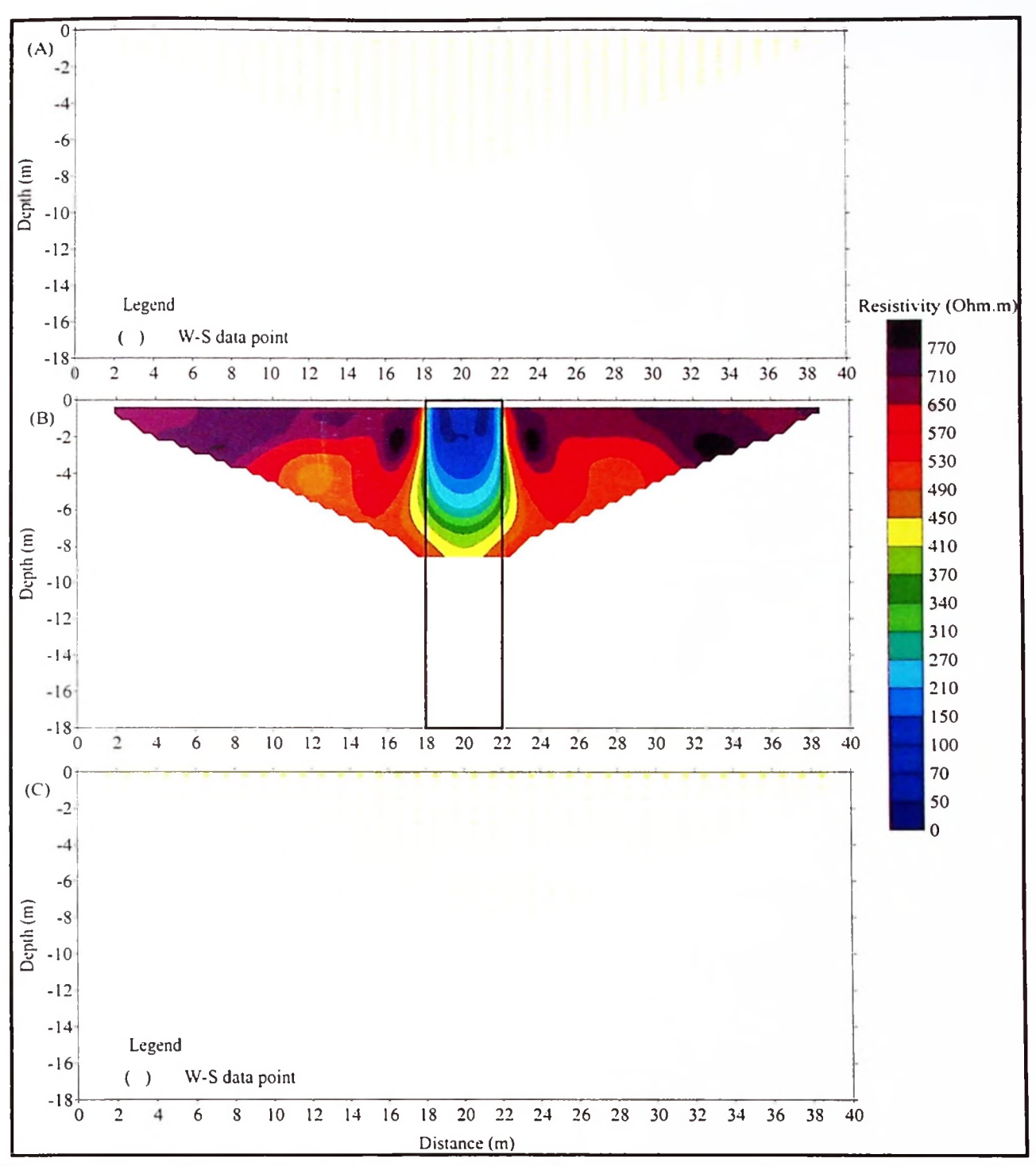


Figure 4.34: The vertical dyke model results given by W-S array. A) Apparent resistivity data points arrangement. B) 2-D resistivity model result and C) Model resistivity data points.

All of the 2-D resistivity imaging results for the DLA technique data sets recover the target of vertical dyke (70  $\Omega$ .m) as shown in Figures 4.35 until 4.40. From the results, it shows that the vertical dyke is resolved well by all the models using the DLA technique (D-D+P-D, D-D+W, D-D+W-S, P-D+W, P-D+W-S and

W+W-S). All of the models of the DLA technique are able to image the vertical dyke with the acceptable shape and the right resistivity value.

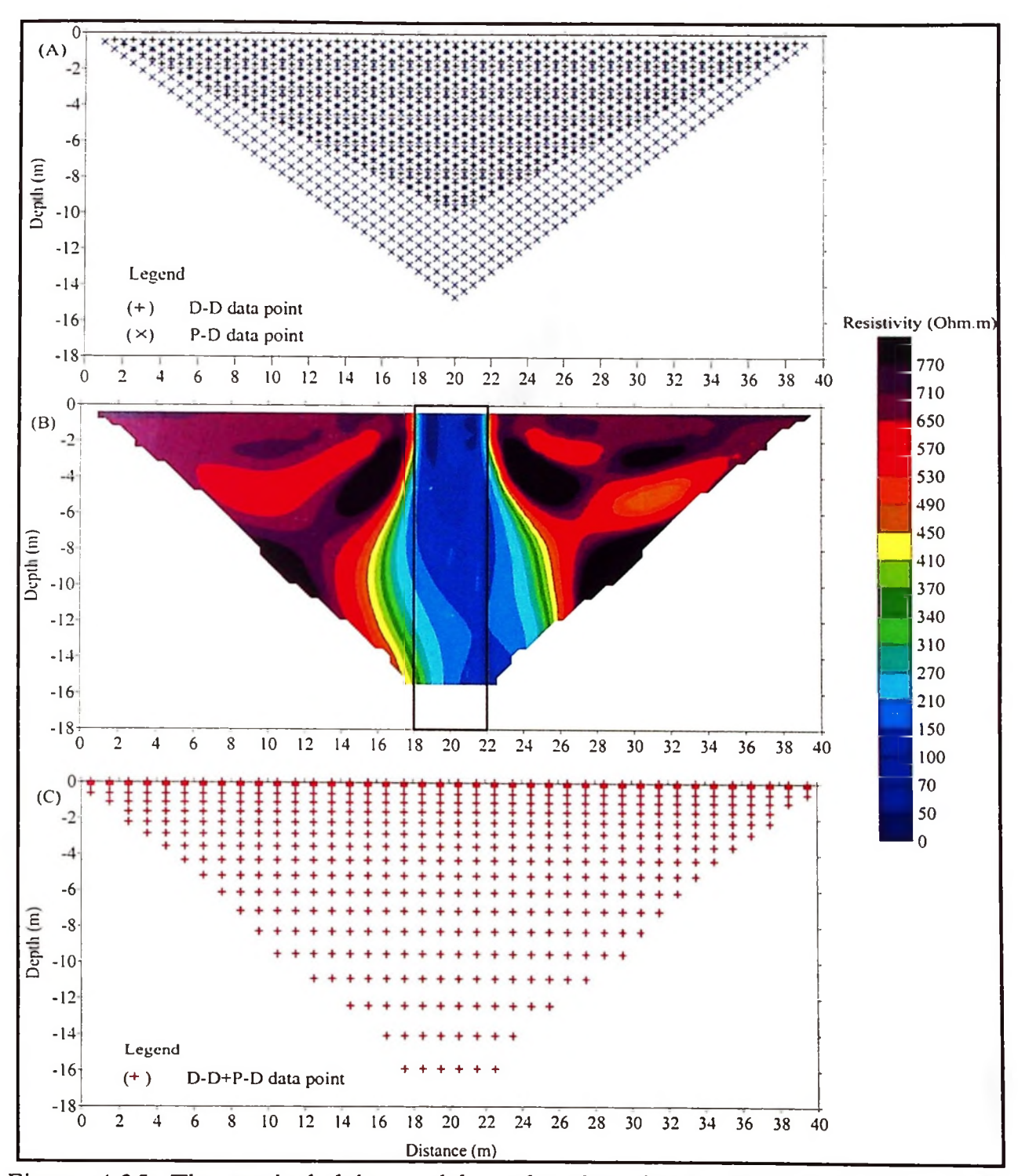


Figure 4.35: The vertical dyke model results given by the DLA technique of (D-D+P-D) arrays. A) Apparent resistivity data points arrangement. B) 2-D resistivity model result and C) Model resistivity data points.

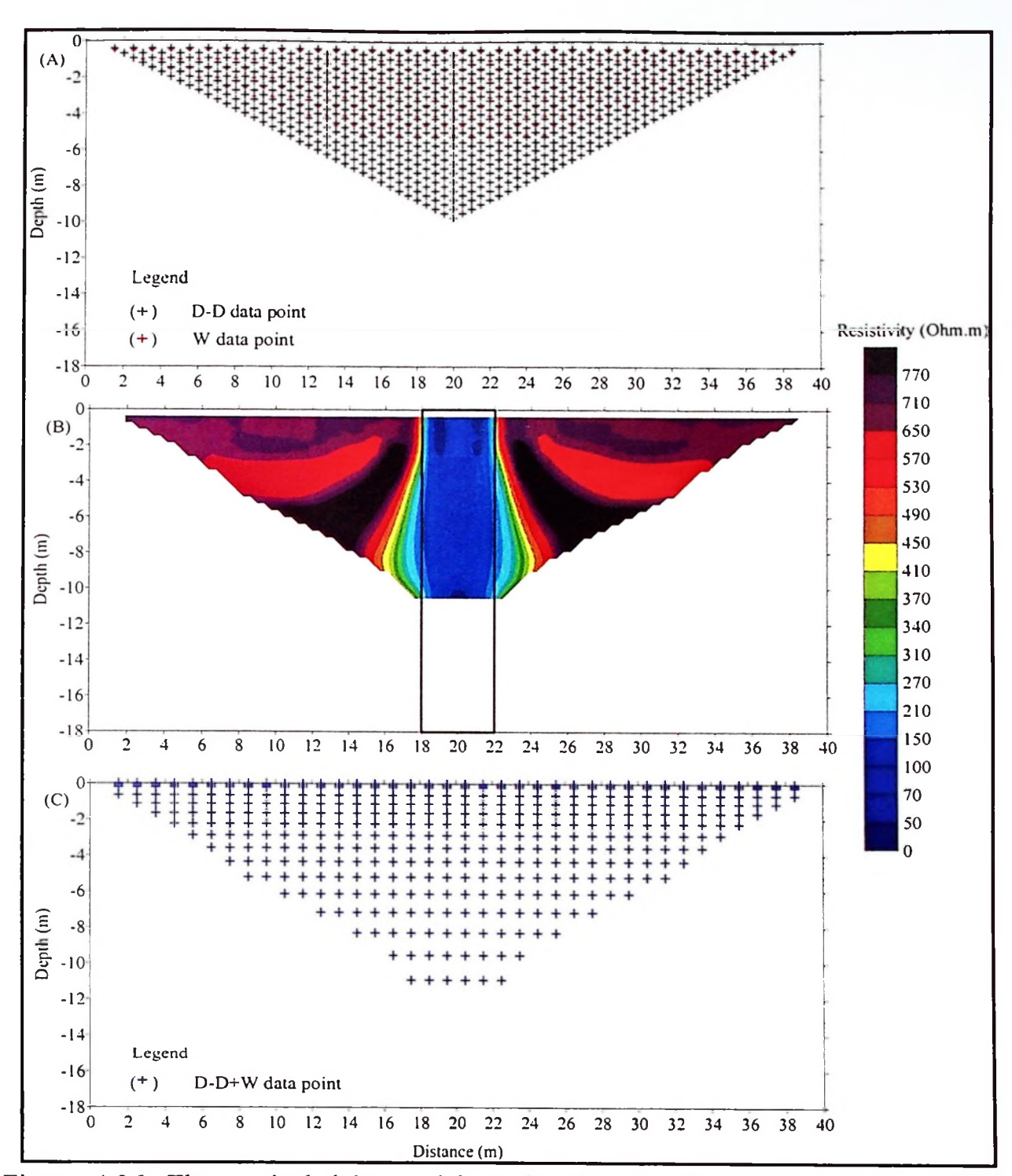


Figure 4.36: The vertical dyke model results given by the DLA technique of (D-D+W) arrays. A) Apparent resistivity data points arrangement. B) 2-D resistivity model result and C) Model resistivity data points.

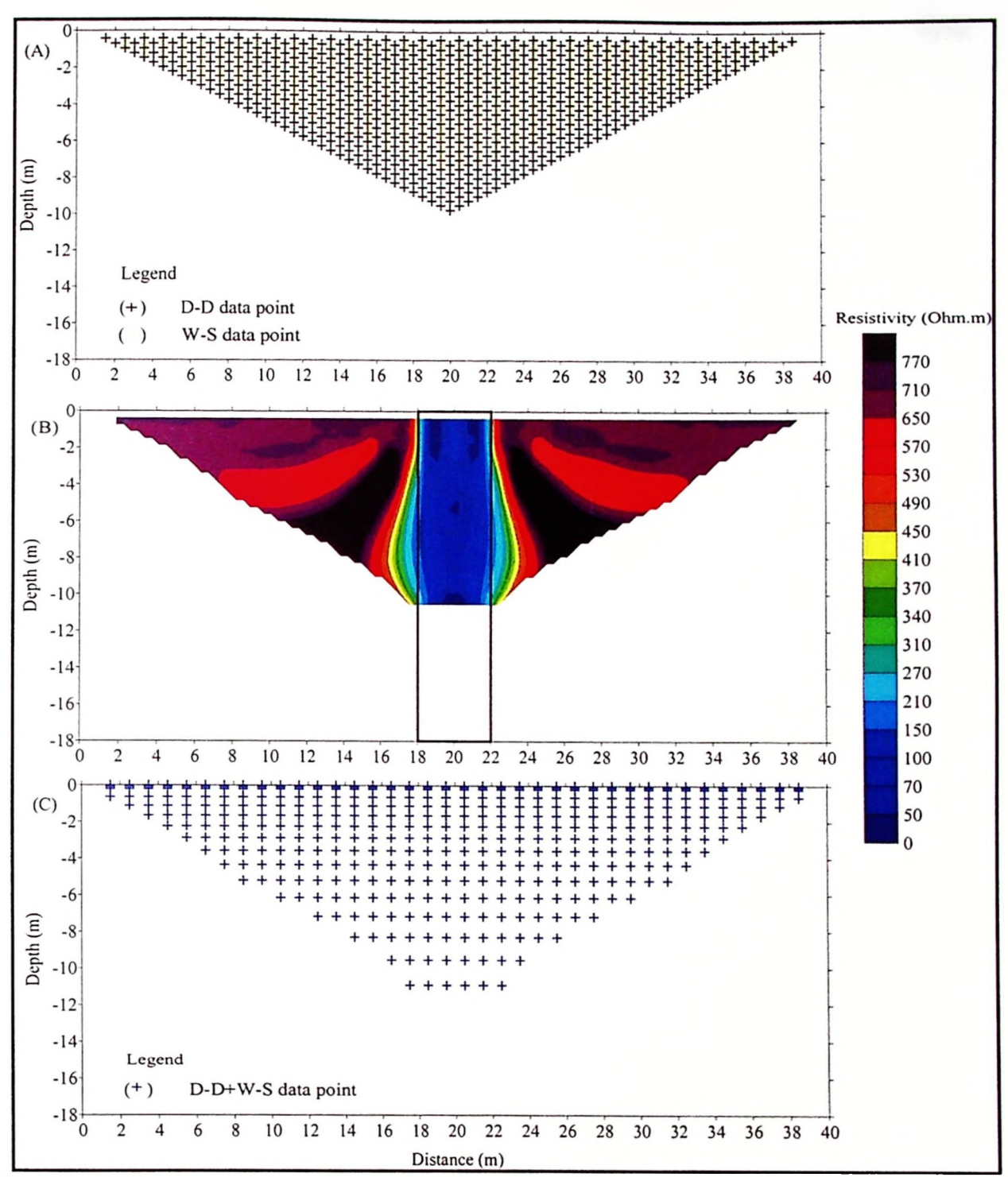


Figure 4.37: The vertical dyke model results given by the DLA technique of (D-D+W-S) arrays. A) Apparent resistivity data points arrangement. B) 2-D resistivity model result and C) Model resistivity data points.

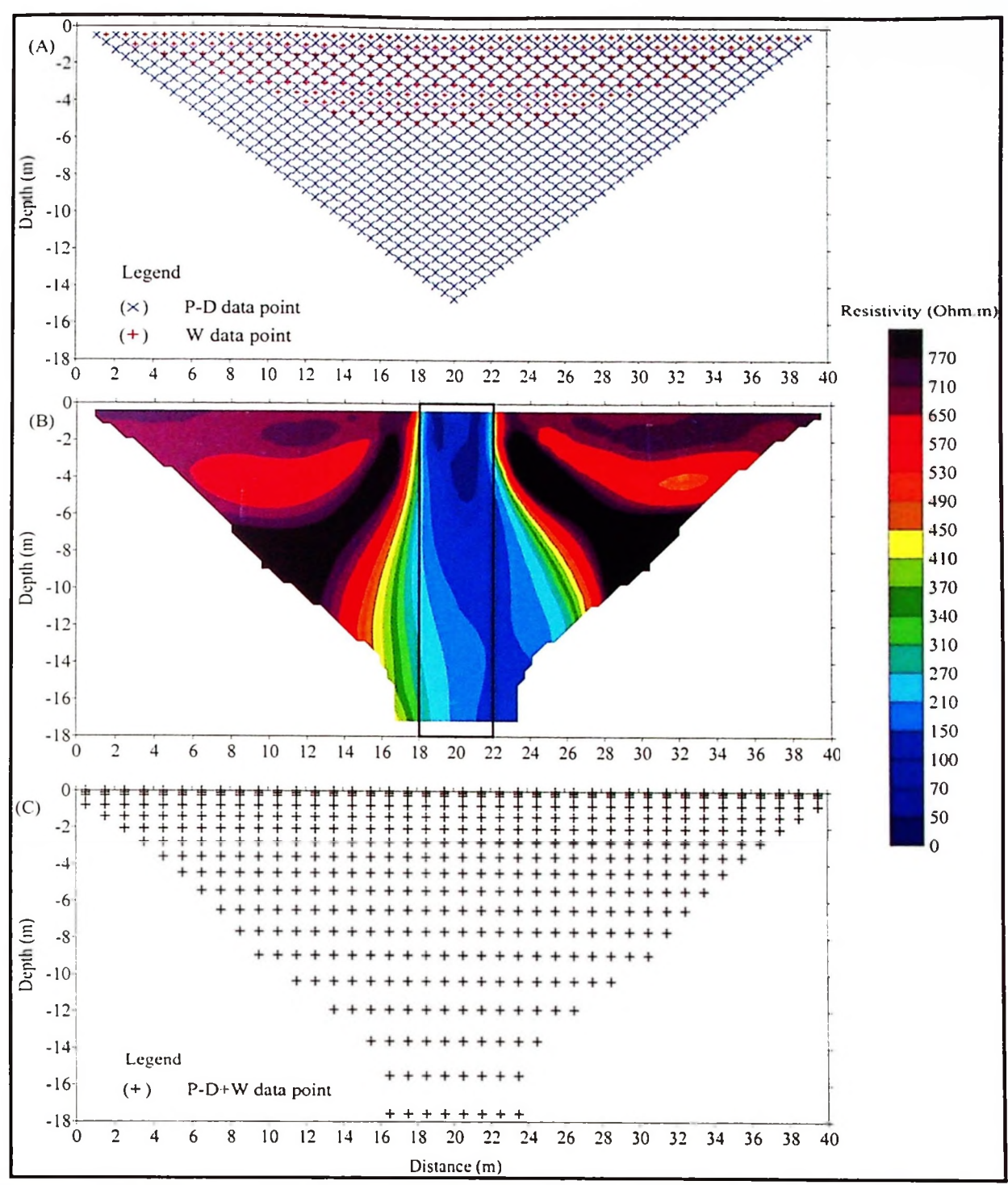


Figure 4.38: The vertical dyke model results given by the DLA technique of (P-D+W) arrays. A) Apparent resistivity data points arrangement. B) 2-D resistivity model result and C) Model resistivity data points.

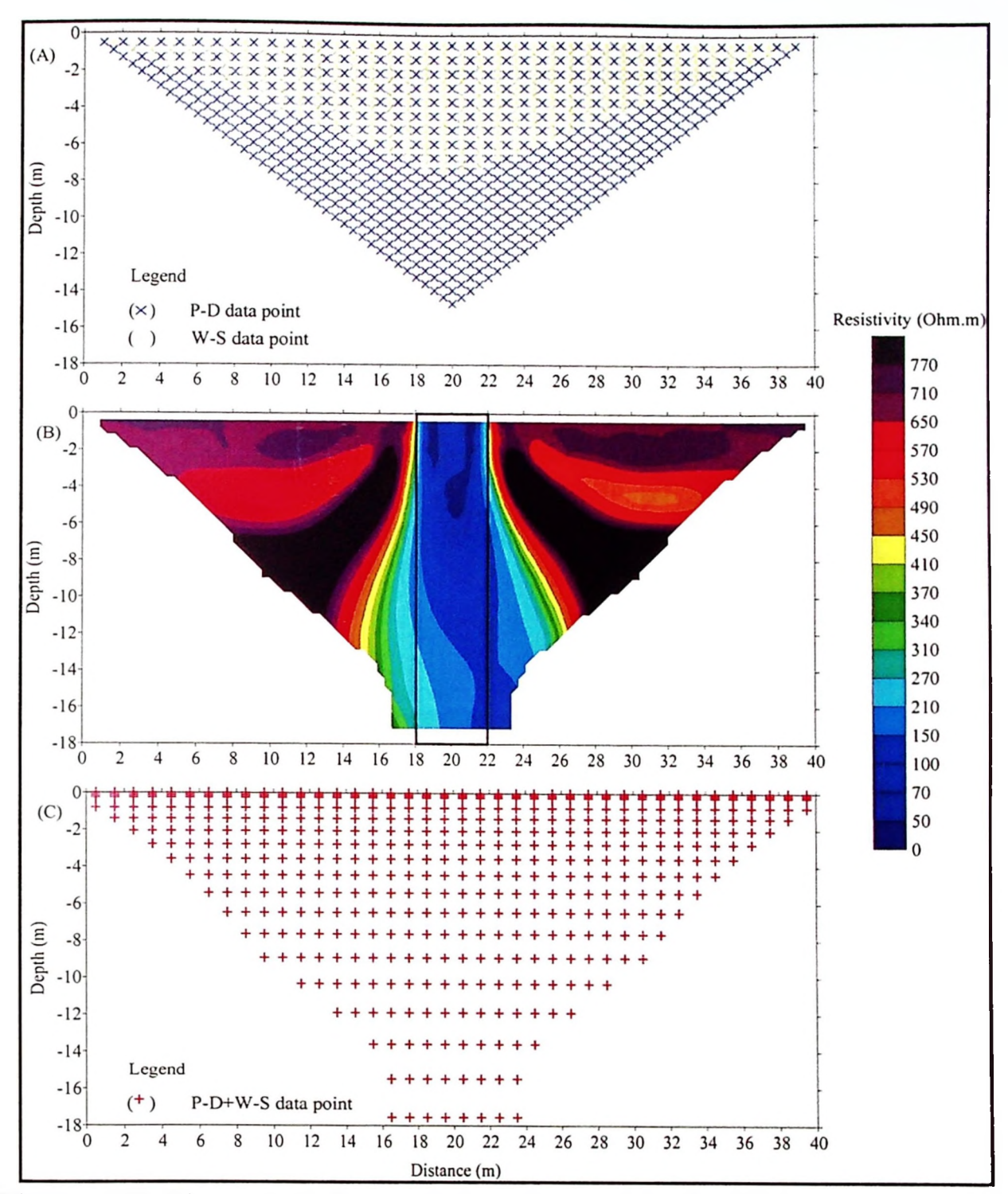


Figure 4.39: The vertical dyke model results given by the DLA technique of (P-D+W-S) arrays. A) Apparent resistivity data points arrangement. B) 2-D resistivity model result and C) Model resistivity data points.

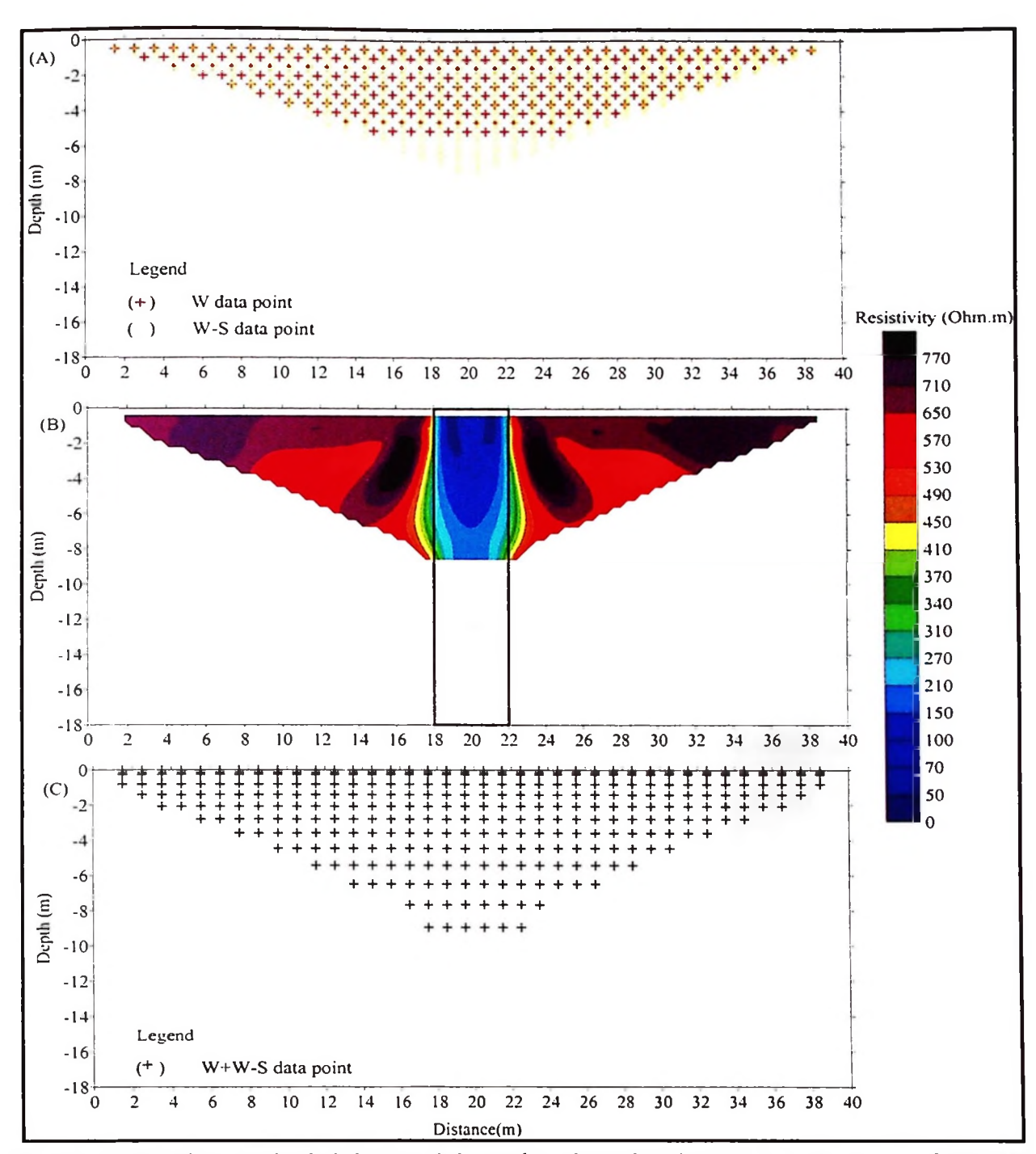


Figure 4.40: The vertical dyke model results given by the DLA technique of (W+W-S) arrays. A) Apparent resistivity data points arrangement. B) 2-D resistivity model result and C) Model resistivity data points.

## 4.1.5 Fault model

Some 2-D resistivity imaging results for individual array data sets recover the targets of the fault images as shown in Figures 4.41 until 4.44. From the results, it shows that the fault (100  $\Omega$ .m) images are fairly well resolved by D-D, P-D and W-S

arrays with the acceptable shape and the right resistivity values. However, W array was only able to resolve image of the fault with moderate results. The results show that these three arrays are able to give the right resistivity value of the fault. The bottom part of the fault is not imaged with good enough. The reason is because this array is less sensitive to resistivity horizontal changes (Loke, 2004; 2014).

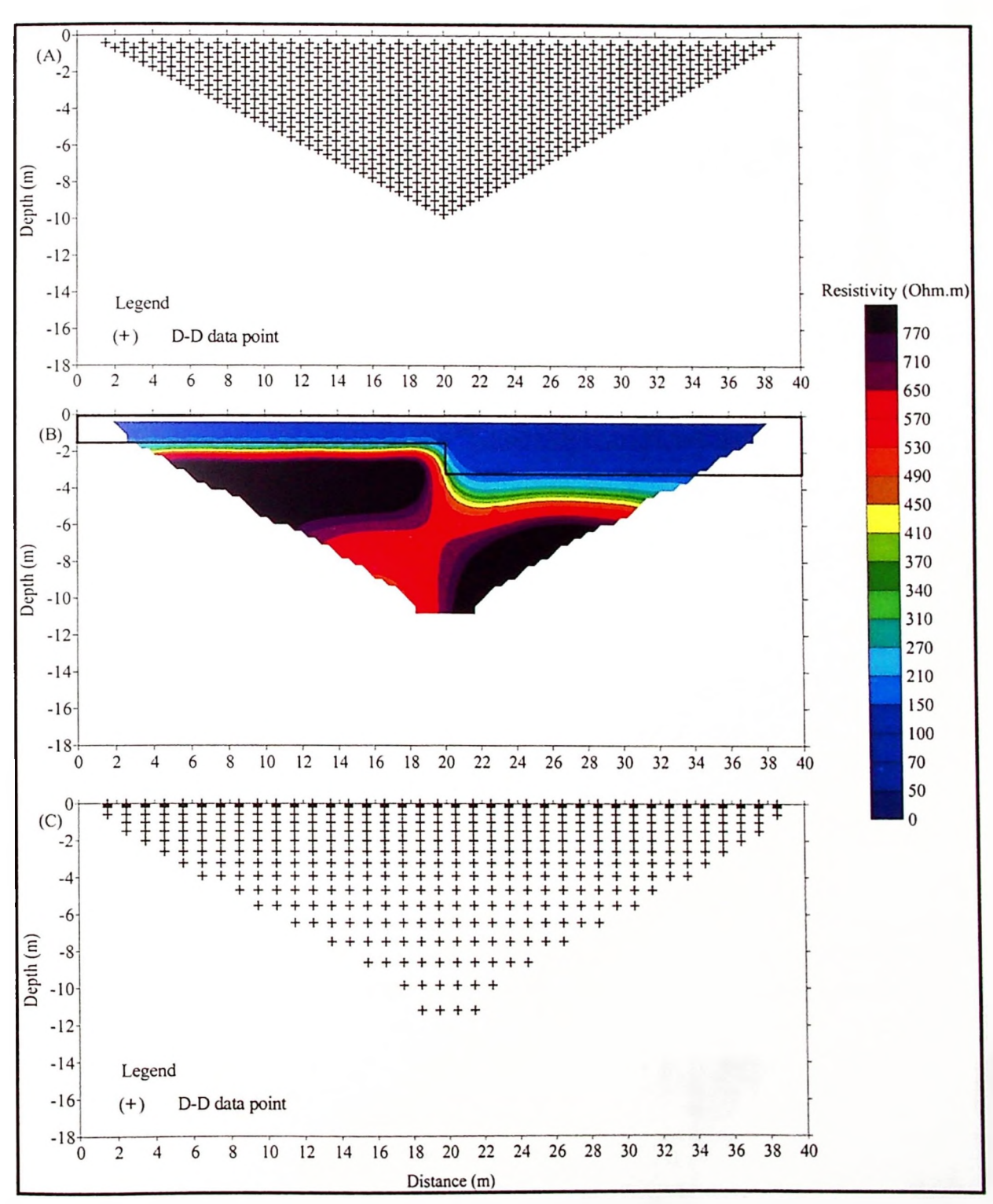


Figure 4.41: The fault model results given by D-D array. A) Apparent resistivity data points arrangement. B) 2-D resistivity model result and C) Model resistivity data points.

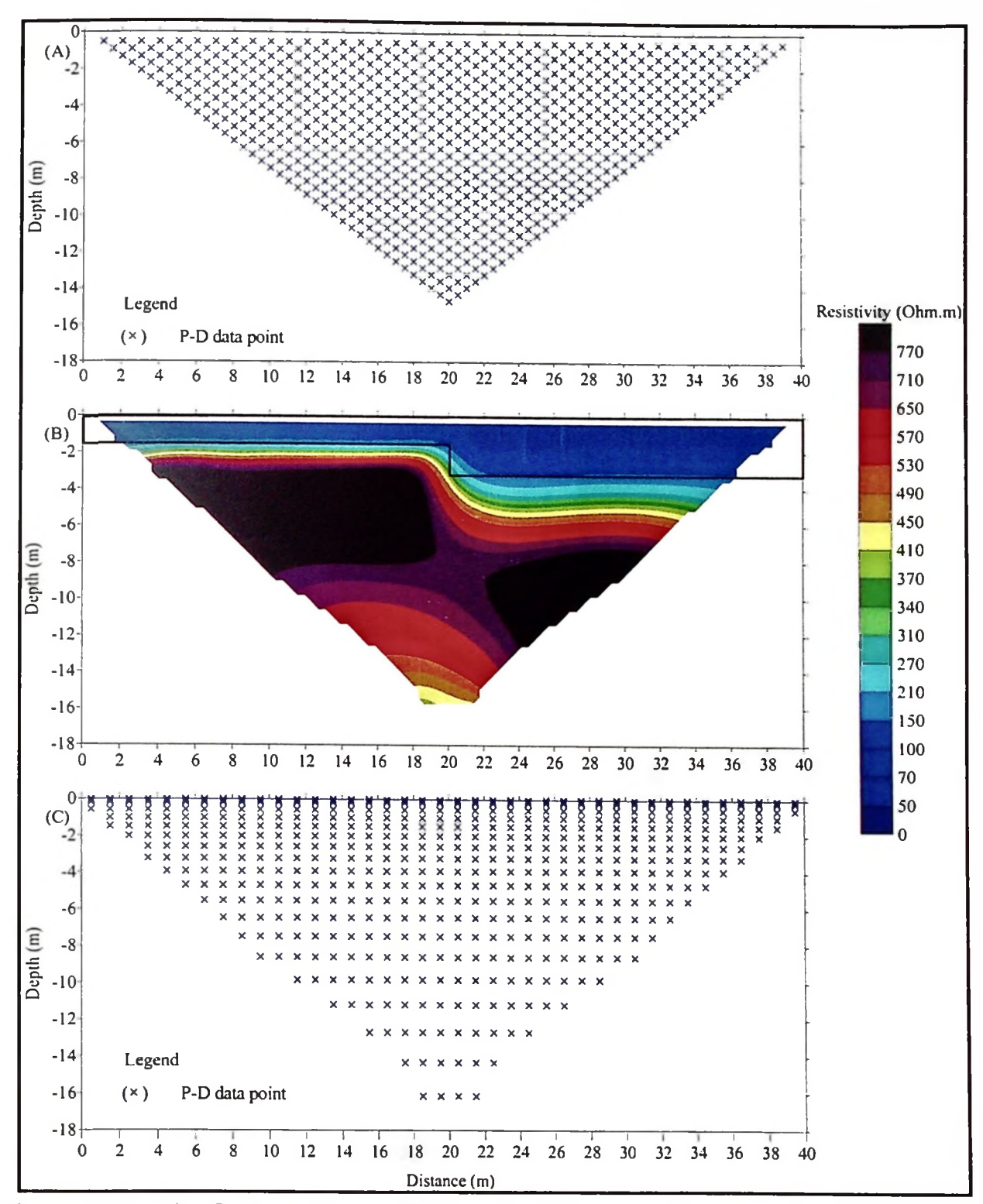


Figure 4.42: The fault model results given by P-D array. A) Apparent resistivity data points arrangement. B) 2-D resistivity model result and C) Model resistivity data points.

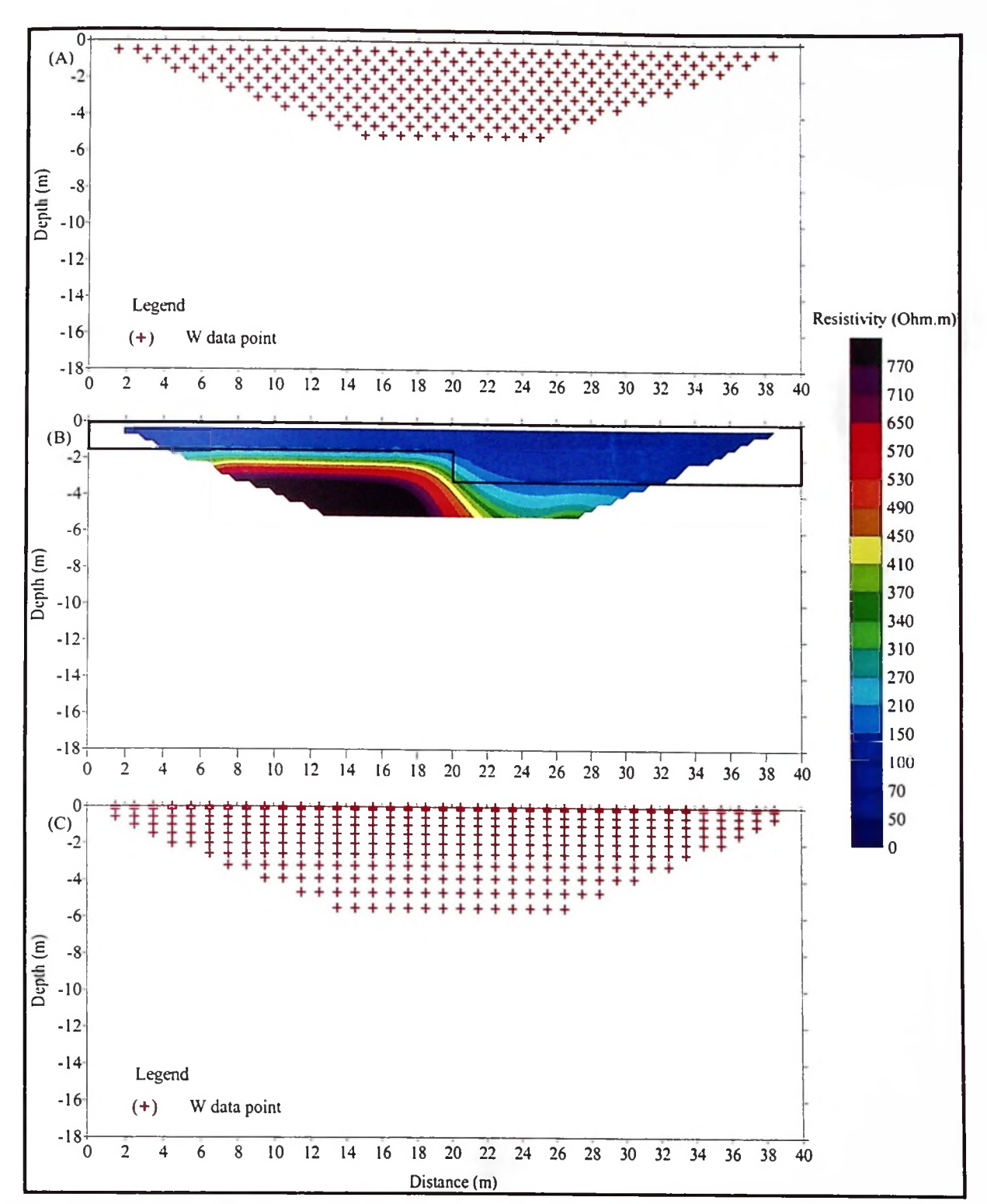


Figure 4.43: The fault model results given by W array. A) Apparent resistivity data points arrangement. B) 2-D resistivity model result and C) Model resistivity data points.

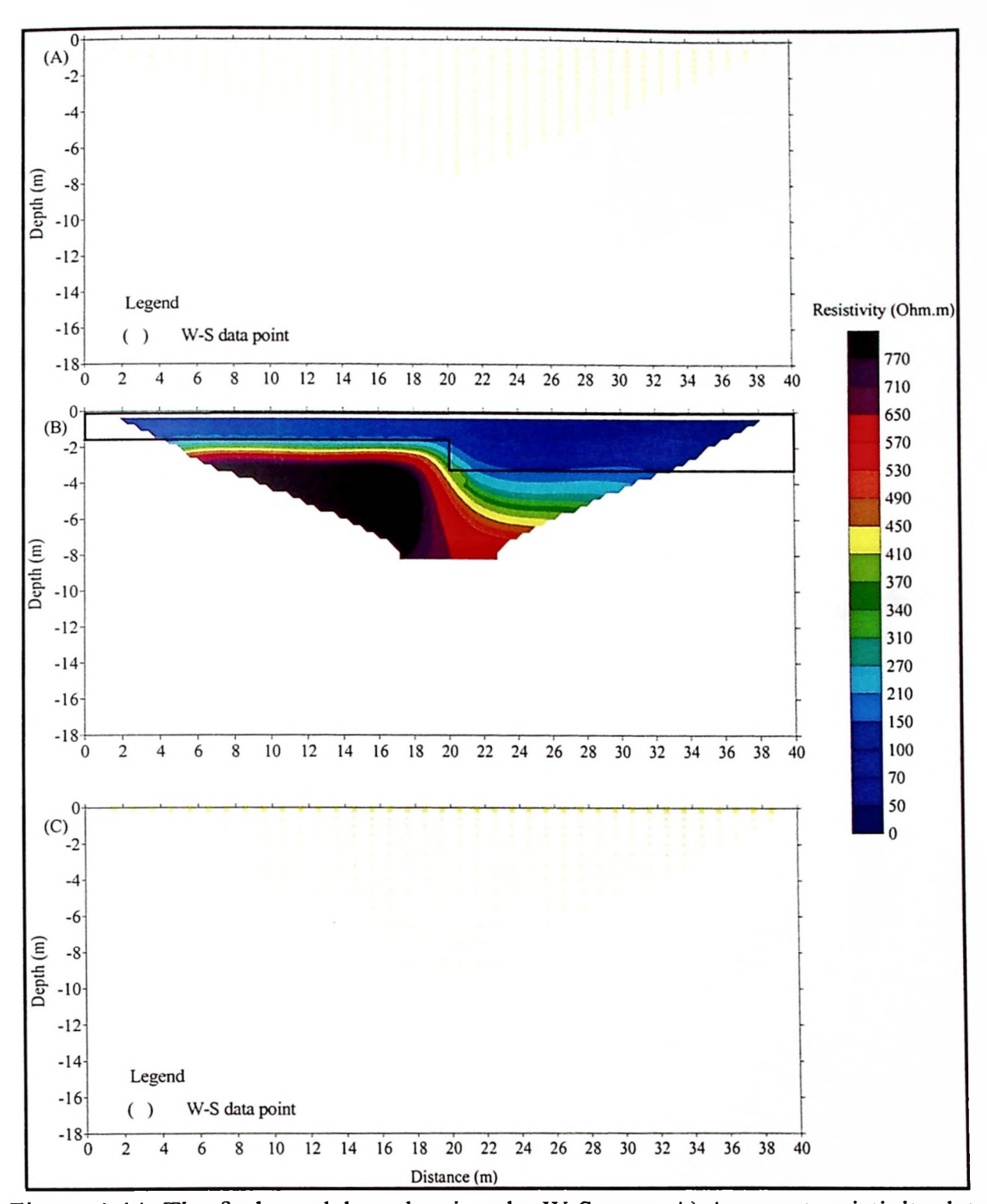


Figure 4.44: The fault model results given by W-S array. A) Apparent resistivity data points arrangement. B) 2-D resistivity model result and C) Model resistivity data points.

All the 2-D resistivity imaging results for the DLA technique data sets recover the target of fault (70  $\Omega$ .m) as shown in Figures 4.45 until 4.50. From the results, it shows that the fault is resolved with good results by all models using the DLA technique (D-D+P-D, D-D+W, D-D+W-S, P-D+W, P-D+W-S and W+W-S).

All of the DLA models are able to image the fault with acceptable shape and right resistivity value.

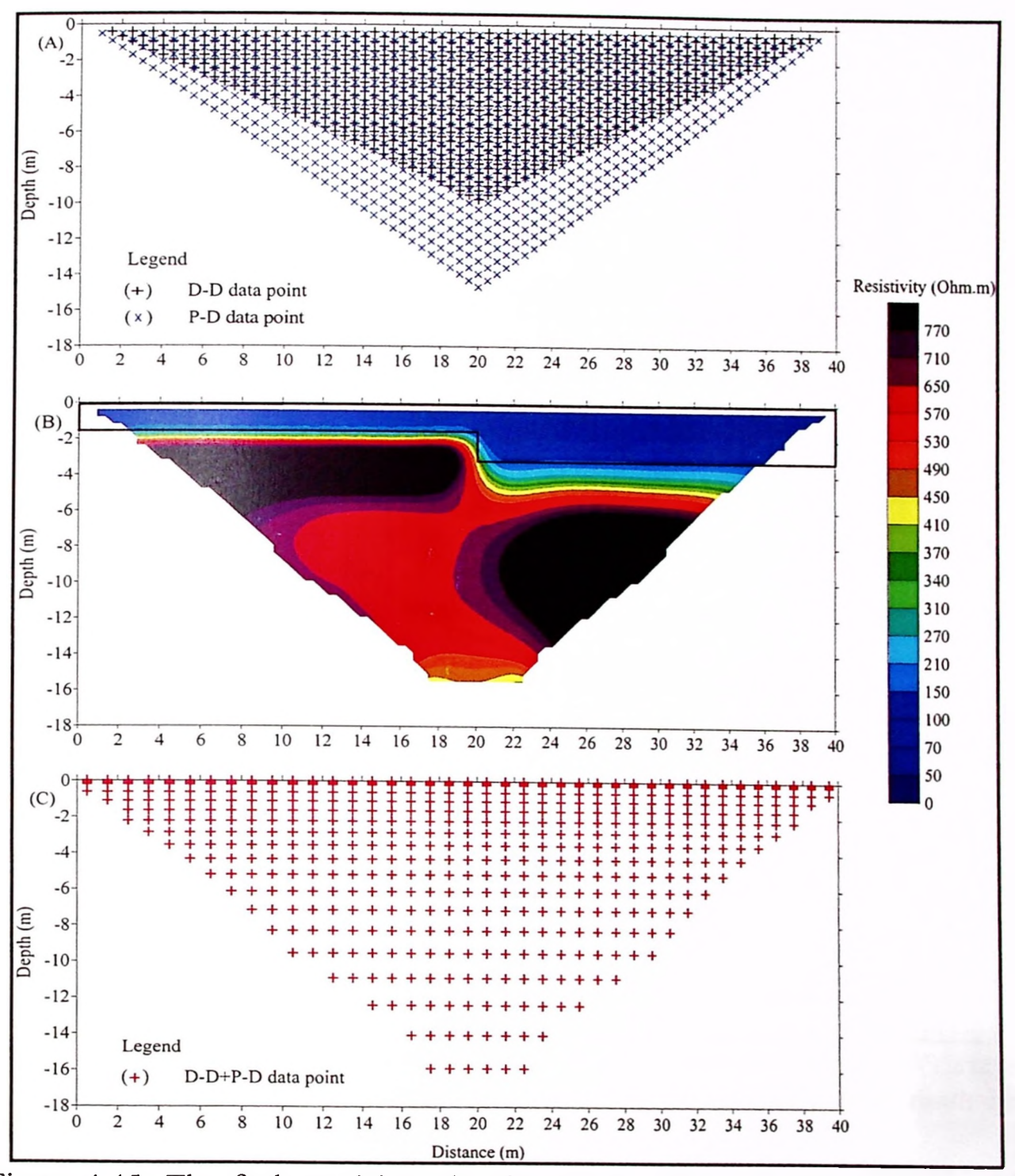


Figure 4.45: The fault model results given by the DLA technique of (D-D+P-D) arrays. A) Apparent resistivity data points arrangement. B) 2-D resistivity model result and C) Model resistivity data points.

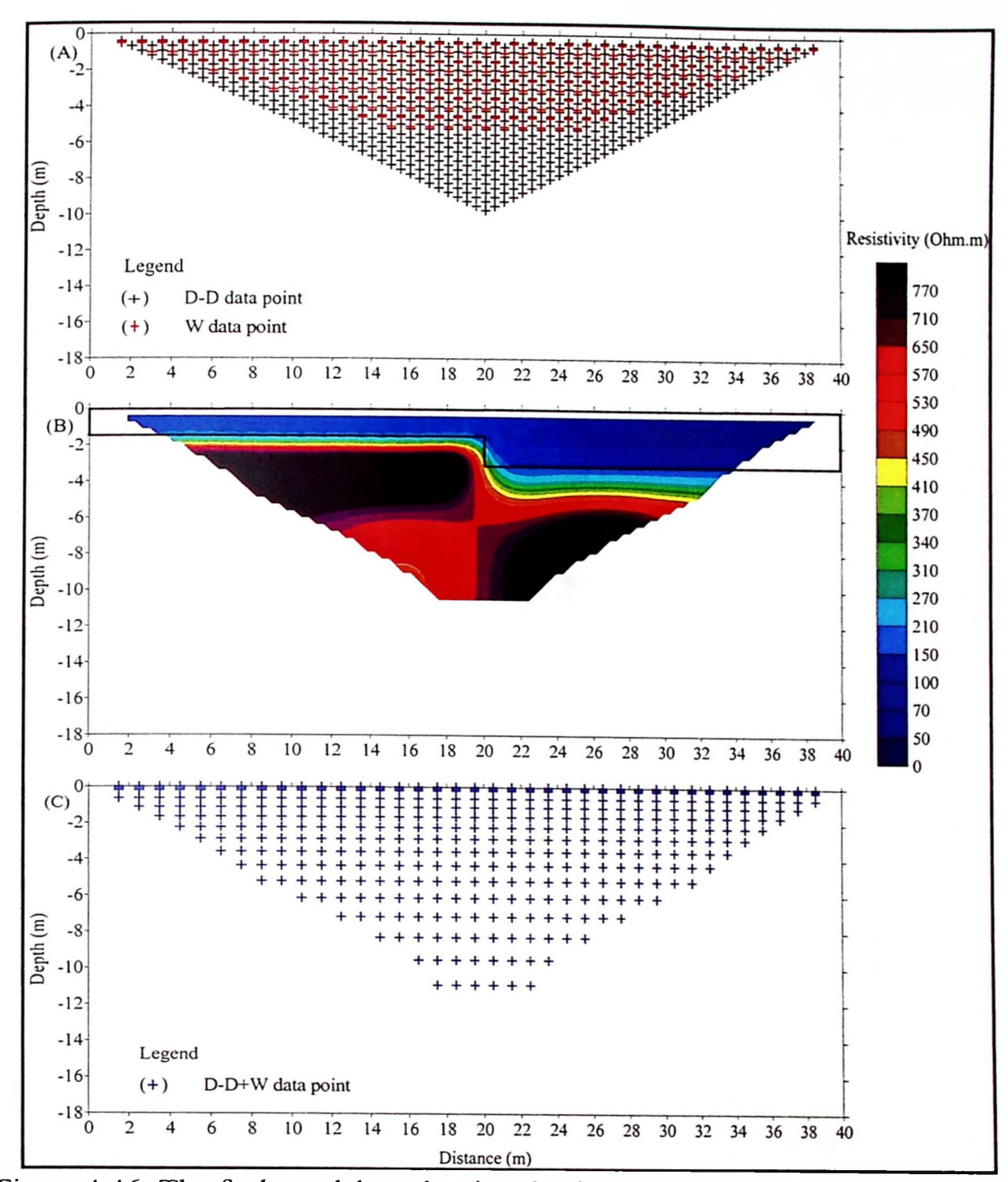


Figure 4.46: The fault model results given by the DLA technique of (D-D+W) arrays. A) Apparent resistivity data points arrangement. B) 2-D resistivity model result and C) Model resistivity data points.

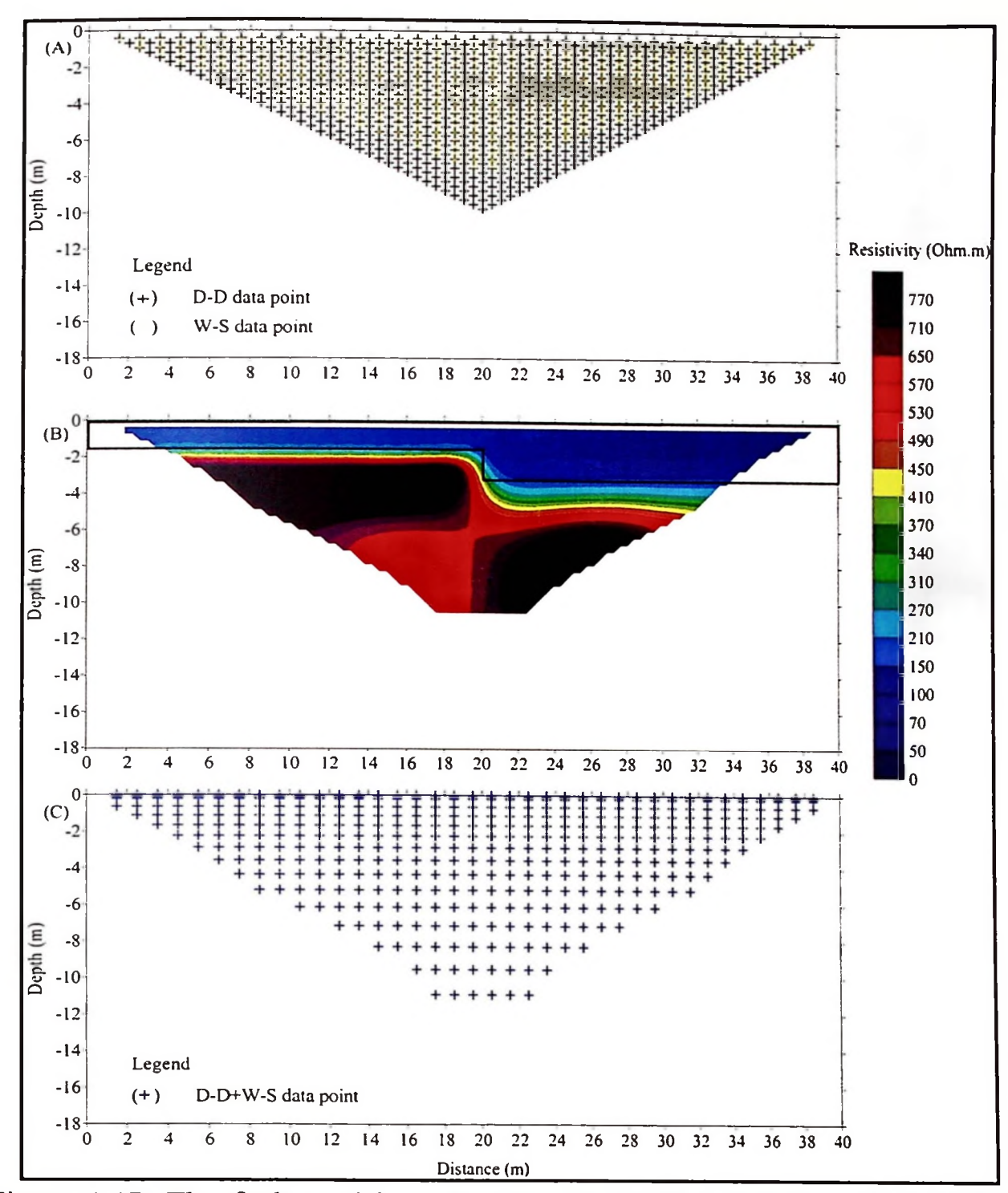


Figure 4.47: The fault model results given by the DLA technique of (D-D+W-S) arrays. A) Apparent resistivity data points arrangement. B) 2-D resistivity model result and C) Model resistivity data points.

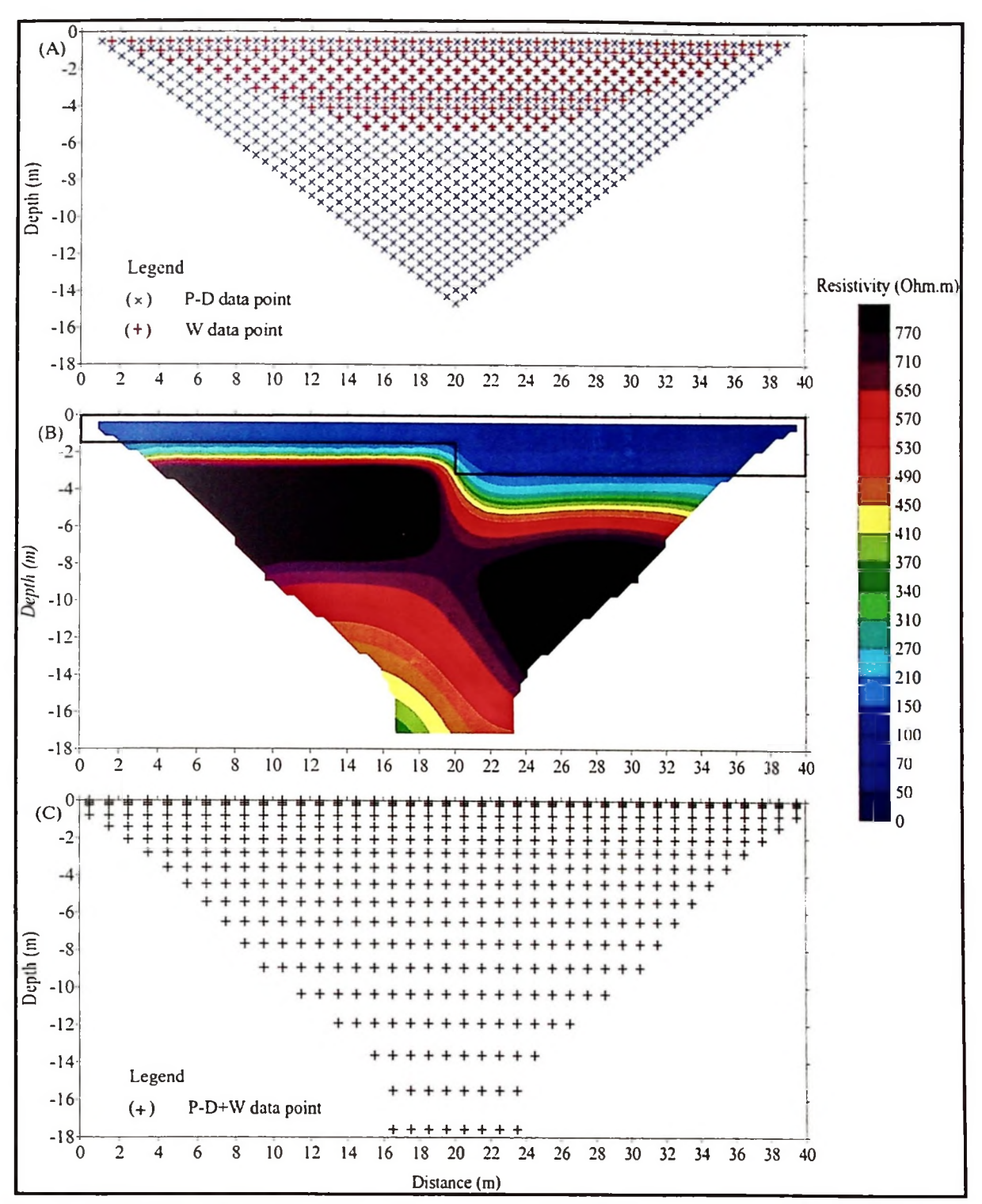


Figure 4.48: The fault model results given by the DLA technique of (P-D+W) arrays. A) Apparent resistivity data points arrangement. B) 2-D resistivity model result and C) Model resistivity data points.

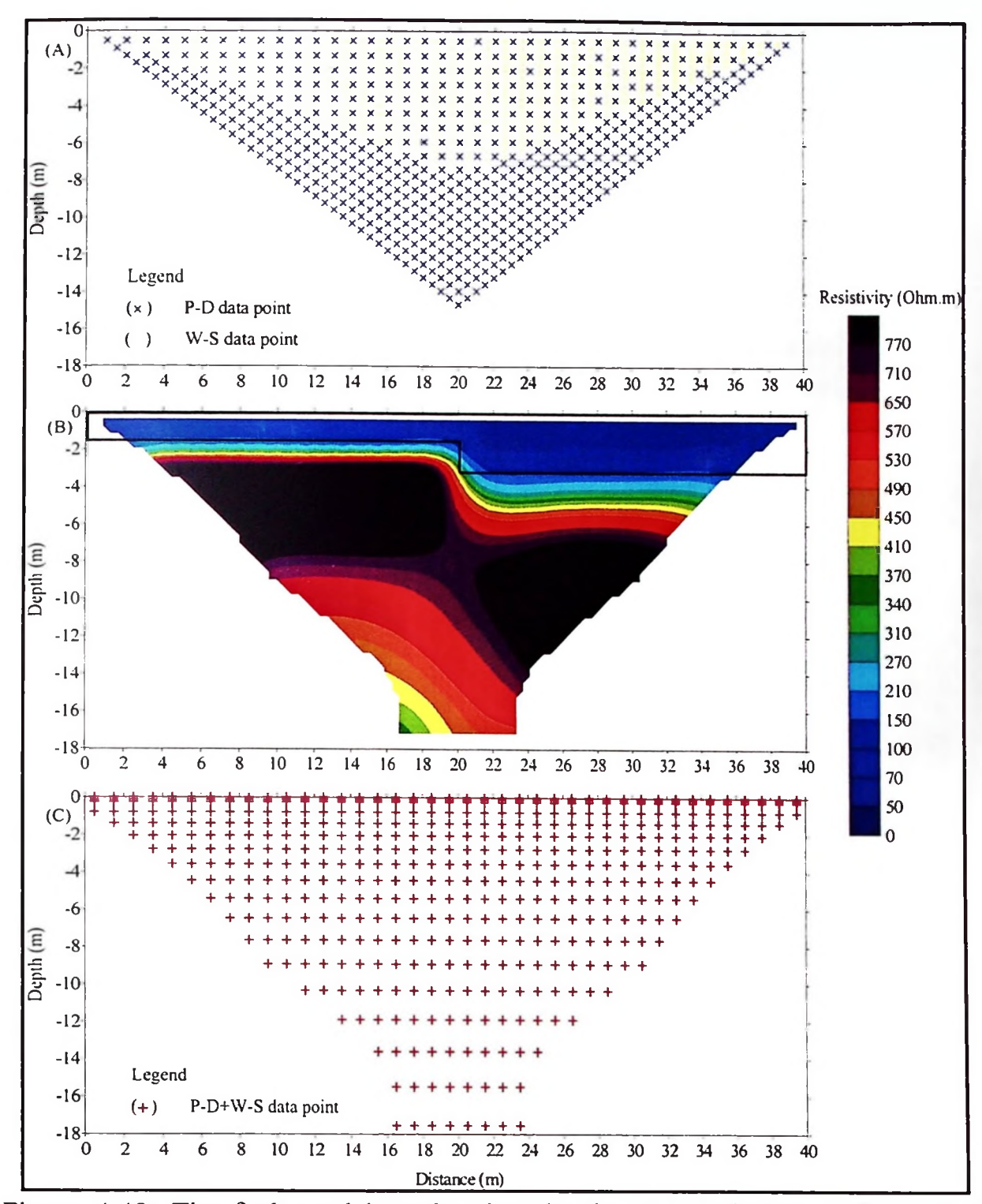


Figure 4.49: The fault model results given by the DLA technique of (P-D+W-S) arrays. A) Apparent resistivity data points arrangement. B) 2-D resistivity model result and C) Model resistivity data points.

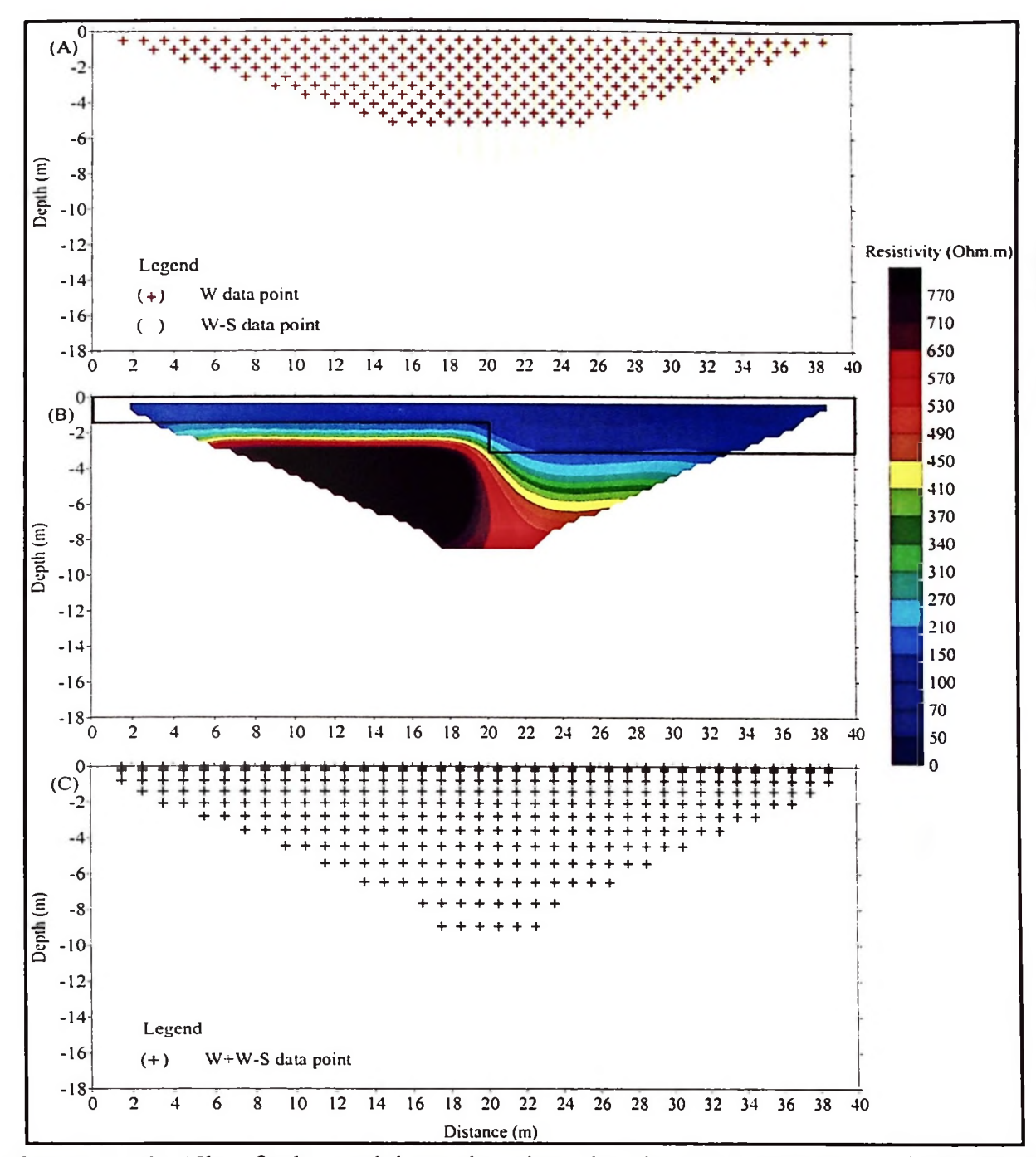


Figure 4.50: The fault model results given by the DLA technique of (W+W-S) arrays. A) Apparent resistivity data points arrangement. B) 2-D resistivity model result and C) Model resistivity data points.

### 4.1.6 The numerical comparative assessment

Based on 2-D computerized models' results, the numerical comparative assessment is carried out to determine the data quality for the individual array and the DLA models. Tables 4.1–4.5 show the summaries of the individual array and the

DLA technique for two different arrays. Two investigated parameters used in this assessment are total number of apparent resistivity data (before inversion) and total number of model data points (in inversion). These two parameters are important because the inversion models are generated by them. All the values for these two parameters can be obtained from RES2DINV program. Then, the third parameter is number of overlapping inversion of model resistivity data (OD). The main reason these parameters were used in this assessment is to study the percentage of overlapping in the DLA technique (ΔPO<sub>DLA</sub>) given by Equation (3.3). In this study, greater than 79 % of overlapping data levels of data points (in inversion) is selected as suitable margin point for the DLA technique. This parameter indicates that the denser the data set used in the DLA technique, the better information about the subsurface can be obtained from the 2-D resistivity imaging survey.

Based on this analysis, it shows that the DLA technique of (D-D+P-D and P-D+W-S) arrays are able to provide good data quality with the total number of apparent resistivity of 1521 and 1160 respectively. The percentage of overlapping inversion data points for these two combination in the DLA technique are also good with values greater than 79 %. This assessment is based on the five computerized models (Tables 4.1–4.3 and 4.5). However, in the fourth model of the vertical dyke (Table 4.4), only the DLA techniques of (P-D+W-S and W+W-S) arrays are able to give the percentage of overlapping in model data points of 79.10 % and 89.02 %, whereas other DLA techniques gave less than 79 %. However, the total number of apparent resistivity data (625) of the DLA technique of (W+W-S) arrays collected is not sufficient to give more information about the subsurface. Nevertheless, the DLA technique of (P-D+W-S) arrays is able to provide dense resistivity data with total number of apparent data points of 1160. In conclusion based on this numerical

comparative assessment have revealed that the DLA technique of different arrays would not be useful in all situations (Berge and Drahor, 2009). Therefore, only two best and suitable arrays will be selected to be used for the real field study which are selected from the 2-D computerized models and the numerical comparative assessment results.

In this study, another parameter is used in the numerical assessment which is the percentage change in inversion depth of investigation. However, this parameter is not main parameter used in consideration of selection the best two arrays. The main purpose of including this parameter in the numerical comparative assessment is to determine the depth of investigation changes. In conclusion, the DLA technique of two different arrays would not necessarily enhance the depth of investigation and model resolution. This is because of this parameter was not constantly change or no pattern. This finding has shown that the statement claimed by de la Vega et al. (2003) is not right. This happened because in that previous study, only two different arrays were used in the joint inversion technique, which are D-D and W arrays.

### 4.1.7 Conclusion of 2-D computerized models

From the results of 2-D computerized models and the numerical comparative assessment, the selection of the two best and suitable arrays is made based on three criteria. They are (i) total number of apparent resistivity data points, (ii) the percentage of overlapping in model data points and (iii) the ability to image the target. The conclusion from all 2-D resistivity models and the numerical comparative assessment shows that the DLA technique is suitable for P-D and W-S arrays.

Table 4.1: The numerical comparative assessment for a block model.

Атау / DLA	Apparent data points (DPApp.)	∑DPApp.(DLA)	Inversion data points (IM)	MDLA	Overlapping inversion data points (OD)	% Overlapping data points (ΔPO)	Inversion Depth of investigation (m)	% Change in inversion depth of investigation (m) (\DDLA)
D-D	741		446				11.203	
P-D	780		554				16.152	
D-D+P-D		1521		528	472	89.39%	15.911	-1.49%
D-D	741		446				11.203	
A	245		362				5.534	
D-D+W		986		424	384	90.57%	10.92	-2.53%
D-D	741		446				11.203	
W-S	380		398				8.608	
D-D+W-S		1121		424	420	%90.66	10.92	-2.53%
P-D	780		554				16.152	
W	245		362				5.534	
P-D+W		1025		488	428	87.70%	17.574	8.80%
P-D	780		554	3 7			16.152	
W-S	380		398				8.608	
P-D+W-S		1160		488	464	%80.56	17.574	8.80%
A	245		362				5.534	
N-S	380		398				8.608	
N+W-S		625		346	414	119.65%	8.945	3.91%

Table 4.2: The numerical comparative assessment for two blocks model.

Array / DLA	Apparent data points (DPApp.)	ΣDP App.(DLA)	Inversion data points (IM)	IMDLA	Overlapping inversion data points (OD)	% Overlapping data points (ΔPO)	Inversion Depth of investigation (m)	% Change in inversion depth of investigation (m)
D-D	741		446				11.203	
P-D	780		528				15.911	
D-D+P-D		1521		528	446	84.47%	15.911	0.00%
D-D	741		446				11.203	
*	245		362				5.534	
D-D+W		986		424	384	90.57%	10.92	-2.53%
D-D	741		446				11.203	
W-S	380		398				8.608	
D-D+W-S		1121		424	420	%90.66	10.92	-2.53%
P-D	780		528				115.911	
*	245		362				5.534	
P-D+W		1025		488	402	82.38%	17.574	10.45%
P-D	780		528				15.911	
W-S	380		398				8.608	
P-D+W-S		1160		488	438	89.75%	17.574	10.45%
*	245		362				5.534	
W-S	380		398				809.8	
W+W-S		625		346	414	119.65%	8.945	3.91%

Table 4.3: The numerical comparative assessment for contact zone model.

Array / DLA	Apparent data points (DPApp.)	ZDPApp.(DLA)	Inversion data points (IM)	IMDLA	Overlapping inversion data points (OD)	% Overlapping data points ( $\Delta PO$ )	Inversion Depth of investigation (m)	% Change in inversion depth of investigation (m) (ADDLA)
D-D	741		446				11.203	
P-D	780		554				16.152	
D-D+P-D		1521		528	472	89.39%	15.911	-1.49%
D-D	741		446				11.203	
W	245		308				5.429	
D-D+W		986		424	330	77.83%	10.92	-2.53%
D-D	741		446				11.203	
W-S	380		346				8.945	
D-D+W-S		1121		424	368	86.79%	10.92	-2.53%
P-D	780		554				16.152	
W	245		308				5.429	
P-D+W		1025		488	374	76.64%	17.574	8.80%
P-D	780		554				16.152	
W-S	380		346				8.945	
P-D+W-S		1160		488	412	84.43%	17.574	8.80%
W	245		308				5.429	
W-S	380		346				8.945	
W+W-S		625		346	308	89.02%	8.945	0.00%

Table 4.4: The numerical comparative assessment for vertical dyke model.

Array / DLA	Apparent data points (DPApp.)	ΣDP App.(DLA)	Inversion data points (IM)	IMDLA	Overlapping inversion data points (OD)	% Overlapping data points ( $\Delta PO$ )	Inversion Depth of investigation (m)	% Change in inversion depth of investigation (m) (\DDLA)
D-D	741		382				10.358	
P-D	780		528				15.911	
D-D+P-D		1521		528	382	72.35%	15.911	%00.0
D-D	741		382				10.358	
W	245		308				5.429	
D-D+W		986		424	266	62.74%	10.92	5.43%
D-D	741		382				10.358	
W-S	380		346				8.945	
D-D+W-S		1121		424	304	71.70%	10.92	5.43%
P-D	780		528				15.911	
*	245		308				5.429	
P-D+W		1025		488	348	71.31%	17.574	10.45%
P-D	780		528				15.911	
W-S	380		346		•		8.945	
P-D+W-S		1160		488	386	79.10%	17.574	10.45%
8	245		308		_		5.429	
W-S	380		346		•		8.945	
W+W-S		625		346	308	89.02%	8.945	%00.0

Table 4.5: The numerical comparative assessment for fault model.

Array / DLA	Apparent data points (DPApp.)	ΣDPApp.(DLA)	Inversion data points (IM)	IMDLA	Overlapping inversion data points (OD)	% Overlapping data points (ΔPO)	Inversion Depth of investigation (m)	% Change in inversion depth of investigation (m) (ADDLA)
D-D	741		446				11.203	
P-D	780		554		Ä		16.152	
D-D+P-D		1521		528	472	89.39%	15.911	-1.49%
D-D	741		446				11.203	
W	245		362			N.	5.534	
D-D+W		986		424	384	90.57%	10.92	-2.53%
D-D	741		446				11.203	
W-S	380		398				8.608	
D-D+W-S		1121		424	420	%90.66	10.92	-2.53%
P-D	780		554				16.152	
*	245		362				5.534	
P-D+W		1025		488	428	87.70%	17.574	8.80%
P-D	780		554				16.152	
W-S	380		398				8.608	
P-D+W-S		1160		488	464	%80.26	17.574	8.80%
M	245		362				5.534	
W-S	380		398				809.8	
W+W-S		625		346	414	119.65%	8.945	3.91%

### 4.2 Field model

Field model is chosen in this study because the protocol to be used in the real field is different from the 2-D computerized model. In addition, the actual conditions for the field model is different such as high noise level, negative apparent resistivity values is rejected by the equipment (SAS4000) during data acquisition and different amount of current is injected into the ground surface. Therefore, the numerical comparative assessment is important in order to select the best two arrays for the real field study.

The results of reconstructed 2-D resistivity imaging for the field model using individual inversion and the joint-inversion technique are presented in this section as shown by figures and tables. In addition, the results of the reconstructed numerical comparative analysis approach which was explained in Chapter 3 are presented too.

### 4.2.1 The buried bunker, USM, Penang

Some 2-D resistivity imaging results for individual array data sets recover image of the buried bunker as shown in Figures 4.51–4.54. The buried bunker was indicated by low resistivity values (Saad, 2009; Muztaza, 2013). The low resistivity values (less than 20  $\Omega$ .m) given by the target is because to the structure is made of concrete and the corrosion of concrete have occurred. The low values of this buried bunker was due to increases in both concrete water content and porosity (Neville, 2006). Therefore, the rate of corrosion increases (Broomfield, 2003). From the buried bunker results, it shows that image of the buried bunker is resolved well using P-D array (Figure 4.52). This array is able to image the target with good results and it is

represented with the low resistivity values. However, D-D, W and W-S arrays are only able to resolve image of the buried bunker with moderate results, giving low resistivity values of the target but with unclear shape. D-D array is able to gives a moderate image about the buried bunker which is due to small signal strength (Loke, 2004). W array gives moderate results about the target which is due to less sensitive in resistivity horizontal changes (Loke, 2004). Meanwhile, W-S array gives moderate result which is due to moderate sensitive to horizontal changes in resistivity (Loke, 1999a; 2004).

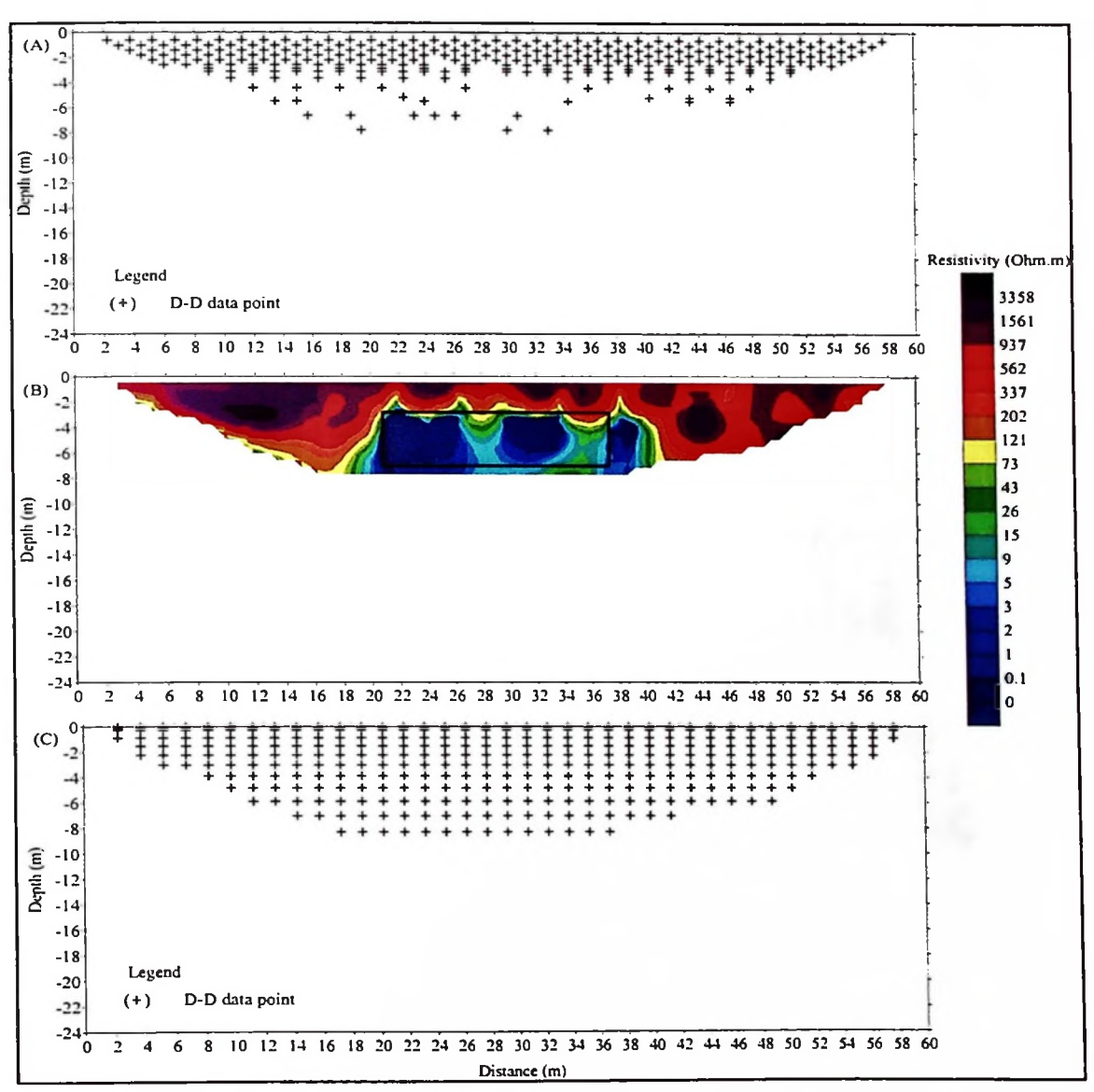


Figure 4.51: The buried bunker model results given by D-D array. A) Apparent resistivity data points arrangement. B) 2-D resistivity model result and C) Model resistivity data points.

represented with the low resistivity values. However, D-D, W and W-S arrays are only able to resolve image of the buried bunker with moderate results, giving low resistivity values of the target but with unclear shape. D-D array is able to gives a moderate image about the buried bunker which is due to small signal strength (Loke, 2004). W array gives moderate results about the target which is due to less sensitive in resistivity horizontal changes (Loke, 2004). Meanwhile, W-S array gives moderate result which is due to moderate sensitive to horizontal changes in resistivity (Loke, 1999a; 2004).

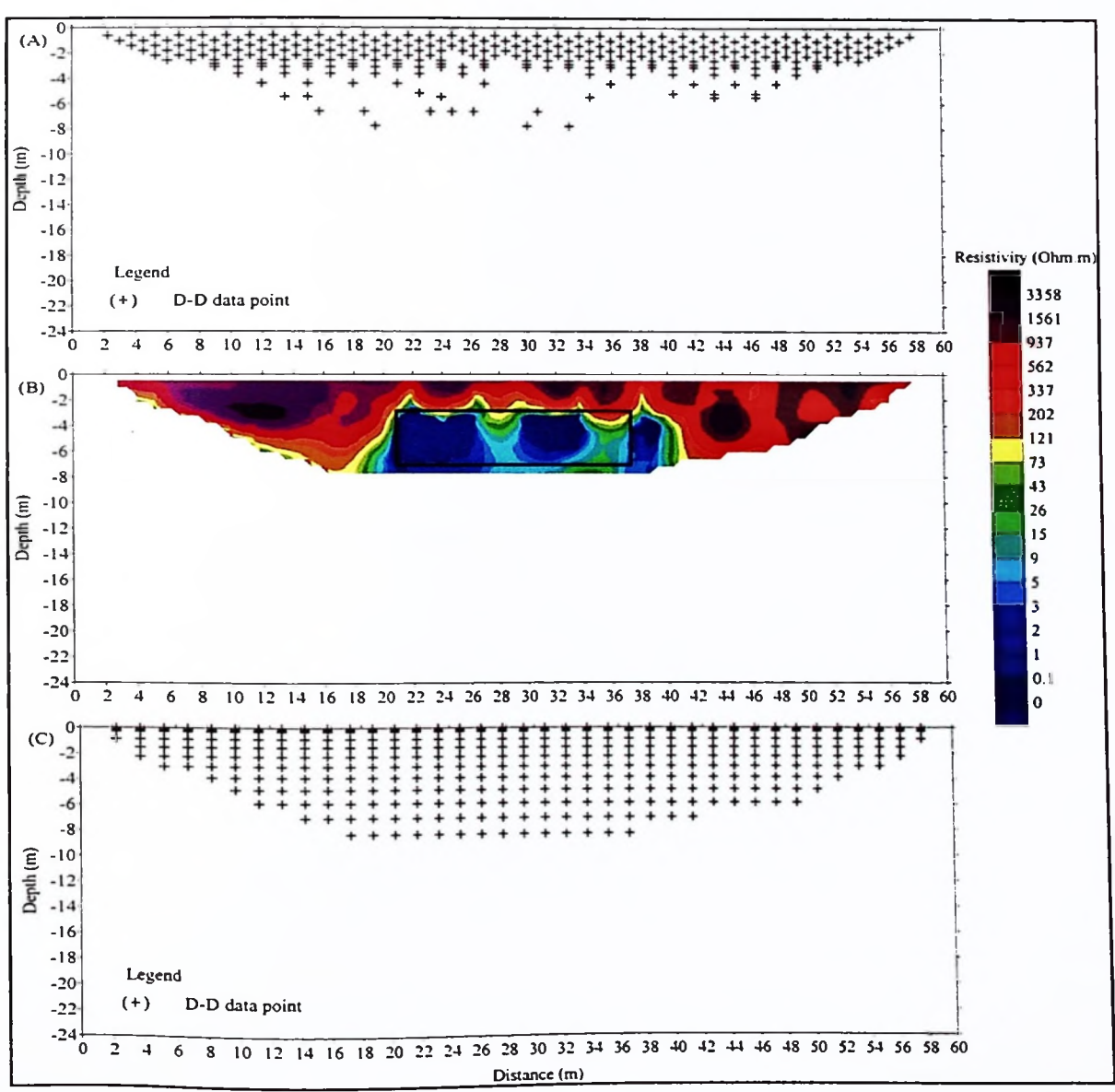


Figure 4.51: The buried bunker model results given by D-D array. A) Apparent resistivity data points arrangement. B) 2-D resistivity model result and C) Model resistivity data points.

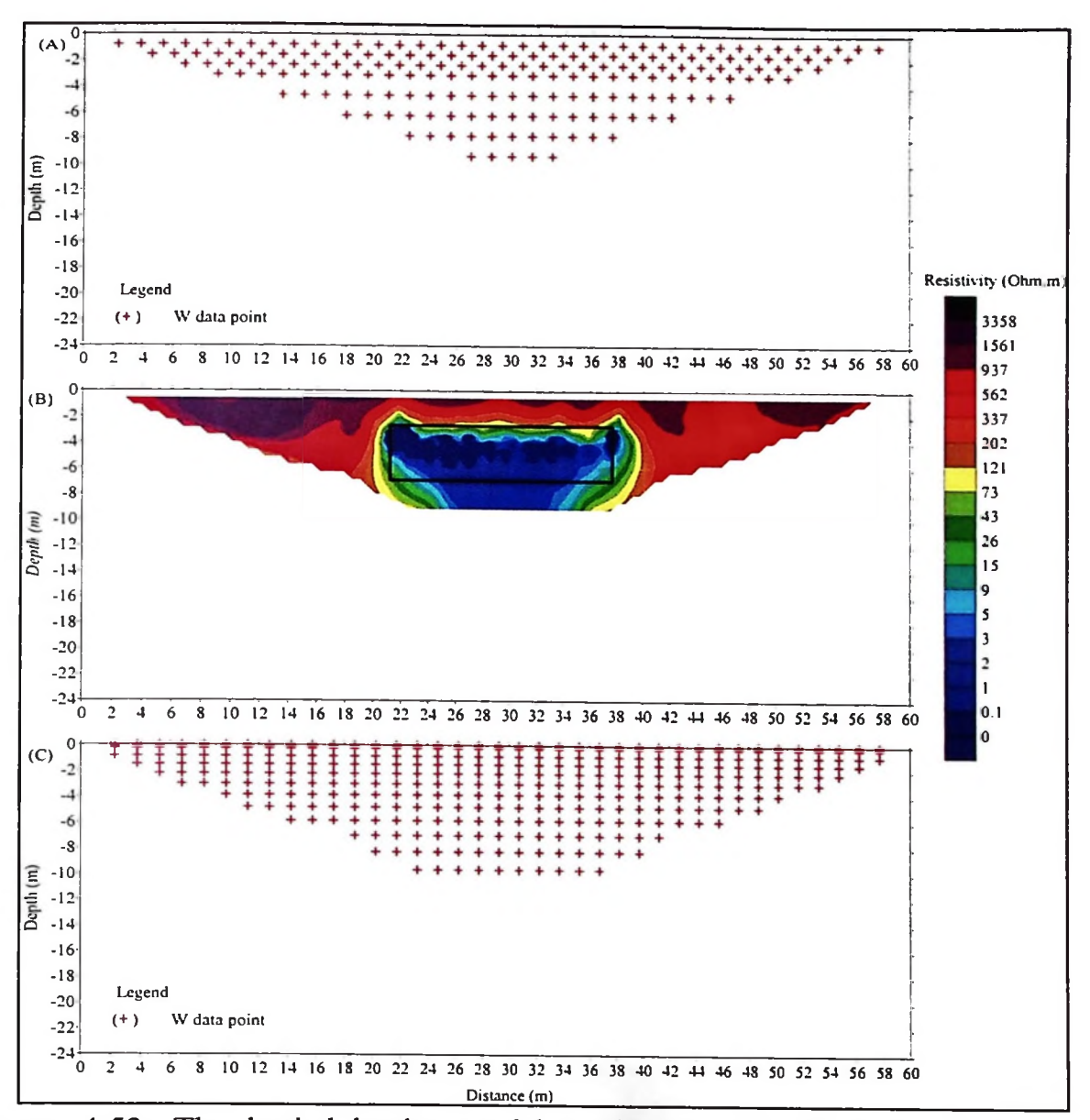


Figure 4.53: The buried bunker model results given by W array. A) Apparent resistivity data points arrangement. B) 2-D resistivity model result and C) Model resistivity data points.

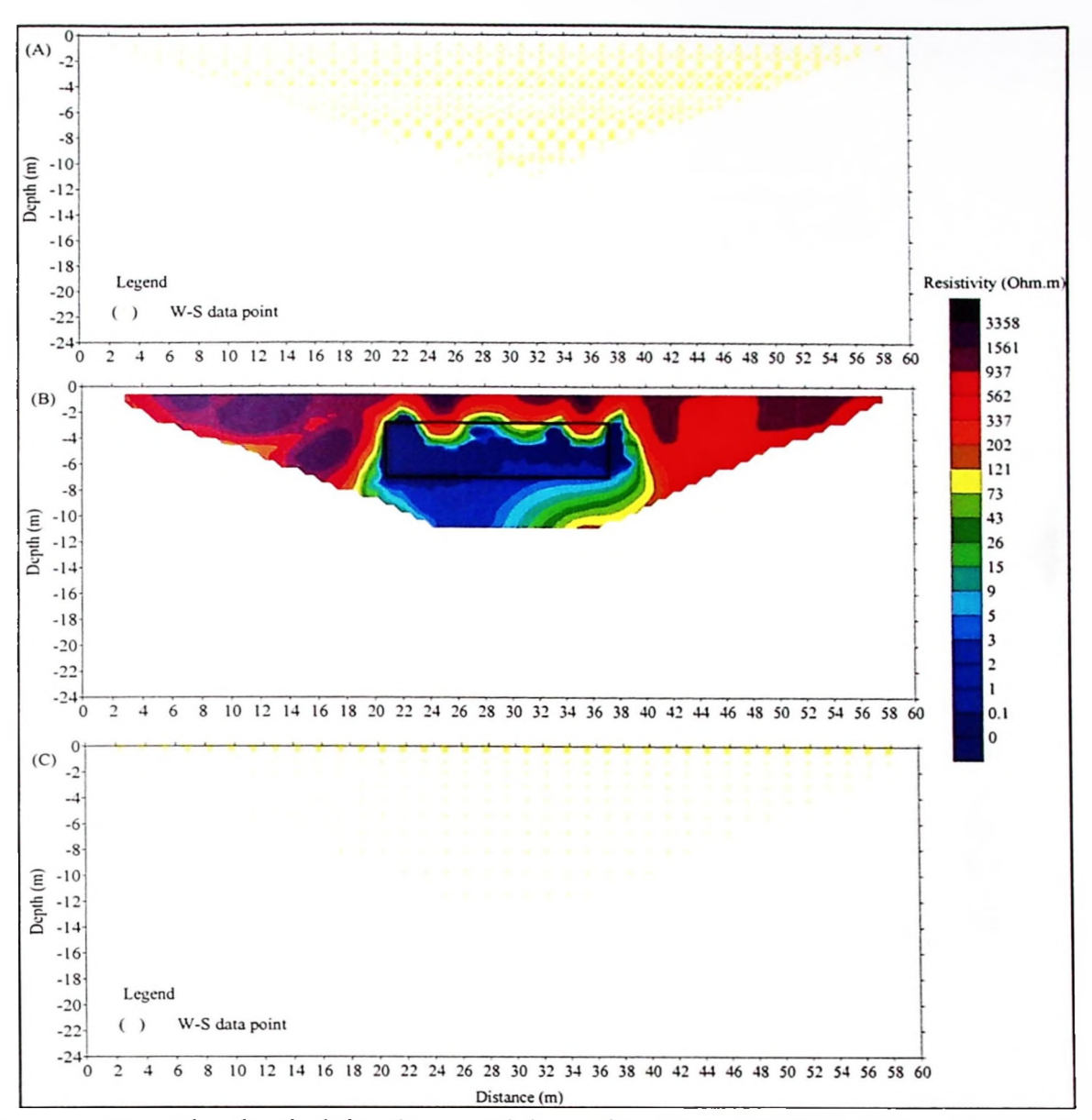


Figure 4.54: The buried bunker model results given by W-S array. A) Apparent resistivity data points arrangement. B) 2-D resistivity model result and C) Model resistivity data points.

Some of the 2-D resistivity imaging results for the DLA technique data sets recovered the buried bunker (less  $20~\Omega.m$ ) as shown in Figures 4.55 until 4.60. From the results, it shows that the buried bunker is resolved with good results by three models using the DLA technique of (D-D+P-D, P-D+W and P-D+W-S). These three DLA models are able to image the buried bunker with good results and give low resistivity values. Meanwhile, the other three models using the DLA technique of (D-D+W, D-D+W-S and W+W-S) are only able to resolve the buried bunker with

moderate results. These three DLA models are unable to image the shape of bunker with well but they are able to give low resistivity values.

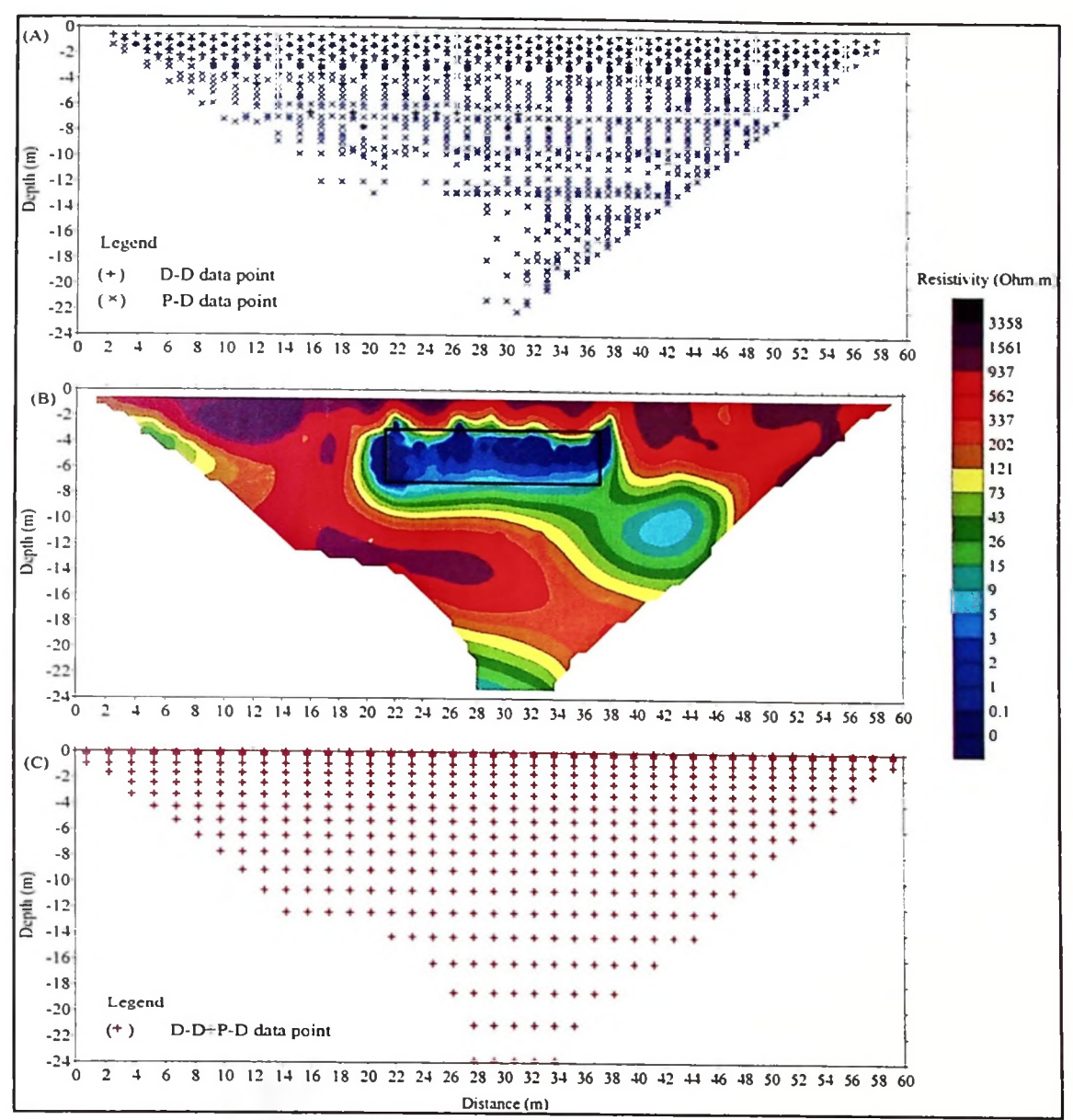


Figure 4.55: The buried bunker model results given by the DLA technique of (D-D+P-D) arrays. A) Apparent resistivity data points arrangement. B) 2-D resistivity model result and C) Model resistivity data points.

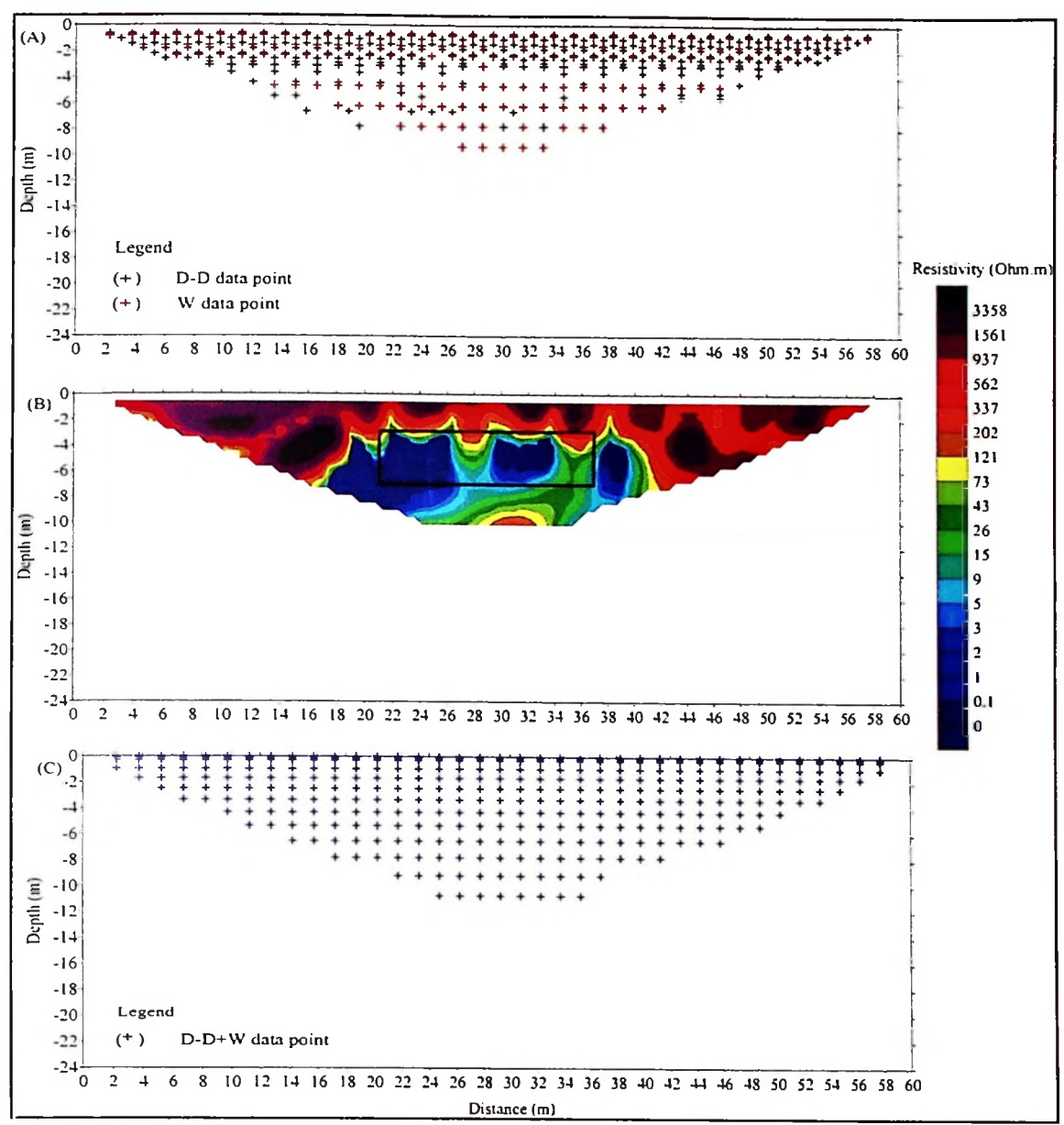


Figure 4.56: The buried bunker model results given by the DLA technique of (D-D+W) arrays. A) Apparent resistivity data points arrangement. B) 2-D resistivity model result and C) Model resistivity data points.

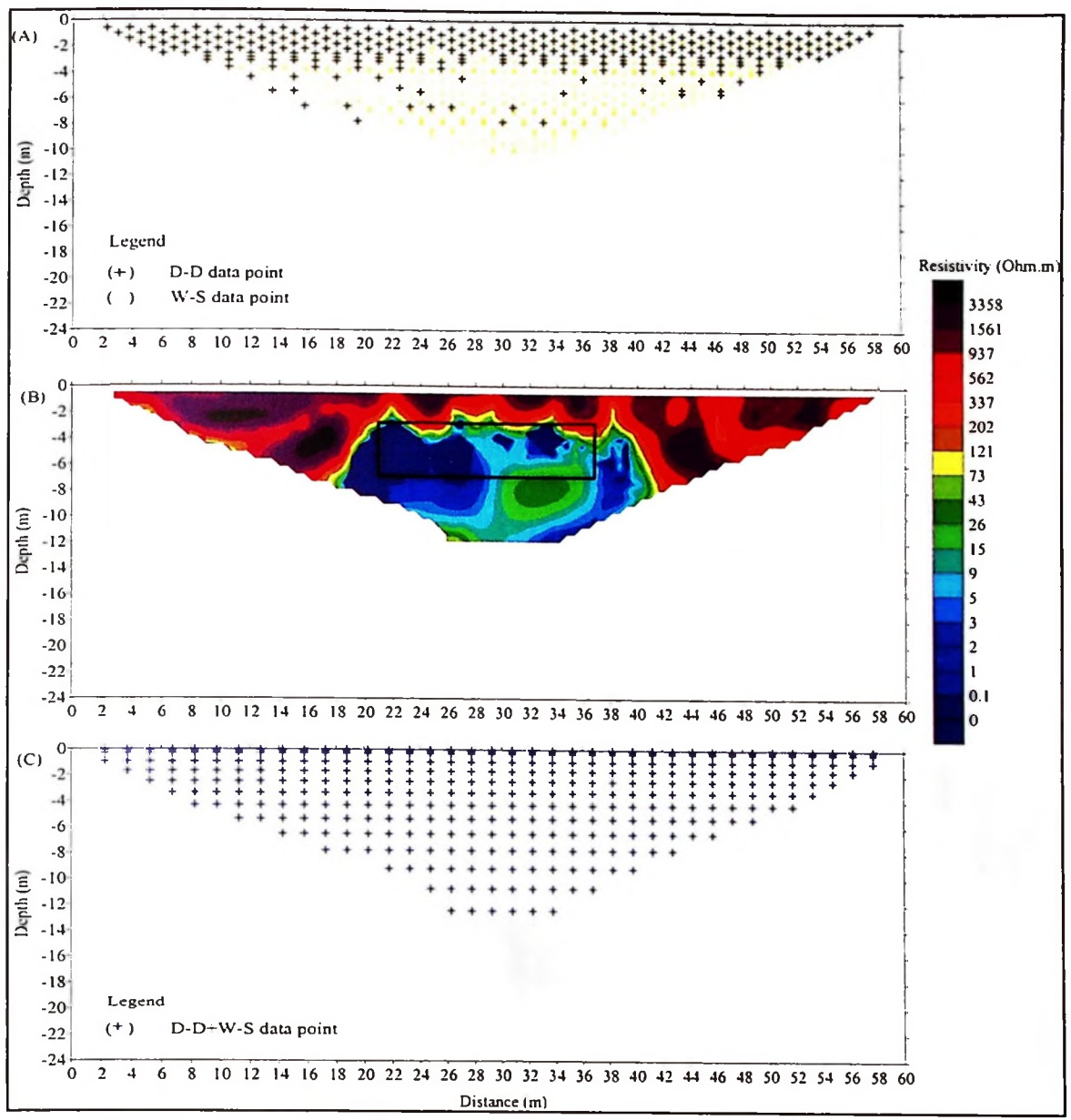


Figure 4.57: The buried bunker model results given by the DLA technique of (D-D+W-S) arrays. A) Apparent resistivity data points arrangement. B) 2-D resistivity model result and C) Model resistivity data points.

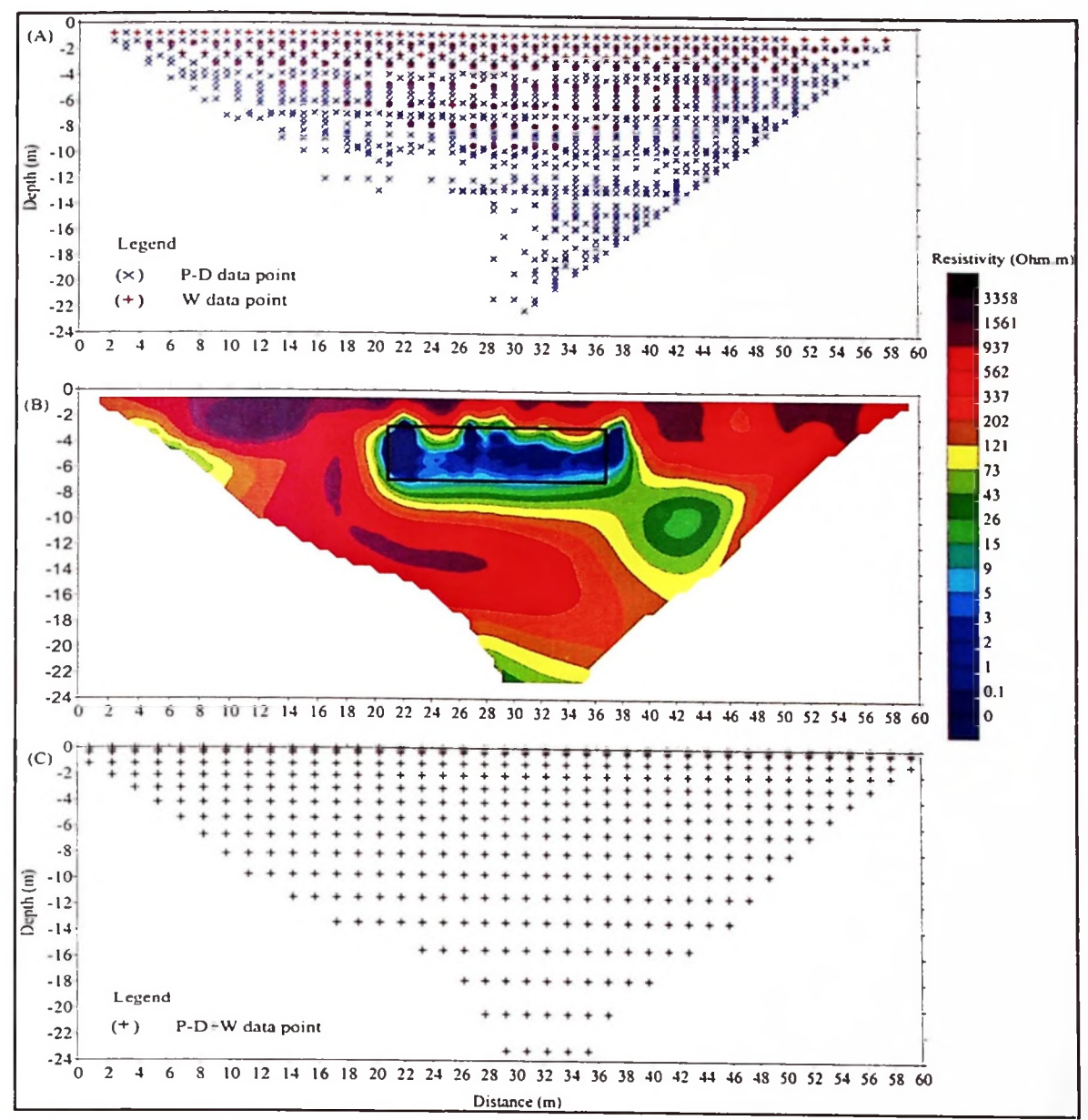


Figure 4.58: The buried bunker model results given by the DLA technique of (P-D+W) arrays. A) Apparent resistivity data points arrangement. B) 2-D resistivity model result and C) Model resistivity data points.

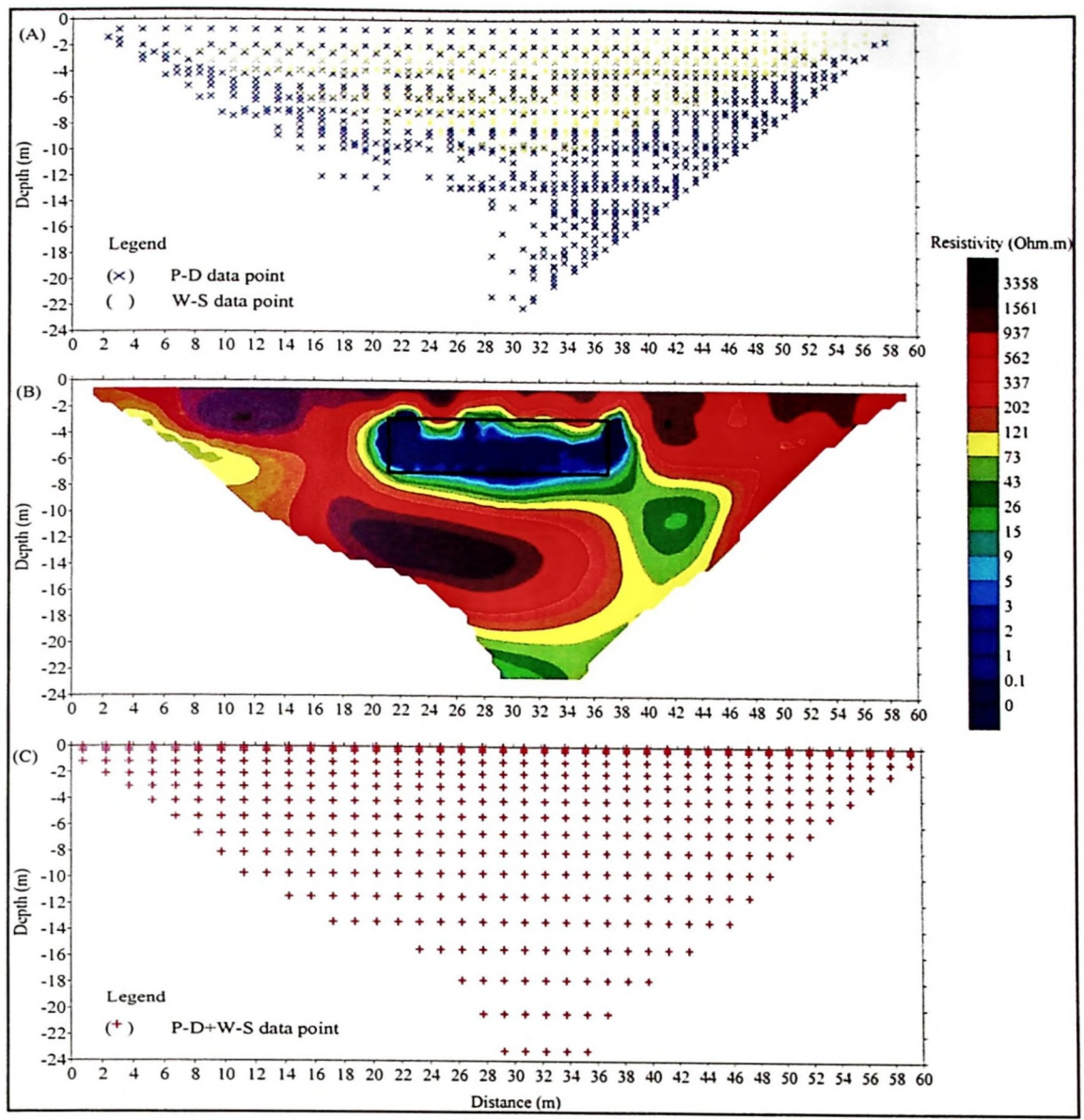


Figure 4.59: The buried bunker model results given by the DLA technique of (P-D+W-S) arrays. A) Apparent resistivity data points arrangement. B) 2-D resistivity model result and C) Model resistivity data points.

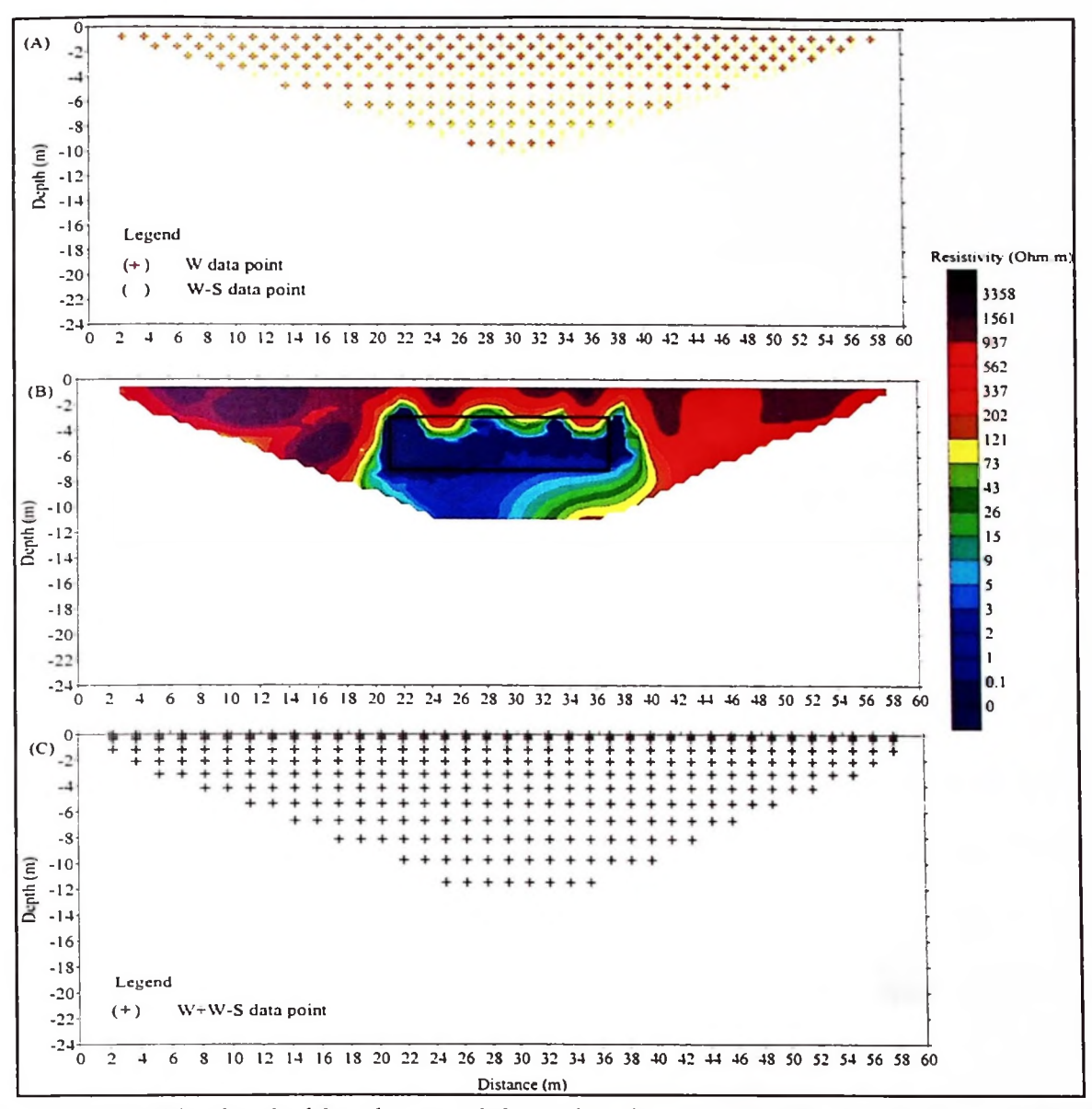


Figure 4.60: The buried bunker model results given by the DLA technique of (W+W-S) arrays. A) Apparent resistivity data points arrangement. B) 2-D resistivity model result and C) Model resistivity data points.

### 4.2.2 The numerical comparative assessment

Table 4.5 shows the summary of the individual array and the DLA technique for two different arrays. Two investigated parameters used in this assessment are the total number of apparent resistivity data (before inversion) and total number of model data points (in inversion). These two parameters is are important because the inversion models are generated by them. All the values for these two parameters can

be obtained from RES2DINV program. Then, the third parameter is the number of overlapping inversion of model resistivity data (OD). The main reason this parameters is used in this assessment is to study the percentage of overlapping in the DLA technique (ΔPO<sub>DLA</sub>) given by Equation (3.3). In this study, greater than 79 % of overlapping data levels of data points (in inversion) is selected as suitable margin point for the DLA technique. This indicates that the denser the data set used in the DLA technique, the better information about the subsurface can be obtained from the 2-D resistivity imaging survey. In addition, it can increases the confident level of an interpreter (a geophysicist) on the 2-D resistivity imaging results.

Based on this analysis, it shows that the DLA technique of (P-D+W-S and P-D+W) arrays are able to provide good data quality with total number of apparent resistivity of 1716 and 1384. Overlapping inversion data points for the DLA technique of (P-D+W-S) is good with value of 86.61 %. However, only the DLA technique of (D-D+P-D) gives the percentage of overlapping in model data points of 75.10 % which is less than the required margin bar (Table 4.6).

In this study, another parameter is used in the numerical assessment which is the percentage change in inversion depth of investigation. This parameter is not the main parameter used in consideration of the selection of the two best and suitable arrays. From Table 4.6, it shows that the depth of investigation is reduced by 2.55% for the DLA technique of (P-D+W-S and P-D+W). This is due to overlapping in data levels (Loke, 2004; 2014).

# 4.2.3 Conclusion of field model

From the results of 2-D computerized models and the numerical comparative assessment, selection of the two best and suitable arrays is made based on three criteria. They are (i) total number of apparent resistivity data points, (ii) the percentage of overlapping in model data points and (iii) the ability to image the target. The conclusion from 2-D computerized models and the numerical comparative assessment shows that the DLA technique is suitable for two different arrays which are P-D and W-S.

Table 4.6: The numerical comparative assessment for the buried bunker, USM.

Apparent data points	ΣDPApp.(DLA)	Inversion data points	IMDLA	Overlapping inversion data points	% Overlapping data points	Inversion Depth of investigation	% Change in inversion depth of investigation (m)
				(QO)	(APO)	(m)	(ADDLA)
		375				8.302	
		525				23.866	
	1384		514	386	75.10%	23.866	0.00%
		375				8.302	
		370				9.694	
	483		366	379	103.55%	10.754	10.93%
ļ		375				8.302	
		339				11.489	
	918		378	336	88.89%	12,454	8.40%
1.6		525				23.866	
190		370				9.694	
	1281		463	432	93.30%	23.257	-2.55%
1001		525				23.866	
625		339				11.489	
	1716		463	401	86.61%	23.257	-2.55%
		370				9.694	
		339				11.489	
	815	,	339	370	109.14%	11.489	%00.0

# 4.3 Field studies

Results are shown from two field studies which were carried out at Minden, USM, Penang and Bukit Bunuh, Lenggong, Perak are discussed. The following discussions are a summary of obtained results followed by the figures and to give more insight into the results' explanation. The borehole data were used to validate the 2-D resistivity imaging results.

# 4.3.1 Minden, USM, Penang

All of the 2-D resistivity imaging results give fairly good information about the subsurface. Figure 4.61 shows the results of the individual array and the DLA technique (W-S+P-D) respectively. Total number of apparent data points for W-S array is 665, P-D array is 1188 and the DLA technique is 1843. The number of apparent data points is obtained after the filtering process. The overburden is made up of clay/silt/sand material mixed with some gravels at depth range of 38.5-7.0 m. It is represented by resistivity values of  $160-1400 \Omega \text{ m}$ . Meanwhile, the weathered/fractured granite has resistivity values of  $100-1600 \Omega \text{ m}$ . The interpretation of these values were made from the resistivity values along two borehole data (BH 1 and BH 2).

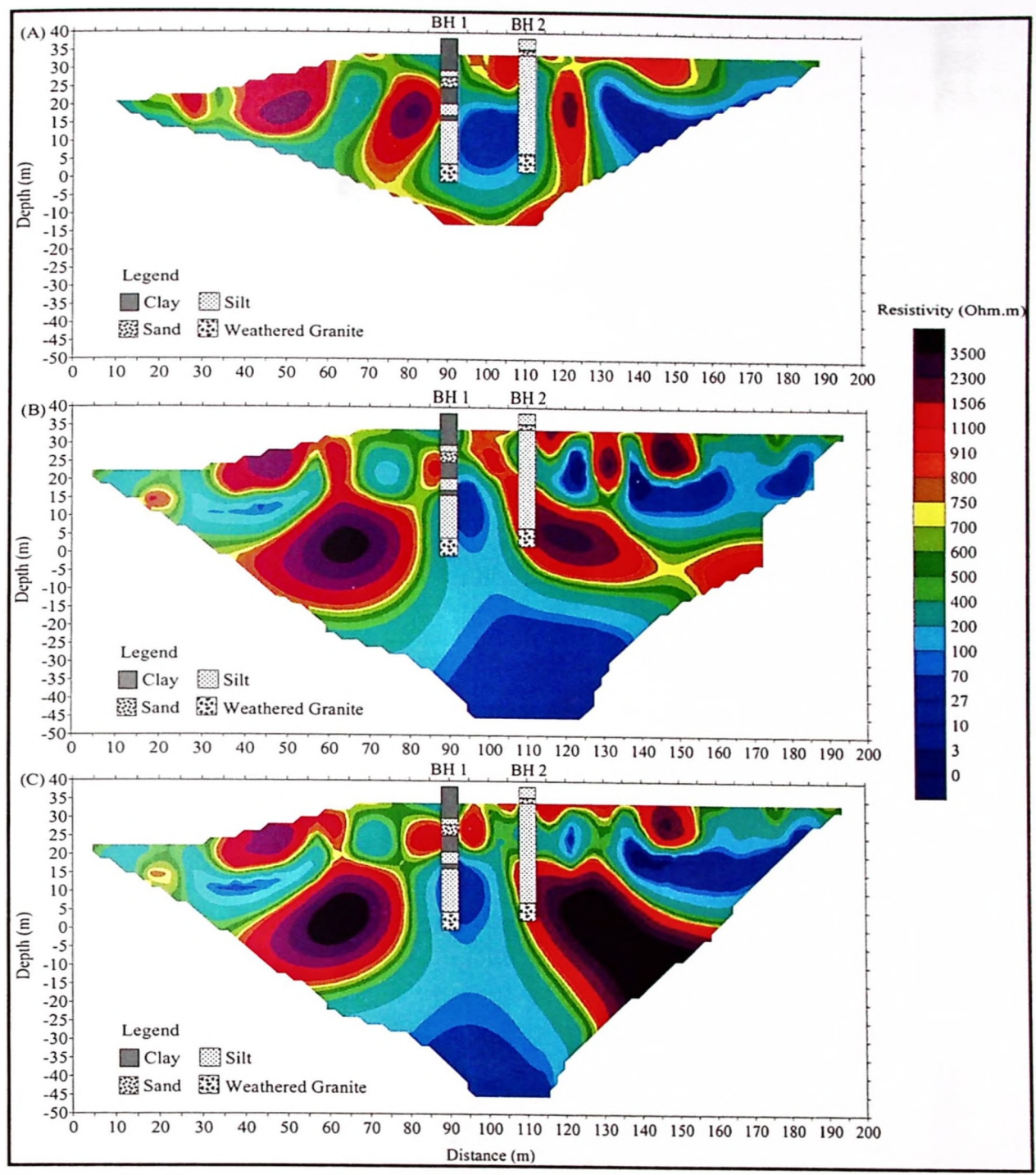


Figure 4.61: Inversion of model resistivity results at Minden, USM, Penang. A) W-S array; B) P-D array and C) the DLA technique.

### 4.3.2 Bukit Bunuh, Perak

Figure 4.62 shows inversion of model resistivity results for W-S array, P-D array and the DLA technique respectively. Total of datum points for W-S array is

665, P-D array is 1317 and the DLA technique is 1982. The number of apparent data points is obtained after the filtering process. It shows that the subsurface is made up of overburden (sandy and silty soils) at depth of 81.5–70.0 m. It is represented by resistivity values of 120–400  $\Omega$ .m. The weathered granite has resistivity values of 300–2100  $\Omega$ .m. The interpretation of these values were made from the resistivity values along a borehole data (BH 6).

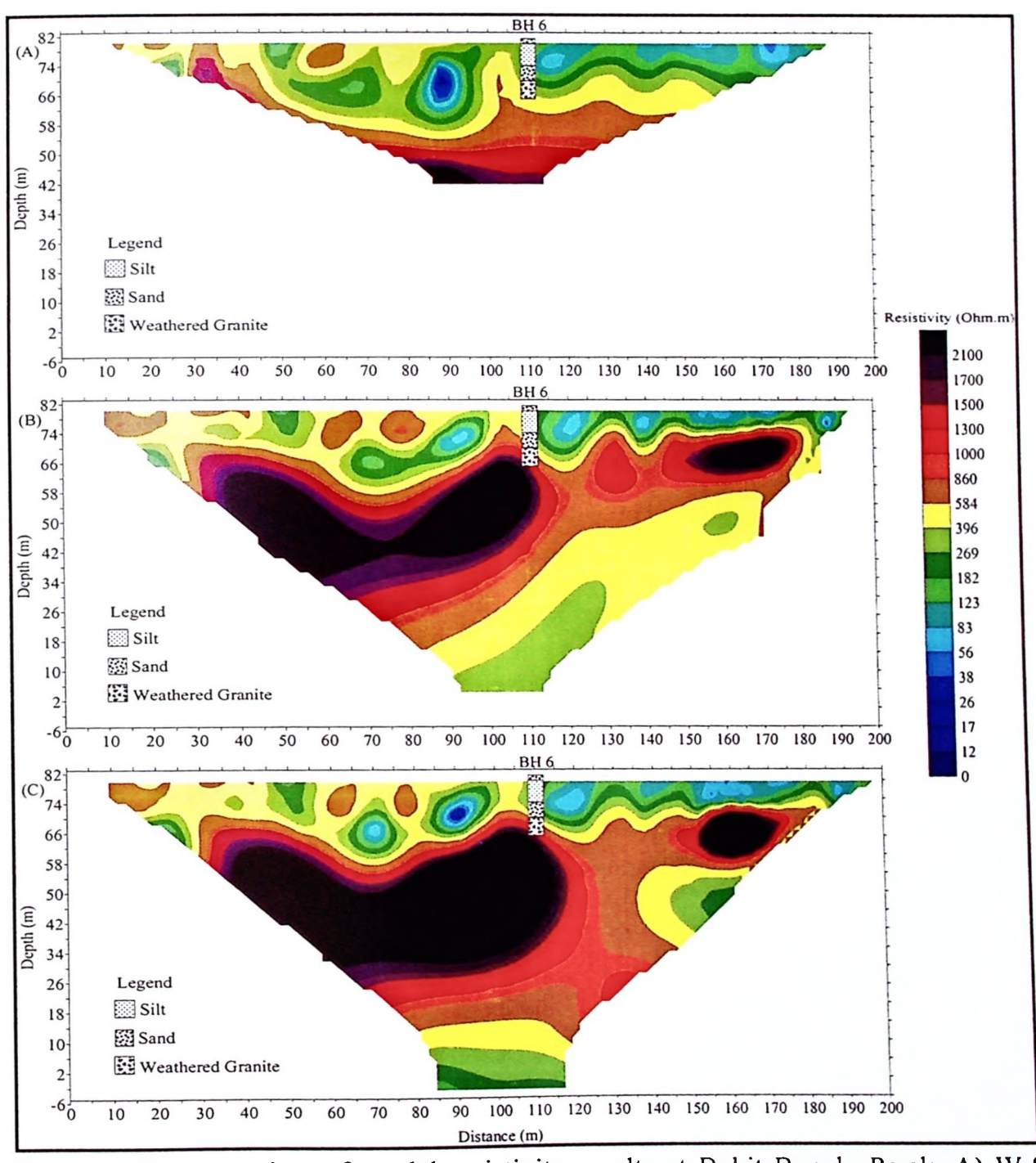


Figure 4.62: Inversion of model resistivity results at Bukit Bunuh, Perak. A) W-S array; B) P-D array and C) the DLA technique.

### 4.4 Chapter summary

In this chapter, the results of the 2-D computerized models or namely synthetic models and a field model are presented. Four different synthetic models were created and were used to investigate the imaging capabilities using four different arrays and the DLA technique of two different arrays. Secondly, the numerical comparative assessment was introduced for individual array and the DLA technique. The best and suitable two arrays were determined which was based on the numerical comparative analysis results and their ability to image the known target. Lastly, validation of the DLA technique using the two best and suitable arrays are applied to the actual field studies.

In conclusion, the field study results show that the DLA technique is good in producing and enhancing the resolution of inversion of model resistivity results. This was supported by the increase of total datum point (dense data quality) of model resistivity when compared to individual array (Dahlin and Zhou, 2004). The DLA technique is also more acceptable in subsurface study compared to individual array (de la Vega et al. 2003; Candansayar, 2008; Berge and Drahor, 2009; Neyamadpour, 2010a; 2010b). In addition, by using this approach, the effect of noisy apparent resistivity data points can be reduced (Loke, 2004; 2014). Even though, the time taken using the DLA technique was twice, the outcome is reliable and this technique has good technical merit. Therefore, good quality and reliability of the field study data is a more important matter than speed of data acquisition. However, this condition can only be achieved if a proper selection of arrays is made.

#### **CHAPTER 5**

## CONCLUSION AND RECOMMENDATIONS

### 5.0 Conclusion

With proper array selection, 2-D electrical resistivity method seems to be the most suitable geophysical method in all study fields such as engineering and environmental. However, the depth and size of the target is very critical in the 2-D resistivity imaging (Loke, 2004; 2014). Resolution is decreased when current travels away from electrodes at the surface (Loke, 1999a). Poor scalability of electrode spacing, wrong array selection and poor ground contact lead to bad interpretation and improper use of the electrical resistivity method (Loke, 2014).

The 2-D electrical resistivity survey with common arrays such as Dipole-Dipole (D-D), Pole-Dipole (P-D, Wenner (W) and W-S has advantages and disadvantages (Loke, 2004; 2014). This research aims to realize the modification in data processing of common 2-D electrical resistivity method. This research is classified into three phases.

The first phase involved 2-D computerized models or namely synthetic models and a field model was presented. Four different synthetic models were created and used to investigate the imaging capabilities using four different arrays and the DLA technique for two different arrays. In the second phase, the numerical comparative assessment was introduced for each individual array and the DLA technique of two different arrays. The two best and suitable arrays were determined

which is based on the numerical comparative analysis results and their ability to image the known target. In phase three, validation of the DLA technique using two best and suitable arrays were applied to the actual field surveys. The field study was carried out at Minden, USM, Penang and Bukit Bunuh, Lenggong, Perak respectively.

In this study, inversion of model resistivity results (individual and the DLA technique) were validated with inline borehole data. The DLA technique used in the data processing is successful in enhancing inversion of model resistivity results. This can only happen when proper consideration is given to type of arrays used. For the array selection, the numerical comparative analysis was carried out for three main investigated parameters. They are (i) total number of data points (apparent resistivity) (ΣDP<sub>App.(DLA)</sub>), (ii) percentage of overlapping inversion of model resistivity data (ΔPO<sub>DLA</sub>) and (iii) the ability to resolve the known target. This research indicates that the DLA technique has its technical merit and was successfully applied in this research.

In addition, the DLA technique can increase the confidence level of geophysicists in data interpretation. The technical merit of this geophysical method can also be improved well with this approach in data processing and data interpretation works. Even though, the time taken in data acquisition using the DLA technique is twice as long, the result is reliable and acceptable which is helpful in the subsurface interpretation. In conclusion, all the three study objectives were successfully identified in this study. The first objective of the study is to compare the numerical comparative assessment for individual array and the DLA technique of two different arrays. The second objective of the study is to improve resolution in data processing using the DLA technique on two different arrays. The last objective

of the study is to validate the DLA technique of two different arrays to provide significant improvement in 2-D resistivity imaging data quality.

#### 5.1 Recommendations for future research

An application of 2-D resistivity imaging method with the DLA technique has proven beneficial and useful for shallow subsurface investigation. In future research, it is recommended that the processing software should be improved so that the computer used is more stable during handling the large number of data points. It is also recommended to use portable battery pack for injecting current especially for complex geological studies and long period of field survey. Lastly, wireless electrodes can be developed in the future to be more cost and time effective. That means, heavy resistivity cables would no longer be needed and travelling cost would be more effective.

#### REFERENCES

- Abdul Nassir, S. S. A. (1997). A study of the use different electrode array for electrical imaging surveys. Unpublished MSc thesis, Universiti Sains Malaysia, Malaysia.
- ABEM (2006). ABEM instruction manual terrameter SAS4000/SAS1000. ABEM Instrument AB, Sundbyberg, Sweden.
- Adiat, K. A. N., Nawawi, M. N. M., Abdullah, K., Ishola, K. S. & Abdulrahman, A. (2013). Effect of electrode spacing and inversion techniques on the efficacy of 2-D resistivity imaging to delineate subsurface features. American Journal of Applied Sciences, 10(1), 64-72.
- Alwan, I. A. K. (2013). Comparison between conventional arrays in 2-D electrical resistivity imaging technique for shallow subsurface structure detection of the University of Technology. *Engineering and Technology Journal*, 31(10), 1817-1824.
- al Hagrey, S. A. (2012). 2D optimized electrode arrays for borehole resistivity tomography and CO2 sequestration modelling. *Pure and Applied Geophysics*, 169(7), 1283-1292.
- Archie, G. E. (1942). The electrical resistivity log as an aid in determining some reservoir characteristics. Transactions of the American Institute of Mining, Metallurgical and Petroleum Engineers (AIME), 146, 54-62.
- Araffa, S. A. S., Helaly, A. A., Khozium, A., Lala, A. M. S., Soliman, S. A. & Hassan, N. M. (2015). Delineating groundwater and subsurface structures by using 2D resistivity, gravity and 3D magnetic data interpretation around Cairo-Belbies Desert road, Egypt. NRIAG Journal of Astronomy and Geophysics, 4(1), 134-146.
- Athanasiou, E. N., Tsourlos, P. I., Papazachos, G. N. & Tsokas, G. N. (2007). Combined weighted inversion of electrical resistivity data arising from different array types. Journal of Applied Geophysics, 62(2), 124-140.
- Azwin, I. N., Saad, R., Saidin, M., Nordiana, M. M., Bery, A. A. & Hidayah, I. N. E. (2015). Combined analysis of 2-D electrical resistivity, seismic refraction and geotechnical investigation for Bukit Bunuh complex crater. *IOP Conference Series Earth and Environmental Science*, 23(1), 012013.
- Barker, R. D. (1979). Signal contribution sections and their use in resistivity studies. Geophysical Journal of the Royal Astronomy Society, 59(1), 123-129.

- Barker, R. D. (1992). A simple algorithm for electrical imaging of the subsurface. *First Break*, 10, 53-62.
- Berge, M. A. & Drahor, MG. (2009). Optimum electrical resistivity tomography (OERT) approach using combination of different arrays in archaeological investigations. Archaeo Sciences, Suppl. 33, 263-265.
- Blome, M., Maurer, H. & Greenhalgh, S. (2011). Geoelectric experimental design Efficient acquisition and exploitation of complete pole-bipole data sets. *Geophysics*, 76(1), F15-F26.
- Broomfield, J. P. (2003). Corrosion of steel in concrete. Understanding, investigation and repair. Spoon Press.
- Candansayar, M. E. (2008). Two-dimensional individual and joint inversion of threeand four-electrode array dc resistivity data. Journal of Geophysics and Engineering, 5, 290-300.
- Chambers, J. E., Ogilvy, R., Meldrum, P. & Nissen, J. (1999). 3-D resistivity imaging of buried oil-and tar-contaminated waste deposits. European Journal of Environmental and Engineering Geophysics, 4, 3-15.
- Chambers, J. E., Ogilvy, R. D., Kuras, O., Cripps, J. C., & Meldrum, P. I. (2002). 3D electrical imaging of known targets at a controlled environmental test site. *Environmental Geology*, 41(6), 690-704.
- Chambers, J. E., Gunn, D. A., Wilkinson, P. B., Meldrum, P. I., Haslam, E., Holyoake, S., Kirkham, M., Kuras, O., Merritt, A., & Wragg, J. (2014). 4D electrical resistivity tomography monitoring of soil moisture dynamics in an operational railway embankment. *Near Surface Geophysics*, 12(1), 61-72.
- Cho, I. K., Ha, I. S., Kim, K. S., Ahn, H. Y., Lee, S., & Kang, H. J. (2014). 3D effects on 2D resistivity monitoring in earth-fill dams. *Near Surface Geophysics*, 12(1), 73-81.
- Coles, D. A., & Morgan, F. D. (2009). A method of fast, sequential experimental design for linearized geophysical inverse problems. *Geophysical Journal International*, 178(1), 145-158.
- Constable, S. C., Parker, R. L. & Constable, C. G. (1987). Occam's inversion: A practical algorithm for generating smooth models from electromagnetic sounding data. *Geophysics*, 52(3), 289-300.
- Dahlin, T. (1996). 2-D resistivity surveying for environmental and engineering applications. First Break, 14, 275-284.
- Dahlin, T., Bernstone, C. & Loke, M. H. (2002). A 3-D resistivity investigation of a contaminated site at Lemacken in Sweden. *Geophysics*, 60(6), 1682-1690.

- Dahlin, T., Lofroth, H., Schalin, D. & Suer, P. (2013). Mapping quick clay using geoelectrical imaging and CPTU- resistivity. *Near surface geophysics*, 11(6), 659-670.
- Dahlin, T., Aronsson, P. & Thornelof, M. (2014). Soil resistivity monitoring of an irrigation experiment. *Near surface Geophysics*, 12(1), 35-43.
- Dahlin, T. & Zhou, B. (2004). A numerical comparison of 2-D resistivity imaging with 10 electrode arrays. Geophysical Prospecting, 52(5), 379-398.
- de la Vega, M., Osella, A. & Lascano, E. (2003). Joint inversion of Wenner and Dipole-Dipole data to study a gasoline-contaminated soil. Journal of Applied Geophysics, 54, 97-109.
- deGroot-Hedlin, C. & Constable, S. (1990). Occam's inversion to generate smooth two dimentional models from magnetotelluric data. Geophysics, 55, 1613-1624.
- Dey, A. & Morrison, H. F. (1979a). Resistivity modelling for arbitrary shaped two-dimensional structures. Geophysical Prospecting, 27, 1020-1036.
- Donohue, S., Long, M., O'Connor, P., Helle, T. E., Pfuffhuber, A. A. & Romoen, M. (2012). Multi-method geophysical mapping of quick clay. *Near Surface Geophysics*, 10(3), 207-219.
- Ellis, R. G. & Oldenburg, D. W. (1994). Applied geophysical inversion. Geophysical Journal International, 116, 5-11.
- Ezersky, M. G., Eppelbaum, L. V., Al-Zoubi, A., Keydar, S., Abueladas, A., Akkawi, E. & Medvedev, B. (2013). Geophysical prediction and following development sinkholes in two Dead Sea areas, Israel and Jordan. *Environmental Earth Sciences*, 70(4), 1463-1478.
- Farquharson, C. G. & Oldenburg, D. W. (2004). A comparison of automatic techniques for estimating the regularization parameter in non-linear inverse problems. Geophysical Journal International, 156, 411-425.
- Fauziah, A., Yahaya, A. S. & Farooqi, M. A. (2006). Characterization and geotechnical properties of Penang residual soils with emphasis on landslide. *American Journal of Environmental Sciences*, 2(4), 121-128.
- Fox, R. C., Hohmann, G. W., Killpack, T. J. & Rijo, L. (1980). Topographic effect in resistivity and induced-polarization surveys. *Geophysics*, 45(1), 75-93.
- Furman, A., Ferre, T. P. A. & Heath, G. L. (2007). Spatial focusing of electrical resistivity surveys considering geological and hydrologic layering. *Geophysics*, 72(2), F65-F73.

- Giang, N. V., Duan, N. B., Thanh, L. N., & Hida, N. (2013). Geophysical techniques to aquifer locating and monitoring for industrial zones in North Hanoi, Vietnam. *Acta Geophysica*, 61(6), 1573-1597.
- Gharibi, M. & Bentley, L. R. (2005). Resolution of 3-D electrical resistivity images from inversions of 2-D orthogonal lines. *Journal of Environmental and Engineering Geophysics*, 10(4), 339-349.
- Griffiths, D. H. & Turnbull, J. (1985). A multi-electrode array for resistivity surveying. First Break, 3, 16-20.
- Griffiths, D. H., Turnbull, J. & Olayinka, A. I. (1990). Two-dimensional resistivity mapping with a computer controlled array. *First Break*, 8, 121-129.
- Hamdan, H. A. & Vafidis, A. (2013). Joint inversion of 2D resistivity and seismic travel time data to image saltwater intrusion over karstic areas. *Environmental Earth Sciences*, 68(7), 1877-1885.
- Hatanaka, H., Aono, T., Mizunaga, H. & Ushijima, K. (2005). Three-dimensional modeling and inversion of the mise-a-la-masse data using a steel-casing borehole. *Proceedings World Geotermal Congress* 2005. Antalya, Turkey, April 24<sup>th</sup> -29<sup>th</sup>, 2005.
- Heenan, J., Slater, L. D., Ntarlagiannis, D., Atekwana, E. A., Fathepure, B. Z., Dalvi, S., Ross, C., Werkema, D. D. & Atekwana, E. A. (2015). Electrical resistivity imaging for long-term autonomous monitoring of hydrocarbon degradation: Lessons from the Deewater Horizon oil spill. *Geophysics*, 80(1), B1-B11.
- Imam, M. H., Hossain, D. & Woobaid Ullah, A. S. M. (2013). Geoelectrical resistivity survey for the evaluation of hydrogeological condition of Bagerhat Sadar and the adjacent areas, Bangladesh. *Journal of the Geological Society of India*, 82(3), 290-294.
- Ishola, K. S., Nawawi, M. N. M., Abdullah, K., Sabri, A. I. A. & Adiat, K. A. N. (2014a). Assessment of the reliability of producing two-dimensional models using an image processing technique. SpringPlus, 3:214, 1-12.
- Ishola, K. S., Nawawi, M. N. M. & Abdullah, K. (2014b). Combining multiple electrode arrays for 2-D electrical imaging using unsupervised classification technique. Pure and Applied Geophysics, 172(6), 1615-1642.
- Ishola, K. S. (2015). Development of united integrated model to characterize geophysical data using image processing technique. Unpublished PhD thesis. Universiti Sains Malaysia.
- Jabatan Mineral dan Geosains Malaysia, (1985). Peta Geologi Semenanjung Malaysia. (<a href="http://www.jmg.gov.my//add\_on/mt/smnjg/tiles/">http://www.jmg.gov.my//add\_on/mt/smnjg/tiles/</a>). Online on March 17<sup>th</sup>, 2015.

- Juhojuntti, N. & Kamm, J. (2015). Joint inversion of seismic refraction and resistivity data using layered models Applications to groundwater investigation. *Geophysics*, 80(1), E43-E55.
- Jupp, D. L. & Vozoff, K. (1975). Stable iterative methods for the inversion of geophysical data. Geophysical Journal of Royal Astronomy Society, 42, 957-976.
- LaBrecque, D. & Daily, W. (2008). Assessment of measurement errors for galvanic-resistivity electrodes of different composition. *Geophysics*, 73(2), F55-F64.
- Lehmann, H. (1995). Potential representation by independent configuration on a multi electrode array. *Geophysical Journal International*, 120(2), 331-338.
- Loke, M. H. (1994). The inversion of two-dimensional resistivity data. Unpublished PhD thesis, University of Birmingham.
- Loke, M. H. & Barker, R. D. (1995a). Improvements to the Zohdy method for the inversion of resistivity sounding and pseudosection data. *Computers and Geosciences*, 21, 321-332.
- Loke, M. H. & Barker, R. D. (1995b). Least-squares deconvolution of apparent resistivity pseudosection. *Geophysics*, 60(6), 1682-1690.
- Loke, M. H. & Barker, R. D. (1996). Rapid least-squares inversion of apparent resistivity pseudosection: by a Quasi-Newton method. *Geophysical Prospecting*, 44, 131-152.
- Loke, M. H. (1999a). Electrical imaging surveys for environmental and engineering studies. Universiti Sains Malaysia, Penang, Malaysia.
- Loke, M. H. (199b). Time-lapse resistivity imaging inversion. Proceedings of the 5<sup>th</sup> Metting of the Environmental and Engineering European Society, Em1.
- Loke, M. H. (2001). Instruction manual for the 2D resistivity forward modeling program RES2DMOD. Universiti Sains Malaysia, Penang, Malaysia.
- Loke, M., Acworth, I. & Dahlin, T. (2003). A comparison of smooth and blocky inversion methods in 2D electrical imaging surveys. Exploration Geophysics, 34(3), 182-187.
- Loke, M. H. (2004). Tutorial: 2-D and 3-D electrical imaging surveys. A practical guide to 2-D and 3-D surveys and interpretation for environmental and engineering studied. Universiti Sains Malaysia, Penang, Malaysia.
- Loke, M. H., Wilkinson, P. B. & Chambers, J. E. (2010). Fast computation of optimized electrode arrays for 2-D resistivity surveys. *Computers and Geosciences*, 36(11), 1414-1426.

- Loke, M. H. & Dahlin, T. (2010). Methods to reduce banding effects in 3-D resistivity inversion. *Proceedings the 16<sup>th</sup> European Meeting of Environmental and Engineering Geophysics*, Zurich, Switzerland, p. A16.
- Loke, M.H., Chambers, J.E., Rucker, D.F., Kuras, O. & Wilkinson, P.B. (2013). Recent developments in the direct-current geoelectrical imaging method. Journal of Applied Geophysics, 95, 135-156.
- Loke, M. H. (2014). Tutorial: 2-D and 3-D electrical imaging surveys. Geotomo, Malaysia.
- Lowrie, W. (1997). Fundamental of geophysics. Cambridge University Press, Switzerland, 254-257.
- Martinez-Moreno, F. J., Pedrera, A., Ruano, P., Galindo-Zaldivar, J., Martos-Rosillo, S., Gonzalez-Castillo, L., Sanchez-Ubeda, J. P. & Marin-Lechado, C. (2013). Combined microgravity, electrical resistivity tomography and induced polarization to detect deeply buried caves: Algaidilla cave (Southern Spain). Engineering Geology, 162, 67-78.
- Martorana, R., Fiandaca, G, Casas Ponsati, A. & Cosentino, P. L. (2009). Comparative test on different multi-electrode arrays using models in near-surface geophysics. Journal Geophysics and Engineering, 6, 1-20.
- Moller, I., Jacobsen, B. H. & Christensen, N. B. (2001). Rapid inversion of 2-D geoelectrical data by multichannel deconvolution. *Geophysics*, 66(3), 800-808
- Muztaza, N. M. (2013). Development of enhancing horizontal resolution (EHR) technique in 2-D resistivity survey. Unpublished PhD thesis, Universiti Sains Malaysia, Malaysia.
- Narayan, S., Dusseault, M. B. & Nobes, D.C. (1994). Inversion techniques applied to resistivity inversion problems. Inverse problem, 10, 669-686.
- Nenna, V., Pidlisecky, A. & Knight, R. (2011). Informed experimental design for electrical resistivity imaging. *Near Surface Geophysics*, 9(5), 469-482.
- Neville, A. M. (2006). Properties of concrete. Pearson Education Limited.
- Neyamadpour, A., Wan Abdullah, W. A. T., Taib, S. & Neyamadyur, B. (2010a). Comparison of wenner and dipole-dipole arrays in the study of an underground three-dimensional cavity. Journal of Geophysics and Engineering, 7(1), 30-40.
- Neyamadpour, A., Wan Abdullah, W. A. T., Taib, S. & Neyamadyur, B. (2010b). Use of four-electrode arrays in three-dimensional electrical resistivity imaging survey. Studia Geophysica et Geodaetica, 54(2), 299-311.

- Norman, H. S. & Fujita, K. (1997). Principle of geophysics. Malden, MA: Blackwell Science Inc.
- Nordiana, M. M., Saad, R., Mokhtar, S. M. Nawawi, N. M. M. & Azwin, I. N. (2012). Iamging subsurface characterization at Bukit Bunuh using 2-D resistivity method: The effectiveness of enhancing horizontal resolution (EHR) technique. *International Journal of Environmental Science and Development*, 3(6), 569-573.
- Nyquist, J. E., Peake, J. S. & Roth, M. J. S. (2007). Comparison of an optimized resistivity array with dipole-dipole soundings in karst terrain. *Geophysics*, 72(4), F139-F144.
- Oladunjoye, M. & Jekayinfa, S. (2015). Efficacy of hummel (modified schlumberger) arrays of vertical electrical sounding in groundwater exploration: case study of parts of Ibadan Metropolis, Southwestern Nigeria. *International Journal of Geophysics*, 2015. ID 612303, 24 pages.
- Olayinka, A. I. & Yaramanci, U. (2000). Assessment of the reliability of 2D inversion of apparent resistivity data. Geophysical Prospecting, 48(2), 293-316.
- Oldenburg, D. W. (1978). The interpretation of direct current resistivity measurements. *Geophysics*, 43(3), 610-625.
- Ong, W. S. (1993). The geology and engineering geology of Penang Island. Geological Society of Malaysia, Malaysia.
- Paul, E. T. (2007). Physics. 7th Ed. McGraw-Hill Higher Education.
- Pelton, W. H., Ward, S. H., Hallof, P. G., Sill, W. R. & Nelson, P. H. (1978). Mineral discrimination and removal of inductive coupling with multifre-quency IP. *Geophysics*, 43(3), 588-609.
- Perren, L. J. (2005). *Investigating the performance of electrical resistivity arrays*. MSc thesis, Virginia Polytechnic Institute and State University.
- Petrick, W. R., Pelton, W. H. & Ward, S. H. (1977). Ridge regression inversion applied to crustal resistivity sounding data from South Africa. *Geophysics*, 42(5), 995-1005.
- Pradhan, B., Chaudhari, A., Adinarayana, J. & Buchroithner, M. F. (2012). Soil erosion assessment and its correlation with landslide events using remote sensing data and GIS: a case study at Penang Island, Malaysia. *Environmental Monitoring and Assessment*, 184(2), 715-727.
- Pustika, R., Nikolaj, M., Dostal, I. & Kusnirak, D. (2012). Determination of cavities using electrical resistivity tomography. *Contributions to Geophysics and Geodesy*, 42(2), 201-211.

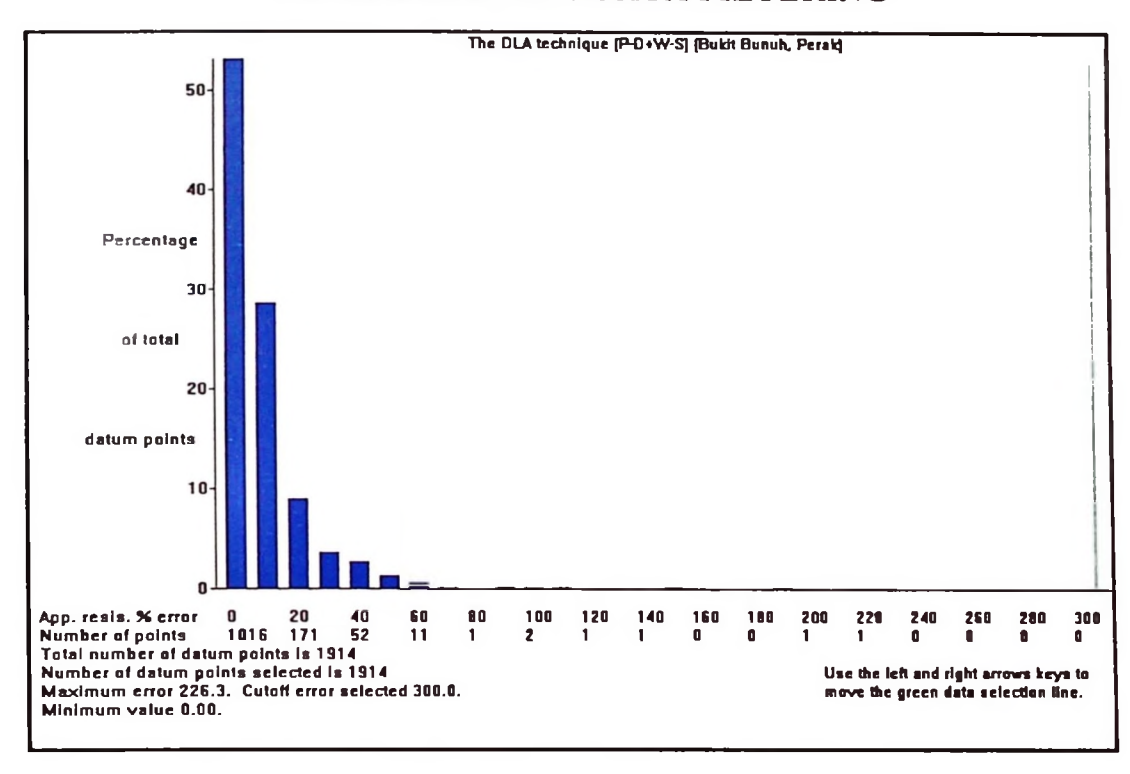
- Ramirez, A., Daily, W., LaBrecque, K., Owen, E. & Chesnut, D. (1993). Monitoring an underground stream injection process using electrical resistance tomography. *Water Resources Research*, 29(1), 73-87.
- Ramirez, A. L., Newmark, R. L. & Daily, W. D. (2003). Monitoring carbon dioxide floods using electrical resistance tomography (ert): sensitivity studies. *Journal of Environmental and Engineering Geophysics*, 8(3), 187-208.
- Reynolds, J. M. (1997). An introduction to applied and environmental geophysics. John Willey & Sons Ltd. West Sussex, England.
- Rijo, L., Pelton, W. H., Feitosa, E. C. & Ward, S. H. (1977). Interpretation of apparent resistivity data from Apodi Valley, Rio Grande Do Norte, Brazil. *Geophysics*, 42(4), 811-822.
- Robinson, J., Johnson, T. & Slater, D. (2015). Challenges and opportunities for fractured rock imaging using 3-D cross-borehole electrical resistivity. *Geophysics*, 80(2), E49-E61.
- Roy, A. & Apprao, A, (1971). Depth of investigation in direct current methods: Geophysics, 36, 943-959.
- Rucker, D. F. & Noonan, G. E. (2013). Using marine resistivity to map geotechnical properties: a case study in support of dredging the Panama Canal. *Near Surface Geophysics*, 11(6), 625-637.
- Saad, R. (2009). Novel protocol of engineering geophysics in urban environments, Unpublished PhD thesis, Universiti Sains Malaysia, Malaysia.
- Saad, R., Muztaza, N. M., Nordin, M. N. M., Nafiu, A. K. A., Ismail, N. E. H., Ismail, N., Bery, A. A. & Mohamad, E. T. (2011). Correlation between 2-D resistivity and seismic refraction methods in shallow subsurface investigation. Paper presented at *National Geosciences Conference 2011*. The Puteri Pasific Johor Bahru, Johor, Malaysia.
- Saidin, M. M. (1997). Monograf: Kajian perbandingan tapak paleolitik kampong temelong dengan kota tampan dan sumbangan terhadap kebudayaan zaman pleistosen akhir di asia tenggara. *Malaysia Museums Journal*, 32.
- Samsudin, A. R., Mohammed, A. S. & Hamzah, U. (1998). The use of electrical and seismic methods for imaging shallow subsurface structure of limestone at Batu Caves, Kuala Lumpur, Malaysia. Proceedings of the 9<sup>th</sup> Regional Congress on Geology, Mineral and Energy Resources of Southeast Asia, 72-75.
- Samsudin, A. R., Haryono, A., Hamzah, U. & Rafek, A. G. (2008). Salinity mapping of coastal groundwater aquifers using hydrochemical and geophysical methods: A case study from North Kelantan, Malaysia. *Environmental Geology*, 55(8), 1737-1743.

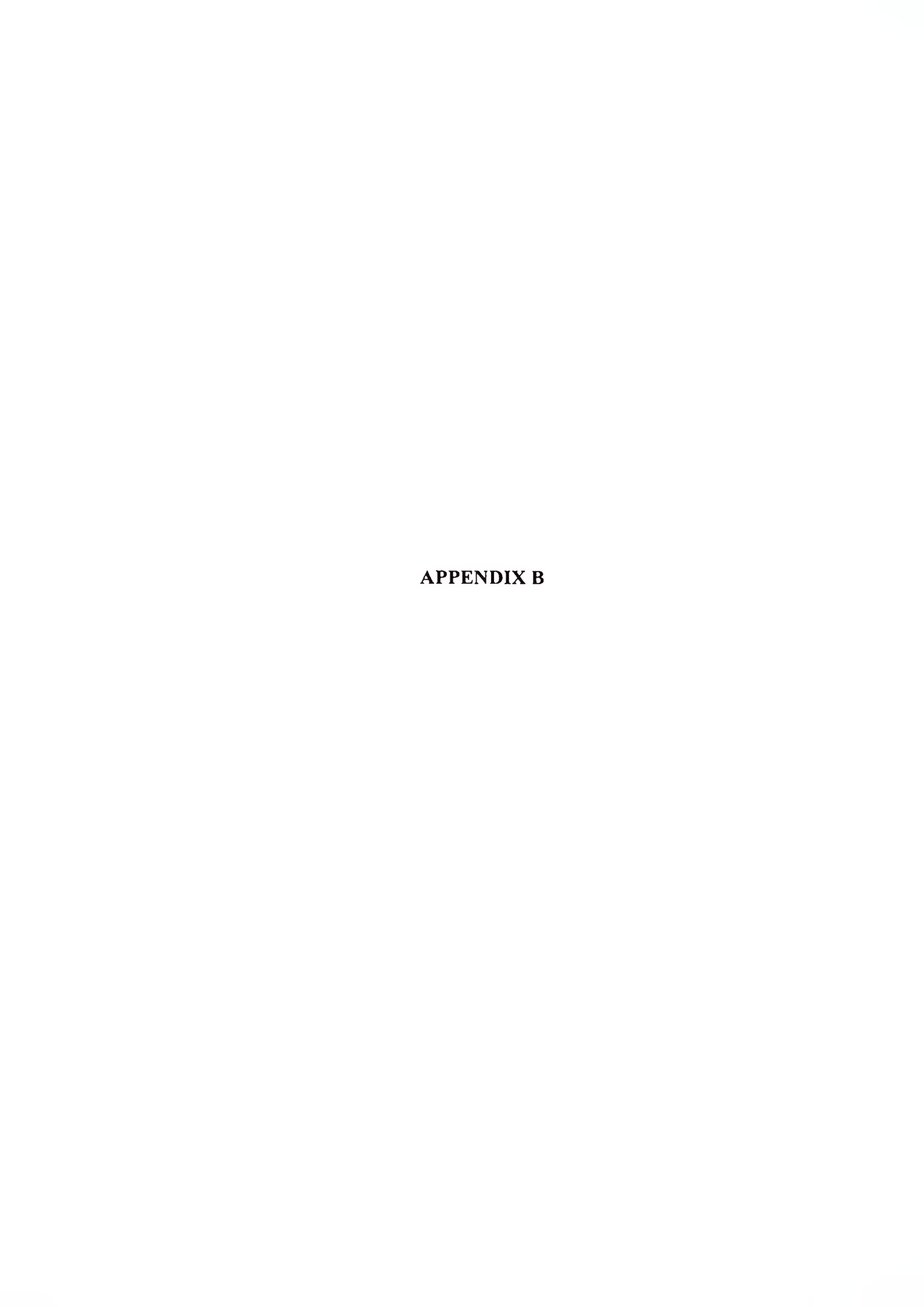
- Sasaki, Y. (1992). Resolution of resistivity tomography inferred from numerical simulation. *Geophysical Prospecting*, 40(4), 453-464.
- Schwarzbach, C, Borner, R.-U. & Spitzer, K. (2005). Two dimensional inversion of direct current resistivity data using a parallel, multi-objective genetic algorithm. Geophysical Journal International, 162, 685-695.
- Seaton, W. J. & Burby, T. J. (2000). Aquifer characterization in the Blue Ridge physiographic province using resistivity profiling and borehole geophysics: geologic analysis. *Journal of Environmental and Engineering Geophysics*, 5(3), 45-58.
- Shima, H. (1990). Two-dimensional automatic resistivity inversion technique using alpha centers. *Geophysics*, 55(3), 354-361.
- Shima, H. (1992). 2-D and 3-D resistivity image reconstruction using crosshole data. *Geophysics*, 57(10), 1270-1281.
- Smith, D. L. (1986). Application of the pole-dipole resistivity technique to the detection of solution cavities beneath highways. *Geophysics*, 51(3), 833-837.
- Spiegel, R. J., Sturdivant, V. R. & Owen, T. E. (1980). Modeling resistivity anomalies from localized voids under irregular terrain. *Geophysics*, 45(7), 1164-1183.
- Streckeisen, A. L (1967). Classification and nomenclature of igneous rocks, N Jahrbuch fur Mineralogie Abhandlungen. 107(2&3), Schweizerbart'sche Verlagsbuchhandlung, Stuttgart, 144-240.
- Storz, H., Stroz, W. & Jacobs, F. (2000). Electrical resistivity tomography to investigate geological structures of the earth's upper crust. *Geophysical Prospecting*, 48(3), 455-471.
- Stummer, P., Maurer, H. & Gree, A. (2004). Experimental design: electrical resistivity data sets that provide optimum subsurface information. *Geophysics*, 69(1), 120-129.
- Szalai, S. & Szarka, L. (2008). On the classification of surface geoelectric arrays. Geophysical Prospecting, 56(2), 159-175.
- Szalai, S., Kis, A., Metwaly, M., Lemperger, I. & Szokoli, K. (2015). Increasing the effectiveness of electrical resistivity tomography using γlln configurations. Geophysical Prospecting, 63(2), 508-524.
- Talib, K., Abdullah, J. & Saidin, M. (2009). Evidence of meteorite impact in Bukit Bunuh and its contribution to archaeology", Saidin, M., & Razak K. A. (eds.). Proceedings of the International Seminar on Sharing Our Archaeological Heritage, Yayasan Warisan Johor, Johor Baharu, 173-186.

- Tong, L. T. & Yang, C. H. (1990). Incorporation of topography into two-dimensional resistivity inversion. *Geophysics*, 55(3), 354-361.
- Tripp. A. C., Hohmann, G. W. & Swift Jr, C. M. (1984). Two-dimensional resistivity inversion. *Geophysics*, 49(10), 1708-1718.
- Tsokas, G. N., Tsourlos, P. I., Vargemezis, G. N. & Novack, M. (2008). Non-destructive electrical resistivity tomography for indoor investigation: In the case of Kapnikarea Church in Athens. *Archaeological Prospection*, 15(1), 47-61.
- Ward, S. H. (1990). Resistivity and induced polarization methods. In: Ward, H. S. (ed.), Geotechnical and Environmental Geophysics. Investigation in Geophysics', No. 5, SEG, United States of America, 147-190.
- White, R. M. S., Collins, S., Denne, R. & Brown, P. (2001). A new survey design for 3D IP modelling at Copper hill. *Exploration Geophysics*, 32(4), 152-155.
- Wilkinson, P. B., Chambers, J. E., Meldrum, P. I., Ogilvy, R. D. & Caunt, S. (2006a). Optimization of array configurations and panel combinations for the detection and imaging of abandoned mineshafts using 3-D cross-hole electrical resistivity tomography. *Journal of Environmental and Engineering Geophysics*, 11(3), 213-221.
- Wilkinson, P. B., Meldrum, P. I., Chambers, J. E., Kuras, O. & Ogilvy, R. D. (2006b). Improved strategies for the automatic selection of optimized sets of electrical resistivity tomography measurement configuration. *Geophysical Journal International*, 167(3), 1119-1126.
- Zhou, B. & Greenhalgh, S. A. (2000). Cross-hole resistivity tomography using different electrode configurations. Geophysical Prospecting, 48, 887-917.
- Zhu, T. & Feng, R. (2011). Resistivity tomography with a vertical line source and its application to the evaluation of residual oil saturation. *Journal of Applied Geophysics*, 73(2), 155-163.
- Zohdy, A. A. R. (1989). A new method for the automatic interpretation of Schlumberger and Wenner sounding curves. *Geophysics*, 54(2), 245-253.

APPENDIX A

### 2-D RESISTIVITY DATA FILTERING





### **GENERAL ARRAY FORMAT**

General array format file	Comments
Bunker USM	Name of surfey line
1.5	Unit electode spacing
11	Array type (11 for general array)
0	Array type, 0 to indicate non-specific; 1 for Wenner
Type of measurement (0=Apparent resistivity, 1=resistive	Header
0	0 to indicate apparent resistivity
1716	Number of data points
2	Type of x-location, 2 for surface distance
0	Flag for IP data, 0 for none (1 if present)
4 0.0,0.0 3.0,0.0 1.0,0.0 2.0,0.0 10.753	The format for each data points is :-
4 1.0,0.0 4.0,0.0 2.0,0.0 3.0,0.0 10.309	Number of electrode used,
4 2.0,0.0 5.0,0.0 3.0,0.0 4.0,0.0 10.007	x- and z-location of C1, C2, P1, P2,
4 3.0,0.0 6.0,0.0 4.0,0.0 5.0,0.0 10.538	Apparent resistivity value
4 4.0,0.0 7.0,0.0 5.0,0.0 6.0,0.0 10.957	
	Same format for other data points
4 0.0,0.0 20.0,0.0 40.0,0.0 60.0,0.0 10.312	Last data point
Topography in separate list	Extra header required for the general array
2	2 to indicate surface distance
17	Number of of topography data points
0,15	Horizontal and vertical location of 1st point
3,16	2nd topography data point
5,17	3rd topography data point
	This is follow by similar topogarphy data point
60,15	Last topography data point
1	The topography data point number with first electrode
0	End with zero.

### APPENDIX C

BOREHOLE DATA (BH 1) AT MINDEN, USM, PENANG.



#### **DEEP BORING LOG.**

PROJECT:

KAJIAN SUB-PERMUKAAN DI KAWASAN RUMAH TETAMU, USM, PULAU PINANG.

	0:		meter		Sup	pervi	sor :	Osn	nan l	B Abo	dullah.			
Sheet No:	1	of:	4	Type of Drill:	YWE (Wash)			Dat	e :		03.1	2.20	)13	
DEPTH			DEC	COURTION OF COM				SAI	MPL					
(meter)	COL	OUR (	CONS	CRIPTION OF SOIL ISTENCY, RELATI\	/F DENSITY	DEPTH	No			_	d Tes			REMARKS
		G	RAIN	SIZE, TEXTURE E	TC.	(meter)	No. (Cls.)	75 mm		75 mm	75 mm	75 mm		
1.50	Medium s	tiff, lig	ht bro	wn reddish CLAY wi	th	1.50 -	P1	1	0	1	1	2	2	N = 6
	traces of	gravel	and d	ecayed wood.		1.95	D1							Rr = 300/450 mi
3.00	Very stiff,	yellow	ish br	own reddish CLAY		3.00 -	P2	2	3	4	4	5	6	N = 19
	with a little	grave	el. (roc	k fragment)		3.45	D2	_			,	ا ا		Rr = 370/450 mi
						0.10	52							KI = 3/0/450 mr
4.50	Stiff, redd	sh gre	ey yello	ow CLAY		4.50 -	P3	1	2	3	3	4	3	N = 13
	with trace:	s of gr	avel.			4.95	D3	·	_	ľ	ľ		ŭ	Rr = 350/450 m
														TXI = 330/430 IIII
6.00	Stiff, reddi	sh gre	y brov	vn CLAY		6.00 -	P4	2	2	3	4	4	4	N = 15
						6.45	D4							Rr = 310/450 m
7.50	Very stiff,	ditto				7.50								
7.50	very sum,	ditto.				7.50 -	P5	2	3	3	4	5	5	N = 17
						7.95	D5							Rr = 280/450 m
9.00	Stiff, light	grey y	ellow i	eddish CLAY		9.00 -	P6	2	3	3				N = 44
	with some							-	٥	l °	3	4	4	N = 14
		g	••			9.45	D6							Rr = 200/450 m
10.50	Very stiff,	reddis	h light	yellow SILT		10.50 -	P7	3	3	4	5	5	5	N = 19
	with some	grave	ıl.			10.95	D7				Ĭ	Ĭ	Ĭ	Rr = 320/450 m
							J.							- 020/400 [[

UD = Undisturbed sample D = Disturbed Sample V.S = Vane Shear Test C = Core Sample W = Water Sample

W.L = Water Level . CR = Core Recovery (mm) R/r = Recovery Ratio (%) RQD = Rock Quality Designation

COHESIVE SOIL (N) 0-2: Very Soft 2 - 4 Soft 4 - 8 Medium Stiff 8 - 15 : Stiff 15 - 30 : 30 - Above : Very Stiff

Very Loose 4 - 10 : Loose 10 - 30 : Medium Dense 30 -50 : Dense 50 - Above : - Very Dense



#### DEEP BORING LOG.

PROJECT:

KAJIAN SUB-PERMUKAAN DI KAWASAN RUMAH TETAMU, USM, PULAU PINANG.

Borehole N	lo: BH 1		meter Supervisor : Osman B Abdullah.							dullah.		
Sheet No:	2 of: 4	Type of Drill:	YWE (Wash)	<del></del>								
DEDTIL	DECOR	DTION 65 65				SAI	MPLI	 E				
DEPTH (meter)	COLOUR CONSIST	PTION OF SOIL ENCY, RELATIV E, TEXTURE E	E DENSITY	DEPTH (meter)	No. (Cls.)	75 mm	75	Field 75 mm		75 mm	- 1	REMARKS
12.00	Medium dense, reddish S	SAND		12.00 - 12.45	P8 P8	4	6	5	5	6	6	N = 22 Rr = 320/450 mm
13.50	Medium dense, ditto.			13.50 - 13.95	P9 D9	4	5	5	6	6	6	N = 23 Rr = 280/450 mm
15.00	Medium dense, ditto.			15.00 - 15.45	P10 D10	5	6	5	5	6	5	N = 21 Rr = 450/450 mm
16.50	No Recovery			16.50 - 16.95	P11	2	2	2	2	2	3	N = 9 Rr = NIL
18.00	Very stiff, light grey yellow with traces of gravel.	rish CLAY		18.00 - 18.45	P12	2	3	3	4	4	5	N = 16 Rr = 400/450 mm
19.50	Stiff, light grey yellowish S	SILT		19.50 - 19.95	P13	3	3	4	3	4	4	N = 15 Rr = 450/ 450 mm
	Hard, reddish light grey S with traces of gravel.	ILT		21.00 - 21.45	P14 D13	8	7	7	10	10	12	N = 39 Rr = 320/450 mm

NOTES

= Standard Penetration Test (S.P.T)

UD = Undisturbed sample

D = Disturbed Sample

V.S = Vane Shear Test

C = Core Sample

W = Water Sample W.L = Water Level .

CR = Core Recovery (mm)
R/r = Recovery Ratio ( = Recovery Ratio (%) CRR

= Core Recovery Ratio (%)

= Rock Quality Designation RQD

COHESIVE SOIL (N) 0 - 2 :

2 - 4

4 - 8

8-15 :

15 - 30 : 30 - Above :

Medium Stiff Stiff Very Stiff Hard

Very Soft

Soft

NON COHE SIVE SOIL (N)

0-4 : 4-10 : Very Loose

Loose

10 - 30 : Medium Dense

30 -50 : Dense

50 - Above : · Very Dense



### DEEP BORING LOG.

PROJECT:

KAJIAN SUB-PERMUKAAN DI KAWASAN RUMAH TETAMU, USM, PULAU PINANG.

Borehole N		ВН			Reduce level:	·	meter Supervisor : Osman B Abdullah.								
Sheet No:	3	of:	4		Type of Drill:	YWE (Wash)			Dat	e :		05.1	2.20	)13	
DEPTH			חרי	C C D I	DTION OF SOM		<u></u>		SAI	MPL	E				
(meter)	COL	OUR (	CON	SURI	PTION OF SOIL ENCY, RELATI	-, VE DENSITY	DEDT				_	Tes			REMARKS
(		G	RAIN	N SIZ	E. TEXTURE E	TC.	DEPTH (meter)	No.	75			75	75	75	
							(moter)	(Cls.)	ши	ının	mm	mm	mm	mm	
22.50	Stiff, yello	wish li	ght g	grey (	CLAY		22.50 -	P15	3	4	ارا				
	with some						22.95		٦	4	3	4	4	4	N = 15
							22.95	D14							Rr = 400/450 m
24.00	Hard, light	t arev	vello	wich	CII T										
				WISII	SILI		24.00 -	P16	5	7	11	9	10	13	N = 43
	with some	grave	21.				24.45	D15							Rr = 280/450 m
05.50	11 1 120														
25.50	Hard, ditto	).					25.50 -	P17	13	17	28	22			N = 50
							25.75	D16				25 1	nm I		Rr = 220/250 m
	=														
27.00	No Recov	ery					27.00 -	P18	9	8	7	7	8	8	N = 30
							27.45								Rr = NIL
28.50	Hard, redo	lish ye	llowi	sh lig	ht grey SILT		28.50 -	P19	9	10	10	10	12	13	N = 45
							28.95	D17							Rr = 300/450 m
20.00	111 0 0			<u>.</u>	_										
	Hard, light			n SIL	Т		30.00 -	P20	11	9	12	13	10	10	N = 45
[	with some	grave	I.				30.45	D18							Rr = 120/450 m
31.50	Hard rod	lich !:-	h												
31.50	Hard, redd	nsn lig	nt gr	ey Si	LI		31.50 -	P21	29	21					N = 50
							31.60	D19		25	mm 				Rr = 100/100 n
OTES					<del></del>	<del></del>									
= Standard D = Undistur = Disturbe		est (S.P.	.T)			ecovery Ratio (%)		NON C			OIL (N	_			

= Disturbed Sample

V.S = Vane Shear Test C = Core Sample W = Water Sample

W. = Water Gample
W.L = Water Level.
CR = Core Recovery (mm)
R/r = Recovery Ratio (%)

COHESIVE SOIL (N) 0 - 2 : 2 - 4 : Very Soft Soft 4 - 8 Medium Stiff 8 - 15 : Stiff Very Stiff Hard 15 - 30 : 30 - Above :

0-4 : 4-10 : 10-30 : 30-50 : Loose Medium Dense Dense 50 - Above : - Very Dense



#### DEEP BORING LOG.

PRO.	JECT

KAJIAN SUB-PERMUKAAN DI KAWASAN RUMAH TETAMU, USM, PULAU PINANG.

Borehole N	lo:							meter Supervisor : Osman B Abdullah.							dullah
Sheet No:	4	of:	4	Type of	f Drill:	YWE (Wash)			Dat			05.1			
DEPTH			DEC	ODIDTION					SA	MPL	—- Е				
(meter)	COL	OUR (	CONS	CRIPTION ( SISTENCY, F SIZE, TEXT	RELATI	VE DENSITY	DEPTH (meter)							REMARKS	
33.00	Hard, ligh with trace			wish SILT			33.00 - 33.12	P22		24					N = 50 Rr = 100/120 mm
34.50	No Recov	ery					34.50 - 34.52	P23	<u>50</u> 20						N = 50 Rr = NIL
36.00	Brown ligh	nt grey	mode	erately weat	hered G	RANITE.	36.00 - 37.50	C1							CR = 1500 CRR= 600/1500 RQD= 100/600
37.50	Light grey	browr	ı high	tly weathere	d GRAN	NITE.	37.50 - 39.00	C2							CR = 1500 CRR= 650/1500 RQD= 0
39.00	Brown ligh	nt grey	mode	erately weatl	nered G	RANITE.	39.00 - 40.50	C3							CR = 1500 CRR= 1100/1500 RQD= 150/1100
40.50	Ditto.						40.50 - 41.00	C4							CR = 500 CRR= 300/500 RQD= 180/300
		E	nd Of	f Borehole A	it 41.00	m									
		Grou	ınd W	/ater Level A	At 5.93 ı	m									
NOTES	<u> </u>	<u> </u>													

= Standard Penetration Test (S.P.T) UD = Undisturbed sample

D = Disturbed Sample

V.S = Vane Shear Test C = Core Sample

W = Water Sample

W.L = Water Level .

CR = Core Recovery (mm) R/r = Recovery Ratio (%)

CRR Core Recovery Ratio (%)Rock Quality Designation

RQD COHESIVE SOIL (N)

0 - 2 :

2 - 4

4 - 8

8 - 15 :

15 - 30 : 30 - Above :

Very Stiff

Medium Stiff Stiff

Very Soft

Soft

0-4 : 4-10 : 10-30 :

Medium Dense 30 -50 : Dense

50 - Above : · Very Dense

NON COHE SIVE SOIL (N)

Very Loose

Loose

### APPENDIX D

BOREHOLE DATA (BH 2) AT MINDEN, USM, PENANG.



## DEEP BORING LOG.

PROJECT:

KAJIAN SUB-PERMUKAAN DI KAWASAN RUMAH TETAMU, USM, PULAU PINANG.

No: BH 2 Reduce level:						meter Supervisor : Osman B Abdullah.							dullah.	
1	of:	4	Type of Dr	ill: ——	YWE (Wash)									
COL	OUR (	CONS	ISTENCY, REL	_ATI	VE DENSITY	DEPTH (meter)	No.	75	75	Field 75	75	75		REMARKS
No Reco	very					1.50 - 1.95	P1	1	2	2	1	2	1	N = 6 Rr = NIL
			ı SILT			3.00 - 3.45	P2 D1	2	2	3	2	2	2	N = 9 Rr = 300/450 mm
						4.50 - 4.95	P3 D2	2	2	2	2	2	2	N = 8 Rr = 350/450 mm
			ı SILT			6.00 - 6.45	P4 D3	2	2	3	3	2	2	N = 10 Rr = 400/450 mm
Stiff, ditto.						7.50 - 7.95	P5 D4	2	2	2	3	2	2	N = 9 Rr = 380/450 mn
			sh reddish SILT	Г		9.00 - 9.45	P6 D5	2	3	3	2	3	3	N = 11 Rr = 420/450 mm
			ey reddish SILT	-		10.50 - 10.95	P7 D6	3	3	4	3	3	4	N = 14 Rr = 450/450 mn
	COL No Recov Stiff, light with some Stiff, light with some Stiff, ditto. Stiff, light with some	COLOUR CO	DES COLOUR CONS GRAIN  No Recovery  Stiff, light grey reddish with some gravel.  Loose, reddish SAND with traces of gravel.  Stiff, light grey reddish with some gravel.  Stiff, light grey reddish with some gravel.	DESCRIPTION OF COLOUR CONSISTENCY, REIGRAIN SIZE, TEXTURE  No Recovery  Stiff, light grey reddish SILT with some gravel.  Loose, reddish SAND with traces of gravel.  Stiff, light grey reddish SILT with some gravel.  Stiff, ditto.  Stiff, ditto.  Stiff, light grey yellowish reddish SILT with some gravel.	DESCRIPTION OF SOIL COLOUR CONSISTENCY, RELATIGRAIN SIZE, TEXTURE EN No Recovery  Stiff, light grey reddish SILT with some gravel.  Loose, reddish SAND with traces of gravel.  Stiff, light grey reddish SILT with some gravel.  Stiff, ditto.  Stiff, ditto.  Stiff, light grey yellowish reddish SILT with some gravel.	DESCRIPTION OF SOIL, COLOUR CONSISTENCY, RELATIVE DENSITY GRAIN SIZE, TEXTURE ETC.  No Recovery  Stiff, light grey reddish SILT with some gravel.  Loose, reddish SAND with traces of gravel.  Stiff, light grey reddish SILT with some gravel.  Stiff, light grey reddish SILT with some gravel.  Stiff, light grey yellowish reddish SILT with some gravel.	1 of: 4 Type of Drill: YWE (Wash)  DESCRIPTION OF SOIL, COLOUR CONSISTENCY, RELATIVE DENSITY GRAIN SIZE, TEXTURE ETC.  No Recovery  1.50 - 1.95  Stiff, light grey reddish SILT with some gravel.  3.00 - 3.45  Loose, reddish SAND with traces of gravel.  4.50 - 4.95  Stiff, light grey reddish SILT with some gravel.  6.00 - 6.45  Stiff, ditto.  7.50 - 7.95  Stiff, light grey yellowish reddish SILT with some gravel.  9.00 - 9.45	1 of: 4 Type of Drill: YWE (Wash)  DESCRIPTION OF SOIL, COLOUR CONSISTENCY, RELATIVE DENSITY GRAIN SIZE, TEXTURE ETC.  No Recovery  1.50 - P1 1.95  Stiff, light grey reddish SILT with some gravel.  Loose, reddish SAND with traces of gravel.  Stiff, light grey reddish SILT 6.00 - P4 with some gravel.  Stiff, light grey reddish SILT 6.45 D3  Stiff, light grey reddish SILT 9.00 - P5 7.95 D4  Stiff, light grey yellowish reddish SILT 9.00 - P6 Stiff, light grey yellowish reddish SILT 9.45 D5  Stiff, light grey yellowish reddish SILT 9.45 D5  Stiff, light grey yellowish reddish SILT 9.45 D5  Stiff, yellowish light grey reddish SILT 9.45 D5	1 of: 4 Type of Drill: YWE (Wash)  DESCRIPTION OF SOIL, COLOUR CONSISTENCY, RELATIVE DENSITY GRAIN SIZE, TEXTURE ETC.  No Recovery  1.50 - P1 1 1.95  Stiff, light grey reddish SILT with some gravel.  Loose, reddish SAND with traces of gravel.  Stiff, light grey reddish SILT with some gravel.  Stiff, light grey yellowish reddish SILT 9.00 - P6 2 9.45 D5  Stiff, light grey yellowish reddish SILT 9.00 - P6 2 9.45 D5	1	1	1 of: 4 Type of Drill: YWE (Wash)  DESCRIPTION OF SOIL, COLOUR CONSISTENCY, RELATIVE DENSITY GRAIN SIZE, TEXTURE ETC.  No Recovery  1.50 - P1 1 2 2 1 1 1.95 P1 1 2 2 1 1.95 P1 1 2 2 2 1 1.95 P1 1 2 2 2 1 1.95 P1 1 2 2 3 3 2 1.95 P1	1 of: 4 Type of Drill: YWE (Wash)  Date: 31.12 20  DESCRIPTION OF SOIL, COLOUR CONSISTENCY, RELATIVE DENSITY GRAIN SIZE, TEXTURE ETC.  No Recovery  1.50 - P1 1 2 2 1 1 2 1.95  Stiff, light grey reddish SILT with some gravel.  Stiff, light grey yellowish reddish SILT 9.00 - P6 2 3 3 2 2 3 2 3 3 2 3 3 2 3 3 3 3 3 3	1 of: 4 Type of Drill: YWE (Wash)  Date: 31.12.2013  DESCRIPTION OF SOIL, COLOUR CONSISTENCY, RELATIVE DENSITY GRAIN SIZE, TEXTURE ETC.  No Recovery  1.50- P1 1 2 2 1 1 2 1  1.95  Stiff, light grey reddish SILT with some gravel.  Stiff, light grey reddish SILT with some gravel.  Stiff, light grey yellowish reddish SILT with some gravel.  Stiff, light grey yellowish reddish SILT with some gravel.  Stiff, light grey yellowish reddish SILT with some gravel.  Stiff, light grey yellowish reddish SILT with some gravel.  Stiff, light grey yellowish reddish SILT with some gravel.  Stiff, light grey yellowish reddish SILT with some gravel.  Stiff, light grey yellowish reddish SILT with some gravel.  Stiff, light grey yellowish reddish SILT with some gravel.  Stiff, light grey yellowish reddish SILT with some gravel.  Stiff, light grey yellowish reddish SILT with some gravel.  Stiff, light grey yellowish light grey reddish SILT with some gravel.  Stiff, light grey yellowish light grey reddish SILT with some gravel.

D ≃ Disturbed Sample V.S = Vane Shear Test

C = Core Sample W = Water Sample W.L = Water Level .

CR = Core Recovery (mm)
R/r = Recovery Ratio (%)

COHESIVE SOIL (N) 0-2 : Very Soft 2-4 : Soft 4-8 : Medium Stiff 8 - 15 : Stiff

15 - 30 : Very Stiff Hard 30 - Above :

0-4 : 4-10 : Very Loose

Loose 10 - 30 : Medium Dense 30 -50 ; Dense 50 - Above : - Very Dense



DEEP BORING LOG.

PROJECT:

KAJIAN SUB-PERMUKAAN DI KAWASAN RUMAH TETAMU, USM, PULAU PINANG.

Borehole N	10:	вн		meter	1	Sur		sor :	Osn	าลก	B Aby	dullah.		
Sheet No:	2	of:	4	Type of Drill:	YWE (Wash)			Dat			03.0			Julian.
DEDTIL			DE000					SAI	MPL					7
DEPTH (meter)	COLO	OUR (	DESCI	RIPTION OF SOIL TENCY, RELATIV	··· /E DENCITY					Field	J Tes			REMARKS
(		G	RAIN SI	ZE, TEXTURE E	TC.	DEPTH (meter)	No. (Cls.)	75				75	1 1	112.00 (1110
						1	(0.0.)	11211	11411	пип	1000	mm	mm.	
12.00	Very stiff,	light g	rey yello	owish SILT		12.00 -	P8	4	4	3	4	4	5	N = 16
	with some	grave	el.			12.45	D7					,	ľ	Rr = 300/450 mm
]														14 = 300/430 MM
13.50	Very stiff,	light g	rey redo	lish yellowish SILT	Г	13.50 -	P9	4	3	5	4	4	4	N = 17
	with some	grave	el.			13.95	D8							Rr = 320/450 mm
														10 - 020/430 mm
15.00	Very stiff, I	ight b	rown re	ddish SILT		15.00 -	P10	4	5	5	4	4	5	N = 18
	with some	grave	el.			15.45	D9							Rr = 450/450 mm
														100, 100 11111
						1								
16.50	Stiff, light of	grey b	rown SI	LT		16.50 -	P11	3	3	4	4	3	4	N = 15
	with some	grave	ıl.			16.95	D10							Rr = 400/450 mm
İ														
												ĺ		
18.00	Very stiff, o	dark g	rey redo	lish SILT		18.00 -	P12	4	5	5	4	4	5	N = 18
	with some	grave	d.			18.45	D11							Rr = 350/450 mm
19.50	Very stiff, li	ight gi	rey to da	ark grey brown SIL	_T	19.50 -	P13	5	5	5	5	5	5	N = 20
ľ	with some	grave	l.			19.95	D12		ľ					Rr = 400/ 450 mm
						İ								
<u> </u>														
	Very stiff, li	-		wish SILT		21.00 -	P14	3	4	6	5	5	5	N = 21
[	with some	grave	l.			21.45	D13							Rr = 300/450 mm
													Ì	
ł										1				
						1								
NOTES														
N = Standari	d Penetration T	oet /S D	T)	CPP - Core B										

= Standard Penetration Test (S.P.T)

UD = Undisturbed sample

D = Disturbed Sample

V.S = Vane Shear Test

C = Core Sample

W = Water Sample W.L = Water Level .

CR = Core Recovery (mm) R/r = Recovery Ratio (%)

CRR = Core Recovery Ratio (%) RQD = Rock Quality Designation

COHESIVE SOIL (N) Very Soft

0-2 :

Soft 4 - 8 Medium Stiff

8-15 :

15 - 30 : 30 - Above :

Stiff Very Stiff Hard

NON COHE SIVE SOIL (N)

0 - 4 : Very Loose

4-10 :

Loose

10 - 30 : Medium Dense 30 -50 : Dense

50 - Above : - Very Dense



**DEEP BORING LOG.** 

PROJECT:

KAJIAN SUB-PERMUKAAN DI KAWASAN RUMAH TETAMU, USM, PULAU PINANG.

No: BH 2		meter Supervisor : Osman B Abdullah.						dullah.							
3 of: 4	3 of: 4 Type of Drill: YWE (W							Date: 03.01.2014							
					SAM										
COLOUR CONSIST	TENCY, RELATI	VE DENSITY	DEPTH (meter)	No. (Cls.)	75 mm n	75	75	75	75		REMARKS				
Very stiff, light grey brow with some gravel.		22.50 - 22.95	P15 D14	4	4	5	5	4	4	N = 18 Rr = 320/450 mm					
Very stiff, ditto.			24.00 - 24.45	P16 D15	5	5	5	4	4	4	N = 17 Rr = 350/450 mm				
Very stiff, light grey redd with some gravel.	ish brown SILT		25.50 - 25.95	P17 D16	5	5	5	5	5	5	N = 20 Rr = 400/450 mm				
Very stiff, dark brown rewith some gravel.	ddish SILT		27.00 - 27.45	1	1 1	5	6	6	6	5	N = 23 Rr = 400/450 mm				
Very stiff, ditto.			28.50 - 28.95		1	5	5	5	4	6	N = 20 Rr = 300/450 mm				
Very stiff, light grey dark with some gravel.	c brown SILT		30.00 - 30.45		1	5	6	6	5   (	6   8	N = 26 Rr = 300/450 mm				
Hard, yellowish dark bro	own SILT		31.50 - 31.62		- 1		'	n			N = 50 Rr = 120/120 mm				
	DESCR COLOUR CONSIST GRAIN SIZ  Very stiff, light grey brown with some gravel.  Very stiff, ditto.  Very stiff, ditto.  Very stiff, dark brown rewith some gravel.  Very stiff, ditto.  Very stiff, ditto.	DESCRIPTION OF SOIL COLOUR CONSISTENCY, RELATIVE GRAIN SIZE, TEXTURE E  Very stiff, light grey brown SILT with some gravel.  Very stiff, ditto.  Very stiff, light grey reddish brown SILT with some gravel.  Very stiff, dark brown reddish SILT with some gravel.  Very stiff, ditto.	DESCRIPTION OF SOIL, COLOUR CONSISTENCY, RELATIVE DENSITY GRAIN SIZE, TEXTURE ETC.  Very stiff, light grey brown SILT with some gravel.  Very stiff, ditto.  Very stiff, dark brown reddish SILT with some gravel.  Very stiff, ditto.  Very stiff, dark brown reddish SILT with some gravel.  Very stiff, ditto.	DESCRIPTION OF SOIL, COLOUR CONSISTENCY, RELATIVE DENSITY GRAIN SIZE, TEXTURE ETC.  Very stiff, light grey brown SILT with some gravel.  22.50 - 22.95  Very stiff, ditto.  24.00 - 24.45  Very stiff, light grey reddish brown SILT with some gravel.  25.50 - 25.95  Very stiff, dark brown reddish SILT with some gravel.  27.00 - 27.45  Very stiff, ditto.  28.50 - 28.95  Very stiff, light grey dark brown SILT with some gravel.  28.50 - 28.95  Very stiff, light grey dark brown SILT with some gravel.  30.00 - 30.45  Hard, yellowish dark brown SILT 31.50	DESCRIPTION OF SOIL,   COLOUR CONSISTENCY, RELATIVE DENSITY   GRAIN SIZE, TEXTURE ETC.   DEPTH (meter)   No. (Cls.)	DESCRIPTION OF SOIL, COLOUR CONSISTENCY, RELATIVE DENSITY GRAIN SIZE, TEXTURE ETC.  Very stiff, light grey brown SILT with some gravel.  Very stiff, ditto.  24.00 - P16 5 24.45 D15  Very stiff, light grey reddish brown SILT with some gravel.  25.50 - P17 5 D16  Very stiff, dark brown reddish SILT with some gravel.  Very stiff, dark brown reddish SILT with some gravel.  27.00 - P18 5 27.45 D17  Very stiff, ditto.  28.50 - P19 4 28.95 D18  Very stiff, light grey dark brown SILT with some gravel.  30.00 - P20 5 30.45 D19  Hard, yellowish dark brown SILT 31.50 - P21 28	DESCRIPTION OF SOIL, COLOUR CONSISTENCY, RELATIVE DENSITY GRAIN SIZE, TEXTURE ETC.  Very stiff, light grey brown SILT with some gravel.  Very stiff, light grey reddish brown SILT with some gravel.  Very stiff, dark brown reddish SILT with some gravel.  Very stiff, dark brown reddish SILT with some gravel.  Very stiff, ditto.  22.50 - P15	DESCRIPTION OF SOIL,   COLOUR CONSISTENCY, RELATIVE DENSITY   DEPTH (meter)   Field   Colour (Cls.)   mm mm mm mm mm mm mm mm mm mm mm mm m	DESCRIPTION OF SOIL, COLOUR CONSISTENCY, RELATIVE DENSITY GRAIN SIZE, TEXTURE ETC.  Very stiff, light grey brown SILT with some gravel.  Very stiff, light grey reddish brown SILT with some gravel.  Very stiff, dark brown reddish SILT with some gravel.  Very stiff, ditto.  24.00 - P16 5 5 5 5 5  4  Very stiff, light grey reddish brown SILT with some gravel.  Very stiff, dark brown reddish SILT with some gravel.  Very stiff, ditto.  27.00 - P18 5 5 6 6  Wery stiff, ditto.  28.50 - P19 4 5 5 5  Very stiff, ditto.  28.50 - P19 3 5 5 6  Wery stiff, ditto.  28.50 - P19 4 5 5 5  Wery stiff, ditto.  Very stiff, light grey dark brown SILT with some gravel.  Very stiff, light grey dark brown SILT with some gravel.  Very stiff, light grey dark brown SILT with some gravel.  30.00 - P20 5 5 6 6  Hard, yellowish dark brown SILT 31.50 - P21 28 22	DESCRIPTION OF SOIL, COLOUR CONSISTENCY, RELATIVE DENSITY GRAIN SIZE, TEXTURE ETC.   DEPTH   No.   75   75   75   75   75   75   75   7	DESCRIPTION OF SOIL,				

UD = Undisturbed sample D = Disturbed Sample
V.S = Vane Shear Test C = Core Sample

W = Water Sample W.L = Water Level. CR = Core Recovery (mm) R/r = Recovery Ratio (%) ROD = Rock Quality Designation

COHESIVE SOIL (N) 0-2 : 2-4 : 4-8 : 8-15 : Very Soft Soft Medium Stiff Stiff Very Stiff Hard 15 - 30 : 30 - Above :

Very Loose 4 - 10 : Loose 10 - 30 : Medium Dense 30 -50 : Dense 50 - Above : - Very Dense



#### DEEP BORING LOG.

PROJECT:

KAJIAN SUB-PERMUKAAN DI KAWASAN RUMAH TETAMU, USM, PUŁAU PINANG.

Borehole N	lo:	ВН	2	Reduce level:		meter		Sur	pervi		Osm	120	R Ab	dullah.
Sheet No:	4	of:	4	Type of Drill:	YWE (Wash)			Dat			04.0			Julian,
									MPLI					
DEPTH (meter)	COLC	א פו וע	DESCRI	PTION OF SOIL				L		Field	Tes	st		REMARKS
(meter)	OOLC	G	RAIN SIZ	ENCY, RELATI E, TEXTURE E	TC.	DEPTH (meter)	No. (Cls.)	75		75		75		NEMARKS
								mm	mm	mm r	mu	mm	mm	
33.00	Light grey	slight	ly weathe	red GRANITE.		33.00 -	C1							CR = 1500
						34.50								CR = 1450/1500
						01.00								RQD= 1450/1450
														RQD= 1450/1450
34.50	Yellowish li	ight g	rey slight	y weathered GF	RANITE.	34.50 -	C2							CR = 1500
						36.00								CRR= 1380/1500
														RQD= 1380/1380
														1380/1380
36.00	Light grey s	slight	ly weathe	red GRANITE.		36.00 -	C3							CR = 1500
						37.50								CR = 1300/1500
														RQD= 1300/1300
														KQD= 1300/1300
37.50	Ditto.					37.50 -	C4							CR = 500
						38.00								
														CRR= 500/500
														RQD= 500/500
		Е	nd Of Bo	rehole At 38.00	m									
		Grou	und Wate	r Level At 4.70 n	n									
-														
1														
NOTES					<del></del>	<u></u>	<u> </u>	<u>L_</u>		<u>L</u>				<u>L</u>

N	= Standard Penetration Test (S.P.T)
	= Undisturbed sample
D	= Disturbed Sample
V.S	≃ Vane Shear Test
С	= Core Sample

W = Water Sample W.L = Water Level . CR = Core Recovery (mm) R/r = Recovery Ratio (%) CRR = Core Recovery Ratio (%) RQD = Rock Quality Designation COHESIVE SOIL (N)

0-2 : Very Soft 2 - 4 Soft 4-8 : Medium Stiff 8 - 15 : Stiff 15 - 30 : Very Stiff 30 - Above : Hard

NON COHE SIVE SOIL (N) 0-4 : 4-10 : Vary Loose Loose 10 - 30 : Medium Dense 30 -50 : Dense 50 - Above : · Very Dense

### APPENDIX E

BOREHOLE DATA (BH 6) AT BUKIT BUNUH, PERAK.



#### DEEP BORING LOG.

	ICCT
PRU	JECT

# REGIONAL GEOPHYSICS FEILDCAMP 2013, BUKIT BUNUH CRATER STUDY.

Borehole N	No:	вн	BH 6 Reduce level:					neter Supervisor : Osman B Abdullah.							
Sheet No:	1	of:	2	Ty	pe of Drill:	YWE (Wash)		-	Dat			_			
							Date: 07.07.2013 - 08.07.2013  SAMPLE								
DEPTH (meter) COLO		OUR (	DESCRIPTION OF SOIL, UR CONSISTENCY, RELATIVE DENSITY GRAIN SIZE, TEXTURE ETC.				DEPTH (meter)	No.	75	75	Field 75	ld Test 5 75 75 75 1 mm mm mm		75 mm	REMARKS
1.50	Loose raddish SAND with a little gravel and fine soil.						1.50 - 1.95	P1 D1 S-F	2	2	3		2	3	N = 10 Rr = 220/450 mm
3.00	Very stiff plasticity v				sandy SILT	of intermediate	3.00 - 3.45	P2 D2 MIS	3	3	4	5	5	7	N = 21 Rr = 300/450mm
4.50	Very stiff I				sandy SILT	of high	4.50 - 4.95	P3 D3 MHS	4	4	5	5	4	6	N = 20 Rr = 230/450 mm
6.00	Very stiff I plasticity v				rownish SILT	of very high	6.00 -	P4 D4 MV	4	4	4	4	5	4	N = 17 Rr = 210/450 mm
7.50	Very stiff y				reddish SILT	of high	7.50 - 7.95	P5 D5 MH	5	5	6	4	4	5	N = 19 Rr = 400/450mm
9.00	Medium de	ense li	ght b	orown S	AND.		9.00 - 9.45	P6 D6	5	4	5	5	4	6	N = 20 Rr = 240/450 mm
10.50	Medium de	ense li	ght b	orown S	AND with trad	ces of fine soil.	10.50 -	P7 D7	5	5	5	6	6	6	N = 23 Rr = 360/450 mn

UD = Undisturbed sample D = Disturbed Sample

VS = Vane Shear Test C = Core Sample W = Water Sample W.L = Water Level . CR = Core Recovery (mm)
R/r = Recovery Ratio (%) = Rock Quality Designation

RQD COHESIVE SOIL (N) 0-2 : 2-4 : 4-8 : Very Soft Soft Medium Stiff 8 - 15 : Stiff 15 - 30 : 30 - Above : Very Stiff Hard

0 - 4 : 4 - 10 : Very Loose Loose 10 - 30 : Medium Dense 30 -50 : Dense 50 - Above : • Very Dense



### DEEP BORING LOG.

_		$\sim$	- 1	_	$\sim$	~	
$\mathbf{r}$	×	O		_	ι.		

REGIONAL GEOPHYSICS FEILDCAMP 2013, BUKIT BUNUH CRATER STUDY.

Borehole No: BH 6					Reduce level: meter Supervisor : Osman B						R Ah	dullah			
Sheet No: 2 of: 2					Type of Drill:	YWE (Wash)		Date: 07.07.2013 - 08.07.2013							
DEPTH (meter)	er) COLOUR CONSIST			SISTE	PTION OF SOIL, ENCY, RELATIVE DENSITY E, TEXTURE ETC.		DEPTH (meter)	No. (Cls.)	75	75	E Field	Tes		75	REMARKS
12.00	No Recov	very					12.0 -	P8	<u>50</u> 20	mm 					N = 50 Rr =NIL
13.00	Yellowish	light g	rey ł	nighly	weathered GR	ANITE.	13.0- 14.5	C1							CR = 500 CRR=300/1500 RQD= 0
14.50	Yellowish	light g	rey n	nodera	ately weathere	d GRANITE.	14.5- 16.0	C2							CR = 1500 CRR=500/1500 RQD = 0
16.00	Light grey	slightl	y we	athere	ed GRANITE		16.0- 17.5	C3							CR = 1500 CRR=850/1500 RQD = 850/850
17.50	Ditto.						17.5- 18.0	C4							CR = 500 CRR = 450/500 RQD = 450/450
		E	nd C	of Bore	ehole At 18.00	m									
NOTES		Grou	and V	Vater	Level At 4.70 เ	m									

1	П		c
	J	ŌΠ	OTE

N = Standard Penetration Test (S.P.T)
UD = Undisturbed sample
D = Disturbed Sample
V.S = Vane Shear Test

D = Disturbed Sample
V.S = Vane Shear Test
C = Core Sample
W = Water Sample
W = Water Level

W.L = Water Level .

CR = Core Recovery (mm)

R/r = Recovery Ratio (%)

CRR = Core Recovery Ratio (%)
RQD = Rock Quality Designation

COHESIVE SOIL (N)

0 - 2 : Very Soft

2 - 4 : Soft

4 - 8 : Medium Stiff

8 - 15 : Stiff

15 - 30 : Very Stiff

30 - Above : Hard

NON COHE SIVE SOIL (N)
0 - 4 : Very Loose

0 - 4 : Very Loose 4 - 10 : Loose 10 - 30 : Medium Dense 30 - 50 : Dense 50 - Above : - Very Dense



## 2-D RESISTIVITY SURVEYS'S EQUIPMENT

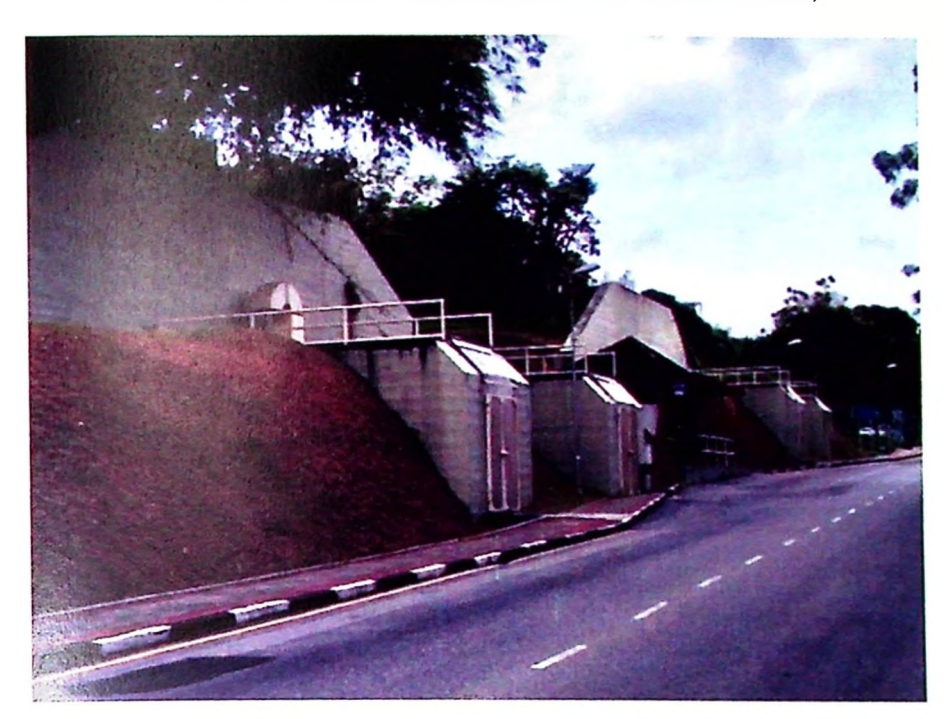


## LIST OF 2-D RESISTIVITY SURVEYS'S EQUIPMENT

No.	Equipment	Label
1	ABEM Terrameter SAS4000	A
2	ABEM Electrode-Selector (ES10-64)	В
3	ABEM LUND Multi-Electrode cables	С
4	Remote cable	D
5	Jumper clips	E
6	Stainless steel electrodes	F
7	Connecting cable SAS4000-to-ES10-64	G
8	Transfer cable	Н
9	Cable-Joint	I
10	Brunton compass	J
11	Battery sealed acid 12 volt	K
12	Hammer	L
13	Global Positioning System	M
14	Log book	N
15	Measuring tape	0
16	Walky-Talky	P
17	ABEM Terrameter manual book	Q
18	Chopping knife	R



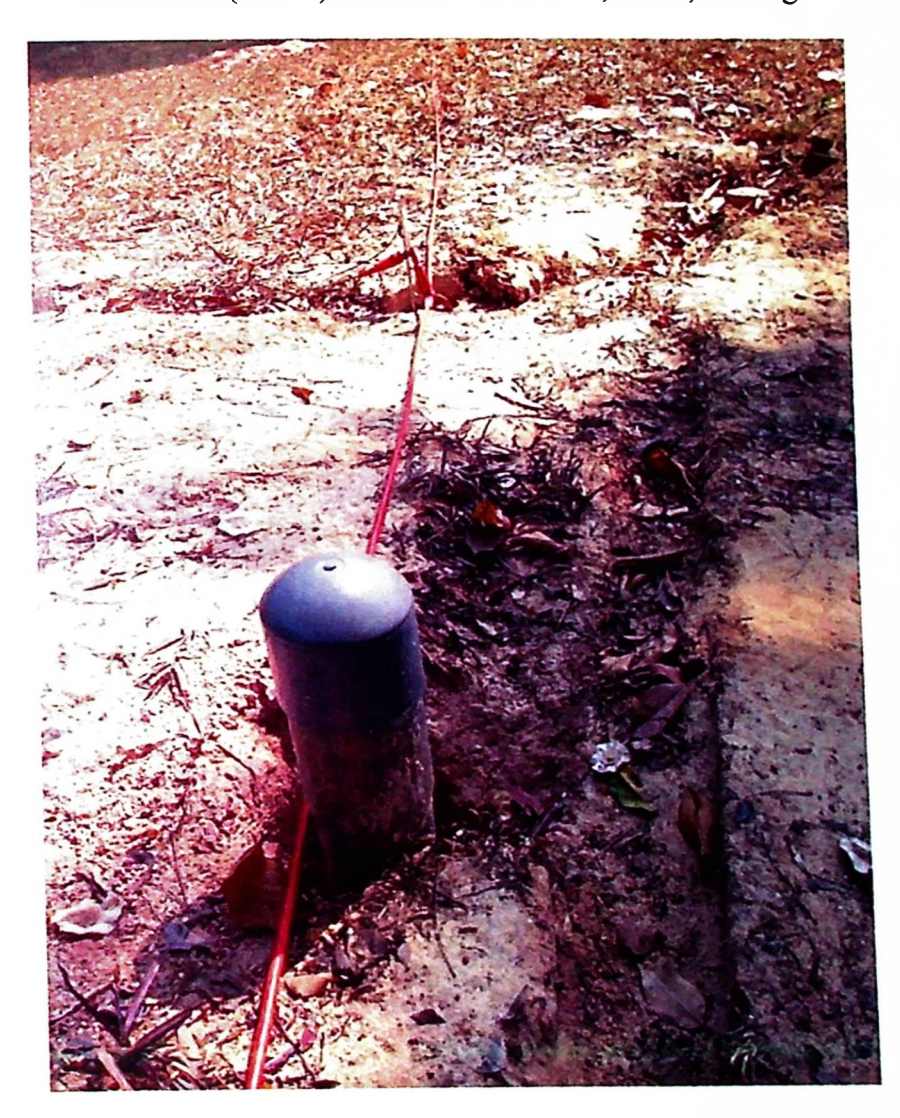
View from outside the buried bunker (Field model).



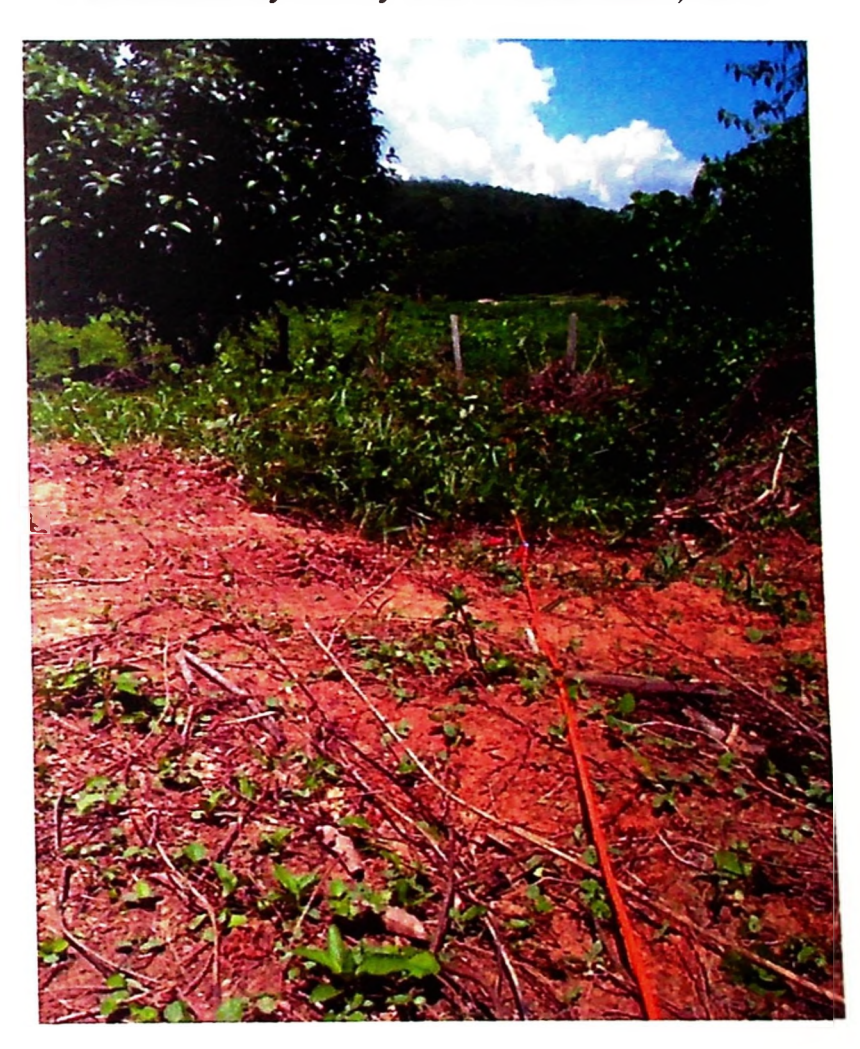
Inside the buried bunker (Field model).



Borehole (BH 1) location at Minden, USM, Penang.



2-D resistivity survey line at Bukit Bunuh, Perak.



Boring (BH 6) work in progress at Bukit Bunuh, Perak.



#### **APPENDIXES**

APPENDIX A: 2-D resistivity data filtering.

APPENDIX B: General array format.

APPENDIX C: Borehole data (BH 1) at Minden, USM, Penang.

APPENDIX D: Borehole data (BH 2) at Minden, USM, Penang.

APPENDIX E: Borehole data (BH 6) at Bukit Bunuh, Perak.

APPENDIX F: Electrical resistivity survey's equipment.

APPENDIX G: Site photos.

#### LIST OF PUBLICATIONS

#### A. Journals

Bery, A.A. & Saad, R. (2013). Merging Data Levels using Two Different Arrays for High Resolution Resistivity Tomography. *Electronic Journal of Geotechnical Engineering*, 18(V), 5507-5514.

#### **B.** Conference Proceedings

Bery, A.A., Saad, R., Hidayah, I.N.E., Azwin, I.N. & Saidin, M. (2015). Enhancement in resistivity resolution based on the data sets amalgamation technique at Bukit Bunuh, Perak, Malaysia. *IOP Conference Series: Earth and Environmental Science*, 23(1), 012009.

Bery, A.A., Saad, R., Hidayah, I.N.E., Azwin, I.N. & Saidin, M. (2014). Enhancement in resistivity resolution based on the data sets amalgamation technique at Bukit Bunuh, Perak, Malaysia. Proceedings of the 2<sup>nd</sup> International Conferences on Geological, Geographical. Aerospaces and Earth Sciences 2014 (AeroEarth 2014), 69-74, Kuta, Bali, Indonesia, October 11<sup>th</sup> -12<sup>th</sup>, 2014.

#### C. Chapter in books

Bery, A.A. & Saad, R. (2015). Enhancement in electrical resistivity tomography resolution for environmental and engineering geophysical study. In the International Civil and Infrastructure Engineering Conference (InCIEC) 2014, Springer-Verlag, 459-467.

DOI: 10.1007/978-981-287-290-6. ISBN: 978-981-287-289-0.

Bery, A.A. & Saad, R. (2014). Enhanced Horizontal and Vertical Resolution in 4-D Electrical Resistivity for Environmental Slope Study in Penang Island. *Chapter: Applied Solution of Engineering Science in Applied Mechanics and Materials*, 661, Trans Tech Publication Ltd, Switzerland, 73-80.

DOI: 10.4028/www.scientific.net/AMM.661.73.